



Design of Nanocarriers to Deliver Small Hydrophobic Molecules for Glioblastoma Treatment

Reatul Karim

► To cite this version:

Reatul Karim. Design of Nanocarriers to Deliver Small Hydrophobic Molecules for Glioblastoma Treatment. Human health and pathology. Université d'Angers; Université de Liège. Faculté de médecine, 2017. English. NNT: 2017ANGE0055 . tel-02155439

HAL Id: tel-02155439

<https://theses.hal.science/tel-02155439>

Submitted on 13 Jun 2019

HAL is a multi-disciplinary open access archive for the deposit and dissemination of scientific research documents, whether they are published or not. The documents may come from teaching and research institutions in France or abroad, or from public or private research centers.

L'archive ouverte pluridisciplinaire **HAL**, est destinée au dépôt et à la diffusion de documents scientifiques de niveau recherche, publiés ou non, émanant des établissements d'enseignement et de recherche français ou étrangers, des laboratoires publics ou privés.



Design of Nanocarriers to Deliver Small Hydrophobic Molecules for Glioblastoma Treatment

Reatul KARIM

Master of Research in Drug Delivery Systems

Promoters:

Dr. Géraldine PIEL and Prof. Catherine PASSIRANI

A dissertation submitted to obtain the degree of
Doctor in Biomedical and Pharmaceutical Sciences

Academic year: 2017-2018



The jury of thesis defense (12 October 2017)

Prof. Brigitte EVRARD (President)	University of Liege, Belgium
Dr. Géraldine PIEL (Promoter)	University of Liege, Belgium
Prof. Catherine PASSIRANI (Promoter)	University of Angers, France
Prof. Claus-Michael LEHR	Saarland University, Germany
Prof. Stefaan DE SMEDT	Ghent University, Belgium
Prof. Christine JEROME	University of Liege, Belgium
Prof. Marianne FILLET	University of Liege, Belgium
Prof. Vincent BOURS	University of Liege, Belgium
Dr. Claudio PALAZZO	University of Liege, Belgium



ERASMUS MUNDUS



Education and Culture DG



This thesis was financially supported by the Erasmus Mundus NanoFar Consortium and Fonds Léon Fredericq.

The thesis was performed in collaboration between the Laboratory of Pharmaceutical Technology and Biopharmacy (LPTB), Prof. B. EVRARD of the University of Liege (Belgium) and Micro and Nanomedicine Translational (MINT) at University of Angers (France).

Abstract

The aim of this thesis was to develop nanocarriers for efficient delivery of two low molecular weight hydrophobic drugs, apigenin (AG) and a ferrocifen-derivative (FcTriOH) to glioblastoma (GBM) as potential therapeutic strategies. Firstly, two liposomes, a lipid nanocapsule (LNC), and a polymer-based nanocapsule were developed and compared by their physicochemical characteristics, drug loading capacity, storage stability, stability in biological serum, drug release profiles, complement consumption and toxicity. Due to various advantageous characteristics, the LNCs were selected for further optimization.

Secondly, the LNCs were surface functionalized by adsorbing a GBM-targeting cell-penetrating peptide (CPP). The CPP concentration increased to significantly enhance LNC internalization in human GBM cells. The uptake mechanisms observed in U87MG cells were: micropinocytosis, clathrin-dependent and caveolin-dependent endocytosis. Moreover, the optimized CPP-functionalized LNCs were internalized preferentially in the GBM cells compared to normal human astrocytes. Additionally, the *in vitro* efficacy of the AG-loaded and FcTriOH-loaded LNCs was evaluated. The FcTriOH-loaded LNC-CPP showed the most promising activity with a low IC₅₀ of 0.5 μ M against U87MG cells. Intracerebral administration of the LNCs in a murine orthotopic U87MG tumor model showed possible toxic effects and the need for dose optimization. Finally, studies in murine ectopic U87MG tumor model showed promising activity after parenteral administration of the FcTriOH-loaded LNCs. Overall, these results exhibit the promising activity of FcTriOH-loaded LNCs as potential alternative GBM therapy strategy.

Keywords: Nanocarrier, lipid nanocapsule, liposome, glioblastoma, cell-penetrating peptide, apigenin, ferrocifen.

Résumé

Le but de cette thèse de doctorat fut de développer des nanoparticules pour la délivrance de deux molécules hydrophobes de faible poids moléculaire, l'apigénine (AG) et un ferrocifène (FcTriOH), comme stratégie innovante pour le traitement du glioblastome (GBM). Dans un premier temps, différents types de nanoparticules, liposomes, nanocapsules lipidiques (LNC), et nanocapsules à base de polymères, furent formulés et comparés en termes de caractéristiques physico-chimiques, de libération en drogue ou encore de toxicité. Les LNCs furent ainsi sélectionnées. Dans un deuxième temps, les LNCs furent fonctionnalisées en surface par un peptide pénétrant (CPP). La concentration de peptide fut augmentée afin d'améliorer significativement l'internalisation des LNCs dans des cellules humaines de GBM. Les mécanismes de macropinocytose et d'endocytose dépendant de la clathrine et de la cavéoline furent observés. De plus, il fut montré que l'internalisation de ces LNCs fonctionnalisées était réduite dans les cellules saines humaines d'astrocyte. L'efficacité biologique des LNCs chargées en AG et chargées en FcTriOH fut évaluée et comparée : le résultat le plus prometteur fut obtenu avec les LNCs chargées en FcTriOH. Une administration intracérébrale des LNCs sur un modèle tumoral murin orthotopique montra une potentielle toxicité et un besoin d'optimiser la dose administrée. Pour finir, les études menées sur un modèle tumoral ectopique murin montrèrent des résultats prometteurs, après une administration parentérale des LNCs chargées en FcTriOH. Ainsi, cette dernière formulation pourrait ouvrir la voie au développement d'une stratégie thérapeutique alternative pour le traitement du GBM.

Mots-clés : nanoparticule, nanocapsule lipidique, liposome, peptide pénétrant, apigénine, ferrocifène.

Table of Contents

1. General Introduction.....	2
1.1. Glioblastoma	2
1.1.1. GBM pathology and molecular biology.....	3
1.1.2. Diagnosis and current treatments	5
1.1.3. Natural flavonoid apigenin for GBM treatment.....	6
1.1.4. Organometallic ferrocifens for GBM treatment.....	9
1.2. Nanocarriers for the treatment of glioblastoma multiforme.....	12
1.2.1. Publication 1: Journal of Controlled Release 227 (2016) 23–37	12
1.2.2. Update since the review	47
1.3. References	49
2. Thesis aim and objectives	70
3. Development and comparison of injectable nanocarriers for delivery of low molecular weight hydrophobic drug molecules.....	73
3.1. Introduction	73
3.2. Summary of the results.....	75
3.3. Results	80
3.3.1. Publication 2: ‘Development and evaluation of injectable nanosized drug delivery systems for apigenin’, International Journal of Pharmaceutics xxx (2017) xxx–xxx (article in press).....	80
3.3.2. Additional unpublished data	108
3.4. Conclusion of chapter 3.....	120
3.5. References	123

4. Surface-functionalization of lipid nanocapsules for targeted drug delivery to human glioblastoma cells131

4.1. Introduction	131
4.2. Summary of the results	135
4.3. Results	140
4.3.1. Publication 3 (to be submitted in ACS Nano): Enhanced and targeted internalization of lipid nanocapsules in human glioblastoma cells: effect of surface-functionalizing NFL peptide	140
4.3.2. Additional data	173
4.4. Conclusion of chapter 4.....	184
4.5. References	186

5. General discussion, conclusion and perspectives193

5.1. General discussion.....	193
5.2. Conclusion and Perspectives	212
5.3. References	214

List of abbreviations

ABC	ATP-binding cassette
ABCB1	ATP-binding cassette sub-family member 1
ABM	astrocyte basal medium
AC-LNCs	Aqueous-core lipid nanocapsule
AG	Apigenin
AJ	Adherens junction
AL	Anionic liposome
AME	adsorptive-mediated endocytosis
AmpB	Amphotericin B
AMT	Adsorptive-mediated transcytosis
ANOVA	Analysis of variance
Apo	Apolipoprotein
AUC	Area under the curve
BBB	Blood-brain barrier
BBTB	Blood-brain tumor barrier
BCNU	Carmustine
BCRP	Breast cancer cell resistance protein
BCS	Biopharmaceutical Classification System
cBSA	Cationic bovine serum albumin
CEC	Cerebral endothelial cell
CED	Convection-enhanced delivery
CH50	50% hemolytic complement activity
Chol	Cholesterol
CI	Combination index
CK2	casein kinase 2
CL	Cationic liposome
CMC-PEG	Polyethylene glycol grafted carboxymethyl chitosan
CMT	Carrier-mediated transport
CNS	Central nervous system
CP	Chlorpromazine
CPP	Cell-penetrating peptide
cRGD	Cyclic arginine–glycine–aspartic acid
CT	Computerized tomography
DAM	5-(N,N-dimethyl) amiloride hydrochloride
DAPI	4',6-diamidino-2-phenylindole
DC-Chol	3 β -[N-(N',N'-dimethylaminoethane)-carbamoyl]cholesterol hydrochloride
DCL	Drug-in-cyclodextrin-in-liposome
DiA	4-(4-(dihexadecylamino)styryl)-N-methylpyridinium iodide)
DLS	Dynamic light scattering

DMEM	Dulbecco's modified Eagle's medium
DN	Daunorubicin
DOPE	1,2-dioleoyl-sn-glycero-3-phosphoethanolamine
DOX	Doxorubicin
DPPC	1,2-dipalmitoyl-sn-glycero-3-phosphocholine
DSPE-mPEG₂₀₀₀	1,2-distearoyl-sn-glycero-3-phosphoethanolamine-N-[methoxy(polyethylene glycol)-2000] ammonium salt
DTI	Diffusion tensor imaging
EAhy926	A human macrovascular endothelial cell line
EE	Entrapment efficiency
EGFR	Epidermal growth factor receptor
EPC	Egg phosphatidylcholine
EPR	Enhanced permeability and retention
FACS	Fluorescence-activated cell sorting
FBS	Fetal bovine serum
FcDiOH	Ferrociphenol
FcTriOH	4-ferrocenyl-5,5-bis(4-hydroxyphenyl)-pent-4-en-1-ol
FDA	Food and Drug Administration
fluoNFL	Fluorescent-labelled NFL-TBS.40-63 peptide
GBM	Glioblastoma multiforme
GM1	Monosialoganglioside
GRAS	Generally recognized as safe
GSH	Reduced glutathione
hCMEC/D3	An immortalized human cerebral microvascular endothelial cell line
HEPES	4-(2-hydroxyethyl)piperazine-1-ethanesulfonic acid
HIR	Human insulin receptor
HIV-1	Human immune deficiency virus type 1
HPI	Hydrogenated phosphatidylinositol
HPβCD	Hydroxypropyl- β -cyclodextrin
HS15	A polyethylene glycol associated hydrophilic surfactant
HSA	human serum albumin
IDH	Isocitrate dehydrogenase
IL13	Interleukin-13
IR	Insulin receptor
Kolliphor HS15	Macrogol 15 hydroxystearate
LDH	Lactate dehydrogenase
LDLR	Low density lipoprotein receptor
Lipoid S PC- 3	Hydrogenated phosphatidylcholine from soybean
Lipoxal	Liposomal oxaliplatin
LNC	Lipid nanocapsule
LUV	Large unilamellar vesicle

LY	Lucifer yellow
mAb	Monoclonal antibody
MAN	p-aminophenyl- α -D-mannopyranoside
MCT	Monocarboxylate transporter
MDR	Multidrug resistance
MGMT	O ⁶ -methylguanine–DNA methyltransferase
MLV	Multilamellar vesicle
MPS	Mononuclear phagocytic system
MRI	Magnetic resonance imaging
MRP4	Multiple drug resistance protein 4
MTS	3-carboxymethoxyphenyl-2-(4-sulfophrenyl)-2H-tetrazolium
MWCO	Molecular weight cut off
MβCD	Methyl- β -cyclodextrin
NaCl	Sodium chloride
NDDS	Nanosized drug delivery system
NEAA	non-essential amino acid
Neuro2a	A mouse neuroblastoma cell line
NFL	NFL-TBS.40-63 (a neurofilament light subunit derived tubulin binding site peptide)
NHA	Normal human astrocytes
NHS	Normal human serum
NP	Nanoparticle
NTA	Nanoparticle tracking analysis
OC-LNC	Oily core lipid nanocapsule
OCT	Organic cationic transporter
OHTam	Hydroxyl-tamoxifen
P908	Poloxamine 908
PACA	Poly(alkyl cyanoacrylate)
PBCA	Poly(butyl cyanoacrylate)
PBS	Phosphate buffer saline
PCL	Polycaprolactone
PDI	Polydispersity index
PEG	Polyethylene glycol
PEI	Polyethyleneimine
P-gp	P-glycoprotein
Phalloidin-TRITC	Phalloidin–tetramethylrhodamine-B-isothiocyanate
pHB	p-hydroxybenzoic acid
PHDCA	Poly(cyanoacrylate-co-hexadecylcyanoacrylate)
PIT	Phase inversion temperature
PLA	Poly lactide
PLGA	Poly(lactide-co-glycolide)
PMA	Phorbol-12-myristate-13- acetate

PMS	Phenazine methosulfate
PNC	Polymer-based nanocapsule
PNP	Polymeric nanoparticle
POPC	1-palmitoyl-2-oleoyl-sn-glycerol-3-phosphocholine
PS80	Polysorbate 80
PTEN	Phosphatase and tensin homolog
PVA	Poly(vinyl alcohol)
RES	Reticuloendothelial system
RME	Receptor-mediated endocytosis
RMT	Receptor mediated transcytosis
ROS	Reactive oxygen species
RT	Radiation therapy
SD	Standard deviation
SR-BI	Scavenger receptor B class I
SUV	Small unilamellar vesicle
TAT	trans-activating transcriptor
TEER	Transendothelial electrical resistance
TEM	Transmission electron microscopy
TfR	Transferrin receptor
TJ	Tight junction
TMZ	Temozolomide
TNFα	Tumor necrosis factor α
UPW	Ultra-pure water
V_d	Volume of distribution
VEGF	Vascular endothelial growth factor
WHO	World Health Organization

Chapter 1: General Introduction

1. GENERAL INTRODUCTION

A part of this introduction has been published in the form of a review article entitled ‘Nanocarriers for the treatment of glioblastoma multiforme: Current state-of-the-art’ in the ‘Journal of Controlled Release’ (Karim et al., 2016), and available at 1.2.1.

1.1. Glioblastoma

Glioblastoma, or historically mentioned ‘glioblastoma multiforme’ (GBM), is the most frequently occurring and deadliest primary malignant tumor of the central nervous system (CNS). Due to its malignant and highly invasive characteristics, GBM is categorized by the World Health Organization (WHO) as a grade IV CNS tumor (Louis et al., 2016). Median survival of GBM patients receiving current treatments is about 14.6 months (Stupp et al., 2005) and merely 5.5% patients survive more than 5 years after diagnosis (Ostrom et al., 2016). GBM is an aggressive form of glioma, a type of CNS tumors that arises from the non-neuronal glial cells i.e. astrocytes, oligodendrocytes, and microglia, which outnumbers neurons in the brain by about 3-folds and normally perform a supporting role to aid synaptic signaling of neurons (Purves et al., 2001). GBM constitutes 14.9% of all primary CNS tumors (3rd most frequent), 46.6% of primary malignant CNS tumors (Figure 1.1) and 55.4% of gliomas (Ostrom et al., 2016).

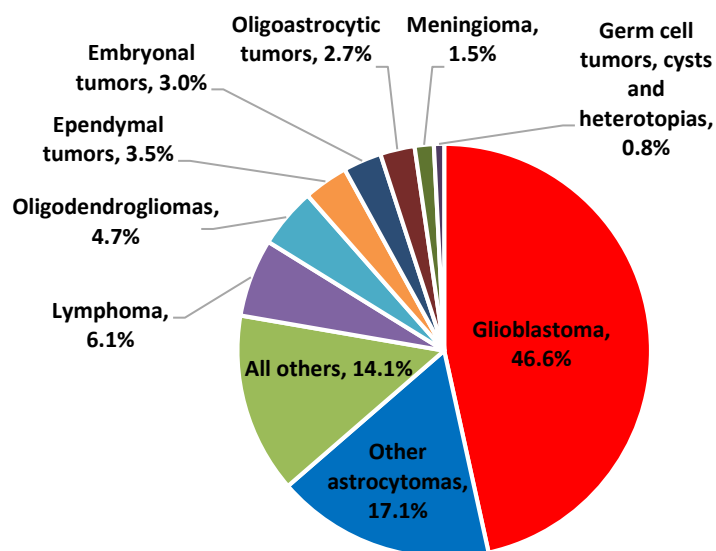


Figure 1.1: Distribution of malignant primary brain and other CNS tumors [adapted from CBTRUS Statistical Report: NPCR and SEER, 2009-2013 (Ostrom et al., 2016)]

1.1.1. GBM pathology and molecular biology

The term GBM was first introduced by Percival Bailey and Harvey Cushing in 1926 (Bailey and Cushing, 1926). GBM tumors generally have enhanced mitotic activity, proangiogenic properties, atypical cells and nucleus, reduced apoptosis, a central necrotic area with pseudopalisades (Adamson et al., 2009; Bianco et al., 2017) and occur 57.9% cases in frontal, temporal or parietal lobe (Ostrom et al., 2013). High angiogenesis and presence of pseudopalisades are key characteristics that distinguish GBM from lower grade gliomas. Although GBM tumors are highly aggressive, they generally do not metastasize outside CNS, which can be due to the quick death of the patients or to the deficiency of lymphatic passage of GBM cells (Robert and Wastie, 2008).

Regardless of their overlapping histology and phenotypes, the genetic variations and molecular characteristics, GBM tumors are heterogeneous. For instance-

- Epidermal growth factor receptor (EGFR) amplification occurs in 40% GBM patients (Hatanpaa et al., 2010). EGFR amplification is often connected with the occurrence of EGFR protein variants. For example, 68% EGFR amplified patients have deletion of exon 2-7 which is part of the ligand binding domains of EGFR (the variant is termed as EGFRvIII), resulting in therapeutic resistance to tyrosine kinase inhibitors like erlotinib (Schulte et al., 2013).
- p53 mutation is a frequent genetic event that is linked with the transition from low grade glioma to glioblastoma (Sidransky et al., 1992). Fults et al. reported to observe p53 mutation and loss of heterozygosity (LOH) on chromosome 10 in 28% and 61% GBM patients respectively (Fults et al., 1992). However, p53 mutation and concurrent LOH on chromosome 10 was observed only in 22% GBM patients, but not in patients with anaplastic astrocytoma or low-grade astrocytoma (Fults et al., 1992). Moreover, p53 mutation is often (6 out of 10 cases) associated with inactivation of phosphatase and tensin homolog (PTEN) (Zheng et al., 2008), a phosphatase tumor suppressor which generally facilitates homeostasis and aids in maintaining neural cell population. Mice with nonsense PTEN mutant GBM xenografts survived significantly shorter compared to wild-type (Xu et al., 2014).
- Overexpression of O⁶-methylguanine–DNA methyltransferase (MGMT) gene is often observed in GBM patients resulting in high levels of the MGMT protein, that

removes O⁶ alkyl groups of guanine and counteracts the anticancer effects of alkylating agents like temozolomide (TMZ) (Hegi et al., 2005).

- Isocitrate dehydrogenase (IDH) 1 mutation is observed in only 10% primary GBM cases (Louis et al., 2016) and more frequently (83%) observed for secondary GBM patients (Kloosterhof et al., 2011). The normal IDH-1 converts isocitrate to α -ketoglutarate, whereas the mutant IDH-1 can further convert α -ketoglutarate to 2-hydroxyglutarate which is an oncometabolite aiding in gliomagenesis (Losman and Kaelin, 2013).
- Genetic mutations are observed often with loss of tumor suppressor genes. This loss is spread throughout the genome and the altered regions frequently include e.g. 1p, 6q, 9p, 10p, 10q, 13q, 14q, 15q, 17p, 18q, 19q, 22q, and Y (Adamson et al., 2009).

The importance of identifying genetic/molecular variations along with the tumor histology for improved targeted-personalized therapy for CNS tumors has been recently acknowledged by WHO. Previously, CNS tumors were classified based on histology and malignancy (Louis et al., 2007). But the latest 2016 WHO CNS tumor classification is more dynamic and based on both phenotype and genotype so that tumors of same group have similar prognostic markers and are genetically more alike to aid in the choice of therapy in clinical setting (Louis et al., 2016). GBM is now subcategorized into three groups- IDH mutant GBM (about 10% cases), IDH wild-type GBM (about 90% cases), and GBM NOS (where IDH evaluation was not performed or inconclusive) (Louis et al., 2016). The IDH wild-type GBM has a median diagnosis age of 62 years, a median survival of 15 months after surgery, radiation therapy (RT) and chemotherapy, occurs mainly in the supratentorial region of the brain, has extensive necrosis, and shows P53 mutation (27%), EGFR amplification (35%) and PTEN mutation (24%) (Louis et al., 2016). In comparison, the IDH mutant GBM has median diagnosis age of 44 years, median survival is 31 months, occurs mainly at the frontal region, has limited necrosis, and shows p53 mutation (81%), but rarely has EGFR amplification or PTEN mutation (Louis et al., 2016).

Due to the heterogeneous genetic and molecular characteristics of GBM tumors, a drug molecule can be efficacious in some patients, but may not be able to cure other GBM patients as the tumor cells may be resistant to the therapy due to their altered molecular

characteristics. Therefore, the treatment may need to be chosen based on the genetic and molecular profile of the GBM tumor of the patient.

1.1.2. Diagnosis and current treatments

For last few decades, standard diagnosis of GBM began with magnetic resonance imaging (MRI) to detect suspicious changes in brain anatomy. T1-weighted MRI images with and without gadolinium and T2-weighted MRI images are commonly taken to determine the size, shape and location of the tumor. Several other potential MRI techniques are emerging which may provide more detailed images. Diffusion-weighted MRI uses differential diffusion of water molecules in healthy brain tissue and in tumors to create contrast enhanced MR images. Additionally, perfusion-weighted MRI uses tracer agent to compute relative cerebral blood volume, flow and mean transit time to determine the level of tumor neoangiogenesis (Korfiatis and Erickson, 2014). If MRI is not possible, contrast enhanced ‘computerized tomography’ (CT) scan can be performed. Once the size, shape and location of the tumor is confirmed, biopsy samples are taken to perform histological and molecular characterization to confirm GBM.

Present standard of care therapy for GBM involves surgical resection followed by RT and chemotherapy (Stupp et al., 2005). Surgical resection has been the cornerstone of the treatment for many decades. With the aid of modern imaging techniques, size-shape-location of the GBM tumor can be confirmed, maximal tumor resection (>98%) is possible (if intolerable brain damage can be avoided) and so, survival can be improved (Lacroix et al., 2001; Simpson et al., 1993). However, complete tumor removal is not achievable as the highly invasive GBM cells infiltrate surrounding healthy brain tissues. Maximal tumor resection significantly improves median survival to 13 months compared to 8.8 months for submaximal resection, and possibly enhances response to RT and chemotherapy (Lacroix et al., 2001; Stummer et al., 2008). Partial resection is not helpful as the remaining tumor can become very hostile and malignant, may cause massive edema and severe mass effect (Adamson et al., 2009). However, maximal tumor resection only improves short-term survival as a recent study observed no significant difference in baseline survival after 2 years between maximal resection and biopsy alone groups (Stewart, 2002). Therefore, RT is routinely given about 2 weeks after surgery as 60 Gray units (Gy) in 30 therapy sessions over 6 weeks targeting 2-3 cm ring of the tumor periphery that was observed in MRI

before surgery. RT induces DNA damage by breaking the double-strand and resulting apoptosis of the cells. Post-operative RT significantly improves median survival to 12.1 months.

Concomitant and adjuvant chemotherapy with TMZ, a blood-brain barrier (BBB) penetrating alkylating agent that methylates the purine bases of DNA, further improves the survival only to 14.6 months and has been the primary choice of treatment after surgery with concomitant RT (Stupp et al., 2005). Besides TMZ, Giladel® wafers have been used in the resection cavity after tumor removal for local delivery of the alkylating agent carmustine (BCNU) for a sustained period, although its median survival improvement capability is similar to TMZ (Brem et al., 1995). In 2009, FDA approved the use of bevacizumab, a vascular endothelial growth factor (VEGF) targeting monoclonal antibody (mAb) which inhibits angiogenesis, although the European Medicines Agency still hasn't approved it for GBM treatment (Wick et al., 2010). Moreover, two recent clinical trials have shown that bevacizumab treatment was unable to improve median survival of GBM patients (Chinot et al., 2014; Gilbert et al., 2014). Similar results were observed by numerous other clinical trials performed in the last decade, e.g. nimustine, estramustine, ¹³¹I-labelled human/murine chimeric 81C6 anti-tenascin mAb (ch81C6) and Anti-EGFR ¹²⁵I-mAb 425 failed to improve median survival of GBM patients (Henriksson et al., 2006; Imbesi et al., 2006; Sampson et al., 2006; Wygoda et al., 2006). Therefore, **new therapeutic approaches for GBM** are urgently necessary to improve efficacy of the treatment.

Among numerous promising molecules, flavonoids and ferrocifens are two hydrophobic group of molecules which showed promising activity against GBM that were therefore further evaluated in this study.

1.1.3. Natural flavonoid apigenin for GBM treatment

Apigenin (AG), or 4', 5, 7,-trihydroxyflavone (Figure 1.2) is a low molecular weight (MW = 270.24 g.mol⁻¹) yellow colored natural flavonoid, found in fruits i.e. oranges and grapefruit; plant beverages i.e. tea; vegetables i.e. parsley, onions and wheat sprouts; and in chamomile (Patel et al., 2007; Zheng et al., 2005a). Like several other flavonoids (Middleton et al., 2000), AG shows several promising bioactivities e.g. antimutagenic (Birt et al., 1986), antioxidant (Romanova et al., 2001), and anti-inflammatory (Lee et al.,

2007) properties. In recent years, it has gained attention of researchers as promising chemopreventive or chemotherapeutic agent owing not only to its strong antioxidant and anti-inflammatory effects, but also for its differential effects on healthy versus tumor cells (Das et al., 2010; Gupta et al., 2001).

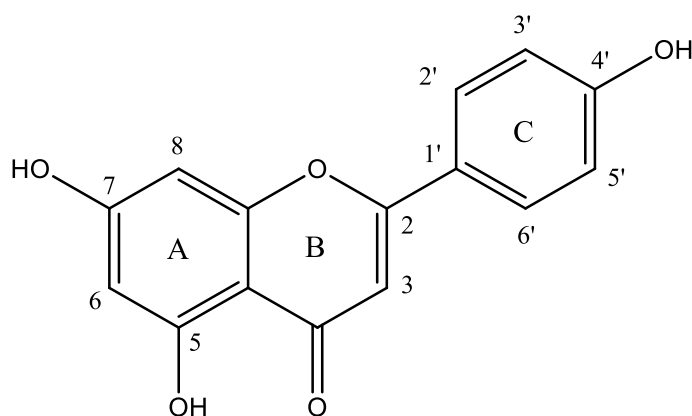


Figure 1.2: Chemical structure of 4', 5, 7,-trihydroxyflavone or apigenin

As a chemopreventive agent, AG can show activity by aiding in metal chelation, free radical scavenging and enhancing activity of the detoxification enzymes (Middleton et al., 2000). Pretreatment with AG gave protective effect in murine skin and colon carcinogenesis models (Birt et al., 1997; Van Dross et al., 2003). Moreover, AG strongly inhibited the tumorigenic ornithine decarboxylase enzyme (Wei et al., 1990), and amplified intracellular glutathione level resulting in an improved protection against oxidative stress (Myhrstad et al., 2002).

As a chemotherapeutic agent, AG showed promising activity against breast cancer (Way et al., 2004), cervical cancer (Zheng et al., 2005b), colon cancer (Wang et al., 2000), leukemia (Ruela-de-Sousa et al., 2010), lung cancer (Lu et al., 2010), prostate cancer (Gupta et al., 2001), ovarian cancer (Li et al., 2009), thyroid cancer (Yin et al., 1999) and neuroblastoma (Torkin et al., 2005) by interfering with various cellular signal transduction pathways. Among these, inhibition of casein kinase 2 (CK2) by AG was observed in various cell lines e.g. myeloma cells (Zhao et al., 2011), mammary epithelial cells (Song et al., 2000) and HeLa cells (Liu et al., 2015). CK2 is a serine/threonine kinase with a large number (>300) of substrates (Bian et al., 2013), has a vital role in maintenance of cell survival, and its amplified activity is observed in numerous types of tumors including GBM (Ji and Lu, 2013). The gene (CSNK2A1) encoding for CK2 α , one of the catalytic

subunits of CK2, is overexpressed in 33.7% of all GBM patients and more commonly (50%) in classical GBM patients (Zheng et al., 2013). CK2 impacts several downstream signal transduction pathways that play fundamental roles in various vital cellular activities (Figure 1.3). For example, CK2 interacts with JAK1/2 and positively regulates JAK and STAT3 (Zheng et al., 2011). Subsequently, it induces gene expression promoting angiogenesis and proliferation, and reduce apoptosis. Increased activity of activated STAT3 (Brantley et al., 2008), JAK1 and JAK2 (McFarland et al., 2011) was reported in GBM tumors. Moreover, CK2 increases the activity of NF- κ B and PI3/AKT pathways and supports cell survival and diminish apoptosis (Duncan and Litchfield, 2008). Additionally, CK2 can regulate Wnt/ β -catenin signaling pathway and aids in gliomagenesis (Seldin et al., 2005). Therefore, CK2 can be a potential target in GBM treatment and CK2 inhibitors can be promising as anti-GBM drug candidates.

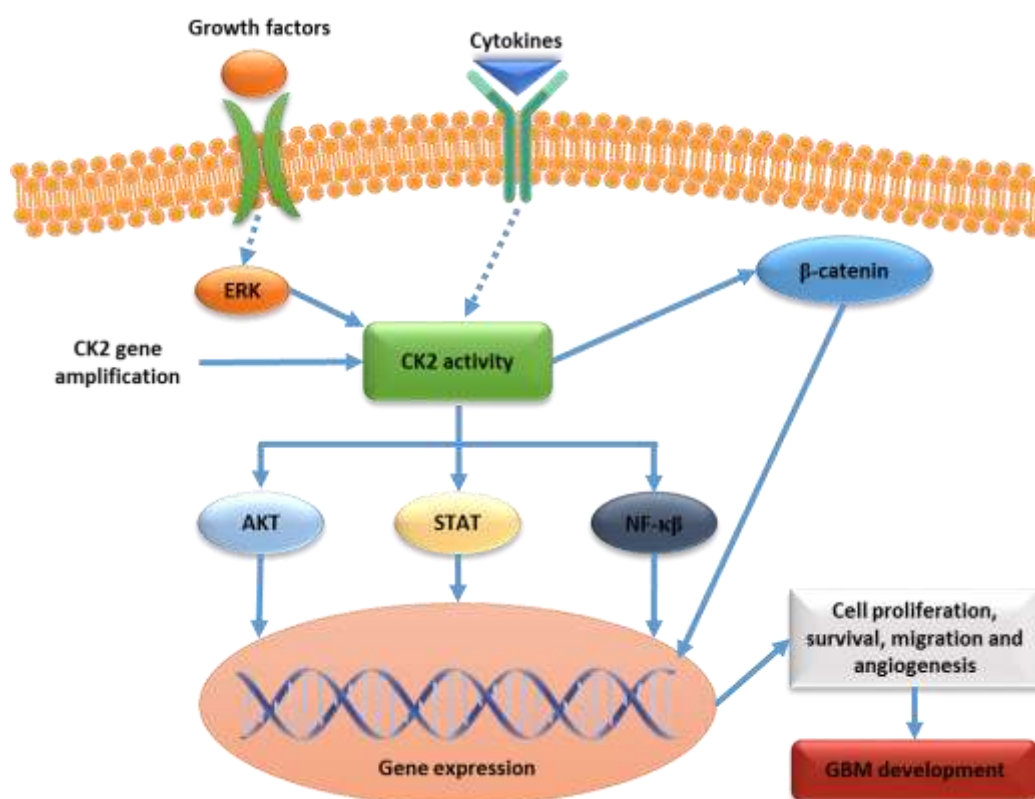


Figure 1.3: CK2 activation and CK2-regulated signaling pathways, aiding GBM development [reproduced from (Ji and Lu, 2013)]

AG, like several other flavonoids, has potent CK2 inhibiting activity with an IC_{50} of 0.8 μ M (Lolli et al., 2012). The presence of hydroxyl groups at position 7 and 4'- of the

flavone backbone is important for the CK2 inhibiting activity. Due to these hydroxyl groups and its appropriated tridimensional form, AG can target the two CK2 polar binding sites and inhibit its activity (Lolli et al., 2012). Against GBM, AG showed promising activities in several *in vitro* studies. Das et al. reported that 24 h of treatment with 50 μM of AG induced apoptosis in 40% T98G and U87MG GBM cells, but did not affect healthy human astrocytes (Das et al., 2010). In another study, 96 h of AG treatment reduced viability of U87MG cells in dose-dependent manner with an IC_{50} around 60 μM (Parajuli et al., 2009). Moreover, 24 h of treatment with varying concentrations of AG sensitized A172, U87MG and T98G GBM cells to tumor necrosis factor α ($\text{TNF}\alpha$) induced apoptosis (Dixit et al., 2012). Additionally, 72 h treatment of AG strongly reduced viability of C6 glioma cells with an IC_{50} of 22.8 μM , about 40-folds more efficient compared to TMZ (1000 μM) (Engelmann et al., 2002). A recent study reported that AG reduced viability of U1242MG and U87MG cells in a dose and time-dependent manner, but not on normal human astrocytes (NHA) (Stump et al., 2017).

Despite these promising *in vitro* results, the use of AG for *in vivo* studies is very constrained, chiefly owing to its very low aqueous solubility (1.35 $\mu\text{g/mL}$) (Li et al., 1997), and unavailability of biocompatible solvents (Zhao et al., 2013).

1.1.4. Organometallic ferrocifens for GBM treatment

Platinum based antitumor agents have been well known and widely used since 1960s, after the discovery of cisplatin by Rosenberg and his colleagues (Rosenberg et al., 1969). At present, platinum based DNA alkylating agents are one of the major chemotherapeutic products used alone or in combination for treatment of several cancers i.e. bladder, colorectal, ovarian and prostate cancers (Kelland, 2007). Platinum-based antitumor agents act mainly by formation of complex with two adjacent guanine residues of the DNA resulting in DNA distortion and apoptosis (Reedijk and Lohman, 1985). However, various problems associated with platinum complexes (i.e. side effects, high toxicity, inefficacy in resistant cells, kidney problems etc.) (Kelland, 2007) led to the development of other metal-based anticancer drugs (Fricker, 2007) i.e. ruthenium based and KP1019 (indazolium trans-[tetrachlorobis(1H-indazole)ruthenate(III)]) (Bergamo and Sava, 2011) or gold based auranofin etc. (Mirabelli et al., 1985). Moreover, organometallic compounds (i.e. compounds having a metal and organic ligands linked via coordination bonds) were

also developed which differ from the platinum complex drugs by binding mechanism and act preferentially on target proteins instead of acting solely on DNA (Jaouen et al., 2015). Among various organometallic anticancer agents, one of the most promising molecules is the iron containing metallocene ferrocene. It was stable in non-oxidative environment, was relatively nontoxic, had reversible oxidation-reduction (redox) characteristics and showed anticancer properties (Braga and Silva, 2013). When a ferrocene was combined with a tamoxifen molecule, one of the first ferrocifens, FcOHTam was developed as potential antitumor agents against breast cancer (Top et al., 1996). Interestingly, ferrocene had IC_{50} of 160 μ M, hydroxyl-tamoxifen (OHTam) had an IC_{50} of 30 μ M, and FcOHTam had an IC_{50} of 0.5 μ M against hormone-dependent breast cancer cells (Top et al., 2003). Some of the earliest ferrocifens, FcDiOH and FcOHTam (Figure 1.4) showed promising activity with low IC_{50} against both hormone-dependent and hormone independent breast cancer cells (Top et al., 2003; Vessieres et al., 2010). This was quite noteworthy and shows the importance of the ferrocenyl ring as OHTam was active only on hormone-dependent breast cancer cells (Vessieres et al., 2005). Such promising results has led to many other studies with ferrocifen type drugs (Jaouen et al., 2015).

Interestingly, the dominant pathway of cellular activity of ferrocifens depends on their concentration in culture medium (Figure 1.4) (Vessieres et al., 2010). At low concentrations, ferrocifens act by senescence, and gradually moves to apoptosis or Fenton reaction as the concentration is increased (Jaouen et al., 2015). This property makes them promising candidates for treating cancer cell lines resistant to apoptosis pathway. Compared to other organometallics (titanium, ruthenium, rhenium), ferrocifens showed better experiment outcomes that can be related to the redox characteristics of Fe, by reversible Fe^{II}/Fe^{III} oxidation (Jaouen and Top, 2014; Jaouen et al., 2001; Top et al., 2004). Multiple mechanisms of action are described for the antiproliferative effects of ferrocifens i.e. generation of reactive oxygen species (ROS) (Vessieres et al., 2010), formation of cytotoxic quinone methides (Hillard et al., 2005), and interaction with DNA (Zanellato et al., 2009), thiols and thioredoxin reductases (Citta et al., 2014). Solutions of several ferrocifen molecules i.e. FcDiOH and ansa-FcDiOH solutions showed promising *in vitro* activity against GBM cells (Laine et al., 2014; Laine et al., 2012). Moreover, ferrocifens were reported to be much more cytotoxic on GBM cells compared to astrocytes (Allard et al., 2008).

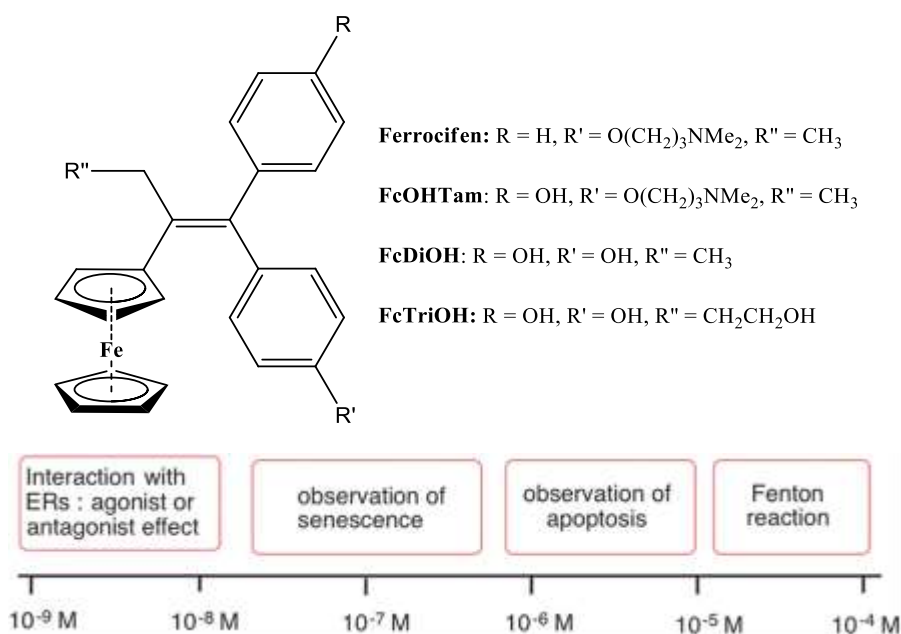


Figure 1.4: Chemical structure of several ferrocifen type anticancer drugs, and their *in vivo* action pathway changes according to concentration in the biological medium (adapted from (Jaouen et al., 2015)).

Despite their promising *in vitro* characteristics, the most promising ferrocifen molecules, generally polyphenols, are lipophilic and insoluble in water. Moreover, they are prone to rapid hepatic metabolism and can be quickly eliminated from the systemic circulation, making their successful delivery to the target site quite challenging.

Utilization of nanocarriers to encapsulate and deliver AG and/or ferrocifens can be a promising approach as efficiently designed nanocarriers may overcome the above-mentioned issues, preferentially accumulate in tumor tissue and thereby may reduce side-effects of chemotherapy.

1.2. Nanocarriers for the treatment of glioblastoma multiforme

1.2.1. Publication 1: Journal of Controlled Release 227 (2016) 23–37

NANOCARRIERS FOR THE TREATMENT OF GLIOBLASTOMA MULTIFORME: CURRENT STATE-OF-THE-ART

Reatul Karim^{a*}, Claudio Palazzo^{a*}, Brigitte Evrard^a, Geraldine Piel^a

^a *Laboratory of Pharmaceutical Technology and Biopharmacy, CIRM, University of Liège (4000), Belgium. Fax: +32 4 366 43 02; Tel: +32 4 366 43 07;*

*equal contribution

Corresponding authors:

Reatul Karim, e-mail address: reatul.karim@ulg.ac.be

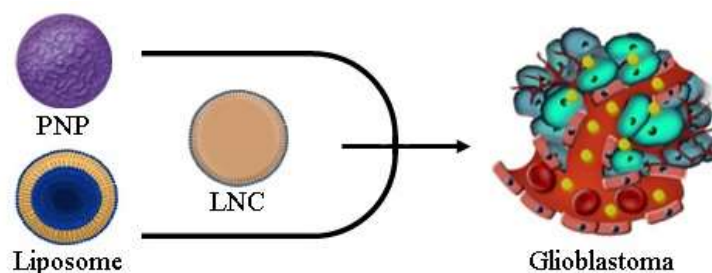
Claudio Palazzo, e-mail address: claudio.palazzo@ulg.ac.be

Journal of Controlled Release 227 (2016) 23–37

<http://dx.doi.org/10.1016/j.jconrel.2016.02.026>

Abstract

Glioblastoma multiforme, a grade IV glioma, is the most frequently occurring and invasive primary tumor of the central nervous system, which causes about 4% of cancer-associated-deaths, making it one of the most fatal cancers. With present treatments, using state-of-the-art technologies, the median survival is about 14 months and 2 year survival rate is merely 3-5%. Hence, novel therapeutic approaches are urgently necessary. However, most drug molecules are not able to cross the blood-brain barrier, which is one of the major difficulties in glioblastoma treatment. This review describes the features of blood-brain barrier, and its anatomical changes with different stages of tumor growth. Moreover, various strategies to improve brain drug delivery i.e. tight junction opening, chemical modification of the drug, efflux transporter inhibition, convection enhanced delivery, craniotomy-based drug delivery and drug delivery nanosystems are discussed. Nanocarriers are one of the highly potential drug transport systems that have gained huge research focus over the last few decades for site specific drug delivery, including drug delivery to the brain. Properly designed nanocolloids are capable to cross the blood-brain barrier and specifically deliver the drug in the brain tumor tissue. They can carry both hydrophilic and hydrophobic drugs, protect them from degradation, release the drug for sustained period, significantly improve the plasma circulation half-life and reduce toxic effects. Among various nanocarriers, liposomes, polymeric nanoparticles and lipid nanocapsules are the most widely studied, and are discussed in this review. For each type of nanocarrier, a general discussion describing their composition, characteristics, types and various uses is followed by their specific application to glioblastoma treatment. Moreover, some of the main challenges regarding toxicity and standardized evaluation techniques are narrated in brief.



Keywords:

Blood-brain barrier, Glioblastoma, Liposome, Polymeric nanoparticle, Lipid nanocapsule

1. Introduction

Glioblastoma multiforme (GBM), a type of glioma, is the most frequently occurring and invasive primary tumor of the central nervous system (CNS). Based on tumor prognosis and survival rates, GBM is defined by the World Health Organization (WHO) as grade IV, the most malignant glioma (Kanu et al., 2009). Although GBM accounts for 54.4% of all gliomas and glioma comprises only 1.35% of all cancer incidents, it causes about 4% of cancer-associated-deaths, making it one of the most fatal cancers (Louis et al., 2007; Ostrom et al., 2013; Sehati and Liao, 2003). Nowadays, the treatment includes surgical removal of the tumoral tissue, followed by post-surgical concomitant radiotherapy and chemotherapy. Despite the combination of these treatment regimens, using state-of-the-art facilities, the median survival is about 14 months and 2 year survival rate is merely 3-5% (Adamson et al., 2009). The GBM cells show chemoresistance due to overexpression of P-gp which causes enhanced drug efflux from tumor cells. Moreover, hypoxic zones can be present in the tumors, not easily reachable by the drug, due to lack of blood flow. The resistant GBM cells relapse inevitably, and rapidly infiltrate healthy brain tissues by their unique cellular heterogeneity, creating one of the toughest challenges in cancer patient management. Hence, novel therapeutic approaches are urgently necessary.

With the in-depth research performed, profound knowledge of the oncogenomics and molecular biology of GBM has been gained in the last few decades. Using these insights, numerous types of *de novo* chemotherapeutics to overcome the drug resistance are under investigation (Adamson et al., 2009). Even though many of these chemotherapeutics showed promising results *in vitro* against GBM, most were unsuccessful to reproduce such effects, when systemically administered *in vivo*. The major reason of the limited success is the incapability of the drugs to cross the blood-brain barrier (BBB) and to penetrate inside the tumor tissue (Ying et al., 2010). In the last few decades, nanocarriers have drawn progressively increasing attention as brain tumor targeted drug delivery systems, due to their capacity (when formulated with appropriate characteristics) to cross the BBB and specifically deliver the drug in the tumor tissue. Various nanocarriers have been investigated and reported as potential brain tumor targeted delivery systems (Bragagni et al., 2012; Chen et al., 2010; Garcion et al., 2006; Lim et al., 2011).

This review will discuss about the features of BBB and the strategies to improve drug delivery to brain tumors. It will focus on liposomes, polymeric nanoparticles (PNPs) and

lipid nanocapsules (LNCs) as potential GBM targeted nanocarriers. Moreover, it will confer the limitations as well as future prospects of such brain targeted nano-therapeutics.

2. The Blood-Brain Barrier and the Blood-Brain Tumor Barrier

2.1. The blood-brain barrier

The BBB is a highly selective active interface which lines the blood vessels in the brain and spinal cord, and regulates the movement of numerous molecules between the systemic circulation and the brain interstitial fluid to maintain homeostasis in the CNS. It is chiefly formed by cerebral endothelial cells (CECs) along with other perivascular cells i.e. astrocytes and pericytes (Fig. 1). A few other cells e.g. neurons, microglial cells and smooth muscle cells also contribute considerably to the function of BBB (Begley, 2004; Bernacki et al., 2008). Primarily, the CECs act as a barrier for most substances due to their distinct morphology and inhibit the transport of these compounds across the BBB. Moreover, it works as a selective carrier for particular molecules due to presence of specific transporters and receptors. Besides their contribution in the formation and maintenance of the BBB, astrocytes are primarily involved in structural formation of the brain, maintaining cerebral homeostasis, modulation of synaptic transmission and brain repair; whereas pericytes contribute in the regulation of capillary blood flow, homeostasis, endothelial proliferation and angiogenesis.

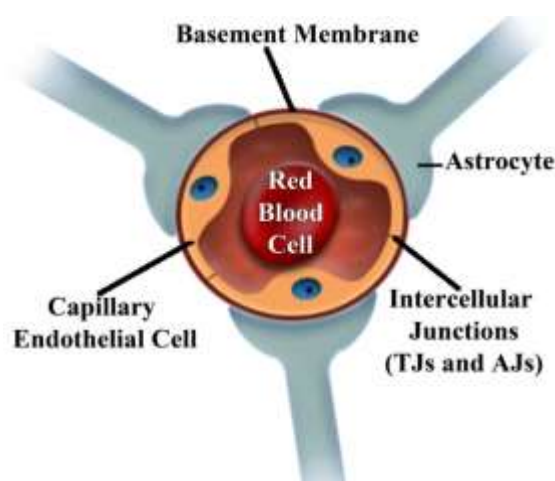


Fig. 1 - Structure of the blood-brain barrier.

The barrier function of the BBB is to block the passage of toxic and harmful molecules from systemic circulation to the brain. This is accomplished due to the presence of different defense mechanisms, i.e. transport barrier (paracellular and transcellular),

enzymatic barrier, immunologic barrier and efflux transport systems (Wilhelm et al., 2011).

The paracellular transport barrier is formed by the presence of tight junctions (TJs) and adherens junctions (AJs) between adjacent CECs, which interconnect these cells and practically replenish the paracellular fenestrations. The TJs are composed of transmembrane proteins (i.e. occludin and claudins) and are found in the apical region of the paracellular space (Matter and Balda, 2003), whereas the AJs are chiefly composed of cadherin and integrin and placed at the basolateral region (Hawkins and Davis, 2005). The TJs prevent paracellular transport of most molecules including macromolecules and hydrophilic compounds (Correale and Villa, 2009). Therefore, these molecules are required to take a transcellular pathway across the BBB, which is distinctive from other endothelia (Hawkins and Davis, 2005; Wolburg and Lippoldt, 2002). The primary transcellular barrier function is carried out by claudins, which substantially restrict even the passage of small ions e.g. sodium and chloride ions, and contribute to the high transendothelial electrical resistance (TEER) (Butt et al., 1990; Wolburg and Lippoldt, 2002), whereas occludin aids possibly by TJ regulation (Yu et al., 2005). Moreover, cadherins of AJs help to maintain structural integrity of CECs, reinforce interactions among them and assist to the formation of TJs by linking with catenin, a membrane bound protein. Thus, AJ disruption may cause compromised paracellular barrier activity (O'Kane and Hawkins, 2003). The presence of TJs and AJs impede the entrance of approximately all macromolecular drugs and over 98% of small-molecule drugs into the cerebral tissue (Pardridge, 2001).

The transcellular transport obstruction is formed due to the small number of pinocytic vesicles in the CECs. As a result, endocytosis and transcytosis in these cells are significantly lower compared to other endothelial cells, which restrict the passage of numerous molecules through their cytoplasm. Additionally, the metabolic obstacle is created by the presence of various types of intra- and extracellular enzymes in the CECs, such as esterase, phosphatase, peptidase, nucleotidase, monoamine oxidase and cytochrome P450, which can degrade or deactivate various drugs and neurotoxins (El-Bacha and Minn, 1999). Furthermore, an immunologic defense is developed due to the presence of microglia, perivascular macrophages and mast cells in the BBB (Aguzzi et al., 2013; Daneman and Rescigno, 2009).

In the perspective of drug permeability, one of the key barriers is the presence of efflux transporters in the BBB, which can actively pump-out a wide range of drugs including various anti-cancer agents, through the cell membrane. Therefore, drug concentration in the targeted pathologic cerebral site may not be sufficient to obtain a pharmacological effect (Borges-Walmsley et al., 2003). The CECs express a large family of membrane bound efflux transport proteins called the ATP-binding cassette (ABC) transporters. The significantly important ABC transporters include P-gp, multiple drug resistance protein 4 (MRP4) and breast cancer cell resistance protein (BCRP). Many antitumor drugs are substrates for these ABC transporter proteins. For example, vincristine, doxorubicin (DOX) and etoposide are substrates for P-gp (Sharom, 2011); 6-mercaptopurine and methotrexate are substrates for MRP4 (Chen et al., 2002); prazosin and nitrofurantoin are substrates for BCRP (Litman et al., 2000; Sharom, 2011).

Besides acting as a barrier for most molecules, the other major task of the BBB is to transport nutrients and other essential molecules to the brain tissues. However, due to the unique morphology of BBB, energy-independent transport of aqueous soluble molecules is exceedingly limited. Only small lipophilic molecules and gaseous molecules can cross the BBB by energy-independent transport mechanisms. In addition, molecules that are substrates of specific transporters or receptors can also cross the BBB adequately (Reiber, 2001).

The CECs express a vast number of membrane transport proteins or solute carriers (SLC transporters). For example, there are several glucose transporters (GLUT 1, 3, 4, 5, 6 and 8) for passage of sugar molecules (Maher et al., 1994), several amino acid transporters (large neutral amino acid transporter or LA-transporter and neutral amino acid transporter or NAA-transporter etc.) which transport amino acids (Wolburg et al., 2009), monocarboxylate transporters (MCTs) which carry several organic acids, organic cationic transporters (OCTs), and nucleoside transporters (Alyautdin et al., 2014). Additionally, numerous receptors are also expressed on the CECs, e.g. transferrin receptor (TfR) (Chen et al., 2010; Ulbrich et al., 2009), insulin receptor (IR) (Pardridge et al., 1985), epidermal growth factor receptor (EGFR) (Halatsch et al., 2006) and low density lipoprotein receptors (LDLR) (Wagner et al., 2012). These receptors facilitate the delivery of selective macromolecules to the brain.

Overall, due to the obstruction of paracellular transport by TJs, presence of efflux pumps and small number of pinocytic vesicles, only highly lipophilic molecules with less than 8 hydrogen bonds and molecular weight below 400 Da can cross the BBB (Pardridge, 2012). Unfortunately, around 98% of the medicinal drugs do not fall into this category.

2.2. The blood-brain tumor barrier

The BBB that is situated between the cerebral tumor tissues and capillary vessels are often termed as blood-brain tumor barrier (BBTB) (Fig. 2). The morphology and permeability of the BBTB can be divided into three types, which chiefly depends on and changes with the progress of the adjacent cerebral tumor (Groothuis, 2000). In the first phase, at very initial phase of malignant brain tumors, the regular brain capillaries are capable to provide enough nutrients for their growth, and therefore the capillaries are continuous and non-fenestrated, and the BBTB integrity is not compromised (Schlageter et al., 1999). However, in the second phase of tumor growth, once the cancer cells invade neighboring healthy cerebral tissues and the tumor volume becomes larger than 2 mm³, tumor neovasculature is formed by angiogenesis. These newly formed capillaries are continuous with fenestrations around 12 nm size. Therefore, the permeability of the BBTB is altered and spherical molecules with size below 12 nm may pass through such areas (Schlageter et al., 1999; Squire et al., 2001). In the final phase (third phase), with further tumor growth, the BBTB integrity is compromised as the inter-endothelial gaps are formed between CECs. *In vitro* studies with rat GBM tumor RG-2 showed mean fenestration size and inter-endothelial gaps of 48 nm and 1 µm respectively. Although the microvessel basement membrane was present between the gaps, it was frequently thinner than regular CECs and junctional proteins were not observed (Schlageter et al., 1999). In such conditions, the BBTB is vulnerable for nanocarriers and enhanced permeability and retention (EPR) effect allows their accumulation preferentially in the tumor tissues (Brigger et al., 2002).

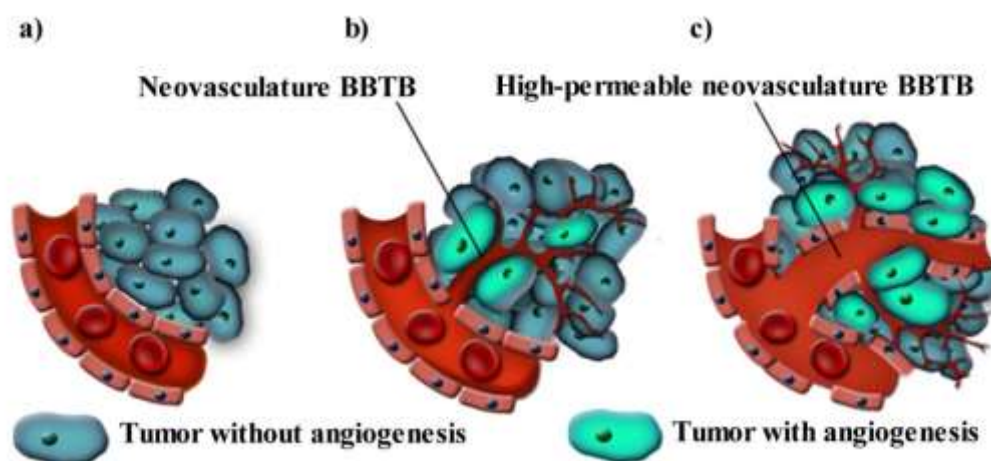


Fig. 2 - Stages of the blood-brain tumor barrier formation: first stage **a)**, second stage **b)** and third stage **c)**.

The leaky BBTB is more common in high-grade gliomas (e.g. GBM) due to their amplified metabolic requirements. In fact, angiogenesis is triggered by hypoxia in certain areas of the high-grade gliomas, which eventually compromises the integrity of the BBB (Plate et al., 2012). However, high-grade gliomas are very aggressive and quickly spread in the surrounding healthy brain tissues, where the BBTB is less damaged and EPR effect is not in action. Therefore, the BBTB still remains as the major hurdle for delivering drugs at therapeutically effective levels to GBM tumors (Juillerat-Jeanneret, 2008; van Tellingen et al., 2015).

3. Drug Delivery Strategies for GBM

3.1. Tight junction opening

In the last few decades, several methods have been investigated to open the TJs of the CECs in a regulated, reversible and transient manner. One of the first reported methods is to intra-arterially infuse hyperosmotic agents e.g. mannitol (Rapoport, 1970). Such infusion provisionally shrinks the CECs and opens the TJs up to a few hours (Siegal et al., 2000), which eventually enhances the passage of drugs across the BBB/BBTB. TJ opening was also reported by using bioactive molecules like bradykinin and its analog RMP-7. Bradykinin acts on B2 receptors of the CECs, increases Ca^{2+} ions concentration within the cells which finally modifies the TJ to increase permeability of the drug (Prados et al., 2003; Regoli and Barabe, 1980). Moreover, surfactants such as sodium dodecyl sulfate (Saija et al., 1997) and polysorbate 80 (PS80) (Sakane et al., 1989) has been reported to

successfully open the TJs. Additionally, the use of ultrasound (Sheikov et al., 2004) and electromagnetic waves (Stam, 2010) has been reported to temporarily and reversibly disrupt the BBB.

Although opening of the TJs by alteration of the BBB is a promising method to increase drug delivery to GBM and other brain disorders, there are many associated drawbacks such as complex technical nature, low specificity, possibility of tumor spreading to the periphery, exposure of cerebral tissues to neurotoxins present in blood, and low efficiency that make this technique poorly exploited.

3.2. Chemical modification of the drug

Chemical modification of the drug to produce a more lipophilic prodrug can be used to increase systemic drug delivery across the BBB (Gabathuler, 2010). This is possible by modifying the hydrophilic groups to lipophilic groups; e.g. esterification of hydroxyl- or carboxylic acid- groups, introduction of methyl- or chlorine- groups. The chemotherapeutic drug chlorambucil was modified by such methods which enhanced its brain delivery (Greig et al., 1990). However, the molecular weight of the lipophilic prodrug should be below 500 Da and it should possess less than 8 hydrogen bonds in order to cross the BBB (Pardridge, 2012). Moreover, increased lipidic nature may also enhance the nonspecific uptake of the pharmaceutical molecule by other tissues, and therefore possibly increase its toxic effects (Scherrmann, 2002).

3.3. Efflux transporter inhibition

As many chemotherapeutic agents are substrates of the efflux transporters present at the BBB, inhibition of such transporters can significantly increase crossing of these drugs into the brain (Lin et al., 2013). This strategy may effectively enhance the brain concentration of drugs without disrupting the integrity of the BBB. For example, cyclosporine A, PSC833 and GF120918 inhibited the activity of P-gp and improved BBB crossing of paclitaxel in mice (Kemper et al., 2003). Pluronic[®] P85 has been reported to improve brain concentrations of paclitaxel and docetaxel (Kabanov et al., 2003). Elacridar and tariquidar, inhibitors of ABC sub-family member 1 (ABCB1) and BCRP, were also investigated (Kuntner et al., 2010). However, ABC transporters at the CECs are more challenging to inhibit compared to ABC transporters at other commonly utilized surrogate markers (Choo et al., 2006). In addition, many of these markers were not successful in clinical trials as

they could not fully inhibit the efflux pumps due to various factors (van Tellingen et al., 2015). Furthermore, inhibition of these efflux pumps will increase the BBB permeability of possible neurotoxic compounds, which can be risky. Further investigations are necessary to fully understand the level of inhibition necessary, the safety profile of the method and to choose the optimum drug-inhibitor combination for using this technique for GBM therapy.

3.4. Convection enhanced delivery

In convection enhanced delivery (CED) technique, a catheter, connected to a syringe pump, is placed in the tumor tissue and the drugs are administered continuously under positive pressure through it. This brain drug delivery technique allows the local distribution of a significant amount of highly concentrated therapeutic molecules with very low systemic secondary effects (Allard et al., 2009b). The convection mechanism consents to obtain a higher drug concentration in the target tissue compared to classical parenteral formulations, with a constant concentration profile during the infusion step (Bobo et al., 1994). To be effective, some important parameters like the target portion of the brain (Laske et al., 1997); catheter placement, design and size (Allard et al., 2009b); rate of infusion (Krauze et al., 2005); brain extracellular matrix dilatation (Neeves et al., 2007); increase of the heart rate (Hadaczek et al., 2006); volume and composition of the injected pharmaceutical formulation have to be taken into account. Despite the advantages of this technique, it is not widely used due to the risk of backflow which may result in the release of drug in brain healthy tissue and consequent reduction of the therapy efficacy (Allard et al., 2009b).

3.5. Craniotomy-based drug delivery

Craniotomy-based drug delivery allows the pharmaceutical molecule to be delivered directly in the brain via intracerebral implantation or intracerebroventricular injection. Although this technique allows the delivery of the pharmaceutical formulation directly in the target tumor brain tissue, it is limited by the diffusion capacity of the drug. Moreover, small drugs can diffuse far away from the injection site (Pardridge, 2002).

3.6. Nanocarrier drug delivery systems

Nanocarriers are one of the highly potential drug transport systems that have gained huge research focus over the last few decades for site specific drug delivery, including for drug delivery to the brain. The enrichment of knowledge about the BBB, especially the transport systems present on it, combined with the advancement in polymer science and nanotechnology has facilitated nanocarrier research remarkably. Their composition, size and other surface characteristics can be easily modified to achieve drug delivery to a specific region of the body. They can carry both hydrophilic and hydrophobic drugs, protect them from degradations, release the drug for sustained period, significantly improve the plasma circulation half-life and reduce toxic effects. An ideal systemic nanocarrier for brain drug delivery to the brain should possess the following properties (Bhaskar et al., 2010; Koo et al., 2006)

- they must be nontoxic, biodegradable and biocompatible;
- they should avoid opsonization and consequent clearance by the reticuloendothelial system (RES) and have a long plasma circulation time;
- their size should be below 200 nm;
- they should not produce immune response;
- they should protect the drug from any means of degradation;
- they should have targeting strategies to be selectively delivered to the brain; and
- they should have controllable release profile.

However, the major properties that govern the *in vivo* characteristics of the brain targeted nanocarriers are their size and surface charge, and the presence of hydrophilic polymers and targeting ligands on the surface. The relationship between the size and the clearance of the systemic nanocarriers has been confirmed by early studies. The nanovectors are cleared chiefly by the RES, a part of the immune system consisting phagocytic cells (monocytes and macrophages) which can engulf and eradicate the nanocarrier from the systemic circulation, and consequently destroy them. The percentage of nanocarrier to be cleared is dependent on particle size (Harashima et al., 1994). Uptake of nanocolloids by

RES increases as size of the particles increases (Senior et al., 1985). In addition, RES uptake follows saturation kinetics and the system can be saturated with high doses of nanocarriers (Oja et al., 1996). However, saturation of the body's defense mechanism can be unsafe. Generally, nanocarriers below 100 nm size are cleared slower and to a lesser extent than larger nanocolloids (Lian and Ho, 2001). Smaller nanovectors can also penetrate through the leaky BBTB and preferentially accumulate in the GBM tumors by EPR effect. The extravasation occurs without the need of energy, and propelled by intravascular and interstitial pressure difference (Yuan et al., 1994).

The type and intensity of the surface charge of the nanocarriers are critical and can influence their pharmacokinetics, bio-distribution and interactions with cells. Both parameters are chiefly controlled by composition of the delivery system. Neutral nanocarriers have low possibility to be captured by RES, but high probability to form aggregates. Moreover, they have little interaction with cells and may release the drug extracellularly (Sharma et al., 1993). On the other hand, nanocarriers with positive or negative surface charge have higher interaction with cells and the charge density influences the extent of interaction. They are more prone to phagocytic uptake by RES which may accelerate their plasma clearance (Gabizon et al., 1990). However, they are less prone to aggregation and have higher shelf-life as dispersed systems. Macrophage uptake of the nanovectors increases when their surface charge moves to higher negative or positive values. In case of non-phagocytic cells, the uptake increases as the surface charge moves from negative to positive values (He et al., 2010). Nevertheless, for brain targeted drug delivery, cationic nanocarriers are more attractive as they may cross the BBB by adsorptive-mediated transcytosis (AMT) (Abbott et al., 2006; Lu et al., 2005).

Plasma circulation half-life of the nanocarriers can be also improved by a technique which is often termed as surface hydration or steric modification. The addition of small amounts (5-10 mol.%) of certain hydrophilic group containing compounds e.g. monosialoganglioside (GM1), hydrogenated phosphatidylinositol (HPI) or polyethylene glycol (PEG) on the nanocarrier surface create an extra hydration layer which causes steric hindrance to plasma opsonins and reduces uptake by RES (Allen et al., 1991; Torchilin, 1994). Hence, these nanovectors are more stable *in vivo* and may have up to 10 times more circulation half-life compared to nanocarriers without hydrophilic surface coating (Klibanov et al., 1991; Lasic et al., 1991). PEG is one of the most frequently used

polymers for surface hydration of nanocarriers. PEG-lipid complexes can be used up to 5-10 mol.% of overall lipid and can produce about 5 nm of hydration layer at the surface (Lian and Ho, 2001; Woodle et al., 1992). However, to reduce opsonization in plasma, and to penetrate the leaky BBTB, even PEG grafted nanocarriers have to maintain their highest size within 150-200 nm (Lian and Ho, 2001).

Another crucial criteria for GBM targeted nanocarrier drug delivery is availing endogenous transport mechanisms across the BBB for improving the passage of the nanocarrier. This is often termed as active targeting strategy which chiefly involves utilization of two types of transports, AMT and receptor mediated transcytosis (RMT). The AMT has achieved substantial focus as increasing number of studies report this strategy to enhance the transport of nanocarriers across the BBB, using cationic proteins or cell-penetrating peptides (CPPs) (Herve et al., 2008). Brain delivery of cationic protein-conjugated nanocarrier, such as cationic bovine serum albumin (cBSA) conjugated nanoparticles (NPs) was reported to increase by 2.3 fold compared to unconjugated NPs (Lu et al., 2007). CPPs, e.g. HIV-1 trans-activating transcriptor (TAT) conjugated NPs and liposomes were capable to cross the BBB and enhance brain drug concentration (Qin et al., 2011; Wang et al., 2010). However, as AMT is a non-specific process, conjugation of such cationic proteins will also increase the adsorptive uptake process of nanocarriers in other parts of the body, which may possibly create toxic and immunogenic concerns. Transport of nanocarriers to the brain using RMT process is more specific than AMT. The RMT involves addition of endogenous molecules on the nanocarrier surface, which are substrates for specific receptors expressed on the BBB. Addition of proteins (e.g. transferrin, lactoferrin, ApoE); peptides (e.g. glutathione) or anti-transferrin receptor antibody OX26 on the surface of liposomes, PNPs and LNCs increased significantly the BBB penetrations of such nanocarriers (Beduneau et al., 2008; Chen and Liu, 2012).

Overall, size of the nanocarrier along with surface charge, surface hydration and targeting strategy are important characteristics for development of a successful brain targeted nanocolloid drug delivery system for GBM treatment. Among various nanocarriers, liposomes, PNPs and LNCs are the most widely studied, and will be discussed in details in the following sections.

4. Liposomes for GBM Treatment

4.1. Introduction to liposomes

Liposomes are vesicles made of minimum one phospholipid bilayer and an aqueous core, with vesicle size typically between 50 nm to 5 μ m. They are self-assembled when dry phospholipid films are hydrated. Liposome was first reported by Alec Bangham, a British hematologist, who noticed its formation while staining dry phospholipids for evaluating an electron microscope (Bangham and Horne, 1964). The structural similarity between liposomes and certain cellular organelles were noticed very quickly. Liposomes were able to uphold concentration gradient of certain ions (Bangham et al., 1965a), but failed to maintain their structure and the ion gradient in presence of detergents (Bangham et al., 1965b). Due to structural resemblance, they were utilized to study biomembrane specific processes since their discovery. Additionally, their potential as biodegradable-biocompatible drug carriers was acknowledged in the 1970s, and numerous studies were conducted with aims to improve efficacy and reduce toxicity of several drugs. In the next few decades, comprehensive knowledge about liposome morphology, biodistribution, interactions at the nano-biointerface etc. was realized (Lian and Ho, 2001).

Liposomes are made of generally biocompatible-biodegradable ingredients. They are able to entrap water-soluble drug molecules within their aqueous core, and lipophilic drug molecules in the lipid bilayer(s). They can also carry bioactive molecules such as enzymes or nucleic acids effectively. They can protect their cargo from unwanted inactivating effects of the body and improve their pharmacological effect. Their preparation is relatively simple and large scale production is possible. Generally, liposomes improve the toxic profile of the drug and increase tissue-specificity. They can transport drug molecules into cells, even within specific cellular components (Goren et al., 2000; Pakunlu et al., 2006).

4.2. Types and applications of liposomes

On the basis of size and number of bilayers, liposomes can be classified into three groups (Fig. 3): small unilamellar vesicles (SUV) large unilamellar vesicles (LUV) and multilamellar vesicles (MLV) (Sharma and Sharma, 1997; Yang et al., 2011).

- The SUVs have a single bilayer, usually up to 100 nm in size and have low aqueous-lipid ratio (0.2-1.5 L/mol lipid)
- The LUVs have a single bilayer membrane, can be from 100 nm to more than 1000 nm in size, have high aqueous-lipid ratio (about 7.0 L/mol lipid) and are suitable for entrapping hydrophilic drugs
- The MLVs have multiple lipid bilayer membrane, more than 100 nm in size, have poor aqueous-lipid ratio (1.0-4.0 L/mol lipid) and are appropriate for entrapping lipophilic or hydrophobic drugs

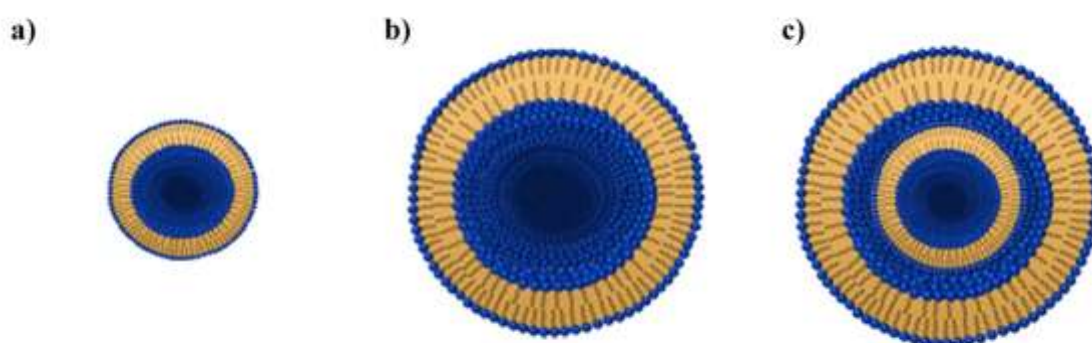


Fig. 3 - Classification of liposomes on the basis of size and number of bilayers: small unilamellar vesicles **a)**, large unilamellar vesicles **b)** and multilamellar vesicles **c)**.

Composition and surface properties of liposomes can be easily engineered to utilize them for vast range of purposes. Liposome entrapped imaging agents have been used for diagnostic bioimaging of vital body organs (e.g. brain, liver and heart), conditions like infections and inflammations, and also for tumors (Torchilin, 1996, 1997). Positively charged liposomes are often used to prepare non-viral gene delivery system called lipoplexes, which are its complex with anionic DNA molecules. Lipoplexes can have high DNA loading and good transfection efficiency (Matsuura et al., 2003). Liposomes are also reported to specifically deliver antisense oligonucleotide to neuroblastoma cells (Brignole et al., 2003; Fattal et al., 2004). Many other types of liposomes e.g. pH-sensitive

liposomes (Asokan and Cho, 2003; Sudimack et al., 2002), ligand or peptide grafted liposomes (Frankel and Pabo, 1988), virosomes (Kaneda, 2000), magnetic liposomes (Nobuto et al., 2004), gold or silver particle-containing liposomes (Park et al., 2006) are under research.

The earliest liposomal product, DaunoXome[®], produced by Nexstar Pharmaceuticals in 1995, contained daunorubicin (DN) and is used against Kaposi's sarcoma (Immordino et al., 2006). At present, about twelve liposome drug delivery systems, such as Ambisome[®], Doxil[®], Depocyt[®], Visudyne[®], are in clinical use and many more are in clinical trials (Chang and Yeh, 2012). The majority of these are for anti-fungal or anti-cancer therapies.

4.3. Liposomes for GBM treatment

Liposomes have been extensively studied as drug delivery systems for CNS disorders in the earlier few decades. Many of these researches were focused on the development of liposomes for brain cancer therapy due to their several advantages. Firstly, they can cross the BBB through the inter-endothelial gaps of the highly vascularized leaky BBTB in case of high grade brain tumors. Moreover, surface-modified brain targeted liposomes may also transport across the intact BBB by means of RMT or AMT (Liu and Lu, 2012). Therefore, they can be used for the treatment of different grades of brain tumors. Secondly, after crossing the BBB/BBTB, the targeted liposomes are known to preferentially accumulate in brain tumor tissues rather than healthy brain tissues (Koukourakis et al., 2000). Thus, the non-specific side effects of the anti-tumor agent on healthy brain cells are reduced and safety profiles of the drugs are improved. Thirdly, they can carry various types of drugs and biomolecules efficiently which enables their use for various types of anti-cancer agents, from simple hydrophilic or hydrophobic chemical entities to macro-molecules like DNAs or RNAs.

To efficiently cross the BBB/BBTB, systemically administered liposomes should maintain certain physicochemical characteristics. Their size should be small (below 200 nm), they should have sufficient plasma circulation time and their surface must be attached to ligands which are recognized and internalized by the CECs (Alyautdin et al., 2014). Plasma circulation time can be increased by two methods, by reducing their size and/or by adding hydrophilic polymer coating for surface hydration or steric hindrance (Lian and Ho, 2001; Torchilin, 2005). The most commonly used excipients are phospholipid-

conjugated PEGs. PEGylation may reduce the clearance of the nanocarrier up to 200 times (Allen, 1994). Additionally, active targeting using specific ligands is essential to achieve sufficient brain drug concentration. Several molecules have been reported to improve BBB passage of liposomes. Transferrin conjugated liposome increased brain delivery of 5-fluorouracil by 17 and 13 times compared to the free drug and non-conjugated liposomes respectively (Soni et al., 2005). The brain uptake of coumarin-6 encapsulated in liposomes attached to lactoferrin also improved by 2.11-fold compared to the non-conjugated liposome (Chen et al., 2010). Addition of anti-TfR antibody OX26 to liposomes significantly increased brain delivery of the drug compared to free drug and the non-targeted liposomes (Huwlyer et al., 1996). Surface conjugation with peptides such as ApoE and TAT also significantly improved drug passage across the BBB (Qin et al., 2011; Re et al., 2011).

Many studies have reported much improved BBB penetration and tumor accumulation of the medical agents using liposome drug delivery systems for glioma treatment (Table 1). One of the most frequently studied drug for GBM treatment using liposomes is DOX. In a clinical study, Koukourakis et al. treated several GBM patients undergoing radiotherapy with stealth® liposomal DOX (Caelyx®) (Koukourakis et al., 2000). Caelyx® is a PEGylated liposome formulation of DOX hydrochloride. The intra-tumoral tissue concentration of DOX was 13-19 folds higher than normal brain tissue possibly due to EPR effect in the highly vascularized GBM tumor tissue.

In another *in vivo* study of DOX on subcutaneous mouse glioma model, interleukin-13 (IL13) grafted liposomal formulation of the drug significantly improved the cytotoxicity and tumor accumulation compared to the free DOX. Intraperitoneal injection of the targeted liposome significantly decreased the tumor size compared to the untargeted liposomes (Madhankumar et al., 2006).

Liposomal formulation of oxaliplatin (Lipoxal®), a platinum analog which acts as radiosensitizer and improves the efficacy of radiotherapy, was tested on F98 glioma model (cells implanted in the right hemisphere) on Fischer rats (Charest et al., 2012). Concentration of oxaliplatin in the tumor was 2.4 times higher for Lipoxal® after 24 h compared to the free oxaliplatin. Moreover, median survival time of the rats was improved to 29.6 ± 1.3 days compared to 21.0 ± 2.6 days. Additionally, the ratio of tumor to adjacent healthy right hemisphere tissue concentration for Lipoxal® was significantly

higher compared to the free drug. The liposomal formulation markedly reduced the toxic effects observed with free oxaliplatin.

Ying *et al.* developed egg phosphatidylcholine (EPC) liposomes containing DN. The liposome surface was then attached with p-aminophenyl- α -D-mannopyranoside (MAN) and transferrin to target both the BBB and C6 glioma tumor. After 24 h, *in vitro* BBB passage of DN-MAN-Transferrin liposomes were 8.0-fold, 2.9-fold, 2.8-fold and 1.4-fold higher compared to free DN, DN liposomes, DN-Transferrin liposomes and DN-MAN liposomes respectively. Additionally, cellular uptake of DN-MAN-Transferrin liposomes increased by 3.3-fold compared to DN liposomes. Moreover, inhibition of C6 glioma cells after crossing the BBB for DN-MAN-Transferrin liposomes were 1.1-fold, 1.4-fold, 1.4-fold and 1.6-fold higher than DN-MAN liposomes, DN liposomes, free DN and DN-Transferrin liposomes respectively. Therefore, targeting of the BBB using MAN and the C6 glioma tumor using Transferrin significantly improved BBB passage, cellular uptake and tumor inhibition property of DN (Ying *et al.*, 2010).

Liposomes were also used for human EGFR antisense gene therapy for GBM (Zhang *et al.*, 2002). The gene was in a nonviral plasmid, which was encapsulated in PEGylated 1-palmitoyl-2-oleoyl-sn-glycerol-3-phosphocholine (POPC) liposomes conjugated to 83-14 murine monoclonal antibodies (mAb) to the human insulin receptor (HIR). The liposome formulation was tested against U87 glioma cell line and about 70-80% cell growth was inhibited.

Although numerous preclinical studies have shown that active-targeting by grafting certain endogenous ligands or mAb on liposome surface improved GBM targeted drug delivery compared to the passively-targeted nanocarrier, translation of this technique to clinical studies can be difficult due to various reasons. Most of the receptors targeted for RMT across BBB are not present only on the CECs, which make active-targeting quite challenging. For example, TfR is expressed in hepatocytes, red blood cells, monocytes and intestinal cells along with CECs (Ponka and Lok, 1999). Additionally, nanocarriers grafted with ligands like transferrin have to compete with endogenously present transferrin for receptor binding which may reduce their efficacy. Although monoclonal antibody i.e. OX26 or 83-14 murine mAb grafted liposomes showed promising results as brain-targeted delivery systems in preclinical studies, none of the two animal derived antibodies can be used directly in human trials. Even if the OX-26 binds the murine TfR, it is not capable to

interact with the human TfR (Pardridge, 1999). Moreover both OX26 and 83-14 murine mAb will cause immunogenic reactions if administered in humans. Furthermore, the TfR and the IR on the BBB are involved in iron and glucose homeostasis of the brain and such mAb grafted nanocarriers may downregulate the activity of these receptors and raise safety concerns (de Boer and Gaillard, 2007). Indeed, most liposomes that reached clinical trials for GBM are passively-targeted, avoiding the ligand-receptor interaction. However, active-targeting is promising for making GBM-targeted delivery more efficient and genetically engineered chimeric antibodies for human receptors, usable for drug targeting through the BBB, have been produced (Coloma et al., 2000).

Therefore, liposomes have been studied extensively for brain targeted drug delivery and also more specifically for GBM treatment. Their simple and large scale manufacturing possibility, easily tunable composition, and ability to cross the BBB and preferential accumulation within the tumor tissue makes them very potential drug delivery systems for the treatment of GBM.

Table 1: Liposomes for the treatment of GBM.

Treatment	Targeting approach	Drug nanocarrier	in Status	References
IL13-grafted liposome	Active	DOX	Preclinical- <i>in vivo</i>	(Madhankumar et al., 2006)
Liposome	Passive	Oxaliplatin	Preclinical- <i>in vivo</i>	(Charest et al., 2012)
MAN and transferrin-grafted liposome	Active	DN	Preclinical- <i>in vivo</i>	(Ying et al., 2010)
83-14 murine mAb-grafted liposome	Active	Human EGFR antisense gene	Preclinical- <i>in vitro</i>	(Zhang et al., 2002)
Liposome	Passive	DN	Phase I clinical trial	(Zucchetti et al., 1999)
PEGylated liposome	Passive	DOX	Phase I/II clinical trial	(Fabel et al., 2001; Hau et al., 2004; Koukourakis et al., 2000)
PEGylated liposome + TMZ	Passive	DOX	Phase II clinical trial	(Ananda et al., 2011; Chua et al., 2004)
PEGylated liposome + radiotherapy + TMZ	Passive	DOX	Phase I/II clinical trial	(Beier et al., 2009)

5. PNPs for GBM Treatment

5.1. Introduction to PNPs

PNPs are solid colloidal drug delivery systems which are generally made from biocompatible hydrophobic polymers or copolymers of natural or synthetic origin with a size range of 1-1000 nm in diameter. The therapeutic molecule can be loaded in the PNPs in several ways. They can be entrapped within the NP matrix in solid form, or in solution if the PNP core is liquid, or linked with the polymer covalently, or adsorbed on the particle surface (Couvreur, 1987; Couvreur et al., 1995). They can entrap both hydrophilic and lipophilic small pharmaceutical molecules as well as macromolecular drugs.

The PNPs have several advantages compared to the drug molecules alone. They can protect the entrapped drug molecule from degradation and may increase the drug concentration at the site of action. Their encapsulation efficiency can be high, and therefore a high number of pharmaceutical molecules can be delivered inside the cells for each PNP (Kreuter, 2007; Tosi et al., 2008). PNPs can improve the plasma circulation half-life of the drug molecules, increase their bioavailability and aid the pharmaceutical molecules to reside in target tissues longer (Ganesh et al., 2013; Schwartz et al., 2014). Moreover, PNPs can be designed to pass through biological barriers such as the BBB and BBTB (Gulyaev et al., 1999), and preferentially deliver the pharmaceutical molecule in the desired tissue by targeting (Shenoy et al., 2005). PNPs can be more stable within the biological system and also during storage, and can have more controlled drug release kinetics, when compared to liposomes, when appropriate polymer is chosen (Andrieux et al., 2009). They can withstand sterilization by radiation and also freeze-drying process which are suitable characteristics for industrial scale manufacturing (Wohlfart et al., 2012).

However, biocompatible-biodegradable-nontoxic nature of the polymers is vital for developing systemically administrable PNPs for brain targeted delivery. The degradation products of the polymers must be also nontoxic and should be easily cleared from the body. However, only a small number of polymers have suitable safety profiles to develop such systems. The most frequently studied polymers for developing brain targeted nanocarriers includes poly(alkyl cyanoacrylate) (PACA), poly(lactide-co-glycolide) (PLGA), polylactide (PLA), polyethyleneimine (PEI), human serum albumin (HSA) and

chitosan (Fazil et al., 2012; Olivier, 2005; Tosi et al., 2008). At present, even if not all of these polymers are approved by the Food and Drug Administration (FDA) for intravenous (i.v.) administration, they have been found to be nontoxic in many studies (Kim et al., 2011; Lukowski et al., 1992; Tosi et al., 2008; Zheng et al., 2007).

Due to their promising features, PNPs have gained lots of research focus and have been studied extensively as brain-targeted nanocarriers in the last few decades.

5.2. Types and applications of PNPs

Depending on the type of the final formulation, the PNPs can be categorized chiefly into two categories, nanospheres and nanocapsules (Fig. 4). Nanospheres are made of a matrix of the polymer, where the pharmaceutical molecule is dissolved or dispersed in the matrix or adsorbed on the particle surface. Nanocapsules are like vesicles where the drug is dissolved in a liquid core walled by a polymer membrane (Griffiths et al., 2010). However, often it is difficult to differentiate among the two types of NPs, therefore the generalized name ‘nanoparticle’ is commonly used (Denora et al., 2009).

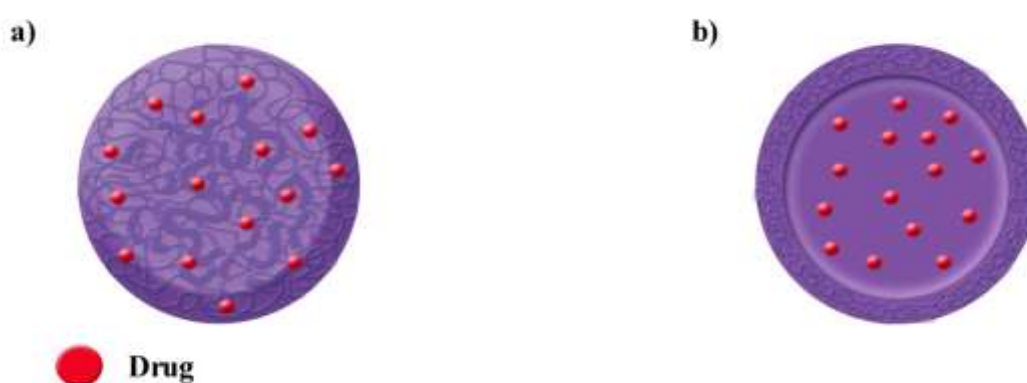


Fig. 4 - Types of polymeric nanoparticles: nanospheres **a)** and nanocapsules **b)**.

The chemical structure of the polymers used for preparing the NPs is easily modifiable, and therefore PNPs can be designed for a wide range of medical applications. Conjugated polymers, designed to have photo- and electroluminescence, have been utilized to prepare fluorescent NPs which are then used for fluorescence bio-imaging (Li and Liu, 2012). Wu and colleagues reported that PNPs encapsulating a fluorescent probe, with chlorotoxin and PEG attached on the PNP surface, were able to cross the BBB and accumulate in the brain tumor regions within 24 h, after tail vein

injection, in a transgenic mouse model (Wu et al., 2011). PNPs are also promising as non-viral gene delivery systems (Liu et al., 2007). They have been studied to carry protein drugs across mucosal tissues (nasal and intestinal) (Jung et al., 2000; Vila et al., 2002). Hydrophobically modified glycol chitosan NPs encapsulating the protein GRGDS, labeled with fluorescent dye FAM, have been reported to be promising to monitor and destroy angiogenic blood vessels near tumor tissue (Park et al., 2004). PNPs are also promising for delivery of multiple drugs (as combinations). Combination of MDR-1 gene silencing siRNA and paclitaxel in NPs has increased the accumulation of the chemotherapeutic agent in resistant ovarian adenocarcinoma cells (Yadav et al., 2009).

As brain-targeted drug delivery systems, PNPs are very promising. Various strategies have been used to improve the BBB permeability of the PNPs. For example, PEGylated poly(cyanoacrylate-co-hexadecylcyanoacrylate) (PHDCA) NPs were able to cross the BBB more than PS80 or poloxamine 908 (P908) coated NPs, due to their extended plasma circulation time (Calvo et al., 2001). In another study, concentration of PEGylated PHDCA NPs in 9L gliosarcoma in Fisher rats was found to be 3.1 times higher compared to the non-PEGylated NPs (Brigger et al., 2002). Moreover, modification of the NPs to make them positively charged can be a useful technique to enhance their brain delivery by AMT. For example, brain permeability of PEG-PLA NP was improved by the addition of cBSA as brain targeting moiety, and their brain concentration was more compared to PEG-PLA NP added with neutral BSA (Lu et al., 2005). Additionally, surfactants such as PS80 or poloxamer 188 (P188) can act as brain targeting agents, and can be used as a coating on the NP surface or can be attached with the polymer. Addition of PS80 on PACA NPs improved the brain delivery of several drugs, e.g. dalargin, loperamide and DOX (Alyautdin et al., 1997; Kreuter et al., 1997). Similar effects were reported for DOX entrapped in P188 coated PACA NPs (Ambruosi et al., 2006a). Although having dissimilar chemistry, both of the surfactants are very similar in terms of plasma protein adsorption on their NP surface. Both of them adsorb high quantities of apolipoprotein A-I (Apo A-I) which interacts with scavenger receptor B class I (SR-BI) on the CECs, and help the NPs to cross the BBB (Petri et al., 2007). Furthermore, brain targeted PNPs can be developed by addition of certain ligands (e.g. transferrin, OX 26 mAb, glutathione etc.) on the nanocarrier surface.

Therefore, PNPs are very promising to carry drugs across the BBB and treat disorders in the CNS such as Alzheimer's, Parkinson's disease, brain tumors etc.

5.3. PNPs for GBM treatment

As mentioned above, PNPs can be designed to have favorable characteristics for brain targeted delivery of many drugs. There are numerous studies focusing on the treatment of disorders of the CNS, including malignant brain tumors. If properly designed, PNPs can cross the leaky BBTB in highly malignant brain tumors by EPR effect, and can also cross the undamaged BBB by active targeting using RMT or AMT process. It is also possible to design PNPs to target both the BBB and the brain tumor cells by either attaching two targeting moieties, or by conjugating a single ligand which targets both the CECs and the brain tumor tissue (Liu and Lu, 2012). Therefore, PNPs have been evaluated in many studies as a potential BBB targeted drug delivery system for the treatment of GBM (Table 2). However, all of the studies reported were at preclinical phase and no clinical trials are ongoing.

Poly(butyl cyanoacrylate) (PBCA) NPs, a type of PACA NPs, with surface coating of PS80 as targeting moiety and DOX as the anti-tumor drug have been evaluated by several researchers against different GBM models and also in healthy rats.

Steiniger et al. developed PBCA NPs encapsulating DOX, with and without PS80 coating, and investigated the potential of these formulations against intracranial 101/8 GBM tumor model in rats (Steiniger et al., 2004). The rats were treated with the drug solution, or drug loaded PBCA NPs, or drug loaded PBCA-PS80 NPs three times (on days 2, 5 and 8 after transplanting the tumor) at a dose of 1.5 mg of drug per kg body weight. The survival time of PBCA-PS80 NP treated animals increased 85% compared to control animals and 24% compared to DOX treated animals. Out of 23 animals treated with PBCA-PS80 NPs, 5 animals survived more than 180 days. Histological study confirmed size reduction of tumor and smaller values for proliferation and apoptosis. Moreover, no signs of neurotoxicity were observed. In a further study using the same GBM model, it was found that the DOX loaded PBCA-PS80 NPs significantly reduced necrosis and inhibited the growth of capillaries, leading to reduced tumor growth (Hekmatara et al., 2009). When the treatment was prolonged by increasing the number of doses from 3 up to 5 (1.5 mg/kg DOX per injection), the survival time was significantly increased (Wohlfart et al., 2009).

Best anti-tumor effect was found in the groups receiving the maximum number of dose with significant reduction in tumor growth, less angiogenesis, and tumor regression in about 40% treated animals. Ambruosi *et al.* investigated the bio-distribution of the C¹⁴ labeled PBCA-PS80 NPs loading DOX in GBM 101/8 bearing rats (Ambruosi *et al.*, 2006b). The dosage was administered intravenously and the NP concentration was determined by radioactive assay. Highest brain concentration of NPs was found after 1 h of treatment with PS80 coated NPs, reaching about 31 µgNP/g tissue (0.93% of initial dose). Gulyaev *et al.* studied the pharmacokinetics of DOX solution, DOX + 1% PS80 solution, DOX loaded PBCA NP and DOX loaded PBCA-PS80 NP in rats. Concentration of DOX in brain was detectable only when the drug was loaded in PS80 coated NP (Gulyaev *et al.*, 1999). Although, this study considered the total brain concentration and could not specify whether the drug could actually cross the BBB, the higher BBB permeability of PS80 coated PBCA NP compared to free DOX solution and DOX loaded PBCA NP was observed in another study in rats using capillary depletion method (Wohlfart *et al.*, 2011a). In the latter study, rats were injected with the formulations at a dosage of 5 mg DOX/kg body weight and were sacrificed at 0.5 h, 2 h and 4 h post-injection to remove the brains. Subsequently, homogenates of the brain samples were prepared and a part of the homogenate was centrifuged to separate it into a pellet (containing vascular elements) and supernatant (containing parenchyma). These samples were then analyzed to determine the time-dependent bio-distribution of DOX in brain. Therapeutically significant concentrations of DOX in the parenchyma were detected only for the PBCA-PS80 NP, which shows their ability to permeate across the BBB. At 0.5 h, drug concentration in the vascular elements was almost 2 times compared to the parenchymal concentration; however it was the opposite after 2 h indicating transcytosis of a huge amount of DOX across the CECs (Wohlfart *et al.*, 2011a). Moreover, Wang *et al.* has reported the blank PBCA-PS80 NPs to be safe after testing it *in vitro* against C6 glioma cells (Wang *et al.*, 2009). Additionally, the DOX loaded PBCA-PS80 NPs significantly reduced cardiotoxicity and testicular toxicity in comparison to the free drug solution (Pereverzeva *et al.*, 2007).

Besides PS80, other surfactants were also evaluated to improve the BBB permeability of PBCA NPs, e.g. P188 and P908. In an *in vitro* investigation against 3 different rat glioma cell lines, cytotoxicity and cellular uptake of DOX loaded PBCA NPs coated with PS80,

or P188 or P908 were evaluated (Sanchez De Juan et al., 2006). Cytotoxicity was evaluated by two methods, i.e. LDH assay and MTT assay, where the NP formulations showed more cytotoxicity compared to the free drug solution, with highest activity for PS80 coated NPs, possibly due to its dual effects as BBB targeting agent and P-gp inhibitor. Confocal microscopy also showed the higher cellular uptake of PBCA-PS80 NP compared to the uncoated NP and the free drug. In an *in vivo* study using rat GBM 101/8 model with similar formulations, comparable results were observed (Ambruosi et al., 2006a). The survival time of the rats treated with surfactant coated DOX loaded NP formulations were significantly improved compared to the drug solution. All control animals died between 18 and 24 days after tumor implantation, whereas 10% animals treated with DOX solution survived up to 65 days. However, 20% animals in case of treatment with P188 coated and P908 coated NPs, and 40% animals in case of treatment with PS80 coated NPs survived more than 180 days.

However, the comparative efficacy of the various surfactant-coated NPs can be dependent on the core polymer, and even on other ingredients. For example, when rats with intracranially transplanted 101/8 GBM were treated with free DOX, and drug loaded PLGA NPs stabilized by poly(vinyl alcohol) (PVA) and coated with PS80 or P188, long term (more than 100 days) tumor regression was observed in only 10% animals receiving PS80 coated NPs which was 40% in case of animals treated with P188 coated NPs (Gelperina et al., 2010). In this study, P188 seems to be more effective coating for brain targeting than PS80, which is opposite to the results described reported by Ambruosi et al. (2006). Additionally, when the stabilizer of the formulation, PVA, which is non-biodegradable and unsuitable for parenteral preparations, was replaced by HSA, long term survival was reduced to 25% (Gelperina et al., 2010). However, inclusion of lecithin in the formulation further improved the anti-tumor activity of the DOX loaded PLGA-HSA-P188 NPs (Wohlfart et al., 2011b).

Besides surfactants, addition of specific ligands on the PNP surface can enhance anti-tumor activity in glioma. Gao and colleagues prepared PEG-polycaprolactone (PEG-PCL) NPs with surface coating IL-13 peptide, which preferentially binds with the receptor IL-13R α 2, which is overexpressed in glioma (Gao et al., 2013). Highest cellular uptake and anti-glioma effect were observed in case of IL-13 coated NPs indicating better site targeted delivery of the targeted NP. This was also confirmed by *ex vivo* imaging with the

help of fluorescence dye. Additionally, conjugation of transferrin on PLGA NPs encapsulating paclitaxel showed promising enhanced cellular uptake and cytotoxicity against C6 rat glioma cell line, in comparison to the uncoated NPs (Shah et al., 2009). For *in vivo* biodistribution of the PLGA-transferrin NPs, the C6 glioma cells were administered on the back of the rat by subcutaneous injection and the tumor was allowed to proliferate. The drug solution, uncoated NPs and coated NPs were administered by tail vein injection. The transferrin-coated NPs showed reduced drug concentration in heart and liver and increased paclitaxel concentration in the tumor, compared to the other formulations.

Moreover, cytotoxicity of PEG grafted carboxymethyl chitosan (CMC-PEG) NPs encapsulating DOX and free DOX solution was studied against DOX-resistant C6 glioma cells (Jeong et al., 2010). For this purpose, regular C6 glioma cells were repeatedly exposed to DOX for short time periods and the drug concentration was gradually increased 100 times of initial concentration over 3 months. The resulting C6 cells were evaluated by MTT assay to test the cytotoxicity of the formulation. The results indicate that the drug solution was less internalized by the cells, whereas the NPs penetrated within the cells more and resulting higher anti-proliferative activity.

Polymeric NPs can act as a carrier for both pharmaceutical small- and macro- molecules. They can be designed with biodegradable-biocompatible polymer cores and to have proper physicochemical characteristics for efficiently crossing the BBB and preferentially accumulate in brain tumor tissue. Therefore, they are very promising nanocarriers for the treatment of GBM.

Table 2: PNPs for the treatment of GBM.

Treatment	Targeting approach	Drug nanocarrier	in Status	References
PEG-grafted CMC NP	Passive	DOX	Preclinical- <i>in vitro</i>	(Jeong et al., 2010)
PS80 coated PBCA NP	Active	DOX	Preclinical- <i>in vivo</i>	(Ambruosi et al., 2006b; Gulyaev et al., 1999; Hekmatara et al., 2009; Pereverzeva et al., 2007; Steiniger et al., 2004; Wang et al., 2009; Wohlfart et al., 2009; Wohlfart et al., 2011a)
PS80 or P188 or P908 coated PBCA NP	Active	DOX	Preclinical- <i>in vitro</i> and <i>in vivo</i>	(Ambruosi et al., 2006a; Sanchez De Juan et al., 2006)
PS80 or P188 coated PLGA NP	Active	DOX	Preclinical- <i>in vivo</i>	(Gelperina et al., 2010)
P188 coated PLGA NP	Active	DOX	Preclinical- <i>in vivo</i>	(Wohlfart et al., 2011b)
Transferrin or Pluronic®P85 coated PLGA NP	Active	Paclitaxel	Preclinical- <i>in vivo</i>	(Shah et al., 2009)
IL-13 coated PLGA-PCL NP	Active	Docetaxel	Preclinical- <i>in vivo</i>	(Gao et al., 2013)
Angiopep-conjugated PEG-PCL NP	Active	Paclitaxel	Preclinical- <i>in vivo</i>	(Xin et al., 2012)

6. LNCs for GBM Treatment

6.1. Introduction to LNCs

LNC formulations are colloidal drug delivery systems with a liquid core surrounded by a shell composed by solid lipid molecules. These novel nanocarriers are hybrids between liposomes and polymeric nanocapsules, and were developed and recently patented by Benoit et al. (Heurtault et al., 2002). If their core material is properly selected to have optimum drug solubility, they can have very high encapsulation efficiency (for both hydrophobic and hydrophilic drugs). Compared to PNPs, LNC formulations require

significantly less amount of raw materials. Moreover, drug release from the LNCs can be more sustained compared to PNPs and liposomes (Lamprecht et al., 2002). Additionally, the drug is generally entrapped within the liquid core of the LNCs which shields it from possible degradations and also protects the body from any irritations. They can be designed to achieve a desired particle size with narrow size distribution (Heurtault et al., 2003).

Depending on the type of materials constituting the liquid core, LNCs can be divided into two types: the more widely used oily core LNCs (OC-LNCs), and aqueous-core LNCs (AC-LNCs) (Huynh et al., 2009). The OC-LNCs are commonly prepared using a simple two step manufacturing process based on phase inversion temperature (PIT) phenomenon: first by preparing oil-in-water (o/w) nanoemulsions, and then by nanoprecipitation of preformed polymers (Heurtault et al., 2000). However, in-situ interfacial polymer synthesis can be also used as the second step (Anton et al., 2008). Principally, the core oily phase is composed of medium chain triglycerides i.e. a mixture of capric and caprylic acid triglycerides; while the shell is composed of a combination of lecithin and a PEG associated hydrophilic surfactant (HS15) which is a mixture of PEG 660 and its hydroxyl stearate; and the aqueous phase is a sodium chloride solution. All of these components are either FDA approved for parenteral administration or generally recognized as safe (GRAS) (Huynh et al., 2009). The size and PDI of the LNC formulations can be controlled by changing the ratio of the constituents. Heurtault et al. established a ternary diagram with various ratios of the constituents and found a region of feasibility where the nanocapsules are formed (Heurtault et al., 2003). Increase of the ratio of the hydrophilic surfactant decreases the LNCs size; increase of the ratio of the oily core material increases the nanocarrier diameter, while the ratio of the aqueous phase has no impact on particle size. The LNCs can be PEGylated by post-insertion method to give stealth properties to the nanocarrier which significantly improves their blood circulation time, improves the plasma AUC, and aids in passive targeting (Hoarau et al., 2004). OC-LNC formulations containing many lipophilic, as well as amphiphilic pharmaceutical molecules have been developed, e.g. the anti-arrhythmic drug amiodarone (Lamprecht et al., 2002), the analgesic drug ibuprofen (Lamprecht et al., 2004), etoposide (Lamprecht and Benoit, 2006), paclitaxel (Lacoeuille et al., 2007) etc. Moreover, LNCs entrapping

radiopharmaceuticals have been developed with the potentials to be used in bio-imaging and radiotherapy (Ballot et al., 2006; Jestin et al., 2007).

The AC-LNCs can be prepared using various techniques including techniques based on the PIT phenomenon. For example, AC-LNCs can be manufactured by the following three steps: preparation of a water-in-oil (w/o) nanoemulsion, followed by *in situ* interfacial polymer synthesis, and lastly elimination of the continuous oil phase by evaporation and addition of the outward aqueous phase (Anton et al., 2009). The AC-LNCs, like liposomes, have the potential to encapsulate hydrophilic (in the aqueous core) or lipophilic (in the lipid shell) drugs, or simultaneously both, and possess huge potential for developing novel drug delivery strategies.

6.2. LNCs for GBM treatment

LNCs can be designed to encapsulate various anti-tumor drugs and to deliver them in malignant brain tumors like GBM. Several *in vitro* and *in vivo* studies have investigated the efficacy of such nanocarriers against glioma (Table 3), but no clinical trials are ongoing. Many of the studies are done by the group of Benoit mostly using the formulation described by Heurtault et al. (Heurtault et al., 2002; Heurtault et al., 2003). As described above, the core oily phase of the LNC is composed of medium chain triglycerides i.e. a mixture of capric and caprylic acid triglycerides; the shell is composed of a combination of lecithin and hydrophilic surfactant HS15. Garcion et al. developed LNCs, with an average size of 50 nm, encapsulating paclitaxel along with blank LNCs and assessed whether they can improve bioavailability and efficacy of the drug, and overcome multidrug resistance (MDR) against glioma cell lines (9L and F98) (Garcion et al., 2006). They reported the interaction among the nanocapsule and the P-gp, with inhibition of ATPase activity (or P-gp inhibition) similar to vinblastine (P-gp inhibitor). Moreover, after only 30 min exposure to low concentrations of the nanocapsules, the retention of $^{99}\text{Tc}^{\text{m}}$ -MIBI, a particular P-gp substrate, was markedly improved in both cell lines. This P-gp suppressing effect was comparable with the one produced by the hydrophilic surfactant HS15 alone at respective concentrations like in the nanocapsules. These results indicate HS15 as the key component producing P-gp suppressing effect. Additionally, a comparable *in vivo* experiment was performed in ectopic glioma models (9L and F98) in rats. Intra-tumoral injections of a P-gp inhibitor, HS15 and LNCs were given and a day later, $^{99}\text{Tc}^{\text{m}}$ -MIBI was injected intravenously. In both tumor models, LNC pre-treatment

significantly improved the tracer concentration in the tumor tissue, which further establishes the P-gp inhibiting activity of the nanocarrier. Furthermore, MDR-substrate antineoplastic drug paclitaxel was loaded in the LNCs and tested against 9L and F98 glioma cells, both *in vitro* and *in vivo*. Compared to a commercially available paclitaxel solution, tumor cell death was improved more than 100 folds and more than 1000 folds, in 9L cells and F98 cells respectively. When these formulations were tested against slowly dividing rat brain astrocytes, their cytotoxic effects were similar, which suggested the preference of the LNCs towards the cancerous cells. The higher efficacy of the paclitaxel loaded LNCs compared to the drug solution was also seen when they were evaluated *in vivo* in a subcutaneous F98 glioma model (Garcion et al., 2006).

Paillard et al. studied the relationship of the size and composition of the LNCs with endocytosis and efficacy against F98 rat-glioma cells (Paillard et al., 2010). Blank, fluorescent labeled, radiolabeled and paclitaxel loaded LNCs of various sizes (20 nm, 50 nm and 100 nm) were prepared. Their results suggest that the nanocapsules start to accumulate within the cells only 2 min after contact using an active and saturable mechanism linked to endogenous cholesterol. LNCs can break the endolysosomal compartment in a size-dependent manner, with smaller particles showing more efficiency. The cellular uptake (after 2 h incubation at 37 °C) experiment with radiolabeled nanocapsules revealed sharply decreasing numbers of LNC uptake with increasing particle size. However, the smaller nanocapsules contain higher ratio of the hydrophilic surfactant HS15 (P-gp inhibitor), and can influence cellular uptake on MDR cancer cells. In fact, when the amounts of the LNC components inside the cells were quantified, the cells treated with 20 nm LNCs had 3-times more HS15 compared to cells treated with 100 nm particles. Moreover, when cytotoxicity of paclitaxel loaded 20 nm and 100 nm LNCs were tested by MTT assay, 20 nm nanocarriers caused higher percentage of tumor cell death compared to 100 nm LNCs, at similar drug concentrations (Paillard et al., 2010). These properties of the LNCs can also be attributed to the amounts of HS15 delivered to the cells which is hypothesized to significantly influence P-gp inhibition and protection of the drugs from lysosomal degradation.

The tolerance of the blank and paclitaxel loaded LNCs after repeated i.v. administration was evaluated in mice (Hureaux et al., 2010). The animals were injected with drug loaded LNCs, or standard drug solutions at a dose of 12mg/kg/day for 5 successive days. Blank

LNCs and saline were also injected to two other groups of animals at a comparable dose in the similar fashion. None of the animals died, or showed any lesions, and the blood cell counts were normal. In comparison to a commercial drug solution, the nanocapsules increased the maximum tolerated dose and the lethal dose 50% (LD₅₀) by 11-fold and 8-fold respectively, which improved the therapeutic index of paclitaxel.

The P-gp inhibiting activity of the LNCs was also observed when blank and etoposide loaded nanocapsules having various diameters (25 nm, 50 nm and 100 nm) were tested against C6, F98 and 9L glioma cell lines (Lamprecht and Benoit, 2006). The smallest LNC produced the most potent P-gp suppression which is similar to the results reported by Paillard (Paillard et al., 2010). Moreover, cytotoxicity of the drug loaded LNCs were significantly higher than the drug solution and the blank LNCs against all three cell lines, and the effect was found to be dependent on nanocarrier size where anticancer efficacy increased as size decreased (Lamprecht and Benoit, 2006). Compared to the drug solution, 25 nm LNCs reduced the IC₅₀ values of the drug by 8-fold, 13-fold and 30-fold in C6, 9L and F98 cells respectively. The LNCs also showed sustained release (up to 7 days) of the drug, which in addition with the P-gp inhibiting affect may have contributed to the improved glioma cell suppressing effect of the formulation compared to the drug alone.

Several organometallic drugs were encapsulated in the LNCs and their *in vitro* and *in vivo* efficacies were tested against 9L glioma model (Allard et al., 2009a; Allard et al., 2008; Laine et al., 2014). Ferrociphenol (FcDiOH), among many organometallic tamoxifen derivatives, generated potent *in vitro* anti-tumor effect in both estrogen-dependent and independent breast cancer cells (Vessieres et al., 2005). However, the *in vivo* activity of this molecule can be hampered as FcDiOH is highly hydrophobic in nature, and formulation development is necessary to ensure its bioavailability at the site of action, especially if it is to be tested against brain tumors like glioma. Allard et al. developed FcDiOH loaded LNCs having diameter around 50 nm and tested its efficacy *in vitro* against 9L glioma cells and newborn rat primary astrocytes; and *in vivo* in an ectopic 9L glioma model in rats (Allard et al., 2008). In the *in vitro* MTT assay, the drug loaded LNCs and the drug solution (solubilized using ethanol) showed analogous cell survival curves, which refers that the activity of the drug was not hampered after entrapment in the nanocapsules. Additionally, the drug loaded LNC produced 150-times more cell death compared to the blank LNC. However, the FcDiOH loaded LNCs and the drug solution

showed much lower cytotoxicity (similar to blank LNCs) against healthy and slowly dividing astrocyte cells, which shows that the preferential activity of the drug towards cancer cell is also maintained by the nanocapsule formulation. Furthermore, the drug loaded LNCs significantly reduced the tumor growth and mass after single intra-tumoral injection of the formulation in an ectopic 9L model in rats (Allard et al., 2008). Allard et al. also evaluated the activity of LNC formulations of two prodrug of FcDiOH (the hydroxyl groups are protected by either acetyl (Fc-diAC) or palmitoyl (Fc-diPal) chains) in similar *in vitro* and *in vivo* experiments (Allard et al., 2009a). Only the Fc-diAC loaded nanocapsules showed similar cytotoxic and anti-tumor activity as FcDiOH loaded nanocapsules. These data shows the successful intracellular delivery of the Fc-diAC prodrug with the aid of the LNCs, and subsequent cleavage of the acetate group by the cell, which converts it into the active drug. The activity of FcDiOH LNCs was also proven in an orthotopic xenograft glioma model, where the treatment was administered by simple stereotaxy and by CED (Allard et al., 2009a).

Another novel organometallic ferrocenyl derivate, ansa-FcDiOH, loaded in PEGylated LNC formulation, was evaluated for its possible anti-tumor effect against 9L glioma cells, both *in vitro* and *in vivo* (Laine et al., 2014). In the *in vitro* antiproliferative assay, the free drug solution and the drug-loaded LNC showed similar cytotoxic profiles evidencing the conservation of its activity even after encapsulation in the nanocarrier. Repeated administration (10 times over 2 weeks) of the ansa-FcDiOH LNC by tail vein injection significantly inhibited the growth of intradermally implanted 9L tumor in fisher rats. Moreover, the number of proliferative cells in the tumor was considerably reduced compared to the saline or blank LNC treated groups. Furthermore, histological study revealed no liver damage after the treatment period.

Curcumin is a natural compound which has shown promising results in treatment of many diseases including cancer. It has been reported to show antiproliferative and apoptotic activity against GBM in several studies (Perry et al., 2010; Zanotto-Filho et al., 2012). However, it might be possible to improve its efficacy incorporating the drug in a brain targeted nanocarrier which can preferentially deliver the drug at the glioma tumors and thereby, may reduce the required dose. In this regard, Zanotto-Filho et al. developed curcumin encapsulated in PS80 coated LNC, which was composed of poly(ϵ -caprolactone), sorbitan monostearate and grapeseed oil (Zanotto-Filho et al., 2013). The

LNC formulation was tested against C6 and U251MG glioma cells *in vitro* and against orthotopic C6 glioma model in rats. The curcumin-LNCs showed sustained drug release kinetics and therefore cytotoxicity similar to the free drug only after 96 h. In the *in vivo* study, the rats were treated by repeated intraperitoneal injections (14 injections in 14 consecutive days) with saline, free curcumin (1.5 mg/kg/day and 50 mg/kg/day), blank LNC (volume respective to curcumin-LNC) and curcumin-LNC (1.5 mg/kg/day). The brain targeted curcumin-loaded LNCs reduced tumor volume and increased survival rate significantly compared to the free drug (at similar concentration). The anti-tumor effect of the free drug was similar to the effect of the nanocapsule formulation only at 33-fold more dosage (50 mg/kg/day of free drug vs 1.5 mg/kg/day). This data demonstrates the capability of nanocapsules to deliver the drug preferentially in the glioma tumor. Moreover, the safety of the LNC treatment was established by serum toxicity marker tests and histological study (Zanotto-Filho et al., 2013).

Finally, LNCs are very promising nanocolloid drug delivery systems for the treatment of GBM. Several LNC formulations are reported to show their preferential accumulation in brain tumors, and to significantly improve the efficacy of the antitumor agents. Additionally, their manufacturing can be simple, solvent free, requires fewer amounts of polymers than PNPs and are more stable than liposomes. Therefore, they have high possibilities to be developed as successful GBM targeted delivery systems.

Table 3: LNCs for the treatment of GBM.

Treatment	Targeting approach	Drug in nanocarrier	Status	References
PEG-grafted LNC	Passive	FcDiOH	Preclinical- <i>in vivo</i>	(Allard et al., 2008)
PEG-grafted LNC	Passive	Fc-diAC or Fc-diPal	Preclinical- <i>in vivo</i>	(Allard et al., 2009a)
PEG-grafted LNC	Passive	ansa-FcDiOH	Preclinical- <i>in vivo</i>	(Laine et al., 2014)
OX26-grafted or peptide coated LNC	Active	FcDiOH	Preclinical- <i>in vivo</i>	(Laine et al., 2012)
PS80 coated LNC	Active	Curcumin	Preclinical- <i>in vivo</i>	(Zanotto-Filho et al., 2013)

7. Challenges in Nanocarrier Development

The nanocolloid drug delivery systems are very promising for treatment of various types of cancers due to their ability of active or passive targeting. Their surface properties can be modified to cross various biological barriers *in vivo* and reach the target tissue, improve cellular uptake, reduce required dosage and decrease toxic effects of the drug. However, the unique characteristic of nanocarriers to pass biomembranes can cause unexpected toxicities as the polymers, lipids or other excipients also reach organs, tissues or cells along with the drug. Inside the cell, nanocarriers can reduce the integrity of intra-cellular membranes, make the different compartments (mitochondria, Golgi apparatus, lysosome, nucleus etc.) of the cell vulnerable, and destroy intracellular homeostasis causing cell death (Elsaesser and Howard, 2012; Ginzburg and Balijepalli, 2007). Moreover, some nanocarriers are capable to reach the nucleus by passing through nuclear pores or by RMT and cause DNA damage (Godbey et al., 1999; Panté and Kann, 2002). Such effects can be dependent on the nanocarrier composition, concentration and physicochemical characteristics (Ginzburg and Balijepalli, 2007; Gou et al., 2010). The nanocolloids can damage cell membranes and DNA (without reaching inside nucleus) also by oxidative stress (Bhabra et al., 2009; Myllynen, 2009). Besides target tissues, nanocarriers may distribute in other organs, especially in the liver. Therefore, it is important to know the biodistribution of the nanocarrier, the biodegradability of the nanomaterials and the elimination process of intact or metabolized chemicals, as well as the possible accumulation along with short and long-term toxic effects.

After i.v. administration, nanocarriers are surrounded by plasma proteins and lipids, which form a corona (Lynch et al., 2007). Bio-distribution and subsequent pharmacological-toxicological effects of the nanocolloids are mainly dependent upon this bio-corona, and therefore it is important to understand the nano-biointerface. The formation of the corona is primarily controlled by NP size and surface characteristics (surface charge, coating etc.). However, the size distribution and related surface characteristics may slightly vary in a batch of nanocarriers. For example, nanocolloids with targeting-moiety grafted on the surface will have a statistical distribution of the ligand. Even a small change in these properties can alter the cellular response (He et al., 2010; Jiang et al., 2008). Some nanocarriers e.g. liposomes and polymeric micelles may have dynamic reorganization property and change their size with time. Moreover, lack of reference materials and

standardized toxicity assays makes it more difficult to precisely predict the possible toxic effects of nanocarriers by comparing it with other studies (Nyström and Fadeel, 2012). Now-a-days, many nanocarriers are designed using novel synthesized polymers, but toxicity profiles of them are not well defined.

These create a big challenge from research and regulatory point of view, as how different nanocarrier properties affect their biological fate is not exactly predictable, and data about possible long-term toxic effects are not readily available. Despite of their promising features, only limited numbers of nanocarrier based drug delivery systems are presently available in the market due to these reasons. Further research is necessary to develop standardized *in vitro-ex vivo* models and assays to more precisely predict *in vivo* biological-toxicological fate of nanocolloid drug delivery systems.

8. Conclusion

Malignant brain tumors like GBM are one of the toughest medical challenges faced around the globe for decades. With the help of modern technologies and in-depth knowledge about tumor biochemistry, numerous novel drug molecules are being designed, synthesized and investigated as possible treatments of such diseases. However, majority of the novel anti-cancer drug molecules are hydrophobic, and require to be incorporated in appropriate formulations to retain their activity *in vivo*. Furthermore, the unique barrier specific functions of the BBB create a greater challenge towards successful treatment of GBM.

Colloidal nanocarriers can be designed to have many favorable characteristics which aid preferential delivery of therapeutic molecules to the brain tumors, and therefore attract many researchers. In fact, nanocarriers like liposomes, PNPs and LNCs have often shown to improve efficacy, reduces non-specific toxicity, and increases stability of drugs. Their biodistribution and drug release kinetics can be more finely controlled than conventional formulations. Although, safety of the raw materials used and regulatory matters still remain as concerns to think about, the significance of nanocarriers as brain-targeted drug delivery systems is increasing with rising incidences of CNS related diseases such as brain cancers.

1.2.2. Update since the review

Since 2016, several promising nanovectors, chiefly liposomes and PNPs, for GBM treatment has been reported. Belhadj et al. developed a Y-shaped multifunctional targeting moiety by linking cyclic RGD and p-hydroxybenzoic acid (pHB) with a short spacer to PEG-DSPE chain and functionalized the surface of DOX-loaded liposomes (Belhadj et al., 2017). Mice with orthotopic GBM tumors were treated by i.v. administration every 2 days between days 7 to 15 after tumor implantation. Median survival was improved by additional 10, 8 and 6.5 days compared to DOX-liposomes, cRGD-DOX-liposomes and pHB-DOX-liposomes respectively. Shi et al. reported that CED of 30 μ g of Lipoxal improved median survival (31 days) of GBM bearing rats to the same extent as CED of 10 μ g of free oxaliplatin compared to untreated animals (23.5 days), but reduced the toxic effects of the free drug (Shi et al., 2016). Madhankumar et al. injected IL-3 grafted liposomes co-encapsulating DOX and farnesyl thiosalicylic acid (FTS), a Ras inhibitor, every 7 days for 7 weeks at 7 mg/kg dose in ectopic U87MG tumor bearing mice and observed slower tumor progression compared to DOX-liposome and control group (Madhankumar et al., 2016). Pi et al. treated orthotopic GBM tumor bearing mice with paclitaxel loaded liposomes that was delivered to brain by ultrasound with microbubbles, and they observed significantly slower tumor growth and 25% longer median survival time compared to untreated group (Pi et al., 2016).

Several studies reported promising results using PNPs against GBM. Zhang et al. delivered cisplatin-polyaspartic acid-PEG NPs by CED to rats bearing F98 intracranial tumors and 80% mouse survived more than 100 days compared to median survival of 40, 12 and 28 days in cisplatin-polyaspartic acid NP, cisplatin and saline treated groups respectively (Zhang et al., 2017). Lin et al. intravenously administered camptothecin-PEG-cyclodextrin NP-drug conjugate in intracranial U87MG tumor bearing mice and improved median survival to 35 days compared to 32 and 22 days in camptothecin treated and untreated mice (Lin et al., 2016). Xu et al. observed significantly better tumor retardation in mice treated with paclitaxel-TMZ co-entrapped in mPEG-PLGA NPs compared to single drug NPs or free drug combination (Xu et al., 2016).

No studies were published reporting the use of LNCs for GBM treatment since 2016. Only one clinical trial focusing GBM treatment using nanocarriers was registered in

ClinicalTrials.gov after 2016, which is in its early phase 1 and trying to assess the safety of their spherical nucleic acid coated gold NPs (Kumthekar, 2017).

1.3. References

- Abbott, N.J., Ronnback, L., Hansson, E., 2006. Astrocyte-endothelial interactions at the blood-brain barrier. *Nat. Rev. Neurosci.* 7, 41-53.
- Adamson, C., Kanu, O.O., Mehta, A.I., Di, C., Lin, N., Mattox, A.K., Bigner, D.D., 2009. Glioblastoma multiforme: a review of where we have been and where we are going. *Expert Opin. Investig. Drugs* 18, 1061-1083.
- Aguzzi, A., Barres, B.A., Bennett, M.L., 2013. Microglia: scapegoat, saboteur, or something else? *Science* 339, 156-161.
- Allard, E., Huynh, N.T., Vessieres, A., Pigeon, P., Jaouen, G., Benoit, J.P., Passirani, C., 2009a. Dose effect activity of ferrocifen-loaded lipid nanocapsules on a 9L-glioma model. *Int. J. Pharm.* 379, 317-323.
- Allard, E., Passirani, C., Benoit, J.P., 2009b. Convection-enhanced delivery of nanocarriers for the treatment of brain tumors. *Biomaterials* 30, 2302-2318.
- Allard, E., Passirani, C., Garcion, E., Pigeon, P., Vessieres, A., Jaouen, G., Benoit, J.P., 2008. Lipid nanocapsules loaded with an organometallic tamoxifen derivative as a novel drug-carrier system for experimental malignant gliomas. *J. Control. Release* 130, 146-153.
- Allen, T.M., 1994. Long-circulating (sterically stabilized) liposomes for targeted drug delivery. *Trends Pharmacol. Sci.* 15, 215-220.
- Allen, T.M., Hansen, C., Martin, F., Redemann, C., Yau-Young, A., 1991. Liposomes containing synthetic lipid derivatives of poly (ethylene glycol) show prolonged circulation half-lives in vivo. *Biochim. Biophys. Acta* 1066, 29-36.
- Alyautdin, R., Khalin, I., Nafeeza, M.I., Haron, M.H., Kuznetsov, D., 2014. Nanoscale drug delivery systems and the blood-brain barrier. *International journal of nanomedicine* 9, 795-811.
- Alyautdin, R.N., Petrov, V.E., Langer, K., Berthold, A., Kharkevich, D.A., Kreuter, J., 1997. Delivery of loperamide across the blood-brain barrier with polysorbate 80-coated polybutylcyanoacrylate nanoparticles. *Pharm. Res.* 14, 325-328.
- Ambruosi, A., Gelperina, S., Khalansky, A., Tanski, S., Theisen, A., Kreuter, J., 2006a. Influence of surfactants, polymer and doxorubicin loading on the anti-tumour effect of poly (butyl cyanoacrylate) nanoparticles in a rat glioma model. *J. Microencapsul.* 23, 582-592.
- Ambruosi, A., Khalansky, A.S., Yamamoto, H., Gelperina, S.E., Begley, D.J., Kreuter, J., 2006b. Biodistribution of polysorbate 80-coated doxorubicin-loaded [14C]-poly(butyl cyanoacrylate) nanoparticles after intravenous administration to glioblastoma-bearing rats. *J. Drug Target.* 14, 97-105.
- Ananda, S., Nowak, A.K., Cher, L., Dowling, A., Brown, C., Simes, J., Rosenthal, M.A., Cooperative Trials Group for, N.-O., 2011. Phase 2 trial of temozolomide and pegylated liposomal doxorubicin in the treatment of patients with glioblastoma multiforme following concurrent radiotherapy and chemotherapy. *J. Clin. Neurosci.* 18, 1444-1448.
- Andrieux, K., Garcia-Garcia, E., Kim, H.R., Couvreur, P., 2009. Colloidal carriers: a promising way to treat central nervous system diseases. *Journal of Nanoneuroscience* 1, 17-34.
- Anton, N., Benoit, J.P., Saulnier, P., 2008. Design and production of nanoparticles formulated from nano-emulsion templates-a review. *J. Control. Release* 128, 185-199.

- Anton, N., Saulnier, P., Gaillard, C., Porcher, E., Vrignaud, S., Benoit, J.-P., 2009. Aqueous-core lipid nanocapsules for encapsulating fragile hydrophilic and/or lipophilic molecules. *Langmuir* 25, 11413-11419.
- Asokan, A., Cho, M.J., 2003. Cytosolic delivery of macromolecules. II. Mechanistic studies with pH-sensitive morpholine lipids. *Biochim. Biophys. Acta* 1611, 151-160.
- Bailey, P., Cushing, H., 1926. A classification of the tumours of the glioma group on a histogenetic basis with a correlated study of prognosis. J.B. Lipponcott, Montreal.
- Ballot, S., Noiret, N., Hindré, F., Denizot, B., Garin, E., Rajerison, H., Benoit, J.-P., 2006. $^{99m}\text{Tc}/^{188}\text{Re}$ -labelled lipid nanocapsules as promising radiotracers for imaging and therapy: formulation and biodistribution. *Eur. J. Nucl. Med. Mol. Imaging* 33, 602-607.
- Bangham, A.D., Horne, R.W., 1964. Negative staining of phospholipids and their structural modification by surface-active agents as observed in the electron microscope. *J. Mol. Bio.* 8, 660-668.
- Bangham, A.D., Standish, M.M., Watkins, J.C., 1965a. Diffusion of univalent ions across the lamellae of swollen phospholipids. *J. Mol. Biol.* 13, 238-252.
- Bangham, A.D., Standish, M.M., Weissmann, G., 1965b. The action of steroids and streptolysin S on the permeability of phospholipid structures to cations. *J. Mol. Biol.* 13, 253-259.
- Beduneau, A., Hindre, F., Clavreul, A., Leroux, J.C., Saulnier, P., Benoit, J.P., 2008. Brain targeting using novel lipid nanovectors. *J. Control. Release* 126, 44-49.
- Begley, D.J., 2004. Delivery of therapeutic agents to the central nervous system: the problems and the possibilities. *Pharmacol. Ther.* 104, 29-45.
- Beier, C.P., Schmid, C., Gorlia, T., Kleinletzenberger, C., Beier, D., Grauer, O., Steinbrecher, A., Hirschmann, B., Brawanski, A., Dietmaier, C., Jauch-Worley, T., Kolbl, O., Pietsch, T., Proescholdt, M., Rummele, P., Muigg, A., Stockhammer, G., Hegi, M., Bogdahn, U., Hau, P., 2009. RNOP-09: pegylated liposomal doxorubicine and prolonged temozolomide in addition to radiotherapy in newly diagnosed glioblastoma--a phase II study. *BMC Cancer* 9, 308.
- Belhadj, Z., Ying, M., Cao, X., Hu, X., Zhan, C., Wei, X., Gao, J., Wang, X., Yan, Z., Lu, W., 2017. Design of Y-shaped targeting material for liposome-based multifunctional glioblastoma-targeted drug delivery. *J. Control. Release* 255, 132-141.
- Bergamo, A., Sava, G., 2011. Ruthenium anticancer compounds: myths and realities of the emerging metal-based drugs. *Dalton Trans* 40, 7817-7823.
- Bernacki, J., Dobrowolska, A., Nierwinska, K., Malecki, A., 2008. Physiology and pharmacological role of the blood-brain barrier. *Pharmacol. Rep.* 60, 600-622.
- Bhabra, G., Sood, A., Fisher, B., Cartwright, L., Saunders, M., Evans, W.H., Surprenant, A., Lopez-Castejon, G., Mann, S., Davis, S.A., 2009. Nanoparticles can cause DNA damage across a cellular barrier. *Nature Nanotechnology* 4, 876-883.
- Bhaskar, S., Tian, F., Stoeger, T., Kreyling, W., de la Fuente, J.M., Grazu, V., Borm, P., Estrada, G., Ntziachristos, V., Razansky, D., 2010. Multifunctional Nanocarriers for diagnostics, drug delivery and targeted treatment across blood-brain barrier: perspectives on tracking and neuroimaging. *Part. Fibre Toxicol.* 7, 3.
- Bian, Y., Ye, M., Wang, C., Cheng, K., Song, C., Dong, M., Pan, Y., Qin, H., Zou, H., 2013. Global screening of CK2 kinase substrates by an integrated phosphoproteomics workflow. *Sci. Rep.* 3, 3460.

- Bianco, J., Bastiancich, C., Jankovski, A., des Rieux, A., Preat, V., Danhier, F., 2017. On glioblastoma and the search for a cure: where do we stand? *Cell. Mol. Life Sci.*, 2451-2466.
- Birt, D.F., Mitchell, D., Gold, B., Pour, P., Pinch, H.C., 1997. Inhibition of ultraviolet light induced skin carcinogenesis in SKH-1 mice by apigenin, a plant flavonoid. *Anticancer Res.* 17, 85-91.
- Birt, D.F., Walker, B., Tibbels, M.G., Bresnick, E., 1986. Anti-mutagenesis and anti-promotion by apigenin, robinetin and indole-3-carbinol. *Carcinogenesis* 7, 959-963.
- Bobo, R.H., Laske, D.W., Akbasak, A., Morrison, P.F., Dedrick, R.L., Oldfield, E.H., 1994. Convection-enhanced delivery of macromolecules in the brain. *Proceedings of the National Academy of Sciences of the United States of America* 91, 2076-2080.
- Borges-Walmsley, M.I., McKeegan, K.S., Walmsley, A.R., 2003. Structure and function of efflux pumps that confer resistance to drugs. *Biochem. J.* 376, 313-338.
- Braga, S.S., Silva, A.M.S., 2013. A New Age for Iron: Antitumoral Ferrocenes. *Organometallics* 32, 5626-5639.
- Bragagni, M., Mennini, N., Ghelardini, C., Mura, P., 2012. Development and characterization of niosomal formulations of doxorubicin aimed at brain targeting. *J Pharm. Pharm. Sci.* 15, 184-196.
- Brantley, E.C., Nabors, L.B., Gillespie, G.Y., Choi, Y.H., Palmer, C.A., Harrison, K., Roarty, K., Benveniste, E.N., 2008. Loss of protein inhibitors of activated STAT-3 expression in glioblastoma multiforme tumors: implications for STAT-3 activation and gene expression. *Clin. Cancer Res.* 14, 4694-4704.
- Brem, H., Piantadosi, S., Burger, P.C., Walker, M., Selker, R., Vick, N.A., Black, K., Sisti, M., Brem, S., Mohr, G., et al., 1995. Placebo-controlled trial of safety and efficacy of intraoperative controlled delivery by biodegradable polymers of chemotherapy for recurrent gliomas. The Polymer-brain Tumor Treatment Group. *Lancet* 345, 1008-1012.
- Brigger, I., Morizet, J., Aubert, G., Chacun, H., Terrier-Lacombe, M.J., Couvreur, P., Vassal, G., 2002. Poly(ethylene glycol)-coated hexadecylcyanoacrylate nanospheres display a combined effect for brain tumor targeting. *J. Pharmacol. Exp. Ther.* 303, 928-936.
- Brignole, C., Pagnan, G., Marimpietri, D., Cosimo, E., Allen, T.M., Ponzoni, M., Pastorino, F., 2003. Targeted delivery system for antisense oligonucleotides: a novel experimental strategy for neuroblastoma treatment. *Cancer Lett.* 197, 231-235.
- Butt, A.M., Jones, H.C., Abbott, N.J., 1990. Electrical resistance across the blood-brain barrier in anaesthetized rats: a developmental study. *J. Physiol.* 429, 47-62.
- Calvo, P., Gouritin, B., Chacun, H., Desmaële, D., D'Angelo, J., Noel, J.-P., Georgin, D., Fattal, E., Andreux, J.P., Couvreur, P., 2001. Long-circulating PEGylated polycyanoacrylate nanoparticles as new drug carrier for brain delivery. *Pharm. Res.* 18, 1157-1166.
- Chang, H.I., Yeh, M.K., 2012. Clinical development of liposome-based drugs: formulation, characterization, and therapeutic efficacy. *International journal of nanomedicine* 7, 49-60.
- Charest, G., Sanche, L., Fortin, D., Mathieu, D., Paquette, B., 2012. Glioblastoma treatment: bypassing the toxicity of platinum compounds by using liposomal formulation and increasing treatment efficiency with concomitant radiotherapy. *Int. J. Radiat. Oncol. Biol. Phys.* 84, 244-249.

- Chen, H., Tang, L., Qin, Y., Yin, Y., Tang, J., Tang, W., Sun, X., Zhang, Z., Liu, J., He, Q., 2010. Lactoferrin-modified procationic liposomes as a novel drug carrier for brain delivery. *Eur. J. Pharm. Sci.* 40, 94-102.
- Chen, Y., Liu, L., 2012. Modern methods for delivery of drugs across the blood-brain barrier. *Advanced drug delivery reviews* 64, 640-665.
- Chen, Z.S., Lee, K., Walther, S., Raftogianis, R.B., Kuwano, M., Zeng, H., Kruh, G.D., 2002. Analysis of methotrexate and folate transport by multidrug resistance protein 4 (ABCC4): MRP4 is a component of the methotrexate efflux system. *Cancer Res.* 62, 3144-3150.
- Chinot, O.L., Wick, W., Mason, W., Henriksson, R., Saran, F., Nishikawa, R., Carpentier, A.F., Hoang-Xuan, K., Kavan, P., Cernea, D., Brandes, A.A., Hilton, M., Abrey, L., Cloughesy, T., 2014. Bevacizumab plus radiotherapy-temozolomide for newly diagnosed glioblastoma. *N. Engl. J. Med.* 370, 709-722.
- Choo, E.F., Kurnik, D., Muszkat, M., Ohkubo, T., Shay, S.D., Higginbotham, J.N., Glaeser, H., Kim, R.B., Wood, A.J., Wilkinson, G.R., 2006. Differential in vivo sensitivity to inhibition of P-glycoprotein located in lymphocytes, testes, and the blood-brain barrier. *J. Pharmacol. Exp. Ther.* 317, 1012-1018.
- Chua, S.L., Rosenthal, M.A., Wong, S.S., Ashley, D.M., Woods, A.M., Dowling, A., Cher, L.M., 2004. Phase 2 study of temozolomide and Caelyx in patients with recurrent glioblastoma multiforme. *Neuro Oncol.* 6, 38-43.
- Citta, A., Folda, A., Bindoli, A., Pigeon, P., Top, S., Vessieres, A., Salmain, M., Jaouen, G., Rigobello, M.P., 2014. Evidence for targeting thioredoxin reductases with ferrocenyl quinone methides. A possible molecular basis for the antiproliferative effect of hydroxyferrocifens on cancer cells. *J. Med. Chem.* 57, 8849-8859.
- Coloma, M.J., Lee, H.J., Kurihara, A., Landaw, E.M., Boado, R.J., Morrison, S.L., Pardridge, W.M., 2000. Transport across the primate blood-brain barrier of a genetically engineered chimeric monoclonal antibody to the human insulin receptor. *Pharm. Res.* 17, 266-274.
- Correale, J., Villa, A., 2009. Cellular elements of the blood-brain barrier. *Neurochem. Res.* 34, 2067-2077.
- Couvreux, P., 1987. Polyalkylcyanoacrylates as colloidal drug carriers. *Crit. Rev. Ther. Drug Carrier Syst.* 5, 1-20.
- Couvreux, P., Dubernet, C., Puisieux, F., 1995. Controlled drug delivery with nanoparticles: current possibilities and future trends. *Eur. J. Pharm. Biopharm.* 41, 2-13.
- Daneman, R., Rescigno, M., 2009. The gut immune barrier and the blood-brain barrier: are they so different? *Immunity* 31, 722-735.
- Das, A., Banik, N.L., Ray, S.K., 2010. Flavonoids activated caspases for apoptosis in human glioblastoma T98G and U87MG cells but not in human normal astrocytes. *Cancer* 116, 164-176.
- de Boer, A.G., Gaillard, P.J., 2007. Drug targeting to the brain. *Annu. Rev. Pharmacol. Toxicol.* 47, 323-355.
- Denora, N., Trapani, A., Laquintana, V., Lopodota, A., Trapani, G., 2009. Recent advances in medicinal chemistry and pharmaceutical technology-strategies for drug delivery to the brain. *Curr. Top. Med. Chem.* 9, 182-196.

- Dixit, D., Sharma, V., Ghosh, S., Mehta, V., Sen, E., 2012. Inhibition of Casein kinase-2 induces p53-dependent cell cycle arrest and sensitizes glioblastoma cells to tumor necrosis factor (TNF α)-induced apoptosis through SIRT1 inhibition. *Cell Death Dis.* 3, e271.
- Duncan, J.S., Litchfield, D.W., 2008. Too much of a good thing: the role of protein kinase CK2 in tumorigenesis and prospects for therapeutic inhibition of CK2. *Biochim. Biophys. Acta* 1784, 33-47.
- El-Bacha, R.S., Minn, A., 1999. Drug metabolizing enzymes in cerebrovascular endothelial cells afford a metabolic protection to the brain. *Cell. Mol. Biol. (Noisy-le-grand)* 45, 15-23.
- Elsaesser, A., Howard, C.V., 2012. Toxicology of nanoparticles. *Advanced drug delivery reviews* 64, 129-137.
- Engelmann, C., Blot, E., Panis, Y., Bauer, S., Trochon, V., Nagy, H., Lu, H., Soria, C., 2002. Apigenin—strong cytostatic and anti-angiogenic action *in vitro* contrasted by lack of efficacy *in vivo*. *Phytomedicine* 9, 489-495.
- Fabel, K., Dietrich, J., Hau, P., Wismeth, C., Winner, B., Przywara, S., Steinbrecher, A., Ullrich, W., Bogdahn, U., 2001. Long-term stabilization in patients with malignant glioma after treatment with liposomal doxorubicin. *Cancer* 92, 1936-1942.
- Fattal, E., Couvreur, P., Dubernet, C., 2004. "Smart" delivery of antisense oligonucleotides by anionic pH-sensitive liposomes. *Advanced drug delivery reviews* 56, 931-946.
- Fazil, M., Md, S., Haque, S., Kumar, M., Baboota, S., Sahni, J.K., Ali, J., 2012. Development and evaluation of rivastigmine loaded chitosan nanoparticles for brain targeting. *Eur. J. Pharm. Sci.* 47, 6-15.
- Frankel, A.D., Pabo, C.O., 1988. Cellular uptake of the tat protein from human immunodeficiency virus. *Cell* 55, 1189-1193.
- Fricker, S.P., 2007. Metal based drugs: from serendipity to design. *Dalton Trans*, 4903-4917.
- Fults, D., Brockmeyer, D., Tullous, M.W., Pedone, C.A., Cawthon, R.M., 1992. p53 mutation and loss of heterozygosity on chromosomes 17 and 10 during human astrocytoma progression. *Cancer Res.* 52, 674-679.
- Gabathuler, R., 2010. Approaches to transport therapeutic drugs across the blood-brain barrier to treat brain diseases. *Neurobiol. Dis.* 37, 48-57.
- Gabizon, A., Price, D.C., Huberty, J., Bresalier, R.S., Papahadjopoulos, D., 1990. Effect of liposome composition and other factors on the targeting of liposomes to experimental tumors: biodistribution and imaging studies. *Cancer Res.* 50, 6371-6378.
- Ganesh, S., Iyer, A.K., Gattacceca, F., Morrissey, D.V., Amiji, M.M., 2013. In vivo biodistribution of siRNA and cisplatin administered using CD44-targeted hyaluronic acid nanoparticles. *J. Control. Release* 172, 699-706.
- Gao, H., Yang, Z., Zhang, S., Cao, S., Shen, S., Pang, Z., Jiang, X., 2013. Ligand modified nanoparticles increases cell uptake, alters endocytosis and elevates glioma distribution and internalization. *Sci. Rep.* 3, 2534.
- Garcion, E., Lamprecht, A., Heurtault, B., Paillard, A., Aubert-Pouessel, A., Denizot, B., Menei, P., Benoit, J.P., 2006. A new generation of anticancer, drug-loaded, colloidal vectors reverses multidrug resistance in glioma and reduces tumor progression in rats. *Mol. Cancer Ther.* 5, 1710-1722.

- Gelperina, S., Maksimenko, O., Khalansky, A., Vanchugova, L., Shipulo, E., Abbasova, K., Berdiev, R., Wohlfart, S., Chepurnova, N., Kreuter, J., 2010. Drug delivery to the brain using surfactant-coated poly (lactide-co-glycolide) nanoparticles: influence of the formulation parameters. *Eur. J. Pharm. Biopharm.* 74, 157-163.
- Gilbert, M.R., Dignam, J.J., Armstrong, T.S., Wefel, J.S., Blumenthal, D.T., Vogelbaum, M.A., Colman, H., Chakravarti, A., Pugh, S., Won, M., Jeraj, R., Brown, P.D., Jaecle, K.A., Schiff, D., Stieber, V.W., Brachman, D.G., Werner-Wasik, M., Tremont-Lukats, I.W., Sulman, E.P., Aldape, K.D., Curran, W.J., Jr., Mehta, M.P., 2014. A randomized trial of bevacizumab for newly diagnosed glioblastoma. *N. Engl. J. Med.* 370, 699-708.
- Ginzburg, V.V., Balijepalli, S., 2007. Modeling the thermodynamics of the interaction of nanoparticles with cell membranes. *Nano letters* 7, 3716-3722.
- Godbey, W.T., Wu, K.K., Mikos, A.G., 1999. Tracking the intracellular path of poly(ethylenimine)/DNA complexes for gene delivery. *Proc. Natl. Acad. Sci. U. S. A.* 96, 5177-5181.
- Goren, D., Horowitz, A.T., Tzemach, D., Tarshish, M., Zalipsky, S., Gabizon, A., 2000. Nuclear delivery of doxorubicin via folate-targeted liposomes with bypass of multidrug-resistance efflux pump. *Clin. Cancer Res.* 6, 1949-1957.
- Gou, N., Onnis-Hayden, A., Gu, A.Z., 2010. Mechanistic toxicity assessment of nanomaterials by whole-cell-array stress genes expression analysis. *Environ. Sci. Technol.* 44, 5964-5970.
- Greig, N.H., Genka, S., Daly, E.M., Sweeney, D.J., Rapoport, S.I., 1990. Physicochemical and pharmacokinetic parameters of seven lipophilic chlorambucil esters designed for brain penetration. *Cancer Chemother. Pharmacol.* 25, 311-319.
- Griffiths, G., Nystrom, B., Sable, S.B., Khuller, G.K., 2010. Nanobead-based interventions for the treatment and prevention of tuberculosis. *Nat. Rev. Microbiol.* 8, 827-834.
- Groothuis, D.R., 2000. The blood-brain and blood-tumor barriers: a review of strategies for increasing drug delivery. *Neuro Oncol.* 2, 45-59.
- Gulyaev, A.E., Gelperina, S.E., Skidan, I.N., Antropov, A.S., Kivman, G.Y., Kreuter, J., 1999. Significant transport of doxorubicin into the brain with polysorbate 80-coated nanoparticles. *Pharm. Res.* 16, 1564-1569.
- Gupta, S., Afaq, F., Mukhtar, H., 2001. Selective growth-inhibitory, cell-cycle deregulatory and apoptotic response of apigenin in normal versus human prostate carcinoma cells. *Biochem. Biophys. Res. Commun.* 287, 914-920.
- Hadaczek, P., Yamashita, Y., Mirek, H., Tamas, L., Bohn, M.C., Noble, C., Park, J.W., Bankiewicz, K., 2006. The "perivascular pump" driven by arterial pulsation is a powerful mechanism for the distribution of therapeutic molecules within the brain. *Molecular therapy : the journal of the American Society of Gene Therapy* 14, 69-78.
- Halatsch, M.E., Schmidt, U., Behnke-Mursch, J., Unterberg, A., Wirtz, C.R., 2006. Epidermal growth factor receptor inhibition for the treatment of glioblastoma multiforme and other malignant brain tumours. *Cancer Treat. Rev.* 32, 74-89.
- Harashima, H., Sakata, K., Funato, K., Kiwada, H., 1994. Enhanced hepatic uptake of liposomes through complement activation depending on the size of liposomes. *Pharm. Res.* 11, 402-406.
- Hatanpaa, K.J., Burma, S., Zhao, D., Habib, A.A., 2010. Epidermal growth factor receptor in glioma: signal transduction, neuropathology, imaging, and radioresistance. *Neoplasia* 12, 675-684.

- Hau, P., Fabel, K., Baumgart, U., Rummele, P., Grauer, O., Bock, A., Dietmaier, C., Dietmaier, W., Dietrich, J., Dudel, C., Hubner, F., Jauch, T., Drechsel, E., Kleiter, I., Wismeth, C., Zellner, A., Brawanski, A., Steinbrecher, A., Marienhagen, J., Bogdahn, U., 2004. Pegylated liposomal doxorubicin-efficacy in patients with recurrent high-grade glioma. *Cancer* 100, 1199-1207.
- Hawkins, B.T., Davis, T.P., 2005. The blood-brain barrier/neurovascular unit in health and disease. *Pharmacol. Rev.* 57, 173-185.
- He, C., Hu, Y., Yin, L., Tang, C., Yin, C., 2010. Effects of particle size and surface charge on cellular uptake and biodistribution of polymeric nanoparticles. *Biomaterials* 31, 3657-3666.
- Hegi, M.E., Diserens, A.C., Gorlia, T., Hamou, M.F., de Tribolet, N., Weller, M., Kros, J.M., Hainfellner, J.A., Mason, W., Mariani, L., Bromberg, J.E., Hau, P., Mirimanoff, R.O., Cairncross, J.G., Janzer, R.C., Stupp, R., 2005. MGMT gene silencing and benefit from temozolomide in glioblastoma. *N. Engl. J. Med.* 352, 997-1003.
- Hekmatara, T., Bernreuther, C., Khalansky, A.S., Theisen, A., Weissenberger, J., Matschke, J., Gelperina, S., Kreuter, J., Glatzel, M., 2009. Efficient systemic therapy of rat glioblastoma by nanoparticle-bound doxorubicin is due to antiangiogenic effects. *Clin. Neuropathol.* 28, 153-164.
- Henriksson, R., Malmstrom, A., Bergstrom, P., Bergh, G., Trojanowski, T., Andreasson, L., Blomquist, E., Jonsborg, S., Edekling, T., Salander, P., Brannstrom, T., Bergenheim, A.T., 2006. High-grade astrocytoma treated concomitantly with estramustine and radiotherapy. *J. Neurooncol.* 78, 321-326.
- Herve, F., Ghinea, N., Scherrmann, J.M., 2008. CNS delivery via adsorptive transcytosis. *The AAPS journal* 10, 455-472.
- Heurtault, B., Saulnier, P., Pech, B., Proust, J., Richard, J., Benoit, J., 2000. Lipidic nanocapsules: preparation process and use as Drug Delivery Systems.
- Heurtault, B., Saulnier, P., Pech, B., Proust, J.E., Benoit, J.P., 2002. A novel phase inversion-based process for the preparation of lipid nanocarriers. *Pharm. Res.* 19, 875-880.
- Heurtault, B., Saulnier, P., Pech, B., Venier-Julienne, M.-C., Proust, J.-E., Phan-Tan-Luu, R., Benoit, J.-P., 2003. The influence of lipid nanocapsule composition on their size distribution. *Eur. J. Pharm. Sci.* 18, 55-61.
- Hillard, E., Vessieres, A., Thouin, L., Jaouen, G., Amatore, C., 2005. Ferrocene-mediated proton-coupled electron transfer in a series of ferrocifen-type breast-cancer drug candidates. *Angew. Chem. Int. Ed. Engl.* 45, 285-290.
- Hoarau, D., Delmas, P., David, S., Roux, E., Leroux, J.C., 2004. Novel long-circulating lipid nanocapsules. *Pharm. Res.* 21, 1783-1789.
- Hureaux, J., Lagarce, F., Gagnadoux, F., Rousselet, M.-C., Moal, V., Urban, T., Benoit, J.-P., 2010. Toxicological study and efficacy of blank and paclitaxel-loaded lipid nanocapsules after iv administration in mice. *Pharm. Res.* 27, 421-430.
- Huwyler, J., Wu, D., Pardridge, W.M., 1996. Brain drug delivery of small molecules using immunoliposomes. *Proc. Natl. Acad. Sci. U. S. A.* 93, 14164-14169.
- Huynh, N.T., Passirani, C., Saulnier, P., Benoit, J.P., 2009. Lipid nanocapsules: a new platform for nanomedicine. *Int. J. Pharm.* 379, 201-209.
- Imbesi, F., Marchioni, E., Benericetti, E., Zappoli, F., Galli, A., Corato, M., Ceroni, M., 2006. A randomized phase III study: comparison between intravenous and intraarterial

- ACNU administration in newly diagnosed primary glioblastomas. *Anticancer Res.* 26, 553-558.
- Immordino, M.L., Dosio, F., Cattel, L., 2006. Stealth liposomes: review of the basic science, rationale, and clinical applications, existing and potential. *International journal of nanomedicine* 1, 297-315.
- Jaouen, G., Top, S., 2014. The ferrocifen family as potent and selective antitumor compounds: mechanisms of action. Wiley: Hoboken, NJ, USA, pp. 563-580.
- Jaouen, G., Top, S., Vessi res, A., Pigeon, P., Leclercq, G., Laios, I., 2001. First anti-oestrogen in the cyclopentadienyl rhenium tricarbonyl series. Synthesis and study of antiproliferative effects. *Chemical Communications*, 383-384.
- Jaouen, G., Vessieres, A., Top, S., 2015. Ferrocifen type anti cancer drugs. *Chem. Soc. Rev.* 44, 8802-8817.
- Jeong, Y.-I., Jin, S.-G., Kim, I.-Y., Pei, J., Wen, M., Jung, T.-Y., Moon, K.-S., Jung, S., 2010. Doxorubicin-incorporated nanoparticles composed of poly (ethylene glycol)-grafted carboxymethyl chitosan and antitumor activity against glioma cells in vitro. *Colloids and Surfaces B: Biointerfaces* 79, 149-155.
- Jestin, E., Mougin-Degraef, M., Faivre-Chauvet, A., Remaud-Le Saec, P., Hindre, F., Benoit, J.P., Chatal, J.F., Barbet, J., Gestin, J.F., 2007. Radiolabeling and targeting of lipidic nanocapsules for applications in radioimmunotherapy. *Q. J. Nucl. Med. Mol. Imaging* 51, 51-60.
- Ji, H., Lu, Z., 2013. The role of protein kinase CK2 in glioblastoma development. *Clin. Cancer Res.* 19, 6335-6337.
- Jiang, W., Kim, B.Y., Rutka, J.T., Chan, W.C., 2008. Nanoparticle-mediated cellular response is size-dependent. *Nature Nanotechnology* 3, 145-150.
- Juillerat-Jeanneret, L., 2008. The targeted delivery of cancer drugs across the blood-brain barrier: chemical modifications of drugs or drug-nanoparticles? *Drug discovery today* 13, 1099-1106.
- Jung, T., Kamm, W., Breitenbach, A., Kaiserling, E., Xiao, J.X., Kissel, T., 2000. Biodegradable nanoparticles for oral delivery of peptides: is there a role for polymers to affect mucosal uptake? *Eur. J. Pharm. Biopharm.* 50, 147-160.
- Kabanov, A.V., Batrakova, E.V., Miller, D.W., 2003. Pluronic® block copolymers as modulators of drug efflux transporter activity in the blood–brain barrier. *Advanced Drug Delivery Reviews* 55, 151-164.
- Kaneda, Y., 2000. Virosomes: evolution of the liposome as a targeted drug delivery system. *Adv. Drug Deliv. Rev.* 43, 197-205.
- Kanu, O.O., Mehta, A., Di, C., Lin, N., Bortoff, K., Bigner, D.D., Yan, H., Adamson, D.C., 2009. Glioblastoma multiforme: a review of therapeutic targets. *Expert Opin. Ther. Targets* 13, 701-718.
- Karim, R., Palazzo, C., Evrard, B., Piel, G., 2016. Nanocarriers for the treatment of glioblastoma multiforme: Current state-of-the-art. *J. Control. Release* 227, 23-37.
- Kelland, L., 2007. The resurgence of platinum-based cancer chemotherapy. *Nat. Rev. Cancer* 7, 573-584.
- Kemper, E.M., van Zandbergen, A.E., Cleypool, C., Mos, H.A., Boogerd, W., Beijnen, J.H., van Tellingen, O., 2003. Increased penetration of paclitaxel into the brain by inhibition of P-glycoprotein. *Clin. Cancer Res.* 9, 2849-2855.

- Kim, T.H., Jiang, H.H., Youn, Y.S., Park, C.W., Tak, K.K., Lee, S., Kim, H., Jon, S., Chen, X., Lee, K.C., 2011. Preparation and characterization of water-soluble albumin-bound curcumin nanoparticles with improved antitumor activity. *Int. J. Pharm.* 403, 285-291.
- Klibanov, A.L., Maruyama, K., Beckerleg, A.M., Torchilin, V.P., Huang, L., 1991. Activity of amphipathic poly (ethylene glycol) 5000 to prolong the circulation time of liposomes depends on the liposome size and is unfavorable for immunoliposome binding to target. *Biochim. Biophys. Acta* 1062, 142-148.
- Kloosterhof, N.K., Bralten, L.B., Dubbink, H.J., French, P.J., van den Bent, M.J., 2011. Isocitrate dehydrogenase-1 mutations: a fundamentally new understanding of diffuse glioma? *Lancet Oncol.* 12, 83-91.
- Koo, Y.E., Reddy, G.R., Bhojani, M., Schneider, R., Philbert, M.A., Rehemtulla, A., Ross, B.D., Kopelman, R., 2006. Brain cancer diagnosis and therapy with nanoplatforms. *Advanced drug delivery reviews* 58, 1556-1577.
- Korfiatis, P., Erickson, B., 2014. The basics of diffusion and perfusion imaging in brain tumors. *Appl. Radiol.* 43, 22-29.
- Koukourakis, M.I., Koukouraki, S., Fezoulidis, I., Kelekis, N., Kyrias, G., Archimandritis, S., Karkavitsas, N., 2000. High intratumoural accumulation of stealth® liposomal doxorubicin (Caelyx®) in glioblastomas and in metastatic brain tumours. *Br. J. Cancer* 83, 1281-1286.
- Krauze, M.T., Saito, R., Noble, C., Tamas, M., Bringas, J., Park, J.W., Berger, M.S., Bankiewicz, K., 2005. Reflux-free cannula for convection-enhanced high-speed delivery of therapeutic agents. *Journal of neurosurgery* 103, 923-929.
- Kreuter, J., 2007. Nanoparticles-a historical perspective. *Int. J. Pharm.* 331, 1-10.
- Kreuter, J., Petrov, V., Kharkevich, D., Alyautdin, R., 1997. Influence of the type of surfactant on the analgesic effects induced by the peptide dalargin after its delivery across the blood-brain barrier using surfactant-coated nanoparticles. *J. Control. Release* 49, 81-87.
- Kumthekar, P., 2017. NCT03020017: NU-0129 in Treating Patients With Recurrent Glioblastoma or Gliosarcoma Undergoing Surgery. *ClinicalTrials.gov*.
- Kuntner, C., Bankstahl, J.P., Bankstahl, M., Stanek, J., Wanek, T., Stundner, G., Karch, R., Brauner, R., Meier, M., Ding, X., Muller, M., Loscher, W., Langer, O., 2010. Dose-response assessment of tariquidar and elacridar and regional quantification of P-glycoprotein inhibition at the rat blood-brain barrier using (R)-[(11)C]verapamil PET. *Eur. J. Nucl. Med. Mol. Imaging* 37, 942-953.
- Lacoeuille, F., Hindré, F., Moal, F., Roux, J., Passirani, C., Couturier, O., Calès, P., Le Jeune, J.-J., Lamprecht, A., Benoit, J.-P., 2007. In vivo evaluation of lipid nanocapsules as a promising colloidal carrier for paclitaxel. *Int. J. Pharm.* 344, 143-149.
- Lacroix, M., Abi-Said, D., Fournay, D.R., Gokaslan, Z.L., Shi, W., DeMonte, F., Lang, F.F., McCutcheon, I.E., Hassenbusch, S.J., Holland, E., Hess, K., Michael, C., Miller, D., Sawaya, R., 2001. A multivariate analysis of 416 patients with glioblastoma multiforme: prognosis, extent of resection, and survival. *J. Neurosurg.* 95, 190-198.
- Laine, A.-L., Clavreul, A., Rousseau, A., Tétaud, C., Vessieres, A., Garcion, E., Jaouen, G., Aubert, L., Guilbert, M., Benoit, J.-P., 2014. Inhibition of ectopic glioma tumor growth by a potent ferrocenyl drug loaded into stealth lipid nanocapsules. *Nanomedicine* 10, 1667-1677.

- Laine, A.L., Huynh, N.T., Clavreul, A., Balzeau, J., Bejaud, J., Vessieres, A., Benoit, J.P., Eyer, J., Passirani, C., 2012. Brain tumour targeting strategies via coated ferrociphenol lipid nanocapsules. *Eur. J. Pharm. Biopharm.* 81, 690-693.
- Lamprecht, A., Benoit, J.P., 2006. Etoposide nanocarriers suppress glioma cell growth by intracellular drug delivery and simultaneous P-glycoprotein inhibition. *J. Control. Release* 112, 208-213.
- Lamprecht, A., Bouligand, Y., Benoit, J.P., 2002. New lipid nanocapsules exhibit sustained release properties for amiodarone. *J. Control. Release* 84, 59-68.
- Lamprecht, A., Saumet, J.-L., Roux, J., Benoit, J.-P., 2004. Lipid nanocarriers as drug delivery system for ibuprofen in pain treatment. *Int. J. Pharm.* 278, 407-414.
- Lasic, D.D., Martin, F.J., Gabizon, A., Huang, S.K., Papahadjopoulos, D., 1991. Sterically stabilized liposomes: a hypothesis on the molecular origin of the extended circulation times. *Biochim. Biophys. Acta* 1070, 187-192.
- Laske, D.W., Morrison, P.F., Lieberman, D.M., Corthesy, M.E., Reynolds, J.C., Stewart-Henney, P.A., Koong, S.S., Cummins, A., Paik, C.H., Oldfield, E.H., 1997. Chronic interstitial infusion of protein to primate brain: determination of drug distribution and clearance with single-photon emission computerized tomography imaging. *Journal of neurosurgery* 87, 586-594.
- Lee, J.H., Zhou, H.Y., Cho, S.Y., Kim, Y.S., Lee, Y.S., Jeong, C.S., 2007. Anti-inflammatory mechanisms of apigenin: inhibition of cyclooxygenase-2 expression, adhesion of monocytes to human umbilical vein endothelial cells, and expression of cellular adhesion molecules. *Arch. Pharm. Res.* 30, 1318-1327.
- Li, B., Robinson, D.H., Birt, D.F., 1997. Evaluation of properties of apigenin and [³H]apigenin and analytic method development. *J. Pharm. Sci.* 86, 721-725.
- Li, K., Liu, B., 2012. Polymer encapsulated conjugated polymer nanoparticles for fluorescence bioimaging. *J. Mater. Chem.* 22, 1257-1264.
- Li, Z.D., Hu, X.W., Wang, Y.T., Fang, J., 2009. Apigenin inhibits proliferation of ovarian cancer A2780 cells through Id1. *FEBS Lett.* 583, 1999-2003.
- Lian, T., Ho, R.J., 2001. Trends and developments in liposome drug delivery systems. *J. Pharm. Sci.* 90, 667-680.
- Lim, K.J., Bisht, S., Bar, E.E., Maitra, A., Eberhart, C.G., 2011. A polymeric nanoparticle formulation of curcumin inhibits growth, clonogenicity and stem-like fraction in malignant brain tumors. *Cancer Biol. Ther.* 11, 464-473.
- Lin, C.J., Lin, Y.L., Luh, F., Yen, Y., Chen, R.M., 2016. Preclinical effects of CRLX101, an investigational camptothecin-containing nanoparticle drug conjugate, on treating glioblastoma multiforme via apoptosis and antiangiogenesis. *Oncotarget* 7, 42408-42421.
- Lin, F., de Gooijer, M.C., Hanekamp, D., Brandsma, D., Beijnen, J.H., van Tellingen, O., 2013. Targeting core (mutated) pathways of high-grade gliomas: challenges of intrinsic resistance and drug efflux. *CNS Oncology* 2, 271-288.
- Litman, T., Brangi, M., Hudson, E., Fetsch, P., Abati, A., Ross, D.D., Miyake, K., Resau, J.H., Bates, S.E., 2000. The multidrug-resistant phenotype associated with overexpression of the new ABC half-transporter, MXR (ABCG2). *J. Cell Sci.* 113 (Pt 11), 2011-2021.
- Liu, J., Cao, X.C., Xiao, Q., Quan, M.F., 2015. Apigenin inhibits HeLa sphere-forming cells through inactivation of casein kinase 2alpha. *Mol Med Rep* 11, 665-669.

- Liu, X., Howard, K.A., Dong, M., Andersen, M.O., Rahbek, U.L., Johnsen, M.G., Hansen, O.C., Besenbacher, F., Kjems, J., 2007. The influence of polymeric properties on chitosan/siRNA nanoparticle formulation and gene silencing. *Biomaterials* 28, 1280-1288.
- Liu, Y., Lu, W., 2012. Recent advances in brain tumor-targeted nano-drug delivery systems. *Expert opinion on drug delivery* 9, 671-686.
- Lolli, G., Cozza, G., Mazzorana, M., Tibaldi, E., Cesaro, L., Donella-Deana, A., Meggio, F., Venerando, A., Franchin, C., Sarno, S., Battistutta, R., Pinna, L.A., 2012. Inhibition of protein kinase CK2 by flavonoids and tyrphostins. A structural insight. *Biochemistry* 51, 6097-6107.
- Losman, J.A., Kaelin, W.G., Jr., 2013. What a difference a hydroxyl makes: mutant IDH, (R)-2-hydroxyglutarate, and cancer. *Genes Dev.* 27, 836-852.
- Louis, D.N., Ohgaki, H., Wiestler, O.D., Cavenee, W.K., Burger, P.C., Jouvet, A., Scheithauer, B.W., Kleihues, P., 2007. The 2007 WHO classification of tumours of the central nervous system. *Acta Neuropathol.* 114, 97-109.
- Louis, D.N., Perry, A., Reifenberger, G., von Deimling, A., Figarella-Branger, D., Cavenee, W.K., Ohgaki, H., Wiestler, O.D., Kleihues, P., Ellison, D.W., 2016. The 2016 World Health Organization Classification of Tumors of the Central Nervous System: a summary. *Acta Neuropathol.* 131, 803-820.
- Lu, H.F., Chie, Y.J., Yang, M.S., Lee, C.S., Fu, J.J., Yang, J.S., Tan, T.W., Wu, S.H., Ma, Y.S., Ip, S.W., Chung, J.G., 2010. Apigenin induces caspase-dependent apoptosis in human lung cancer A549 cells through Bax- and Bcl-2-triggered mitochondrial pathway. *Int. J. Oncol.* 36, 1477-1484.
- Lu, W., Wan, J., She, Z., Jiang, X., 2007. Brain delivery property and accelerated blood clearance of cationic albumin conjugated pegylated nanoparticle. *J. Control. Release* 118, 38-53.
- Lu, W., Zhang, Y., Tan, Y.Z., Hu, K.L., Jiang, X.G., Fu, S.K., 2005. Cationic albumin-conjugated pegylated nanoparticles as novel drug carrier for brain delivery. *J. Control. Release* 107, 428-448.
- Lukowski, G., Müller, R., Müller, B., Dittgen, M., 1992. Acrylic acid copolymer nanoparticles for drug delivery: I. Characterization of the surface properties relevant for in vivo organ distribution. *Int. J. Pharm.* 84, 23-31.
- Lynch, I., Cedervall, T., Lundqvist, M., Cabaleiro-Lago, C., Linse, S., Dawson, K.A., 2007. The nanoparticle-protein complex as a biological entity; a complex fluids and surface science challenge for the 21st century. *Adv. Colloid Interface Sci.* 134-135, 167-174.
- Madhankumar, A., Slagle-Webb, B., Mrowczynski, O., Payne, R., Zacharia, B., Rizk, E., Connor, J., 2016. EXTH-32. Combination of Ras inhibitor and doxorubicin in liposomes enhances therapeutic efficacy in glioblastoma mouse model. *Neuro Oncol.* 18, vi66-vi66.
- Madhankumar, A.B., Slagle-Webb, B., Mintz, A., Sheehan, J.M., Connor, J.R., 2006. Interleukin-13 receptor-targeted nanovesicles are a potential therapy for glioblastoma multiforme. *Mol. Cancer Ther.* 5, 3162-3169.
- Maher, F., Vannucci, S.J., Simpson, I.A., 1994. Glucose transporter proteins in brain. *FASEB J.* 8, 1003-1011.
- Matsuura, M., Yamazaki, Y., Sugiyama, M., Kondo, M., Ori, H., Nango, M., Oku, N., 2003. Polycation liposome-mediated gene transfer in vivo. *Biochim. Biophys. Acta* 1612, 136-143.

- Matter, K., Balda, M.S., 2003. Signalling to and from tight junctions. *Nat. Rev. Mol. Cell Biol.* 4, 225-236.
- McFarland, B.C., Ma, J.Y., Langford, C.P., Gillespie, G.Y., Yu, H., Zheng, Y., Nozell, S.E., Huszar, D., Benveniste, E.N., 2011. Therapeutic potential of AZD1480 for the treatment of human glioblastoma. *Mol. Cancer Ther.* 10, 2384-2393.
- Middleton, E., Jr., Kandaswami, C., Theoharides, T.C., 2000. The effects of plant flavonoids on mammalian cells: implications for inflammation, heart disease, and cancer. *Pharmacol. Rev.* 52, 673-751.
- Mirabelli, C.K., Johnson, R.K., Sung, C.M., Faucette, L., Muirhead, K., Crooke, S.T., 1985. Evaluation of the *in vivo* antitumor activity and *in vitro* cytotoxic properties of auranofin, a coordinated gold compound, in murine tumor models. *Cancer Res.* 45, 32-39.
- Myhrstad, M.C., Carlsen, H., Nordstrom, O., Blomhoff, R., Moskaug, J.O., 2002. Flavonoids increase the intracellular glutathione level by transactivation of the gamma-glutamylcysteine synthetase catalytical subunit promoter. *Free Radic. Biol. Med.* 32, 386-393.
- Myllynen, P., 2009. Nanotoxicology: damaging DNA from a distance. *Nature Nanotechnology* 4, 795-796.
- Neeves, K.B., Sawyer, A.J., Foley, C.P., Saltzman, W.M., Olbricht, W.L., 2007. Dilation and degradation of the brain extracellular matrix enhances penetration of infused polymer nanoparticles. *Brain research* 1180, 121-132.
- Nobuto, H., Sugita, T., Kubo, T., Shimose, S., Yasunaga, Y., Murakami, T., Ochi, M., 2004. Evaluation of systemic chemotherapy with magnetic liposomal doxorubicin and a dipole external electromagnet. *Int. J. Cancer* 109, 627-635.
- Nyström, A.M., Fadeel, B., 2012. Safety assessment of nanomaterials: implications for nanomedicine. *J. Control. Release* 161, 403-408.
- O'Kane, R.L., Hawkins, R.A., 2003. Na⁺-dependent transport of large neutral amino acids occurs at the abluminal membrane of the blood-brain barrier. *Am. J. Physiol. Endocrinol. Metab.* 285, E1167-1173.
- Oja, C.D., Semple, S.C., Chonn, A., Cullis, P.R., 1996. Influence of dose on liposome clearance: critical role of blood proteins. *Biochim. Biophys. Acta* 1281, 31-37.
- Olivier, J.C., 2005. Drug transport to brain with targeted nanoparticles. *NeuroRx* 2, 108-119.
- Ostrom, Q.T., Gittleman, H., Farah, P., Ondracek, A., Chen, Y., Wolinsky, Y., Stroup, N.E., Kruchko, C., Barnholtz-Sloan, J.S., 2013. CBTRUS statistical report: Primary brain and central nervous system tumors diagnosed in the United States in 2006-2010. *Neuro Oncol.* 15 Suppl 2, ii1-56.
- Ostrom, Q.T., Gittleman, H., Xu, J., Kromer, C., Wolinsky, Y., Kruchko, C., Barnholtz-Sloan, J.S., 2016. CBTRUS Statistical Report: Primary Brain and Other Central Nervous System Tumors Diagnosed in the United States in 2009-2013. *Neuro Oncol.* 18, v1-v75.
- Paillard, A., Hindre, F., Vignes-Colombeix, C., Benoit, J.P., Garcion, E., 2010. The importance of endo-lysosomal escape with lipid nanocapsules for drug subcellular bioavailability. *Biomaterials* 31, 7542-7554.
- Pakunlu, R.I., Wang, Y., Saad, M., Khandare, J.J., Starovoytov, V., Minko, T., 2006. *In vitro* and *in vivo* intracellular liposomal delivery of antisense oligonucleotides and anticancer drug. *J. Control. Release* 114, 153-162.

- Panté, N., Kann, M., 2002. Nuclear pore complex is able to transport macromolecules with diameters of ~ 39 nm. *Mol. Biol. Cell* 13, 425-434.
- Parajuli, P., Joshee, N., Rimando, A.M., Mittal, S., Yadav, A.K., 2009. In vitro antitumor mechanisms of various *Scutellaria* extracts and constituent flavonoids. *Planta Med.* 75, 41-48.
- Pardridge, W.M., 1999. Non-invasive drug delivery to the human brain using endogenous blood-brain barrier transport systems. *Pharm. Sci. Technol. Today* 2, 49-59.
- Pardridge, W.M., 2001. Crossing the blood-brain barrier: are we getting it right? *Drug discovery today* 6, 1-2.
- Pardridge, W.M., 2002. Drug and gene delivery to the brain: the vascular route. *Neuron* 36, 555-558.
- Pardridge, W.M., 2012. Drug transport across the blood-brain barrier. *J. Cereb. Blood Flow Metab.* 32, 1959-1972.
- Pardridge, W.M., Eisenberg, J., Yang, J., 1985. Human blood-brain barrier insulin receptor. *J. Neurochem.* 44, 1771-1778.
- Park, J.H., Kwon, S., Nam, J.O., Park, R.W., Chung, H., Seo, S.B., Kim, I.S., Kwon, I.C., Jeong, S.Y., 2004. Self-assembled nanoparticles based on glycol chitosan bearing 5 β -cholanic acid for RGD peptide delivery. *J. Control. Release* 95, 579-588.
- Park, S.H., Oh, S.G., Mun, J.Y., Han, S.S., 2006. Loading of gold nanoparticles inside the DPPC bilayers of liposome and their effects on membrane fluidities. *Colloids Surf B Biointerfaces* 48, 112-118.
- Patel, D., Shukla, S., Gupta, S., 2007. Apigenin and cancer chemoprevention: progress, potential and promise (review). *Int. J. Oncol.* 30, 233-245.
- Pereverzeva, E., Treschalin, I., Bodyagin, D., Maksimenko, O., Langer, K., Dreis, S., Asmussen, B., Kreuter, J., Gelperina, S., 2007. Influence of the formulation on the tolerance profile of nanoparticle-bound doxorubicin in healthy rats: focus on cardio- and testicular toxicity. *Int. J. Pharm.* 337, 346-356.
- Perry, M.C., Demeule, M., Regina, A., Moudmjian, R., Beliveau, R., 2010. Curcumin inhibits tumor growth and angiogenesis in glioblastoma xenografts. *Mol. Nutr. Food Res.* 54, 1192-1201.
- Petri, B., Bootz, A., Khalansky, A., Hekmatara, T., Muller, R., Uhl, R., Kreuter, J., Gelperina, S., 2007. Chemotherapy of brain tumour using doxorubicin bound to surfactant-coated poly(butyl cyanoacrylate) nanoparticles: revisiting the role of surfactants. *J. Control. Release* 117, 51-58.
- Pi, Z., Chen, X., Li, F., Li, Y., Chen, Y., Huang, W., Hu, Y., Shen, Y., Yan, F., Zheng, H., 2016. Therapeutic effect of paclitaxel liposomes delivered by ultrasound with microbubbles on nude mice bearing intracranial glioblastoma xenografts monitored by bioluminescence imaging, *Ultrasonics Symposium (IUS), 2016 IEEE International. IEEE*, pp. 1-4.
- Plate, K.H., Scholz, A., Dumont, D.J., 2012. Tumor angiogenesis and anti-angiogenic therapy in malignant gliomas revisited. *Acta Neuropathol.* 124, 763-775.
- Ponka, P., Lok, C.N., 1999. The transferrin receptor: role in health and disease. *Int. J. Biochem. Cell Biol.* 31, 1111-1137.
- Prados, M.D., Schold, S.J.S., Fine, H.A., Jaeckle, K., Hochberg, F., Mechtler, L., Fetell, M.R., Phuphanich, S., Feun, L., Janus, T.J., Ford, K., Graney, W., 2003. A randomized, double-blind, placebo-controlled, phase 2 study of RMP-7 in combination with carboplatin

- administered intravenously for the treatment of recurrent malignant glioma. *Neuro Oncol.* 5, 96-103.
- Purves, D., Augustine, G.J., Fitzpatrick, D., Katz, L.C., LaMantia, A.-S., McNamara, J.O., Williams, S.M., eds., 2001. *Neuroscience*, 2nd ed. Sinauer Associates, Sunderland (MA).
- Qin, Y., Chen, H., Yuan, W., Kuai, R., Zhang, Q., Xie, F., Zhang, L., Zhang, Z., Liu, J., He, Q., 2011. Liposome formulated with TAT-modified cholesterol for enhancing the brain delivery. *Int. J. Pharm.* 419, 85-95.
- Rapoport, S.I., 1970. Effect of concentrated solutions on blood-brain barrier. *Am. J. Physiol.* 219, 270-274.
- Re, F., Cambianica, I., Zona, C., Sesana, S., Gregori, M., Rigolio, R., La Ferla, B., Nicotra, F., Forloni, G., Cagnotto, A., Salmona, M., Masserini, M., Sancini, G., 2011. Functionalization of liposomes with ApoE-derived peptides at different density affects cellular uptake and drug transport across a blood-brain barrier model. *Nanomedicine* 7, 551-559.
- Reedijk, J., Lohman, P.H., 1985. Cisplatin: synthesis, antitumour activity and mechanism of action. *Pharm. Weekbl. Sci.* 7, 173-180.
- Regoli, D., Barabe, J., 1980. Pharmacology of bradykinin and related kinins. *Pharmacol. Rev.* 32, 1-46.
- Reiber, H., 2001. Dynamics of brain-derived proteins in cerebrospinal fluid. *Clin. Chim. Acta* 310, 173-186.
- Robert, M., Wastie, M., 2008. Glioblastoma multiforme: a rare manifestation of extensive liver and bone metastases. *Biomed Imaging Interv J* 4, e3.
- Romanova, D., Vachalkova, A., Cipak, L., Ovesna, Z., Rauko, P., 2001. Study of antioxidant effect of apigenin, luteolin and quercetin by DNA protective method. *Neoplasma* 48, 104-107.
- Rosenberg, B., VanCamp, L., Trosko, J.E., Mansour, V.H., 1969. Platinum compounds: a new class of potent antitumour agents. *Nature* 222, 385-386.
- Ruela-de-Sousa, R.R., Fuhler, G.M., Blom, N., Ferreira, C.V., Aoyama, H., Peppelenbosch, M.P., 2010. Cytotoxicity of apigenin on leukemia cell lines: implications for prevention and therapy. *Cell Death Dis.* 1, e19.
- Saija, A., Princi, P., Trombetta, D., Lanza, M., De Pasquale, A., 1997. Changes in the permeability of the blood-brain barrier following sodium dodecyl sulphate administration in the rat. *Exp. Brain Res.* 115, 546-551.
- Sakane, T., Tanaka, C., Yamamoto, A., Hashida, M., Sezaki, H., Ueda, H., Takagi, H., 1989. The effect of polysorbate 80 on brain uptake and analgesic effect of D-kyotorphin. *Int. J. Pharm.* 57, 77-83.
- Sampson, J.H., Akabani, G., Friedman, A.H., Bigner, D., Kunwar, S., Berger, M.S., Bankiewicz, K.S., 2006. Comparison of intratumoral bolus injection and convection-enhanced delivery of radiolabeled antitenascin monoclonal antibodies. *Neurosurg. Focus* 20, E14.
- Sanchez De Juan, B., Von Briesen, H., Gelperina, S.E., Kreuter, J., 2006. Cytotoxicity of doxorubicin bound to poly (butyl cyanoacrylate) nanoparticles in rat glioma cell lines using different assays. *J. Drug Target.* 14, 614-622.
- Scherrmann, J.M., 2002. Drug delivery to brain via the blood-brain barrier. *Vascul. Pharmacol.* 38, 349-354.

- Schlageter, K.E., Molnar, P., Lapin, G.D., Groothuis, D.R., 1999. Microvessel organization and structure in experimental brain tumors: microvessel populations with distinctive structural and functional properties. *Microvasc. Res.* 58, 312-328.
- Schulte, A., Liffers, K., Kathagen, A., Riethdorf, S., Zapf, S., Merlo, A., Kolbe, K., Westphal, M., Lamszus, K., 2013. Erlotinib resistance in EGFR-amplified glioblastoma cells is associated with upregulation of EGFRvIII and PI3Kp110delta. *Neuro Oncol.* 15, 1289-1301.
- Schwartz, S.G., Scott, I.U., Flynn, H.W., Jr., Stewart, M.W., 2014. Drug delivery techniques for treating age-related macular degeneration. *Expert opinion on drug delivery* 11, 61-68.
- Sehati, N., Liao, L.M., 2003. Adjuvant treatment for gliomas. *Contemp. Neurosurg.* 25, 1-9.
- Seldin, D.C., Landesman-Bollag, E., Farago, M., Currier, N., Lou, D., Dominguez, I., 2005. CK2 as a positive regulator of Wnt signalling and tumorigenesis. *Mol. Cell. Biochem.* 274, 63-67.
- Senior, J., Crawley, J.C., Gregoriadis, G., 1985. Tissue distribution of liposomes exhibiting long half-lives in the circulation after intravenous injection. *Biochim. Biophys. Acta* 839, 1-8.
- Shah, N., Chaudhari, K., Dantuluri, P., Murthy, R.S., Das, S., 2009. Paclitaxel-loaded PLGA nanoparticles surface modified with transferrin and Pluronic((R))P85, an in vitro cell line and in vivo biodistribution studies on rat model. *J. Drug Target.* 17, 533-542.
- Sharma, A., Sharma, U.S., 1997. Liposomes in drug delivery: progress and limitations. *Int. J. Pharm.* 154, 123-140.
- Sharma, A., Straubinger, N.L., Straubinger, R.M., 1993. Modulation of human ovarian tumor cell sensitivity to N-(phosphonacetyl)-L-aspartate (PALA) by liposome drug carriers. *Pharm. Res.* 10, 1434-1441.
- Sharom, F.J., 2011. The P-glycoprotein multidrug transporter. *Essays Biochem.* 50, 161-178.
- Sheikov, N., McDannold, N., Vykhodtseva, N., Jolesz, F., Hynynen, K., 2004. Cellular mechanisms of the blood-brain barrier opening induced by ultrasound in presence of microbubbles. *Ultrasound Med. Biol.* 30, 979-989.
- Shenoy, D., Little, S., Langer, R., Amiji, M., 2005. Poly(ethylene oxide)-modified poly(beta-amino ester) nanoparticles as a pH-sensitive system for tumor-targeted delivery of hydrophobic drugs: part 2. In vivo distribution and tumor localization studies. *Pharm. Res.* 22, 2107-2114.
- Shi, M., Fortin, D., Paquette, B., Sanche, L., 2016. Convection-enhancement delivery of liposomal formulation of oxaliplatin shows less toxicity than oxaliplatin yet maintains a similar median survival time in F98 glioma-bearing rat model. *Invest. New Drugs* 34, 269-276.
- Sidransky, D., Mikkelsen, T., Schwechheimer, K., Rosenblum, M.L., Cavanee, W., Vogelstein, B., 1992. Clonal expansion of p53 mutant cells is associated with brain tumour progression. *Nature* 355, 846-847.
- Siegel, T., Rubinstein, R., Bokstein, F., Schwartz, A., Lossos, A., Shalom, E., Chisin, R., Gomori, J.M., 2000. In vivo assessment of the window of barrier opening after osmotic blood-brain barrier disruption in humans. *J. Neurosurg.* 92, 599-605.

- Simpson, J.R., Horton, J., Scott, C., Curran, W.J., Rubin, P., Fischbach, J., Isaacson, S., Rotman, M., Asbell, S.O., Nelson, J.S., et al., 1993. Influence of location and extent of surgical resection on survival of patients with glioblastoma multiforme: results of three consecutive Radiation Therapy Oncology Group (RTOG) clinical trials. *Int. J. Radiat. Oncol. Biol. Phys.* 26, 239-244.
- Song, D.H., Sussman, D.J., Seldin, D.C., 2000. Endogenous protein kinase CK2 participates in Wnt signaling in mammary epithelial cells. *J. Biol. Chem.* 275, 23790-23797.
- Soni, V., Kohli, D., Jain, S., 2005. Transferrin coupled liposomes as drug delivery carriers for brain targeting of 5-florouracil. *J. Drug Target.* 13, 245-250.
- Squire, J.M., Chew, M., Nneji, G., Neal, C., Barry, J., Michel, C., 2001. Quasi-periodic substructure in the microvessel endothelial glycocalyx: a possible explanation for molecular filtering? *J. Struct. Biol.* 136, 239-255.
- Stam, R., 2010. Electromagnetic fields and the blood-brain barrier. *Brain research reviews* 65, 80-97.
- Steiniger, S.C., Kreuter, J., Khalansky, A.S., Skidan, I.N., Bobruskin, A.I., Smirnova, Z.S., Severin, S.E., Uhl, R., Kock, M., Geiger, K.D., Gelperina, S.E., 2004. Chemotherapy of glioblastoma in rats using doxorubicin-loaded nanoparticles. *Int. J. Cancer* 109, 759-767.
- Stewart, L.A., 2002. Chemotherapy in adult high-grade glioma: a systematic review and meta-analysis of individual patient data from 12 randomised trials. *Lancet* 359, 1011-1018.
- Stummer, W., Reulen, H.J., Meinel, T., Pichlmeier, U., Schumacher, W., Tonn, J.C., Rohde, V., Oppel, F., Turowski, B., Woiciechowsky, C., Franz, K., Pietsch, T., Group, A.L.-G.S., 2008. Extent of resection and survival in glioblastoma multiforme: identification of and adjustment for bias. *Neurosurgery* 62, 564-576; discussion 564-576.
- Stump, T.A., Santee, B.N., Williams, L.P., Kunze, R.A., Heinze, C.E., Huseman, E.D., Gryka, R.J., Simpson, D.S., Amos, S., 2017. The antiproliferative and apoptotic effects of apigenin on glioblastoma cells. *J. Pharm. Pharmacol.*
- Stupp, R., Mason, W.P., van den Bent, M.J., Weller, M., Fisher, B., Taphoorn, M.J., Belanger, K., Brandes, A.A., Marosi, C., Bogdahn, U., Curschmann, J., Janzer, R.C., Ludwin, S.K., Gorlia, T., Allgeier, A., Lacombe, D., Cairncross, J.G., Eisenhauer, E., Mirimanoff, R.O., 2005. Radiotherapy plus concomitant and adjuvant temozolomide for glioblastoma. *N. Engl. J. Med.* 352, 987-996.
- Sudimack, J.J., Guo, W., Tjarks, W., Lee, R.J., 2002. A novel pH-sensitive liposome formulation containing oleyl alcohol. *Biochim. Biophys. Acta* 1564, 31-37.
- Top, S., Tang, J., Vessieres, A., Carrez, D., Provot, C., Jaouen, G., 1996. Ferrocenyl hydroxytamoxifen: a prototype for a new range of oestradiol receptor site-directed cytotoxics. *Chemical Communications*, 955-956.
- Top, S., Vessieres, A., Leclercq, G., Quivy, J., Tang, J., Vaissermann, J., Huche, M., Jaouen, G., 2003. Synthesis, biochemical properties and molecular modelling studies of organometallic specific estrogen receptor modulators (SERMs), the ferrocifens and hydroxyferrocifens: evidence for an antiproliferative effect of hydroxyferrocifens on both hormone-dependent and hormone-independent breast cancer cell lines. *Chemistry (Easton)* 9, 5223-5236.

- Top, S., Vessieres, A., Pigeon, P., Rager, M.N., Huche, M., Salomon, E., Cabestaing, C., Vaissermann, J., Jaouen, G., 2004. Selective estrogen-receptor modulators (SERMs) in the cyclopentadienylrhodium tricarbonyl series: synthesis and biological behaviour. *Chembiochem* 5, 1104-1113.
- Torchilin, V.P., 1994. Immunoliposomes and PEGylated immunoliposomes: possible use for targeted delivery of imaging agents. *Immunomethods* 4, 244-258.
- Torchilin, V.P., 1996. Liposomes as delivery agents for medical imaging. *Mol. Med. Today* 2, 242-249.
- Torchilin, V.P., 1997. Surface-modified liposomes in gamma-and MR-imaging. *Adv. Drug Deliv. Rev.* 24, 301-313.
- Torchilin, V.P., 2005. Recent advances with liposomes as pharmaceutical carriers. *Nature reviews. Drug discovery* 4, 145-160.
- Torkin, R., Lavoie, J.F., Kaplan, D.R., Yeager, H., 2005. Induction of caspase-dependent, p53-mediated apoptosis by apigenin in human neuroblastoma. *Mol. Cancer Ther.* 4, 1-11.
- Tosi, G., Costantino, L., Ruozi, B., Forni, F., Vandelli, M.A., 2008. Polymeric nanoparticles for the drug delivery to the central nervous system. *Expert opinion on drug delivery* 5, 155-174.
- Ulbrich, K., Hekmatara, T., Herbert, E., Kreuter, J., 2009. Transferrin- and transferrin-receptor-antibody-modified nanoparticles enable drug delivery across the blood-brain barrier (BBB). *Eur. J. Pharm. Biopharm.* 71, 251-256.
- Van Dross, R., Xue, Y., Knudson, A., Pelling, J.C., 2003. The chemopreventive bioflavonoid apigenin modulates signal transduction pathways in keratinocyte and colon carcinoma cell lines. *J. Nutr.* 133, 3800S-3804S.
- van Tellingen, O., Yetkin-Arik, B., de Gooijer, M.C., Wesseling, P., Wurdinger, T., de Vries, H.E., 2015. Overcoming the blood-brain tumor barrier for effective glioblastoma treatment. *Drug resistance updates : reviews and commentaries in antimicrobial and anticancer chemotherapy*, 1-12.
- Vessieres, A., Corbet, C., Heldt, J.M., Lories, N., Jouy, N., Laios, I., Leclercq, G., Jaouen, G., Toillon, R.A., 2010. A ferrocenyl derivative of hydroxytamoxifen elicits an estrogen receptor-independent mechanism of action in breast cancer cell lines. *J. Inorg. Biochem.* 104, 503-511.
- Vessieres, A., Top, S., Pigeon, P., Hillard, E., Boubeker, L., Spera, D., Jaouen, G., 2005. Modification of the estrogenic properties of diphenols by the incorporation of ferrocene. Generation of antiproliferative effects in vitro. *J. Med. Chem.* 48, 3937-3940.
- Vila, A., Sanchez, A., Tobio, M., Calvo, P., Alonso, M.J., 2002. Design of biodegradable particles for protein delivery. *J. Control. Release* 78, 15-24.
- Wagner, S., Zensi, A., Wien, S.L., Tschickardt, S.E., Maier, W., Vogel, T., Worek, F., Pietrzik, C.U., Kreuter, J., von Briesen, H., 2012. Uptake mechanism of ApoE-modified nanoparticles on brain capillary endothelial cells as a blood-brain barrier model. *PLoS One* 7, e32568.
- Wang, C.X., Huang, L.S., Hou, L.B., Jiang, L., Yan, Z.T., Wang, Y.L., Chen, Z.L., 2009. Antitumor effects of polysorbate-80 coated gemcitabine polybutylcyanoacrylate nanoparticles in vitro and its pharmacodynamics in vivo on C6 glioma cells of a brain tumor model. *Brain Res.* 1261, 91-99.
- Wang, H., Xu, K., Liu, L., Tan, J.P., Chen, Y., Li, Y., Fan, W., Wei, Z., Sheng, J., Yang, Y.-Y., 2010. The efficacy of self-assembled cationic antimicrobial peptide nanoparticles

- against *Cryptococcus neoformans* for the treatment of meningitis. *Biomaterials* 31, 2874-2881.
- Wang, W., Heideman, L., Chung, C.S., Pelling, J.C., Koehler, K.J., Birt, D.F., 2000. Cell-cycle arrest at G2/M and growth inhibition by apigenin in human colon carcinoma cell lines. *Mol. Carcinog.* 28, 102-110.
- Way, T.D., Kao, M.C., Lin, J.K., 2004. Apigenin induces apoptosis through proteasomal degradation of HER2/neu in HER2/neu-overexpressing breast cancer cells via the phosphatidylinositol 3-kinase/Akt-dependent pathway. *J. Biol. Chem.* 279, 4479-4489.
- Wei, H., Tye, L., Bresnick, E., Birt, D.F., 1990. Inhibitory effect of apigenin, a plant flavonoid, on epidermal ornithine decarboxylase and skin tumor promotion in mice. *Cancer Res.* 50, 499-502.
- Wick, W., Weller, M., van den Bent, M., Stupp, R., 2010. Bevacizumab and recurrent malignant gliomas: a European perspective. *J. Clin. Oncol.* 28, e188-189; author reply e190-182.
- Wilhelm, I., Fazakas, C., Krizbai, I.A., 2011. *In vitro* models of the blood-brain barrier. *Acta Neurobiol. Exp. (Wars.)* 71, 113-128.
- Wohlfart, S., Bernreuther, C., Khalansky, A., Theisen, A., Weissenberger, J., Gelperina, S., Glatzel, M., Kreuter, J., 2009. Increased numbers of injections of doxorubicin bound to nanoparticles lead to enhanced efficacy against rat glioblastoma 101/8. *Journal of Nanoneuroscience* 1, 144-151.
- Wohlfart, S., Gelperina, S., Kreuter, J., 2012. Transport of drugs across the blood-brain barrier by nanoparticles. *J. Control. Release* 161, 264-273.
- Wohlfart, S., Khalansky, A.S., Gelperina, S., Begley, D., Kreuter, J., 2011a. Kinetics of transport of doxorubicin bound to nanoparticles across the blood-brain barrier. *J. Control. Release* 154, 103-107.
- Wohlfart, S., Khalansky, A.S., Gelperina, S., Maksimenko, O., Bernreuther, C., Glatzel, M., Kreuter, J., 2011b. Efficient chemotherapy of rat glioblastoma using doxorubicin-loaded PLGA nanoparticles with different stabilizers. *PLoS One* 6, e19121.
- Wolburg, H., Lippoldt, A., 2002. Tight junctions of the blood-brain barrier: development, composition and regulation. *Vascul. Pharmacol.* 38, 323-337.
- Wolburg, H., Noell, S., Mack, A., Wolburg-Buchholz, K., Fallier-Becker, P., 2009. Brain endothelial cells and the glio-vascular complex. *Cell Tissue Res.* 335, 75-96.
- Woodle, M.C., Matthay, K.K., Newman, M.S., Hidayat, J.E., Collins, L.R., Redemann, C., Martin, F.J., Papahadjopoulos, D., 1992. Versatility in lipid compositions showing prolonged circulation with sterically stabilized liposomes. *Biochim. Biophys. Acta* 1105, 193-200.
- Wu, C., Hansen, S.J., Hou, Q., Yu, J., Zeigler, M., Jin, Y., Burnham, D.R., McNeill, J.D., Olson, J.M., Chiu, D.T., 2011. Design of highly emissive polymer dot bioconjugates for in vivo tumor targeting. *Angew. Chem. Int. Ed. Engl.* 50, 3430-3434.
- Wygodna, Z., Kula, D., Bierzynska-Macyszyn, G., Larysz, D., Jarzab, M., Wlaszczuk, P., Bazowski, P., Wojtacha, M., Rudnik, A., Stepień, T., Kaspera, W., Etmanska, A., Składowski, K., Tarnawski, R., Kokocinska, D., Jarzab, B., 2006. Use of monoclonal anti-EGFR antibody in the radioimmunotherapy of malignant gliomas in the context of EGFR expression in grade III and IV tumors. *Hybridoma* (2005) 25, 125-132.

- Xin, H., Sha, X., Jiang, X., Zhang, W., Chen, L., Fang, X., 2012. Anti-glioblastoma efficacy and safety of paclitaxel-loading Angiopep-conjugated dual targeting PEG-PCL nanoparticles. *Biomaterials* 33, 8167-8176.
- Xu, J., Li, Z., Wang, J., Chen, H., Fang, J.Y., 2014. Combined PTEN Mutation and Protein Expression Associate with Overall and Disease-Free Survival of Glioblastoma Patients. *Transl. Oncol.* 7, 196-205.e191.
- Xu, Y., Shen, M., Li, Y., Sun, Y., Teng, Y., Wang, Y., Duan, Y., 2016. The synergic antitumor effects of paclitaxel and temozolomide co-loaded in mPEG-PLGA nanoparticles on glioblastoma cells. *Oncotarget* 7, 20890-20901.
- Yadav, S., van Vlerken, L.E., Little, S.R., Amiji, M.M., 2009. Evaluations of combination MDR-1 gene silencing and paclitaxel administration in biodegradable polymeric nanoparticle formulations to overcome multidrug resistance in cancer cells. *Cancer Chemother. Pharmacol.* 63, 711-722.
- Yang, F., Jin, C., Jiang, Y., Li, J., Di, Y., Ni, Q., Fu, D., 2011. Liposome based delivery systems in pancreatic cancer treatment: from bench to bedside. *Cancer Treat. Rev.* 37, 633-642.
- Yin, F., Giuliano, A.E., Van Herle, A.J., 1999. Signal pathways involved in apigenin inhibition of growth and induction of apoptosis of human anaplastic thyroid cancer cells (ARO). *Anticancer Res.* 19, 4297-4303.
- Ying, X., Wen, H., Lu, W.L., Du, J., Guo, J., Tian, W., Men, Y., Zhang, Y., Li, R.J., Yang, T.Y., Shang, D.W., Lou, J.N., Zhang, L.R., Zhang, Q., 2010. Dual-targeting daunorubicin liposomes improve the therapeutic efficacy of brain glioma in animals. *J. Control. Release* 141, 183-192.
- Yu, A.S., McCarthy, K.M., Francis, S.A., McCormack, J.M., Lai, J., Rogers, R.A., Lynch, R.D., Schneeberger, E.E., 2005. Knockdown of occludin expression leads to diverse phenotypic alterations in epithelial cells. *Am. J. Physiol. Cell Physiol.* 288, C1231-1241.
- Yuan, F., Leunig, M., Huang, S.K., Berk, D.A., Papahadjopoulos, D., Jain, R.K., 1994. Microvascular permeability and interstitial penetration of sterically stabilized (stealth) liposomes in a human tumor xenograft. *Cancer Res.* 54, 3352-3356.
- Zanellato, I., Heldt, J.-M., Vessieres, A., Jaouen, G., Osella, D., 2009. Antiproliferative effect of ferrocifen drug candidates on malignant pleural mesothelioma cell lines. *Inorganica Chimica Acta* 362, 4037-4042.
- Zanotto-Filho, A., Braganhol, E., Edelweiss, M.I., Behr, G.A., Zanin, R., Schroder, R., Simoes-Pires, A., Battastini, A.M., Moreira, J.C., 2012. The curry spice curcumin selectively inhibits cancer cells growth in vitro and in preclinical model of glioblastoma. *J. Nutr. Biochem.* 23, 591-601.
- Zanotto-Filho, A., Coradini, K., Braganhol, E., Schroder, R., de Oliveira, C.M., Simoes-Pires, A., Battastini, A.M., Pohlmann, A.R., Guterres, S.S., Forcelini, C.M., Beck, R.C., Moreira, J.C., 2013. Curcumin-loaded lipid-core nanocapsules as a strategy to improve pharmacological efficacy of curcumin in glioma treatment. *Eur. J. Pharm. Biopharm.* 83, 156-167.
- Zhang, C., Nance, E.A., Mastorakos, P., Chisholm, J., Berry, S., Eberhart, C., Tyler, B., Brem, H., Suk, J.S., Hanes, J., 2017. Convection enhanced delivery of cisplatin-loaded brain penetrating nanoparticles cures malignant glioma in rats. *J. Control. Release*.
- Zhang, Y., Jeong Lee, H., Boado, R.J., Pardridge, W.M., 2002. Receptor-mediated delivery of an antisense gene to human brain cancer cells. *J. Gene Med.* 4, 183-194.

- Zhao, L., Zhang, L., Meng, L., Wang, J., Zhai, G., 2013. Design and evaluation of a self-microemulsifying drug delivery system for apigenin. *Drug Dev. Ind. Pharm.* 39, 662-669.
- Zhao, M., Ma, J., Zhu, H.Y., Zhang, X.H., Du, Z.Y., Xu, Y.J., Yu, X.D., 2011. Apigenin inhibits proliferation and induces apoptosis in human multiple myeloma cells through targeting the trinity of CK2, Cdc37 and Hsp90. *Mol. Cancer* 10, 104.
- Zheng, F., Shi, X.-W., Yang, G.-F., Gong, L.-L., Yuan, H.-Y., Cui, Y.-J., Wang, Y., Du, Y.-M., Li, Y., 2007. Chitosan nanoparticle as gene therapy vector via gastrointestinal mucosa administration: results of an *in vitro* and *in vivo* study. *Life Sci.* 80, 388-396.
- Zheng, H., Ying, H., Yan, H., Kimmelman, A.C., Hiller, D.J., Chen, A.J., Perry, S.R., Tonon, G., Chu, G.C., Ding, Z., Stommel, J.M., Dunn, K.L., Wiedemeyer, R., You, M.J., Brennan, C., Wang, Y.A., Ligon, K.L., Wong, W.H., Chin, L., DePinho, R.A., 2008. p53 and Pten control neural and glioma stem/progenitor cell renewal and differentiation. *Nature* 455, 1129-1133.
- Zheng, P.-W., Chiang, L.-C., Lin, C.-C., 2005a. Apigenin induced apoptosis through p53-dependent pathway in human cervical carcinoma cells. *Life Sci.* 76, 1367-1379.
- Zheng, P.W., Chiang, L.C., Lin, C.C., 2005b. Apigenin induced apoptosis through p53-dependent pathway in human cervical carcinoma cells. *Life Sci.* 76, 1367-1379.
- Zheng, Y., McFarland, B.C., Drygin, D., Yu, H., Bellis, S.L., Kim, H., Bredel, M., Benveniste, E.N., 2013. Targeting protein kinase CK2 suppresses prosurvival signaling pathways and growth of glioblastoma. *Clin. Cancer Res.* 19, 6484-6494.
- Zheng, Y., Qin, H., Frank, S.J., Deng, L., Litchfield, D.W., Tefferi, A., Pardanani, A., Lin, F.T., Li, J., Sha, B., Benveniste, E.N., 2011. A CK2-dependent mechanism for activation of the JAK-STAT signaling pathway. *Blood* 118, 156-166.
- Zucchetti, M., Boiardi, A., Silvani, A., Parisi, I., Piccolrovazzi, S., D'Incalci, M., 1999. Distribution of daunorubicin and daunorubicinol in human glioma tumors after administration of liposomal daunorubicin. *Cancer Chemother. Pharmacol.* 44, 173-176.

Chapter 2: Thesis aim and objectives

2. THESIS AIM AND OBJECTIVES

AG is a naturally occurring flavonoid with promising *in vitro* activities against various GBM cell lines. On the other hand, 4-ferrocenyl-5,5-bis(4-hydroxyphenyl)-pent-4-en-1-ol (FcTriOH) is a newly synthesized molecule coming from the organometallic family of ferrocifens. Several other ferrocifen molecules and their formulations showed significant *in vitro* and *in vivo* activity against GBM, making FcTriOH an attractive candidate to investigate against GBM. Moreover, both AG and ferrocifens show their chemotherapeutic activity preferentially in cancer cells rather than in healthy cells, and can help to avoid chemotherapy associated toxicity. Both AG and FcTriOH are low molecular weight ($< 500 \text{ g.mol}^{-1}$) highly hydrophobic water insoluble molecules facing similar challenges towards their successful administration as potential therapy approaches for GBM.

The aim of this thesis was to develop nanosized drug delivery systems (NDDSs) for encapsulation and delivery of these two small hydrophobic drug candidates (AG and FcTriOH) in order to evaluate them as potential therapeutic approaches for GBM.

The main objectives of the study were:

- To develop and compare multiple injectable nanocarriers i.e. liposomes, LNCs and polymer-based nanocapsules (PNCs) as potential vectors of low molecular weight hydrophobic drugs;
- To surface-functionalize one chosen nanocarrier for targeted drug delivery to GBM cells;
- To evaluate *in vitro* and *in vivo* the AG and FcTriOH encapsulating nanocarriers (non-targeted and targeted) against GBM.

The results of these studies are reported in the following two chapters (chapter 3 and 4) of this manuscript.

Chapter 3 is entitled “Development and comparison of injectable nanocarriers for delivery of low molecular weight hydrophobic drug molecules”. The objective of this chapter was to identify the most promising nanovector (among liposomes, LNCs and PNCs) that could deliver the highest amount of drugs in a controlled way while being biocompatible. In Publication 2, the three nanovectors were compared (using AG) in terms of their physicochemical characteristics, drug release, storage stability, stability in serum,

complement consumption and toxicity against a human macrovascular endothelial cell line. Moreover, some additional unpublished results were added reporting the toxicity of the NDDSs against a human brain microvascular endothelial cell line, and a neuronal cell. Furthermore, freeze-drying of a liposome formulation was performed to improve its storage stability.

Chapter 4 is entitled “Surface-functionalization of lipid nanocapsules for targeted drug delivery to human glioblastoma cells”. The objective of this chapter was to functionalize the LNC surface with various concentrations of a GBM targeting CPP to deliver the nanocarrier preferentially in GBM cells than healthy astrocytes. In Publication 3 (in preparation), LNC surface was functionalized with varying concentrations of the CPP and LNC-CPP interaction was characterized. In addition, the effect of CPP concentrations on internalization of LNC in human GBM cells was investigated and the CPP concentration with maximum LNC uptake was determined. Moreover, cellular uptake of the functionalized-LNC in NHA was quantified to analyze the targeting-ability of the nanovector. Possible internalization pathways of the functionalized-LNC in GBM cells were also evaluated. Additionally, *in vitro* efficacy of AG and FcTriOH loaded LNCs (non-targeted and targeted) against human GBM cells were investigated. Finally, preliminary *in vivo* efficacy of the nanovectors was evaluated by i.v. administration in an ectopic murine GBM model, and by CED in an orthotopic murine GBM model.

***Chapter 3: Development and comparison of
injectable nanocarriers for low molecular-weight
hydrophobic drug molecules***

3. DEVELOPMENT AND COMPARISON OF INJECTABLE NANOCARRIERS FOR DELIVERY OF LOW MOLECULAR WEIGHT HYDROPHOBIC DRUG MOLECULES

3.1. Introduction

This chapter concerns about the design and comparison of several different types of NDDSs as potential injectable nanovectors for low molecular weight hydrophobic drugs. Nanocarriers with optimized physicochemical properties for systemic administration can be promising for cancer therapy as they can accumulate into tumors by passive targeting. In the context of brain tumor, systemically administered nanocarriers can reach the brain tumor when the BBTB is ruptured due to tumor growth or temporarily ruptured by chemical or physical means, or if the NDDS surface is functionalized with BBB-targeting moiety (Liu and Lu, 2012). Moreover, the injectable NDDSs can also be administered locally into the brain tumor by stereotactic injection or by CED (Huynh et al., 2012). Due to their capacity to encapsulate hydrophobic drug molecules in different regions of their nano-structure (core or shell), several liposomes and nanocapsules were developed in this study.

As discussed in publication 1, size, zeta potential, shape and hydrophilic surface coating of the NDDSs are key parameters that can influence their *in vivo* fate (Figure 3.1). Therefore, evaluation of nanovector size is an essential characterization step. In this chapter, we have used two particle size distribution techniques i.e. dynamic light scattering (DLS) and nanoparticle tracking analysis (NTA). As NTA measures size distribution based on numbers rather than scattered light intensity, it can measure polydisperse samples more precisely compared to DLS. However, size distribution by NTA is more time consuming and more difficult to operate compared to DLS (Filipe et al., 2010). Additionally, size distribution and morphology of the NDDSs were determined by transmission electron microscopy (TEM).

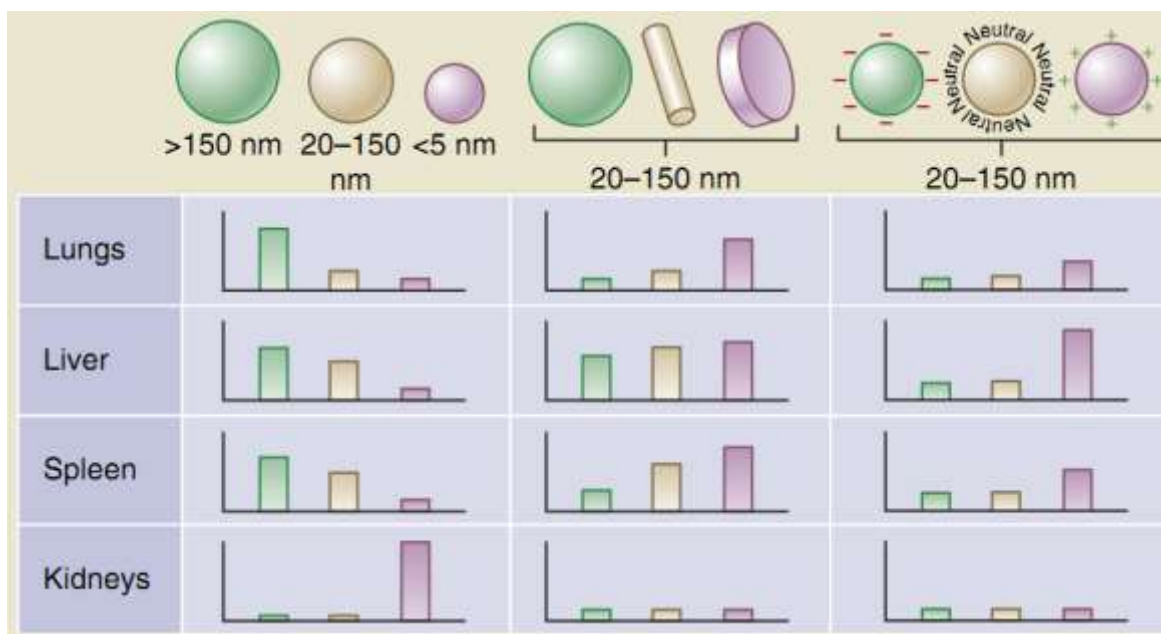


Figure 3.1: Influence of nanocarrier characteristics on its biodistribution (Blanco et al., 2015).

In addition to particle size distribution, zeta potential and surface coating are other parameters that significantly impacts on the *in vivo* fate of the nanovectors (described in publication 1) by regulating its interaction with plasma proteins. Zeta potential was measured using laser Doppler electrophoresis method which calculates the potential by measuring velocity of the particles under electrophoresis (Bhattacharjee, 2016).

The interaction of the NDDSs with serum proteins and their stability in serum was assessed by observing their size distribution in serum overtime using DLS (Palchetti et al., 2016). DLS allowed a quick, less complicated qualitative assessment about particle stability in serum overtime i.e. possibility of protein corona formation, particle aggregation or degradation. Moreover, complement consumption assay was performed to quantify complement protein consumption by the nanovectors.

Drug release profiles of the NDDSs and their storage stability were evaluated. Drug release can be an important factor and an ideal NDDS should have a controlled release profile instead of quick-burst release of the drug. Stability of the NDDSs is another important criterion that was investigated as the nanovectors need to be sufficiently stable during storage until they are used in preclinical or clinical studies. Lyophilization was performed to improve the stability of the nanocarriers.

A part of this chapter has been accepted for publication in the form of an article entitled 'Development and evaluation of injectable nanosized drug delivery systems for apigenin' in the 'International Journal of Pharmaceutics' (Karim et al., 2017a), and available at 3.3.1.

3.2. Summary of the results

The principle objective of this part of the thesis was to identify the nanocarriers that would deliver the highest quantity of AG in a controlled way while being biocompatible and suitable for i.v. administration. AG was used as a model low molecular weight hydrophobic molecule to develop and characterize various nanocarrier formulations. AG is a nearly water-insoluble molecule and therefore required development of suitable formulation for *in vivo* application. Moreover, encapsulating the polyphenolic flavonoid AG within the nanocarrier may protect it from possible degradation during storage and from metabolism after systemic administration. Different nanocarriers were evaluated as their composition and physicochemical characteristics can significantly impact where the drug will be loaded, how much drug can be loaded and how fast the drug will be released in biological environment. Moreover, characteristics of the nanocarriers have profound influence of the *in vivo* fate of itself and its cargo. We evaluated liposomes, LNC and PNC formulations as potential AG-loaded nanocarriers due to their promising characteristics, differences in the composition and possibilities of encapsulating the drug in various regions of the particles (i.e. in the membrane or in the core) in different amounts.

The liposomes developed in this study can be divided into two major categories- i.e. conventional liposomes and drug-in-cyclodextrin-in-liposomes (DCLs). The first category is supposed to entrap the drug in their phospholipid bilayer, whereas the latter is supposed to encapsulate the aqueous soluble complex of the drug in its aqueous core. This can significantly impact on the drug-loading capacity of the nanocarrier. However, encapsulating the drug in the aqueous core will allow the drug to be in contact with aqueous environments and may lead to its degradation. Therefore, it is important to identify the suitable drug entrapment technique to maximize drug loading and better stability of the drug molecule. The DPPC-based conventional liposomes were designed to have similar composition, but different surface charge (cationic and anionic). AG-cyclodextrin complexes was prepared and DCLs were formulated with a similar

CHAPTER 3

composition to the conventional cationic liposomes (CLs) to evaluate the possibility to improve drug-loading. In comparison, the nanocapsules (LNC and PNC) had a core formed by medium-chain triglycerides, and would therefore encapsulate the hydrophobic drug in their core. The PNC was formulated to retain most ingredients of the LNC in its composition, except a newly synthesized tocopherol-modified PEG-b-polyphosphate copolymer (synthesized by the Center for Education and Research on Macromolecules (CERM) in University of Liege, details of the synthesis step are described under 'Materials' and 'Figure S1 in Supplementary material' of Publication 2) was used for its amphiphilic characteristics as the major shell-forming ingredient of a nanocarrier for the first time. The differences in the composition of cores of liposomes and nanocapsules (aqueous and oily respectively) had the possibility to significantly influence on drug loading and therefore was evaluated.

Size of the cationic and anionic liposomes (ALs), LNCs and PNCs were characterized using 3 different techniques i.e. DLS, NTA and TEM. The mean diameters of these liposomes and PNC were around 142-145 nm by DLS, and between 133-141 nm by NTA. Similarly, LNC was 59 nm by DLS, but 54 nm by NTA. The difference between DLS and NTA results can be explained by the intensity-based calculation in DLS compared to number-based calculation in NTA. As DLS calculation is more sensitive to the presence of larger particles/vesicles, the calculated mean diameter in DLS is often larger compared to the mean diameter obtained by NTA (Filipe et al., 2010). Besides their differences in calculation, accuracy and precision of the size measurements in DLS and NTA are about 2 % (www.malvern.com, 2017). Additionally, TEM was used to calculate size distribution and observe morphology of the above mentioned NDDSs. The mean diameter of the CL and the LNC were comparable to the values obtained by NTA. But mean diameter of anionic liposome was significantly higher, whereas it was the opposite for the PNCs. This can occur due to the stress induced during staining (by interaction with the negative stain), or due to the distortion resulted by vacuum (Ruozi et al., 2011). However, TEM was able to show that the NDDSs were nearly spherical in shape and that the liposomes were unilamellar. The size of the DCLs were measured by DLS and they were 11-13 nm smaller compared to the CL. PDI of all the nanovectors (obtained by DLS) were below 0.2, so they can be considered as monodispersed. Overall, the mean diameter of the NDDSs were within acceptable range for i.v. administered nanocarriers according to the

CHAPTER 3

literature (Fu et al., 2009; Huynh et al., 2012; Karim et al., 2017b). The objective was to develop nanocarriers having size within the range of the previously reported parenterally administered nanocarriers that were able to accumulate in brain tumors through the fenestrations of the BBTB by passive targeting (Bernardi et al., 2009; Brigger et al., 2002; Calvo et al., 2001). Therefore, the size of these NDDSs were promising as potential nanocarriers for passively targeting GBM.

Zeta potential of the AL and the nanocapsules were negative. The CL and the DCLs had positive (+43 to +30 mV) zeta potentials due to the presence of the cationic cholesterol substitute in the lipid bilayer. These liposomes had an additional dimethylaminoethane-carbamoyl chain on the cholesterol group to impart the positive surface charge compared to ALs. Surface charge of the nanocarriers would aid to hinder particle aggregation during storage and may improve stability. Moreover, negatively charged nanocarriers are often used to avoid the MPS systems after systemic administration. In contrast, positively charged nanovectors may suffer from non-specific interaction in biological systems, may consume more serum proteins and can be rapidly removed from blood stream by MPS. However, the cationic charge may aid in the crossing of the BBB by AMT, if it can avoid opsonization and non-specific interactions in the blood-stream by its surface PEG-coating.

The positive surface charge possibly impacted drug encapsulation as drug loading of cationic liposome was about 2-folds higher than ALs. We hypothesized that it is due to interactions of charged liposome surface and the partially charged (at pH 7.4) AG. In fact, such electrostatic attraction and repulsion of AG with HSA and sulfo-group containing cyclodextrin (respectively) was reported in literature (Papay et al., 2016; Yuan et al., 2007). The drug-loading capacity of DCLs was significantly lower (even after increasing the initial AG amount by 2-folds) compared to the CLs, although they had the same phospholipid composition and were dissimilar only in drug entrapment technique. Increased CD concentration in AG-HP β CD complex did not allow to increase the encapsulation efficiency of DCL. Among the nanocapsules, the PNCs had higher drug loading compared to LNC possibly due to higher amount of core-oil in its composition (Lertsutthiwong et al., 2008). The objective of preparing the various nanocarriers was to identify the nanovectors with higher drug-loading in order to minimize the possible toxicity of the excipients on the cells.

CHAPTER 3

Drug release from the NDDSs was evaluated by dialysis method. The liposomes formulations showed quick release profiles (anionic liposome > cationic liposome). However, the nanocapsule formulations (LNC and PNC) released the drug at a controlled rate and their release profiles were comparable up to 24 h. After that, release from the LNC was slower compared to PNC possibly due to the higher ratio of shell material in its composition (Watnasirichaikul et al., 2002).

During storage at 4°C, none of the NDDSs showed drug leakage. Their size distribution was stable and remained monodispersed up to 14 days (study period). Drug concentration in the nanovectors was stable except the CL, in which drug concentration gradually decreased to 90% of initial concentration after 14 days. In this formulation, the drug had the possibility to be in contact with water by staying at the lipid-water interface (as hypothesized above) and this may lead to its degradation. Indeed, storage of AG-cyclodextrin aqueous soluble complex (at 50 mM cyclodextrin concentration) showed similar drug concentration reduction tendency. These data support the hypothesis that AG dispersed at molecular level in aqueous solvents will have high contact surface area with water molecules which may aid in the possible degradation. In other formulations, the drug was encapsulated deeper, in the lipid-part of the nanocarriers and was protected from water. When CL were lyophilized and stored at 4°C, drug concentration was stable up to 84 days.

Because of their lowest drug loading capacity and the possible degradation of AG, DCLs encapsulating AG seemed less promising compared to other NNDS and were not further characterized.

The stability of the NDDSs in fetal bovine serum was evaluated by following the size distribution graphs of the formulations (incubated in serum) over time in DLS. The NDDSs were stable in serum up to 6 hours and no particle aggregation, degradation or large protein corona formation was observed. Moreover, in the complement consumption assay, the NDDSs showed very low CH₅₀ unit consumption and therefore would have the possibility of circulating longer in the systemic circulation. The hydrophilic PEG coatings on the NDDS surfaces (DSPE-PEG₂₀₀₀ for the liposomes, combination of DSPE-PEG₂₀₀₀ and PEG₆₆₀-hydroxystearate for LNC, and PEG₅₃₀₀ for PNC) efficiently hindered serum protein adsorption by steric repulsion resulting their stability in serum for up to 6 hours and low consumption of complement proteins.

CHAPTER 3

Toxicity of the NDDSs on a human macrovascular endothelial cell line (EAhy926), an immortalized human cerebral microvascular endothelial cell line (hCMEC/D3) and a mouse neuroblastoma cell line (Neuro2a, commonly used for neurotoxicity study) was evaluated by MTS and LDH assay. The CL showed signs of toxicity on EAhy926 cells at 171 $\mu\text{g/mL}$, on Neuro2a cells at 683 $\mu\text{g/mL}$ in both assays, and on hCMEC/D3 cells at 171 $\mu\text{g/mL}$ in MTS assay. The ALs did not show any toxicity at the tested concentrations on the three tested cell lines. The LNC showed toxicity on Neuro2a cells in both assays from 436 $\mu\text{g/mL}$, and on hCMEC/D3 cells in LDH assay from 109 $\mu\text{g/mL}$. The blank PNC showed toxicity in LDH assay on hCMEC/D3 cells at 189 $\mu\text{g/mL}$ concentration. Overall, the NDDSs were nontoxic on these cell lines up to significantly high concentrations.

Due to their optimum physicochemical characteristics, as systemically administrable nanocarriers, controlled drug release property, stability during storage, optimum stability in serum, low complement protein consumption characteristics and nontoxic nature, the nanocapsules (LNC and PNC) seemed more promising for further optimization as GBM targeting nanovector. Among the nanocapsules, the diameter of LNC was significantly lower compared to PNC that may allow it to pass more efficiently through the fenestrations of BBB. Additionally, its size was less than 100 nm which may allow it to diffuse through the extracellular brain space (Allard et al., 2009). Moreover, its organic solvent free manufacturing technique was more suitable for future scale up (Thomas and Lagarce, 2013). Therefore, LNC was chosen for further optimization to improve its GBM targeting ability.

3.3. Results

3.3.1. Publication 2: ‘Development and evaluation of injectable nanosized drug delivery systems for apigenin’, International Journal of Pharmaceutics xxx (2017) xxx–xxx (article in press)

DEVELOPMENT AND EVALUATION OF INJECTABLE NANOSIZED DRUG DELIVERY SYSTEMS FOR APIGENIN

Reatul Karim^{a,d}, Claudio Palazzo^a, Julie Laloy^b, Anne-Sophie Delvigne^b, Stéphanie Vanslambrouck^c, Christine Jerome^c, Elise Lepeltier^d, Francois Orange^e, Jean-Michel Dogne^b, Brigitte Evrard^a, Catherine Passirani^d, Géraldine Piel^a

^a Laboratory of Pharmaceutical Technology and Biopharmacy, CIRM, University of Liege, Liege, Belgium

^b Namur Nanosafety Centre (NNC), Department of Pharmacy, University of Namur, Namur, Belgium

^c Center for Education and Research on Macromolecules (CERM), University of Liege, UR-CESAM, Liege, Belgium

^d MINT, UNIV Angers, INSERM 1066, CNRS 6021, Université Bretagne Loire, Angers, France

^e Université Côte d’Azur, Centre Commun de Microscopie Appliquée, Nice, France

Corresponding author:

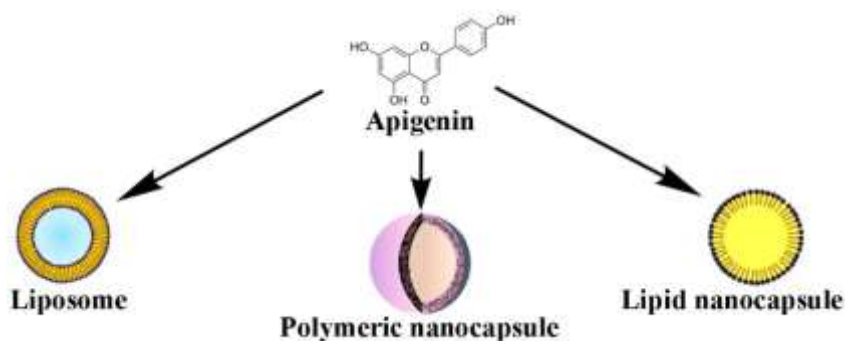
Reatul Karim, email: reatul.karim@ulg.ac.be

International Journal of Pharmaceutics xxx (2017) xxx–xxx (article in press)

<https://doi.org/10.1016/j.ijpharm.2017.04.064>

Abstract

The purpose of this study was to develop different injectable nanosized drug delivery systems (NDDSs) i.e. liposome, lipid nanocapsule (LNC) and polymer-based nanocapsule (PNC) encapsulating apigenin (AG) and compare their characteristics to identify the nanovector(s) that can deliver the largest quantity of AG while being biocompatible. Two liposomes with different surface characteristics (cationic and anionic), a LNC and a PNC were prepared. A novel tocopherol modified poly(ethylene glycol)-b-polyphosphate block-copolymer was used for the first time for the PNC preparation. The NDDSs were compared by their physicochemical characteristics, AG release, storage stability, stability in serum, complement consumption and toxicity against a human macrovascular endothelial cell line (EAhy926). The diameter and surface charge of the NDDSs were comparable with previously reported injectable nanocarriers. The NDDSs showed good encapsulation efficiency and drug loading. Moreover, the NDDSs were stable during storage and in fetal bovine serum for extended periods, showed low complement consumption and were non-toxic to EAhy926 cells up to high concentrations. Therefore, they can be considered as potential injectable nanocarriers of AG. Due to less pronounced burst effect and extended release characteristics, the nanocapsules could be favorable approaches for achieving prolonged pharmacological activity of AG using injectable NDDS.

**Keywords**

Apigenin, Liposome, Lipid nanocapsule, Polymeric nanocapsule, Injectable nanocarriers

1. Introduction

Apigenin (AG) is a natural plant flavonoid (4', 5, 7,-trihydroxyflavone), widely found in many common fruits and vegetables e.g. oranges, grapefruit, chamomile, tea, parsley, onions and wheat sprouts (Patel et al., 2007; Zheng et al., 2005). It showed a number of significant beneficial bioactivities i.e. anti-oxidant (Romanova et al., 2001), anti-inflammatory (Lee et al., 2007) and anti-cancer properties (Shukla and Gupta, 2010). Despite the numerous positive effects, AG is characterized by very low aqueous solubility (1.35 $\mu\text{g/ml}$) and high permeability (log P value 2.87) (Li et al., 1997) and it is then a Biopharmaceutical Classification System (BCS) II molecule (Zhang et al., 2012). Taking these into account, the development of its injectable formulations, useful to overcome the constraint of low oral bioavailability, is challenging as AG is insoluble in most biocompatible solvents (Zhao et al., 2013). Therefore, use of AG for *in vivo* studies is limited.

One of the most interesting strategies to overcome this issue is to encapsulate the AG in nanosized drug delivery systems (NDDSs). NDDSs, also known as nanocarriers, are promising and versatile approach for delivery of hydrophobic drugs (Karim et al., 2017b; Laine et al., 2014a) with several advantageous properties i.e. adaptable characteristics with easily modifiable surface, capacity to entrap large quantities of hydrophobic drug and protect it from degradation, improve bioavailability, release drug in a controlled manner over extended period, prolong plasma circulation half-life and increase pharmacological effects (Peer et al., 2007; Zhang et al., 2008). Moreover, they can be modified for site-specific drug delivery which reduce side-effects and improve the therapeutic window (Karim et al., 2016). Among various nanocarriers, liposome (Eavarone et al., 2000; Felgner and Ringold, 1989), lipid nanocapsule (LNC) (Allard et al., 2008; Lamprecht et al., 2002) and polymer-based nanocapsule (PNC) (De Melo et al., 2012; Mora-Huertas et al., 2010) have been widely studied. Although these nanocarriers can be generally considered as vesicular systems, their composition and morphology are significantly different from each other. Liposomes have structural similarities with cellular organelles and are made of phospholipid bilayer(s) surrounding an aqueous core. Due to their particular structure, liposomes are capable to encapsulate both lipophilic drugs (in the lipidic-bilayer(s)) and hydrophilic drugs (in the core). In comparison, PNCs have a solid polymer-shell surrounding an oily core, where lipophilic drugs are encapsulated. Structure

CHAPTER 3

of LNCs is a hybrid among PNCs and liposomes; characterized by an oily-liquid core surrounded by a solid lipid shell. All three NDDSs, i.e. liposome (Sharma et al., 1996), LNC (Zanotto-Filho et al., 2013) and PNC (Mora-Huertas et al., 2012) have been widely studied to improve the delivery of poorly water soluble drugs. Additionally, these nanocarriers can be designed for parenteral administration, in order to bypass absorption process and maximize the drug bioavailability. AG-loaded injectable NDDSs can be particularly beneficial for treatment of numerous types of cancers (e.g. colon cancer, brain cancer, breast cancer, liver cancer, prostate cancer, cervical cancer, thyroid cancer, skin cancer, gastric cancer etc.) due to the promising activity of AG [reviewed in detail by Patel et al., Shukla and Gupta] (Patel et al., 2007; Shukla and Gupta, 2010) and the capability of NDDSs to extravasate and preferentially accumulate in tumors by enhanced permeability and retention effect (Fu et al., 2009; Iyer et al., 2006). However, after administration into blood circulation, the NDDSs can be destabilized by plasma proteins leading to premature drug release. Moreover, they can form aggregates or adsorb a significant amount of plasma proteins and form a “protein-corona” (Palchetti et al., 2016). If opsonins are adsorbed on the surface, the NDDSs are subsequently captured and rapidly eliminated from the systemic circulation by mononuclear phagocytic system (MPS) (a part of the immune system) which restricts their blood circulation time. Formation of aggregates can also result rapid NDDS uptake by MPS (He et al., 2010). Therefore, stability of NDDSs in serum and low complement protein consumption are necessary for developing of safe and long-circulating nano-therapeutics for future clinical use (Li et al., 2015; Moore et al., 2015).

Different NDDSs are prepared from diverse ingredients and have variations in morphology, surface characteristics, drug loading capacity, drug release rates, toxicity etc. The purpose of this study was to develop and compare the characteristics of different injectable AG-NDDSs in order to identify the nanocarrier(s) that can deliver the largest quantity of AG while being biocompatible. Two liposomes with different surface characteristics (anionic and cationic), a LNC and a PNC were prepared. A novel block-copolymer i.e. tocopherol modified poly(ethylene glycol) (PEG)-b-polyphosphate (Figure S1 in Supplementary material) (Vanslambrouck, 2015) was used for the first time for PNC preparation. Different techniques were used for preparation of the nanocarriers, and the so-obtained NDDSs were physicochemically characterized. Moreover, stability of the

NDDSs in fetal bovine serum (FBS) and their complement protein consumption in normal human serum (NHS) were evaluated. Toxicity of the nanocarriers was assessed against a human macrovascular endothelial cell line to evaluate their biocompatibility.

2. Materials and Methods

2.1. Materials

1,2-dipalmitoyl-sn-glycero-3-phosphocholine (DPPC), 1,2-dioleoyl-sn-glycero-3-phosphoethanolamine (DOPE), 3 β -[N-(N',N'-dimethylaminoethane)-carbamoyl]cholesterol hydrochloride (DC-Chol) and 1,2-distearoyl-sn-glycero-3-phosphoethanolamine-N-[methoxy(polyethylene glycol)-2000] ammonium salt (DSPE-mPEG₂₀₀₀) were purchased from Avanti Polar Lipids, Inc. (USA). Cholesterol (Chol), 4-(2-hydroxyethyl)piperazine-1-ethanesulfonic acid (HEPES), sodium chloride (NaCl) and macrogol 15 hydroxystearate (Kolliphor® HS15) were purchased from Sigma-Aldrich (Germany). Hydrogenated phosphatidylcholine from soybean (Lipoid S PC-3) was provided from Lipoid GmbH (Germany), caprylic/capric triglycerides (Labrafac Lipophile WL1349) was supplied by Gattefosse (France). Polysorbate 80 (PS80) was purchased from Merck (Germany). AG was purchased from Indis NV (Belgium). The tocopherol modified PEG-b-polyphosphate copolymer (PEG₁₂₀-b-(PBP-co-Ptoco)₉) was synthesized by organocatalyzed ring-opening polymerization (Clement et al., 2012) of a butenylphosphate ring from a monomethoxy(polyethylene glycol) macroinitiator (MeO-PEG-OH, MW 5000g/mol, Aldrich) (Yilmaz et al., 2016) followed by the grafting of a tocopherol derivative on the polyphosphate backbone by thiol-ene reaction (Baeten et al., 2016) (Figure S1 in Supplementary material). Ultra-pure water (UPW) was obtained from a Millipore filtration system. All the other reagents and chemicals were of analytical grade. Normal human serum (NHS) was provided by the “Etablissement Français du Sang” (Angers, France). Sheep erythrocytes and hemolysin were purchased from Eurobio (France). EAhy926 cells (human umbilical endothelial cell line), Penicillin-Streptomycin, and Dulbecco's modified Eagle's medium (DMEM) were provided by Lonza (Belgium). Fetal bovine serum (FBS) was provided by Biologicals Industries (USA).

2.2. Preparation of NDDSs

2.2.1. Preparation of cationic liposomes and anionic liposomes

The cationic and anionic liposome formulations (CL-AG and AL-AG respectively, composition shown in Table 1, CL composition is modified from (Bellavance et al., 2010)) were prepared by thin lipid-film hydration, extrusion (Wei et al., 2015) and PEG post-insertion method. Briefly, AG and the excipients were dissolved in absolute ethanol and then dried in a rotary evaporator at 30°C for 1 h to form a dry lipid film. Subsequently, the dried film was hydrated with HEPES buffer (pH 7.4) and hardly agitated for 15 minutes. Afterwards, the lipid dispersion was extruded consecutively through 0.4 μm (3x), 0.2 μm (3x) and 0.1 μm (3x) polycarbonate membranes (Nucleopore®, Whatman) at 50°C (above phase transition temperature of DPPC) to obtain primary liposomes. DSPE-mPEG₂₀₀₀ (in HEPES buffer) was added to the surface of the primary liposomes by post-insertion technique, by incubation at 50°C for 30 min. The liposome formulations were then purified by dialysis (MWCO 20 kD, Spectra/Por® biotech grade cellulose ester membrane, SpectrumLabs, Netherlands) against HEPES buffer (pH 7.4) at 4°C for 2 x 1 h cycles.

Blank liposomes (CL-blank and AL-blank) were prepared following the same procedure but without the addition of AG.

Table 1. Molar ratio of ingredients of CL-AG and AL-AG.

Ingredient	Molar ratio	
	CL-AG	AL-AG
DPPC	1	1
DC-Chol	0.77	-
Chol	-	0.77
DOPE	0.77	0.77
DSPE-mPEG ₂₀₀₀ (during dry lipid film formation)	0.01	0.01
DSPE-mPEG ₂₀₀₀ (post insertion)	0.04	0.04
AG	0.13	0.13

2.2.2. Preparation of lipid nanocapsules

The apigenin-loaded LNCs (LNC-AG) were prepared using phase inversion temperature technique (Laine et al., 2014b). In brief, AG (0.2 % w/w), Kolliphor® HS15 (16.5 % w/w), Lipoid® S PC-3 (1.5 % w/w), Labrafac Lipophile WL1349 (20.1 % w/w), DSPE-mPEG₂₀₀₀ (1.9 % w/w), NaCl (1.7 % w/w) and UPW (58 % w/w) were mixed under magnetic stirring at 60°C. Three heating-cooling cycles were performed between 90°C and 60°C. During the last cooling step, when the temperature was in the phase inversion zone (78-83°C), ice-cold UPW was added (final concentration 69.8 % w/w) to induce irreversible shock and form the LNC-AG. The nanocapsules were then diluted with HEPES buffer and passed through 0.2 µm cellulose acetate filter to remove any aggregates. Purification was done by dialysis method as described in 2.2.1.

Blank LNCs (LNC-blank) were prepared by the same procedure as LNC-AG, but without the addition of AG.

2.2.3. Preparation of polymer-based nanocapsules

The apigenin-loaded PNCs (PNC-AG) were prepared using nanoprecipitation technique followed by solvent evaporation under vacuum (Mora-Huertas et al., 2012). In short, AG (1.2 % w/w), PEG₁₂₀-b-(PBP-co-Ptoco)₉ (20.1 % w/w), Lipoid® S PC-3 (10.8 % w/w), Labrafac Lipophile WL1349 (67.9 % w/w) were dissolved in ethanol:acetone (1:3 v/v). Subsequently, the solution was slowly injected (0.8 mm needle) into an aqueous solution of PS80 (0.25 % w/v) under magnetic stirring at 400 rpm. After 10 minutes stirring, the organic solvent was completely removed by evaporation under reduced pressure at 40°C. The PNC-AG was purified by dialysis method as described in 2.2.1.

Blank PNCs (PNC-blank) were prepared in the same procedure as PNC-AG, but without the addition of AG.

2.3. Size distribution, zeta-potential and morphology

The mean diameter and polydispersity index (PDI) of the NDDSs were determined by dynamic light scattering (DLS) technique using Zetasizer Nano ZS (Malvern Instruments Ltd, UK). NDDSs were diluted 100-folds in UPW before the analysis. The measurements were performed at backscatter angle of 173°. The measured average values were calculated from 3 runs, with 10 measurements within each run.

CHAPTER 3

Additionally, the size distribution of the NDDSs was determined using nanoparticle tracking analysis (NTA), which complements the DLS measurements. The NTA was carried out using the NanoSight NS300 (Malvern Instruments Ltd, UK). Briefly, the NDDS samples were diluted to optimum concentrations with UPW and were infused in the sample chamber using a syringe pump at 30 $\mu\text{L}/\text{min}$ rate. A 405 nm laser was used to illuminate the particles, and their Brownian motion was recorded into three 60 s videos (25 fps) using the sCMOS type camera of the instrument. Subsequently, the NTA software (NTA 3.2 Dev Build 3.2.16) analyzed the recordings, tracked the motion of the particles and calculated the diameter of the particles. The experiment was performed in triplicate.

Zeta potential of the nanocarriers was measured using laser Doppler micro-electrophoresis technique using Zetasizer Nano ZS (Malvern Instruments Ltd, UK).

Morphology and size of the NDDSs were visualized by transmission electron microscopy (TEM) using negative staining technique. Briefly, a drop of the NDDS dispersion was placed for 30 seconds on a TEM copper grid (300 mesh) with a carbon support film. The excess dispersion was removed with a filter paper. Subsequently, staining was done by adding a drop of 1% (w / v) aqueous solution of uranyl acetate on the grid for 1.5 min, followed by removal of excess solution. The TEM observations were carried out with a JEOL JEM-1400 transmission electron microscope equipped with a Morada camera at 100 kV.

2.4. Apigenin dosage via HPLC method

To quantify total (encapsulated and unencapsulated) AG concentration, CL-AG, AL-AG, and LNC-AG were broken by mixing vigorously with an appropriate volume (7-folds dilution for CL-AG and AL-AG, 40-folds dilution for LNC-AG) of ethanol to keep dissolved AG concentration between 5-50 $\mu\text{g}/\text{mL}$. PNC-AG was processed in the similar way, except ethanol:acetone (1:3 v/v, 7-folds dilution) was used as the solvent. To quantify unencapsulated AG concentration, formulations were placed on centrifugal concentrator devices with polyethersulfone membrane (MWCO 30 kD, Vivaspin 500, Sartorius AG) and centrifuged at 14500 g for 20 minutes to separate the free AG from the rest of the formulation. The filtrates containing unencapsulated AG were collected and ethanol (2-folds) was added to solubilize any undissolved drug. AG dosage in the above mentioned samples was performed by a validated method in a HPLC system (LC Agilent

CHAPTER 3

1100 series, Agilent Technologies, Belgium). An Alltima™ HP C18 analytical column (250 x 4.6 mm, 5 µm, Grace Divison Discovery Sciences, Belgium) was used at 30°C. UPW and acetonitrile (55:45, v/v) was used as mobile phase. Flow rate was 1 mL/min, injection volume was 10 µL and AG was quantified by an UV detector at λ of 340 nm. Analysis of the data was performed by Open Lab HPLC Agilent software. Retention time for AG was 4.9 min.

2.5. Entrapment efficiency (EE)

EE (%) was calculated using the following equation:

$$EE (\%) = \frac{(\text{Total AG conc. in NDDS} - \text{unencapsulated AG conc. in NDDS})^* \times 100}{\text{Theoretical AG conc. in NDDS}}$$

* Determined by HPLC (2.4)

2.6. Mass yield and drug loading capacity

Mass yield of NDDSs was calculated by gravimetric analysis of the dried NDDSs dispersions. Briefly, 200 µL of NDDSs were freeze-dried (Drywinner 8, Heto-Holten A/S, Denmark) over a 24 h cycle. Weight of the dried nanocarriers were measured (weights of HEPES buffer and NaCl were taken into account) and mass yield (%) was calculated using the following equation:

$$\text{Mass yield (\%)} = \frac{\text{Weight of 200 } \mu\text{L NDDS} \times 100}{\text{Theoretical weight of 200 } \mu\text{L NDDS}}$$

Drug loading capacity was calculated using the following equation:

$$\text{Drug loading capacity} \left(\frac{\mu\text{gAG}}{\text{mgNDDS}} \right) = \frac{\text{Amount of AG in 200 } \mu\text{L NDDS}^* (\mu\text{g})}{\text{Weight of 200 } \mu\text{L NDDS (mg)}}$$

* Determined by HPLC (2.4)

2.7. *In vitro* drug release profile of the NDDSs

In vitro drug release profiles of the nanocarriers were studied with the dialysis method. In brief, 1 mL of AG loaded NDDSs were taken in a dialysis bag (MWCO 20 kD, Spectra/Por® biotech grade cellulose ester membrane, SpectrumLabs, Netherlands) and dialyzed against HEPES buffer (pH 7.4) (200/1 acceptor/donator volume ratio to obtain sink condition) at 37°C, stirred at 75 rpm (SW22, Julabo GmbH, Germany). The concentration of AG was determined by HPLC method described in 2.4.

2.8. Storage stability

The NDDSs were kept at 4°C and samples were withdrawn at day 0, 1, 3, 7 and 14. Stability during storage was evaluated by size, PDI (using method described in 2.3), AG content (using HPLC method described in 2.4) and AG leakage. The leakage of AG from NDDSs was assessed using the method to quantify unencapsulated AG mentioned in section 2.4.

2.9. Stability of the NDDSs in serum

Stability of the NDDSs in FBS was evaluated by following their size distribution against time (Li et al., 2015; Palchetti et al., 2016). The nanocarrier formulations were diluted using HEPES buffer (pH 7.4) to optimum concentrations (200 µg lipid/mL for CL-AG, AL-AG and PNC-AG; 500 µg lipid/mL for LNC-AG) and mixed with FBS at 1:1 ratio (v/v) at 37°C. The mixture, along with nanocarrier dispersion and FBS (controls), were incubated at 37°C at 75 rpm in a shaking water bath (SW22, Julabo GmbH, Germany). At predetermined time intervals (1 min, 30 min, 1 h, 2 h, 4 h, 6 h and 24 h), 20 µL of samples were withdrawn, diluted 50-folds with UPW and size distribution was measured via DLS method described in 2.3.

2.10. Complement consumption by the NDDSs

Complement activation was evaluated by measuring the residual hemolytic capacity of NHS towards antibody-sensitized sheep erythrocytes after exposure to the different NDDSs (CH50 assay) (Cajot et al., 2011). In brief, aliquots of NHS were incubated with increasing concentrations of the NDDSs at 37°C for 1 h. Subsequently, the different volumes of the NHS were incubated with a fixed volume of hemolysin-sensitized sheep erythrocytes at 37°C for 45 min. The volume of serum that can lyse 50% of the erythrocytes was calculated (“CH50 units”) for each sample and percentage of CH50 unit consumption relative to negative control was determined as described previously (Vonarbourg et al., 2006). Particle number in the NDDS dispersions was determined by NTA described in section 2.3 and particle concentration per mL of NHS was calculated according to following equation-

$$\text{Particle number per mL of NHS} = \text{Particle conc. in NDDS dispersion} \times \frac{\text{vol. of NDDS added}}{\text{vol. of NHS}}$$

CHAPTER 3

Subsequently, surface area of the NDDSs per mL of NHS was calculated according to the following equation-

$$\text{Surface area} = \text{Particle number per mL of NHS} \times \pi \times (\text{average particle diameter})^2$$

The CH50 unit consumption by the different NDDSs were compared by plotting the percentage of CH50 unit consumption as a function of their surface area.

2.11. *In vitro* cytotoxicity of NDDSs on endothelial cell line

The endothelial cells (EAhy926) were seeded in a 96-well plate at a density of 12.5×10^3 cells/well and incubated for 24 hours. AG solution (in DMSO) and NDDSs, at a concentration of 0.6 μM to 40 μM , were added to the cells in 200 μL of cell media and incubated for 24 hours. Cytotoxicity of formulations was determined by evaluating cell viability using methyl tetrazolium (MTS) assay (CellTiter 96[®] Aqueous One Solution Cell Proliferation Assay, Promega, WI, USA) and cell necrosis by lactate dehydrogenase (LDH) assay (Cytotoxicity Detection Kit^{PLUS}, Roche, Basel, Switzerland), according to manufacturer's instructions.

2.12. Statistical analysis

Results obtained from the experiments were analyzed statistically using GraphPad Prism[®] software. Mean and standard deviation (SD) were determined and values are represented as Mean \pm SD. One way analysis of variance (ANOVA) was performed in the respective fields with Bonferroni post-test to compare among individual groups, and Dunnett's post-test to compare with control. P-value less than 0.05 ($p < 0.05$) was considered to be statistically significant.

3. Results

3.1. Characteristics of the NDDSs

Particle size and zeta potential of the developed NDDSs (determined by DLS) are shown in Table 2. The mean hydrodynamic diameter of the AG loaded liposomes (CL-AG and AL-AG) and the PNC-AG was comparable ($p > 0.5$). The sizes of these nanocarriers were around 143 nm. The mean diameter of the LNC-AG was significantly ($p < 0.001$) smaller (59 nm) compared to the other NDDSs. All four NDDSs were monodispersed with PDI < 0.2 . The mean diameter of the CL-AG, AL-AG, LNC-AG and PNC-AG determined by NTA analysis were 133 nm, 136 nm, 54 nm and 141 nm respectively. This was in

agreement with the results obtained from DLS. Morphology of the NDDSs was visualized by TEM images (Figure 1). The NDDSs were nearly spherical and the liposomes were unilamellar. Additionally, mean sizes of CL-AG, AL-AG, LNC-AG and PNC-AG determined by TEM were 111 nm, 214 nm, 55 nm and 87 nm respectively. Mean size (determined by TEM) of CL-AG and LNC-AG were comparable with the results obtained by DLS and NTA, whereas average size of AL-AG and PNC-AG were quite dissimilar. This can possibly occur due to the differences of the physical state of the samples (dry vs hydrated state) and size calculation techniques of TEM compared to DLS (number vs intensity weighted).

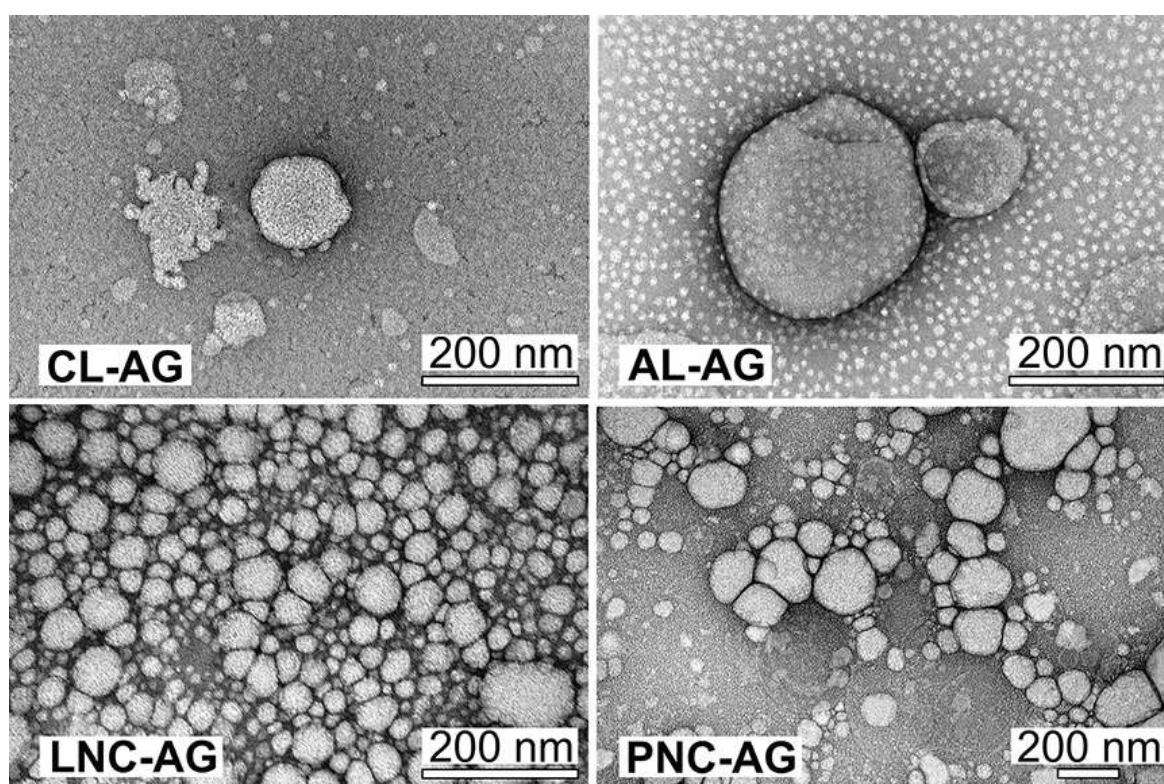


Figure 1. Representative transmission electron microscopy images of CL-AG, AL-AG, LNC-AG and PNC-AG (white bar: 200 nm)

The zeta potential of the CL-AG was 43.2 mV and was significantly different ($p < 0.001$) compared to the other NDDSs, which were negatively charged. Surface charge of AL-AG, LNC-AG and PNC-AG were -27.4 mV, -24.9 mV and -16.2 mV respectively. However, only the zeta potentials of AL-AG and PNC-AG were significantly different ($p < 0.05$) among these three NDDSs.

CHAPTER 3

EE of the CL-AG was 71 % which was significantly higher ($p < 0.001$) compared to the AL-AG. Moreover, EE of the nanocapsules were significantly higher compared to the CL-AG ($p < 0.05$) and AL-AG ($p < 0.001$) but were comparable ($p > 0.05$) with each other (82 % for LNC-AG and 84 % for PNC-AG).

Mass yields of the NDDSs were between 72 and 85 %. The highest yield mass was observed for AL-AG, followed by LNC-AG, PNC-AG and CL-AG. No significant difference ($p > 0.05$) was observed for yield mass of CL-AG and PNC-AG. Drug loading capacity in CL-AG and PNC-AG were more than 2-fold higher (16.5 and 14.3 $\mu\text{gAG/mgNDDS}$ respectively) compared to AL-AG and LNC-AG (6.5 and 6.2 $\mu\text{gAG/mgNDDS}$ respectively). Drug loading capacity of the NDDSs were significantly different ($p < 0.01$) from each other, except for AL-AG and LNC-AG.

Table 2. Physicochemical characteristics of the NDDSs

Characteristics	CL-AG	AL-AG	LNC-AG	PNC-AG
Mean diameter (nm)*	144 \pm 1	142 \pm 6	59 \pm 2	145 \pm 7
PDI	0.04 \pm 0.01	0.12 \pm 0.02	0.11 \pm 0.03	0.11 \pm 0.02
Zeta potential (mV)	43.2 \pm 1.2	-27.4 \pm 2.3	-24.9 \pm 6.0	-16.2 \pm 4.4
EE (%)	71 \pm 2	34 \pm 1	82 \pm 5	84 \pm 4
Mass yield (%)	80 \pm 3	86 \pm 5	72 \pm 2	81 \pm 4
Drug loading capacity ($\mu\text{gAG/mgNDDS}$)	16.5 \pm 0.2	6.5 \pm 0.3	6.2 \pm 0.5	14.3 \pm 0.6

* Measured by DLS.

3.2. *In vitro* drug release profile of the NDDSs

The drug release (%) from the NDDSs was plotted against time to obtain their drug release profiles (Figure 2). Faster release profiles were observed for the liposomes in comparison to the nanocapsules. Although initial release from CL-AGs was slower compared to the AL-AGs, the liposomes released about 85-91 % drug after 6 h.

In comparison, the nanocapsules showed a biphasic and more sustained release profile, with a faster release rate up to 8 h, followed by a much slower rate up to 72 h. Moreover, the release rates of LNC-AG and PNC-AG were very comparable up to 24 h, with a release of 54 % and 58 % drug respectively. However, the drug release rate of PNC-AG

was relatively quicker after 24 h compared to LNC-AG. After 72 h, the LNC-AG released 63 % drug whereas PNC-AG released 85 % drug.

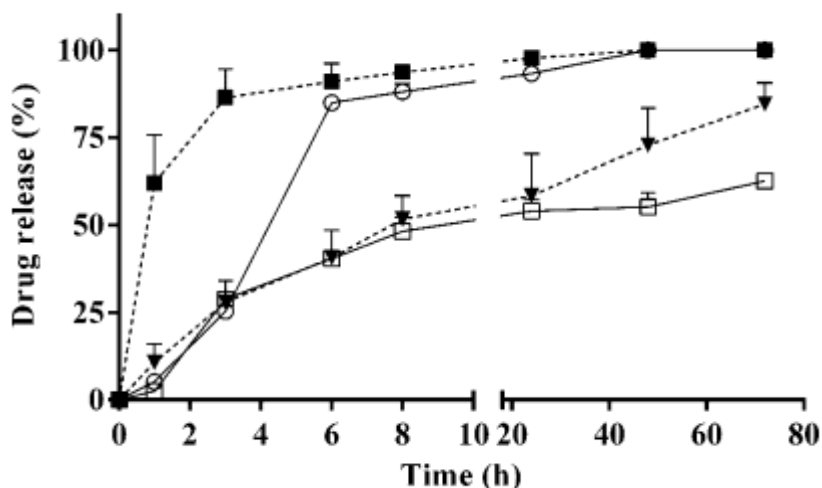


Figure 2: *In vitro* drug release from CL-AG (○), AL-AG (■), LNC-AG (□) and PNC-AG (▼).

3.3. Storage stability of the NDDSs

Stability of the NDDSs during storage was evaluated using several parameters i.e. size distribution (mean diameter and PDI), AG concentration and drug leakage. Mean size and PDI were determined to evaluate the physical stability of the nanocarriers, AG concentration will provide information about chemical stability of the drug within the NDDSs, whereas drug leakage will give evidence of the robustness of the NDDSs during storage. Size of all four NDDSs were stable throughout the study period (Figure 3a). Moreover, PDI of the nanocarriers were below 0.2 up to 14 days showing that the formulations remained monodispersed.

AG concentrations (% of initial) in the nanocarriers are showed in figure 3b. The AG% in AL-AG, LNC-AG and PNC-AG remained unaffected, signifying the stability of the drug in these nanocarriers. However, AG% in CL-AGs gradually reduced to 90 % of initial concentration after 14 days, demonstrating possible drug degradation in this NDDS. No drug leakage from any of the NDDSs was observed up to 14 days.

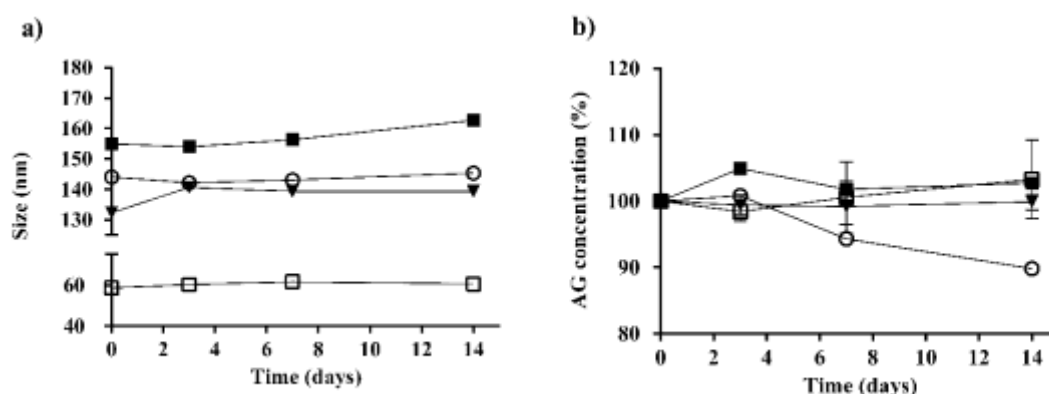


Figure 3: Stability profiles of the NDDSs at 4°C up to 14 days: a) Mean diameter of CL-AG (○), AL-AG (■), LNC-AG (□) and PNC-AG (▼) at 4°C up to 14 days; b) Apigenin concentration (% of day 0) in CL-AG (○), AL-AG (■), LNC-AG (□) and PNC-AG (▼).

3.4. Stability of the NDDSs in serum

Stability of the NDDSs in serum was evaluated by following their size distribution in FBS (at 37°C, 75 rpm) against time using DLS in order to detect any alteration in their diameter and to determine possible particle destabilization, aggregation or protein corona formation. Additionally, the NDDS dispersions and FBS were also incubated under same conditions as controls.

As DLS shows size distribution graphs in relative intensity (%), the height of a unimodal peak will be higher compared to the same peak in a mixed multimodal sample. Moreover, focusing a particular size range (e.g. 0-50 nm or 100-300 nm) and getting information about a specific peak from a mixture is not possible in DLS. Therefore, peak heights of NDDS-FBS mixtures were normalized in the overlaid size graphs (FBS, NDDS, NDDS +FBS) (Figure 4a) for easier qualitative comparison with the controls, while position of the normalized peaks still provided information about possible corona formation.

Throughout the study period, size distributions of the control NDDSs were unimodal and their diameter did not change (Figure 4). Therefore, no signs of particle aggregation or degradation were observed. Size distribution of the control FBS remained bimodal (more frequent, peaks around 10-15 nm and 30-50 nm) or trimodal (less frequent additional small peak around 200 nm) up to 6 h of the study. However, larger aggregates were often observed in control FBS after 24 h with peaks around 300-500 nm.

CHAPTER 3

Up to 6 h, size distributions of the NDDS-FBS mixtures for CL-AG, AL-AG and PNC-AG were trimodal, showing the peaks of the free proteins (around 10-15 nm and 30-50 nm) and the NDDSs (peaks around 120-150 nm). Position of the peaks of NDDS-FBS mixtures were comparable with the corresponding control peaks. However, size distribution graph for LNC-AG-FBS mixture was bimodal as one of the peaks (around 30-50 nm) of FBS overlapped with the peak of LNC-AG, resulting a wider combined peak instead of two separate peaks. Moreover, higher concentration of LNC-AG was necessary, compared to CL-AG, AL-AG and PNC-AG, to observe its peaks in FBS due to the overlapping peaks. However, the peak of the NDDS was identifiable due to the increased height of the second peak in the LNC-AG-FBS mixture. The position of LNC-AG-FBS peaks were comparable with the controls (LNC-AG and FBS), like the other NDDSs. Therefore, up to 6 h, none of the NDDSs showed any signs of particle aggregation or adsorbing large amount of serum proteins, demonstrating their colloidal stability in serum.

The respective peaks of CL-AG, AL-AG and LNC-AG in FBS shifted toward larger diameters after 24 h. However, it is difficult to come into conclusion that the augmentation of diameter is due to protein adsorption and corona formation around the NDDS surface, or due to particle aggregation as the control FBS showed aggregated particle peaks around 300-500 nm after 24 h. However, in the experiment with PNC-AG, the NDDS peak in FBS mixture did not shift toward higher value after 24 h, and the control FBS also did not show any peaks of large aggregated particles.

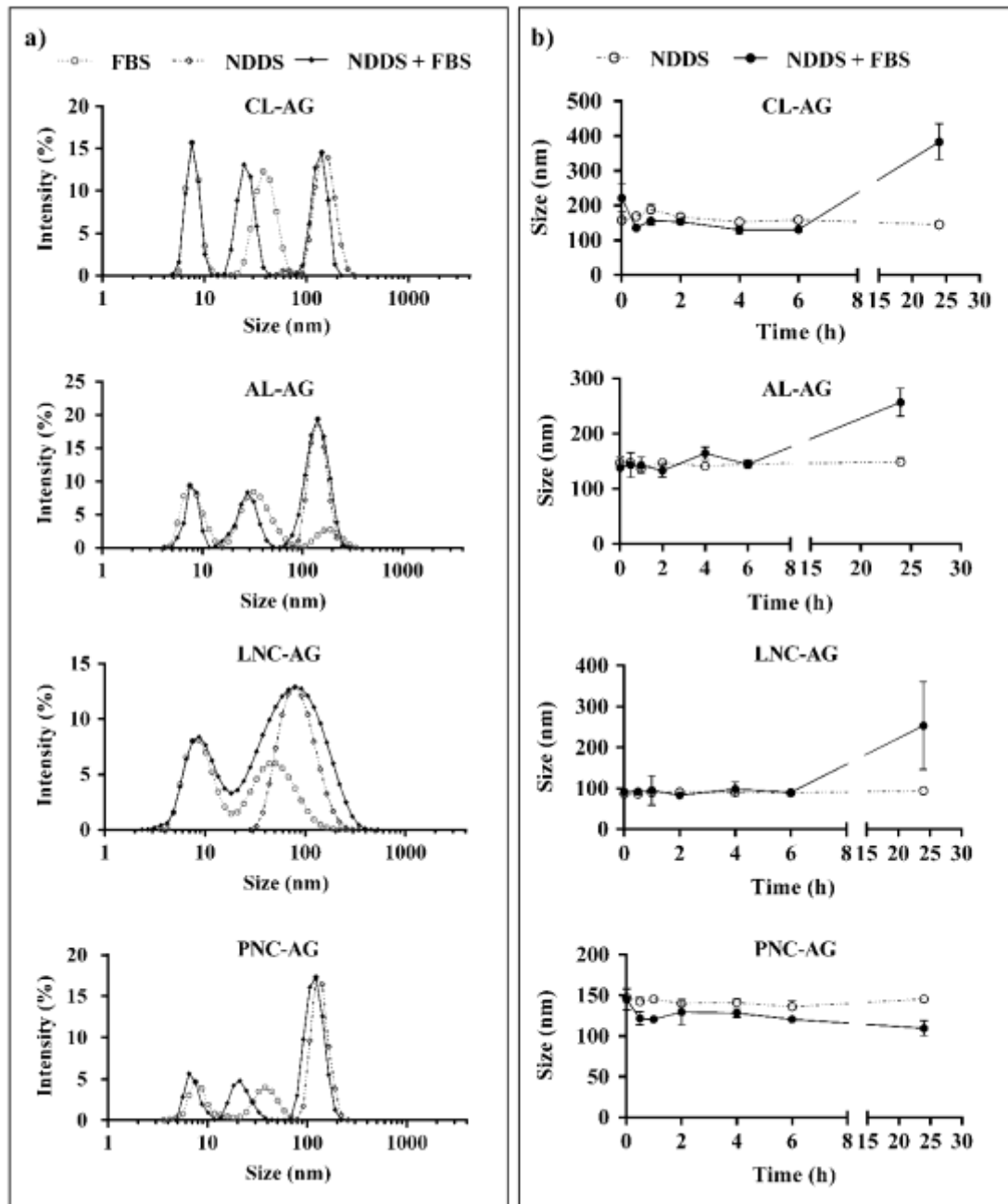


Figure 4. a) Size distribution profiles of CL-AG, AL-AG, LNC-AG and PNC-AG in FBS at 37°C and 75 rpm after 6 h. b) Diameter of CL-AG, AL-AG, LNC-AG and PNC-AG in FBS at 37°C and 75 rpm up to 24 h.

3.5. Complement consumption by the NDDSs

The complement consumption by the different NDDSs were measured by CH50 assay. Their percentage of CH50 unit consumption was plotted as a function of the particle surface area per mL of NHS (Figure 5). As usually observed, the complement

consumption for the four nanocarriers was increasing with the amount of NDDS added in NHS. The LNC-AG showed the lowest CH50 consumption and reached only 2.1 % at 800 cm^2/mL of NHS. The complement consumption of AL-AG and CL-AG increased gradually and reached 17.5% at 852 cm^2/mL of NHS and 26.8% at 752 cm^2/mL of NHS respectively. Although the PNC-AG consumed higher CH50 units at smaller surface areas than the others, its consumption increased slowly when more nanoparticles were added and reached 23.7% at 838 cm^2/mL of NHS.

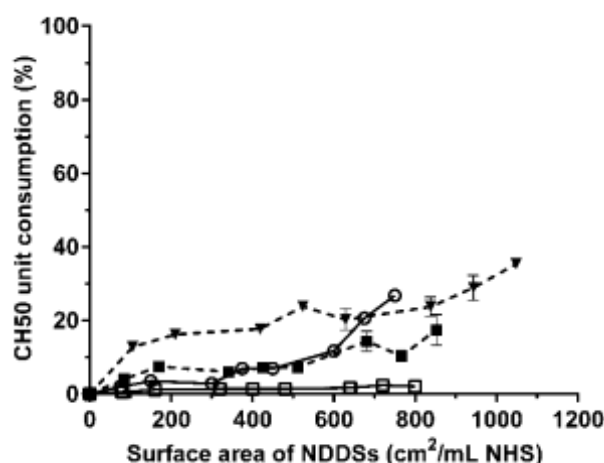


Figure 5. Complement consumption at 37°C by CL-AG (○), AL-AG (■), LNC-AG (□) and PNC-AG (▼).

3.6. *In vitro* cytotoxicity of the NDDSs on endothelial cells

Cytotoxicity of AG solution and the NDDSs on EAhy926, a human endothelial cell line, was evaluated *in vitro* by two different assays i.e. MTS and LDH assay (Figure 6). The drug solution did not show any significant toxicity in both assays. The CL-AG and CL-blank showed no signs of toxicity up to 2.5 μM . However, significant reduction of cell viability was revealed at concentrations ≥ 10 μM , corresponding to ≥ 171 $\mu\text{g}/\text{mL}$ of CL-AG (Table 3). Correspondingly, significant necrosis was observed in LDH assay at similar concentrations of CL-blank and PNC-blank. However, the AL-blank, AL-AG, LNC-blank, LNC-AG and PNC-AG showed no significant reduction in cell viability or any substantial cell necrosis at the test concentrations. Overall, the results observed in MTT and LDH assays were comparable and the nanocarriers were nontoxic up to high concentrations of the NDDSs (AG conc. and corresponding NDDS conc. are shown in Table 3).

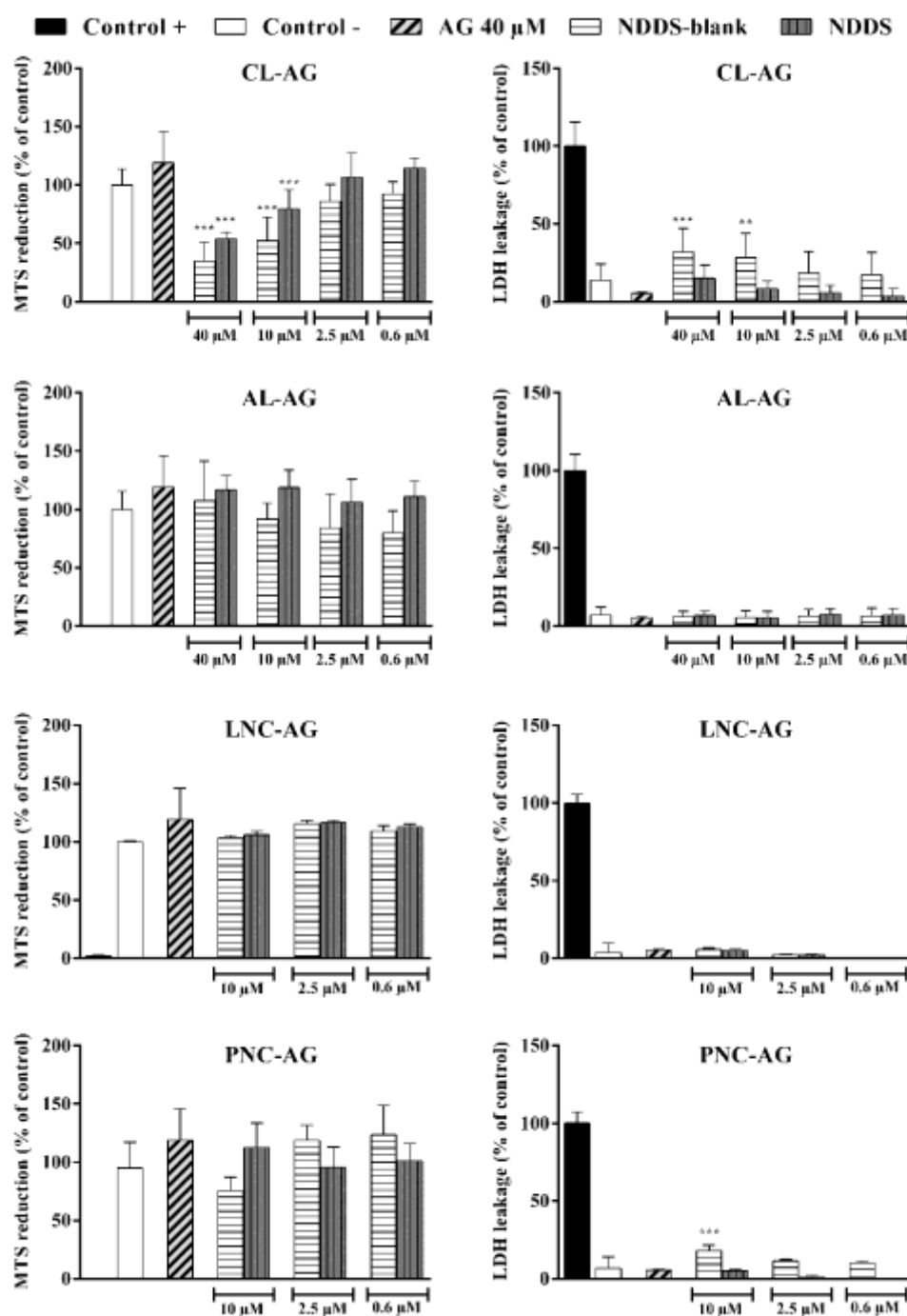


Figure 6. Cytotoxicity of AG, CL-AG, CL-blank, AL-AG, AL-blank, LNC-AG, LNC-blank, PNC-AG and PNC-blank on EAhy926 cells. The cells were treated for 24 h. At the end of the incubation period, cell viability was determined by the MTS reduction assay and cell necrosis was quantified by LDH assay, as described in section 2.11. (Oneway ANOVA with Dunnett's post-test. $p < 0.1$ is denoted by (*), $p < 0.01$ by (**) and $p < 0.001$ by (***)).

Table 3. AG concentrations and corresponding NDDS concentrations

AG conc. (μ M)	Corresponding NDDS concentration (μ g/ml)			
	CL-AG	AL-AG	LNC-AG	PNC-AG
40.0	683	1678	1744	756
10.0	171	420	436	189
2.5	43	105	109	47
0.6	10	25	26	11

4. Discussion

The aim of the present study was to develop injectable dosage forms of AG, to allow their use for *in vivo* studies. AG showed many promising pharmacological activities, but its *in vivo* use is restricted due to very low aqueous solubility. As a result, very slow dissolution would occur after oral administration, which is the rate limiting step causing slow absorption and low bioavailability (Zhang et al., 2013). In fact, a study on pharmacokinetics and metabolism of AG reported that the drug reached the systemic circulation 24 h after oral administration (Gradolatto et al., 2005). Parenteral administration of AG solution formulations can overcome the problem of bioavailability, but face challenges of short plasma half-life (90-105 min) (Wan et al., 2007; Zhang et al., 2013) and nonspecific high tissue distribution (Wan et al., 2007). Moreover, rapid crystallization may occur when these formulations are injected into blood which reduces its availability at diseased tissue (Engelmann et al., 2002). In fact, Engelmann et al. observed enlarged abdominal lymph nodes in mice caused by AG deposition after treatment with such formulation of the drug (Engelmann et al., 2002). Hence, it is necessary to develop suitable drug carrier systems for AG with sufficient stability during storage and in serum. Therefore, three types of NDDSs of AG were developed in this study i.e. liposomes, LNC and PNC; and were evaluated as potential injectable formulations of AG. For PNC preparation, a novel tocopherol modified PEG-b-polyphosphate block-copolymer was used for the first time. The amphiphilic surface active properties of the polymer can aid to improve nanocarrier stability which has been already described in the literature (Lopalco et al., 2015). The use of polyphosphate backbone instead of commonly utilized polylactide or polyglycolide chains is more

CHAPTER 3

biocompatible as the degradation products of polyphosphates do not create extreme acidic environment (Yilmaz and Jerome, 2016). The presence of tocopherol on the polyphosphate chain helps to improve entrapment of hydrophobic drugs like AG (Tripodo et al., 2015). Additionally, it may improve the stability of AG by acting as an antioxidant and protecting its phenol groups from oxidation.

Three key physicochemical properties of the nanocarriers influence their *in vivo* behavior: particle size, surface charge and surface coating (Straubinger et al., 1993). These properties must be optimized in order to achieve favorable drug delivery. Particle size is an important parameter which has profound impact on the uptake of NDDSs by MPS. The rate of MPS uptake increases as size of NDDSs increases (Senior et al., 1985). Size of the CL-AG, AL-AG and PNC-AG were comparable, but the LNC-AG had smaller diameter. Compared to AL-AG, the lipid bilayer of CL-AG had an additional dimethylaminoethane-carbamoyl (DC-) chain on cholesterol molecules which imparted a significant positive surface charge (as ionically bonded chloride ion dissociates from the hydrochloride salt of tertiary amine group of the DC- chain in aqueous environment) without affecting vesicle size. Although most components of the nanocapsule structures of the LNC-AG and PNC-AG were similar, the ratio of the excipients and manufacturing techniques were different, resulting in nanocapsules with dissimilar sizes. However, the major factor governing the higher size of the PNC-AG is possibly its higher weight fraction of core-oil (69%) compared to LNC-AG (50%), which is in accordance with previous reports (Heurtault et al., 2003; Lertsutthiwong et al., 2008). Though, size of all the NDDSs were within acceptable limits and comparable with previously studied systemically administered nanocarriers (Fu et al., 2009; Laine et al., 2014b; Lim et al., 2015; Mosqueira et al., 2001). The surface charge of nanocarriers is another critical parameter that is important from two perspectives- storage stability and *in vivo* distribution. Charged NDDSs are less prone to particle aggregation and more stable as dispersions, compared to neutral nanocolloids. Moreover, their cellular-interaction capacity and possibility of intracellular drug delivery are generally higher, compared to neutral NDDSs. Macrophage engulfment of charged nanocarriers increases as intensity of surface charge amplifies, whereas non-phagocytic cellular uptake increases the charge moves towards comparatively more positive value (He et al., 2010). The surface charges of the AG-loaded NDDSs can be ordered as follows-

CHAPTER 3

CL-AG > PNC-AG > LNC-AG \geq AL-AG, where zeta potential of only CL-AG was positive.

The presence of additional DC- chain on the cholesterol of the lipid bilayer of CL-AG not only altered the zeta potential, but improved the EE by 2 folds, compared to AL-AG. This is possibly due to charged interaction between AG and the DC- chain. AG is a weakly acidic molecule having two pKa values (6.6 and 9.3) (Favaro et al., 2007), and therefore will be partially deprotonated at the pH of the buffer (7.4) with an equilibrium between mono-anionic and neutral species (Papay et al., 2016; Tungjai et al., 2008). Therefore, the neutral species can be entrapped in the lipid bilayer and the mono-anionic species can interact with the positively charged DC- chain on the CL-AG surfaces, resulting significantly improved drug entrapment. Yuan et al. observed similar electrostatic and/or hydrogen bond formation among AG and positively charged human serum albumin (Yuan et al., 2007). Additionally, Papay et al. reported probable electrostatic repulsion among AG and sulfobutylether- β -cyclodextrin, due to presence of negatively charged sulfo group in the cyclodextrin which weakened their complexation as pH was increased (Papay et al., 2016). Moreover, the ionized DC- chain is present both at the inner and outer surfaces of the lipid bilayer facing towards the aqueous core and the surrounding aqueous environment respectively. As AG was added during the formation of dry lipid film, we hypothesize that AG might be electrostatically attached with both inner and outer surfaces during formation of the liposome. The phenomenon is more evident from the drug release characteristics and storage stability (chemical) of CL-AG which is explained in the respective parts of the discussion. The nanocapsules had high EE which can be possibly attributed to the presence of an oily core.

Drug loading capacity of the CL-AG was 2.5 folds higher compared to AL-AG, due to the presence of the additional positively charged DC- chain. Similarly, drug loading capacity of PNC-AG was 2.3 folds more compared to LNC-AG, possibly due to presence of higher % of core oil in its formulation (Lertsutthiwong et al., 2008).

A major parameter evaluated in this study was the drug release characteristics of the different NDDSs, to determine their feasibility as extended release carriers of AG. In previous experiments, plasma concentration of AG was high after intravenous administration, but it rapidly fell with a half-life around 1.75 h (Wan et al., 2007), which can be due to either crystallization of AG in physiological pH (Engelmann et al., 2002), or

CHAPTER 3

formation of its metabolites (Gradolatto et al., 2004). To prolong the pharmacological activity, dosage forms having prolonged plasma circulation time and extended release profile can be beneficial. Drug release at 37 °C in HEPES buffer (pH 7.4, 285-295 mOsm/kg) from the liposomes was more rapid compared to the nanocapsules, which can be attributed to the different composition and morphology of the two types of nanocarriers. The nanocapsules have an oily core surrounded by hydrophobic and amphiphilic polymers. Therefore, majority of hydrophobic drugs like AG will be encapsulated in the core of such nanocarriers. However, liposomes entrap majority of AG within their lipid bilayer and thus released the drug more easily compared to nanocapsules. The release rate from CL-AG was comparatively slower than AL-AG, which can be attributed to two possible reasons. Firstly, the possible electrostatic attraction of AG with the positively charged DC- chain can hinder the movement of the drug from the lipid bilayer. Secondly, the likelihood of presence of a portion of the entrapped AG at the inner surface of the lipid bilayer of CL-AG (as some DC- chains will be present at that surface) which provides more obstacles in the movement pathway of the drug. However, the nanocapsules i.e. LNC-AG and PNC-AG showed much sustained release characteristics than the liposomes. The release rate of the nanocapsules was comparable up to 24 h, but the PNC-AG showed slightly faster release rate afterwards, compared to LNC-AG. The higher % of excipients present on the LNC-AG shell (50% compared to 30% for PNC-AG) may have produced a thicker wall which contributed to the slower release rates at the later stages of the experiment (Watnasirichaikul et al., 2002).

No drug leakage was observed from any of the NDDSs during the storage stability study (14 days at 4°C) showing the robustness of the nanocarriers. Sizes of all the nanocarriers were also stable under the same conditions, and all of them remained monodispersed, demonstrating physical stability of the NDDSs. However, the AG concentration gradually decreased to 90 % after 14 days at 4°C in case of CL-AGs. Based on the difference in the formulation, EE and drug loading capacity of the liposomes, a large portion of the entrapped AG may be present at the surfaces of the CL-AG which puts the drug in contact of the aqueous environment during storage. This may lead to chemical modification or degradation, as pure AG is known to be an unstable molecule (Patel et al., 2007) in aqueous environments with pH below 8.25 (Xu et al., 2006). Further study would be necessary to confirm the mechanism of the possible AG degradation. However, AG

CHAPTER 3

concentration did not alter throughout the experiment period for AL-AG, LNC-AG and PNC-AG. Therefore, these NDDSs can be used to improve aqueous solubility and stability of AG. None of the NDDSs showed any drug leakage at 4°C up to 14 days.

The behavior of nanocarriers at the “bio-nano interface” must be evaluated to predict their *in vivo* fate (Nel et al., 2009; Palchetti et al., 2016). Formation of protein corona around nanocarriers is dependent on their composition, diameter, shape and surface properties along with several experimental parameters, e.g protein concentration, temperature, incubation time and incubation condition (static vs dynamic) etc. (Caracciolo, 2015; Palchetti et al., 2016). From relatively small to huge amounts of proteins may get adsorbed on the nanovector surface, and if plasma opsonins are adsorbed, the NDDSs will be removed from the systemic circulation by the MPS (Palchetti et al., 2016). Additionally, NDDSs can be destabilized or form aggregates in presence of serum proteins which will alter their *in vivo* fate. After injection into systemic circulation, NDDSs will be dispersed, diluted and surrounded by high amounts of proteins very quickly. Therefore, it is necessary to keep nanocarrier concentration as low as possible, compared to serum proteins, while evaluating their stability in serum. The total concentration of serum proteins (average concentration calculated based on manufacture specifications) was 188 folds higher than concentration of the CL-AG, AL-AG and PNC-AG, and 75 folds higher than the LNC-AG, in the nanocarrier-FBS mixtures used in this study. None of the NDDSs showed any signs of particle aggregation or protein corona formation up to 6 h, which indicates that the PEG chains on their surface were adequate to efficiently repel the serum proteins. Although some peaks of larger aggregates were observed in DLS after 24 h in case of CL-AG, AL-AG and LNC-AG, it is not conclusive that they adsorbed proteins on their surface as the control FBS also showed peaks around 200-500 nm at this time point. The nanocarriers may gradually lose their ability to repel proteins due to desorption of PEG chains from their surface, which occurs in a time-dependent way (Nag and Awasthi, 2013; Nag et al., 2013). Conversely, the larger peaks on the NDDS-FBS mixture also may appear due to the aggregated particles from FBS, which overlapped the peaks of the nanocarriers and shifted the peaks toward a higher value. The PNC-AG did not show any signs of particle aggregation or protein adsorption up to 24 h, but its peak shifted slightly towards smaller diameter (approximately 35 nm). As the PNC-AG was prepared using nanoprecipitation technique, tiny aqueous cavities may get entrapped within its oily

CHAPTER 3

core (Rabanel et al., 2014). Water from NDDS core may not escape to the exterior during storage as the particle core and shell membrane are less fluid at colder storage temperature (therefore no change in particle size is observed during storage), but can gradually come out when the NDDS is at physiological temperature in presence of serum due to altered osmotic pressure (Wolfram et al., 2014). Finally, the experiment showed that all of the developed NDDSs (CL-AG, AL-AG, LNC-AG and PNC-AG) were stable after large dilution in serum and did not form significant aggregates or protein corona for extended period which demonstrates their prolonged stability in serum.

Additionally, complement consumption of the NDDSs in human serum was evaluated by CH50 assay, as high consumption can lead to a rapid activation of the complement system and can be followed by clearance from bloodstream. The CH50 assay is an efficient technique for measuring the activation of the total complement system. It correlates well with other complement activation evaluation methods i.e. crossed immunoelectrophoresis and enzyme-linked immunosorbent assay, and represents also a good preliminary experiment to predict the stealth properties of nanocarriers intended for systemic administration (Meerasa et al., 2011). However, previous studies reporting complement consumption of nanocarriers (Cajot et al., 2011; Vonarbourg et al., 2006) plotted percentage of CH50 unit consumption against theoretical surface area of the particles which was calculated using an arbitrary density value. In contrast, NTA was used in this study to determine the number of nanocarriers per mL of NHS. Surface area was calculated using this number and the mean diameter of the NDDS. The previous method of theoretical surface area calculation produced values much higher (1474-1616 cm²/mL of NHS for the NDDS samples in this study) than the actual surface area obtained by NTA. Therefore, careful consideration is necessary when comparing the results with previous reports. The lowest CH50 unit consumption was observed for LNC-AG, which is in agreement with the results described by Vonarbourg et al. and can be possibly attributed to its smaller size (Vonarbourg et al., 2006) and higher percentage of PEG in its composition (due to presence of Kolliphor® HS15 and DSPE-mPEG₂₀₀₀) (Jeon et al., 1991) compared to the other NDDSs. Although, mean diameter of CL-AG, AL-AG and PNC-AG were similar, their CH50 unit consumption was different. Complement consumption of CL-AG was comparable with AL-AG up to 600 cm²/mL of NHS, but augmented comparatively faster then, possibly due to its positive surface-charge (Capriotti et al., 2012). Complement

activation of PNC-AG was higher at surface area $< 600 \text{ cm}^2$ compared to other three NDDSs, but reached only 23.7% at $832 \text{ cm}^2/\text{mL}$ of NHS. The difference can be due to several factors i.e. composition, PEG chain conformation, PEG density or presence of surfactant coating (PS80) (Gao and He, 2014). Further study would be necessary to validate the precise reason. Overall, the NDDSs did not show any strong complement consumption and should not be rapidly removed from systemic circulation by MPS.

Toxicity of the NDDSs on a human endothelial cell line (EAhy926) was evaluated to assess their injectability. The commonly used cytotoxic assays works by different mechanisms and their sensitivity can be dissimilar with alteration of cell lines (Fotakis and Timbrell, 2006; Lappalainen et al., 1994; Lobner, 2000). Moreover, presence of nanoparticles (Holder et al., 2012; Kroll et al., 2009) or the drug molecule (Wang et al., 2010) may interfere with the assay procedures and provide misleading results. Therefore, two common cytotoxicity assays i.e. MTS and LDH assays were used for evaluation and comparison of the possible toxic effects of the NDDSs on the endothelial cells. The two methods for cytotoxicity assessment provided similar results. Among the NDDSs, only CL-AG showed significant toxicity in a dose dependent manner in both assays at concentrations above $171 \text{ }\mu\text{g/mL}$. This is probably due to the presence of the tertiary nitrogen group containing cationic cholesterol derivative (DC-Chol) in CL-AG, which can act as protein kinase C inhibitor and result toxicity (Lv et al., 2006). In comparison, the AL-AG, LNC-AG and PNC-AG were nontoxic at their maximum test concentrations (420, 436 and $189 \text{ }\mu\text{g/mL}$ respectively). Overall, the NDDSs were nontoxic up to high concentrations and can be considered suitable as injectable AG-loaded nanovectors.

5. Conclusion

In this study, novel AG-loaded NDDSs, i.e. liposomes, LNC and PNC were developed as potential injectable dosage forms of AG. The nanovectors were characterized by their size, surface charge, EE, mass yield and drug loading capacity. Moreover, drug release property, drug leakage possibility and stability during storage were evaluated. Furthermore, stability of the NDDSs in serum at physiological temperature and cytotoxicity on a human macrovascular endothelial cell line was evaluated. The size of all the NDDSs was within the acceptable limit for injectable nanocarriers. The surface of the nanocarriers was positively (CL-AG) or negatively charged (AL-AG, LNC-AG and PNC-

CHAPTER 3

AG) which hinder particle aggregation and provided stability during storage. Presence of DC-Chol showed significant increase in AG entrapment at physiological pH, and application of such cationic lipids to improve AG encapsulation can be utilized in future NDDS development of the drug. Although, toxicity due to cationic lipids and chemical stability of the drug have to be carefully considered. Presence of oily core in the NDDSs was beneficial for AG encapsulation, and the LNC-AG and PNC-AG showed high EE. Moreover, this is the first study reporting the suitability and use of the tocopherol grafted PEG-b-polyphosphate amphiphilic block-copolymer PEG₁₂₀-b-(PBP-co-Ptoco)₉ for stable nanocapsule preparation.

Finally, all the nanovectors were stable in FBS for extended periods, showed weak complement system activation and were non-toxic to human macrovascular endothelial cells up to high concentrations, and therefore were suitable as injectable nanocarriers of AG. Due to less pronounced burst effect and extended release characteristics, the nanocapsule formulations i.e. LNC-AG and PNC-AG could be favorable approach for achieving prolonged pharmacological activity or tumor-targeted delivery of AG using injectable NDDS.

Funding

This work was supported by the NanoFar Consortium of the Erasmus Mundus program; and Fonds Léon Fredericq, CHU, University of Liege, Liege, Belgium. CERM is indebted to the Interreg Euregio Meuse-Rhine IV-A consortium BioMIMedics (2011-2014) and IAP VII-05 (FS2) for supporting research on new degradable polymers.

Appendix A. Supplementary data

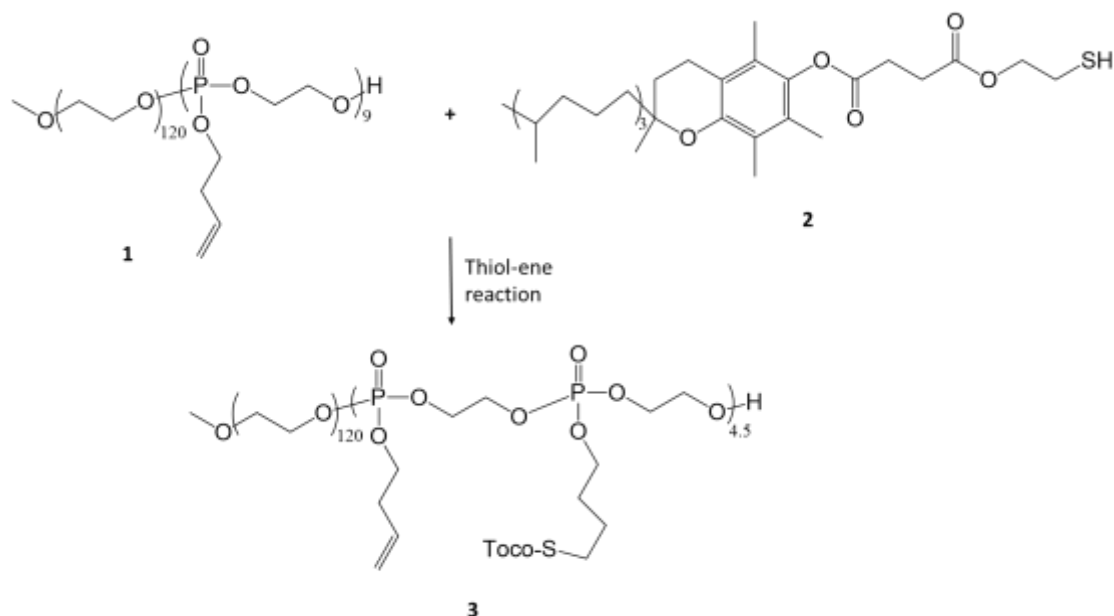


Figure S1: Structure of the poly(ethylene glycol)-b-polyphosphate (PEG)₁₂₀-b-(PBP-co-Ptoco)₉ copolymer used in this study (**3**) obtained by thiol-ene reaction of modified tocopherol (**2**) (toco-SH) on poly(ethylene glycol)₁₂₀-b-poly(butenylphosphate)₉ (**1**).

Table S1: Summary of P-values obtained by One way ANOVA followed by Bonferroni post-test to compare the various characteristics of the NDDSs. p < 0.1 is denoted by (*), p < 0.01 by (**) and p < 0.001 by (***)

Groups	P value summary				
	Mean diameter	Zeta potential	EE	Mass Yield	Drug loading capacity
CL vs AL	ns	***	***	ns	***
CL vs LNC	***	***	*	ns	***
CL vs PNC	ns	***	**	ns	**
AL vs LNC	***	ns	***	**	ns
AL vs PNC	ns	*	***	ns	***
LNC vs PNC	***	ns	ns	ns	***

Table S2: Zeta-potentials of CL-blank, AL-blank, LNC-blank and PNC-blank

Formulation	Zeta potential (mV)
CL-blank	43.8 ± 2.6
AL-blank	-28.2 ± 1.2
LNC-blank	-27.6 ± 6.7
PNC-blank	-15.8 ± 2.8

3.3.2. Additional unpublished data

In publication 2, the AG concentration in CL-AG decreased gradually during storage at 4°C. We hypothesized that AG concentration decreased due to possible degradation of the partially deprotonated drug that was perhaps adsorbed on the CL surface by electrostatic attraction and/or hydrogen bond formation. However, drug entrapment strategy in the CL could be changed by formation of aqueous soluble AG-cyclodextrin complex and encapsulation of this complex in the aqueous core of the vesicle to form DCLs. This may allow to improve drug loading capacity of the liposome. Additionally, formation of cyclodextrin complex may improve the stability of the drug (Tonnesen et al., 2002). Therefore, we developed an AG-cyclodextrin complex, evaluated its stability, prepared DCLs and characterized them. Additionally, lyophilization of the CL-AG in presence of suitable concentration of lyoprotectant was performed to improve the stability by storing it in the freeze-dried form.

3.3.2.1 Materials and methods

3.3.2.1.a. Materials

Hydroxypropyl- β -cyclodextrin (HP β CD) degree of substitution 0.87 was provided by Roquette (Belgium). D-(+)-trehalose dihydrate (trehalose) was collected from TCI Europe N.V. (Belgium). The human cerebral microvascular cells (hCMEC/D3) were provided by CELLutions biosysteme Cederlane (USA). Neuro2a cells were collected from Lonza (Belgium). EMEM basal medium was collected from Lonza (Belgium). EndoGRO-MV complete culture media kit was purchased from Merck (Belgium).

3.3.2.1.b. Apigenin-cyclodextrin complex formation

HP β CD was dissolved in HEPES buffer pH 7.4 to make 50 mM and 100 mM solutions. A 0.250 mg/mL AG solution in methanol was prepared by stirring under dark condition at

CHAPTER 3

room temperature for 30 minutes. Afterwards, the AG solution was mixed with the HP β CD solutions at room temperature for 30 minutes. Methanol was removed from the solution using a rotary evaporator at 30°C for 1 h, and subsequently at 45°C until all methanol was removed and only a viscous syrup-like solution of AG-HP β CD complex remained. Required volumes of UPW were added (if necessary) to make the HP β CD concentration to their original concentration (50 mM and 100 mM).

The resulting solution was then distributed into vials in 1mL aliquots and lyophilized for 23 h 30 min in a freeze-dryer (Heto-Holten, model DW 8030) using a vacuum pump (Vacuubrand RZ8). The samples were primarily frozen at -35°C for 3 h 30 min, followed by a primary drying at -15°C for 3 h at 0.8 bar pressure and at -10°C for 12 h at 0.1 bar pressure. Final drying step was carried out at 10°C for 5 h at 0.1 bar pressure.

3.3.2.1.c. Stability of the AG-HP β CD complex

The complexes were stored at 4°C in the freeze-dried form or in solution. Solutions were prepared by rehydration of freeze dried complexes (1 mL of UPW in each vial to rehydrate them to their starting concentration).

AG concentration was measured by the HPLC method described in Publication 2- section 2.4. on day 0, 1, 3, 7, 14, 28, 56, and 84 for freeze dried complexes and on day 0, 1, 7, and 14 for solutions.

3.3.2.1.d. Drug-in-cyclodextrin-in-liposome formulations

DCL formulations (DCL-AG and DCL-AG2) were prepared according to the formulation and preparation method described for CL-AG in publication 2 section 2.2.1, except AG was added (at 0.13 and 0.26 molar ratio in DCL-AG and DCL-AG1 respectively) as AG-HP β CD complex solution in HEPES buffer pH 7.4 during the dried lipid-film rehydration step. Moreover, purification was performed by centrifugation of the liposomes at 35,000 rpm for 2 h at 4°C (2x). The supernatants were replaced each time with fresh HEPES buffer and the liposomes were redispersed.

The liposomes were characterized for their size distribution, zeta potential, EE, mass yield and drug-loading capacity according to the method described in Publication 2- section 2.3 to section 2.6.

3.3.2.1.e. Lyophilization of CL-AG

Trehalose (concentration range of 0.5-8 % (w/v)) was added to CL-AG dispersion and stirred at room temperature for 30 min. CL-AG samples with or without trehalose were lyophilized by the method described in section 2.4.1.2. The freeze-dried samples were re-dispersed in UPW and size distribution of the CL-AGs were measured.

Thereafter, the CL-AGs were lyophilized using the optimum trehalose concentration, sealed under vacuum and stored at 4°C. The freeze-dried CL-AGs were dispersed in UPW on specified days (day 0, 1, 3, 7, 14, 28, 56 and 84) and storage stability of the lyophilized CLs was determined up to 12 weeks by method described under section 2.3. (Publication 2, section 2.8).

3.3.2.1.f. *In vitro* cytotoxicity of the NDDSs on human cerebral microvascular cells and neuronal cells

The Neuro 2a cells were cultured at 37°C in a humidified atmosphere and 5% CO₂ in EMEM basal medium supplemented with 10% (v/v) heat inactivated FBS and 1% of Penicillin-Streptomycin. The hCMEC/D3 cells were cultured in Endogro-mv complete culture media kit supplemented with 1% Penicillin-Streptomycin. Both Neuro2a and hCMEC/D3 were seeded in a 96-well plate at a density of 12.5×10^3 cells/well and incubated for 24 hours. Cytotoxicity of AG solution (in DMSO) and the NDDSs, at a concentration-range of 0.6 µM to 40 µM, were determined according to the method described under section 2.3. (Publication 2, section 2.11).

3.3.2.2 Results (unpublished)

3.3.2.2.a. Storage stability of AG-HPβCD complex

The AG-HPβCD complexes were prepared in order to develop DCL formulations which is described in the subsequent section. Storage stability at 4°C of the freeze-dried AG-HPβCD complexes was evaluated by rehydrating the samples on day 0, 1, 3, 7, 14, 28, 56, and day 84 and measuring the AG concentrations in the rehydrated samples. The freeze-dried complexes (at 50 mM and 100 mM HPβCD) were stable throughout the study period and their concentrations were 103 ± 2 % and 104 ± 2 % on day 84.

Storage stability of AG-HPβCD complex at 4°C in aqueous solutions was evaluated at day 0, 1, 7 and day 14 (Figure 3.2). AG concentration in AG-HPβCD complexes, at 50 mM HPβCD concentration, was significantly lower at day 7 (compared to day 0) and gradually

decreased to 87.1 ± 2.5 % by day 14. However, at 100 mM HP β CD concentration, AG concentration at day 1, 7 and 14 was not altered significantly compared to day 0.

At day 14, the percentage of AG in AG-HP β CD complex (50 mM HP β CD) was significantly lower compared to the complex in 100 mM HP β CD.

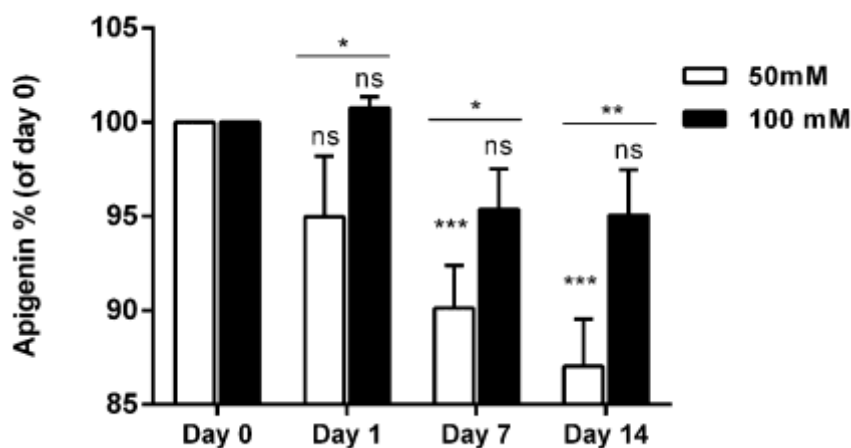


Figure 3.2: AG concentration in AG-HP β CD complexes (at 50 mM and 100 mM HP β CD concentrations) stored at 4°C. (Oneway ANOVA with Tukey's post-test. $p < 0.1$ is denoted by (*), $p < 0.01$ by (**) and $p < 0.001$ by (***)).

3.3.2.2.b. Drug-in-cyclodextrin-in-liposome formulations

The DCL formulations were prepared by encapsulating the aqueous soluble AG-HP β CD complex with the core of the CL. The freeze-dried AG-HP β CD complex (50 mM) was rehydrated using HEPES buffer pH 7.4. This solution was used to rehydrate the dried-lipid film to entrap the soluble AG-HP β CD complex within the core of the liposome. The amount of initially added AG-HP β CD complex was kept equivalent as initial AG concentration in CL-AG (molar ratio 0.13) to prepare the DCL-AG. To further improve the drug loading capacity, the initially added AG-HP β CD complex amount was doubled to prepare DCL-AG2. The sizes of DCL-AG and DCL-AG2 were 136 ± 3 nm and 134 ± 3 nm, which were about 8-10 nm smaller compared to CL-AG (Table 3.1). Zeta potentials of the formulations were 30-32 mV, which were significantly less positive (by 11-13 mV) compared to CL-AG. EE of DCL-AG and DCL-AG2 were 21 ± 6 % and 15 ± 4 % respectively, which were 3.4-folds and 4.7-folds lower compared to CL-AG. Mass yield of the formulations were 77 and 74 % for DCL-AG and DCL-AG2 respectively. However,

CHAPTER 3

drug loading capacity of both the formulations were significantly lower for DCL-AG and DCL-AG2 (3.2 and 2.2-folds respectively), compared to CL-AG.

Therefore, drug-loading capacity of CL could not be improved, rather was reduced by entrapping the drug as its aqueous soluble complex with HP β CD complex inside the liposome core.

Table 3.1. Physicochemical characteristics of the DCLs

Characteristics	DCL-AG	DCL-AG2
Mean diameter (nm)*	136 \pm 3	134 \pm 3
PDI	0.05 \pm 0.01	0.05 \pm 0.03
Zeta potential (mV)	30.2 \pm 1.0	32.2 \pm 3.1
EE (%)	21 \pm 6	15 \pm 4
Mass yield (%)	77 \pm 7	74 \pm 2
Drug loading capacity (μ gAG/mgNDDS)	5.1 \pm 1.6	7.5 \pm 1.6

* Measured by DLS.

3.3.2.2.c. Lyophilization of CL-AG

The CL-AGs were lyophilized with 0.5-8% (w/v) of trehalose and without trehalose. The freeze-dried liposomes were re-suspended by adding UPW and their size distribution was measured by DLS. In absence of trehalose, size of the freeze-dried liposomes increased massively due to fusion and PDI became high (> 0.450) (Figure 3.3). The liposome sizes were below 200 nm when trehalose concentrations were between 3 to 8% and the PDI was below 0.3 at 4, 5 and 8% trehalose concentrations. Among all the samples, liposome size (151 ± 16 nm) and PDI (0.204 ± 0.038) were the lowest in case of lyophilization with 5% trehalose. Therefore, 5% trehalose was used to lyophilize CL-AG for evaluating its storage stability at 4°C.

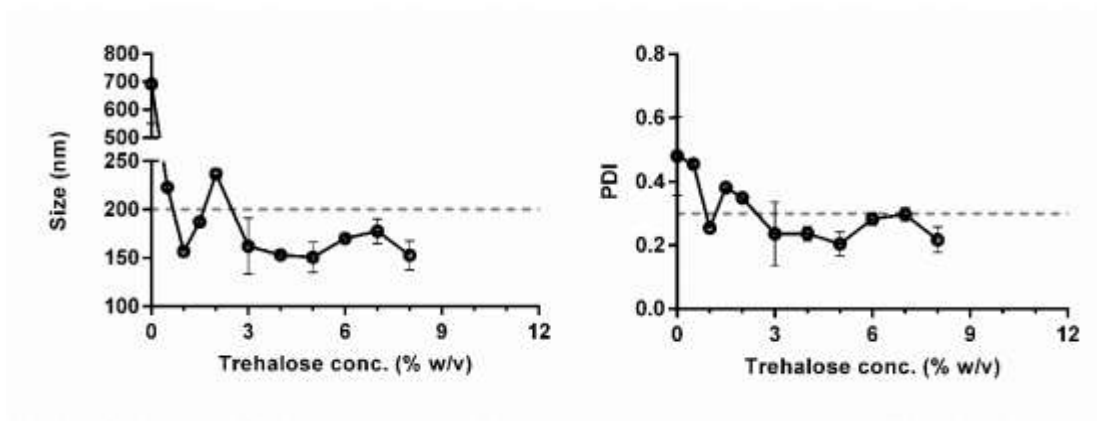


Figure 3.3: Size and PDI of CL-AG after lyophilization with various concentrations of trehalose.

Storage stability of the freeze-dried CL-AGs at 4°C was evaluated by measuring their size distribution (mean diameter and PDI) and AG concentrations after dispersing them in UPW overtime (Figure 3.4). Mean liposome size increased slowly, but were below 200 nm up to day 56 and reached 200 nm at day 84. Similarly, PDI increased very slowly, but remained below 0.3 at day 84. AG concentration (as % of day 0 concentration) was stable and never decreased throughout the study period, unlike the CL-AGs stored as dispersions (in publication 2).

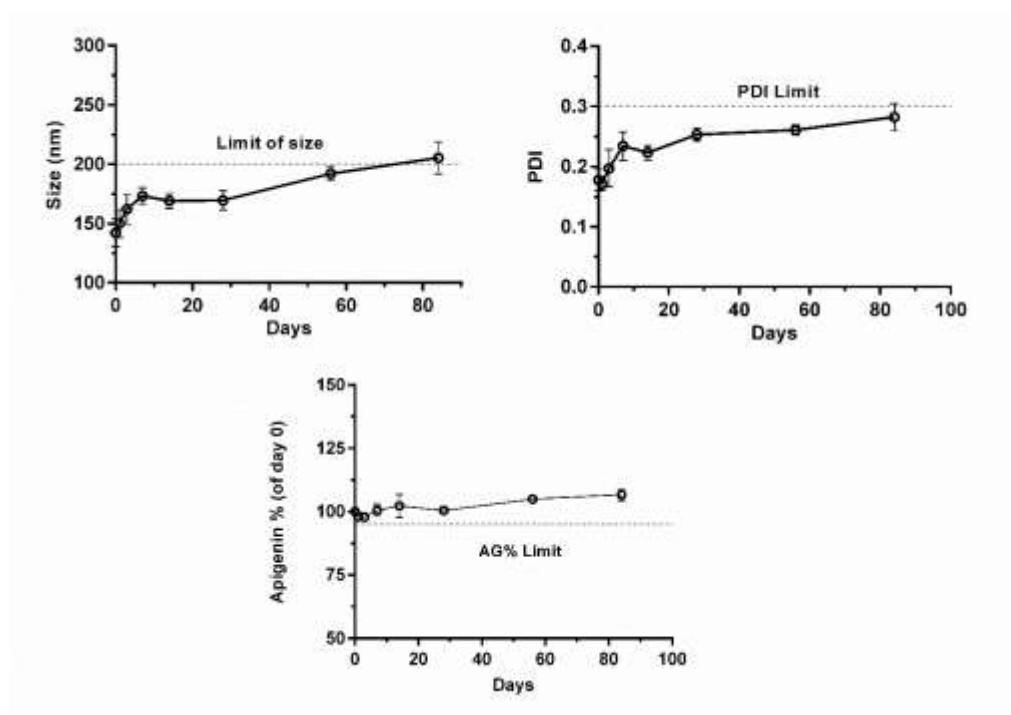


Figure 3.4: Size, PDI and AG concentrations of lyophilized CL-AG (with 5% trehalose) up to 84 days. After lyophilization, samples were stored under vacuum at 4°C and were dispersed in UPW at day 0, 1, 3, 7, 14, 28, 56 and 84 for characterization.

3.3.2.2.d. *In vitro* cytotoxicity of the NDDSs on human cerebral microvascular cells and neuronal cells

Cytotoxicity of AG solution and the NDDSs on hCMEC/D3 cells (a human cerebral microvascular endothelial cell line) (Figure 3.5) and on Neuro2a cells (a mouse neuroblastoma cell that differentiates into neurons) (Figure 3.6) were evaluated *in vitro* by two different tests i.e. MTS and LDH assays. The drug solution did not show any significant toxicity on either of the cell lines in both assays.

In hCMEC/D3 cells, CL-blank showed a significantly reduced cell viability from 10 μ M whereas CL-AG showed similar effect at 40 μ M. Correspondingly, CL-AG showed significantly enhanced LDH release at 40 μ M. However, AL-blank, AL-AG, LNC-blank, LNC-AG, PNC-blank and PNC-AG did not result in a decreased cell viability for the tested concentrations. LNC-blank and LNC-AG showed increased LDH leakage from 2.5 μ M, whereas PNC-blank showed similar effect at 10 μ M. The AL-blank and AL-AG did not show any significant enhanced LDH leakage throughout the tested concentrations.

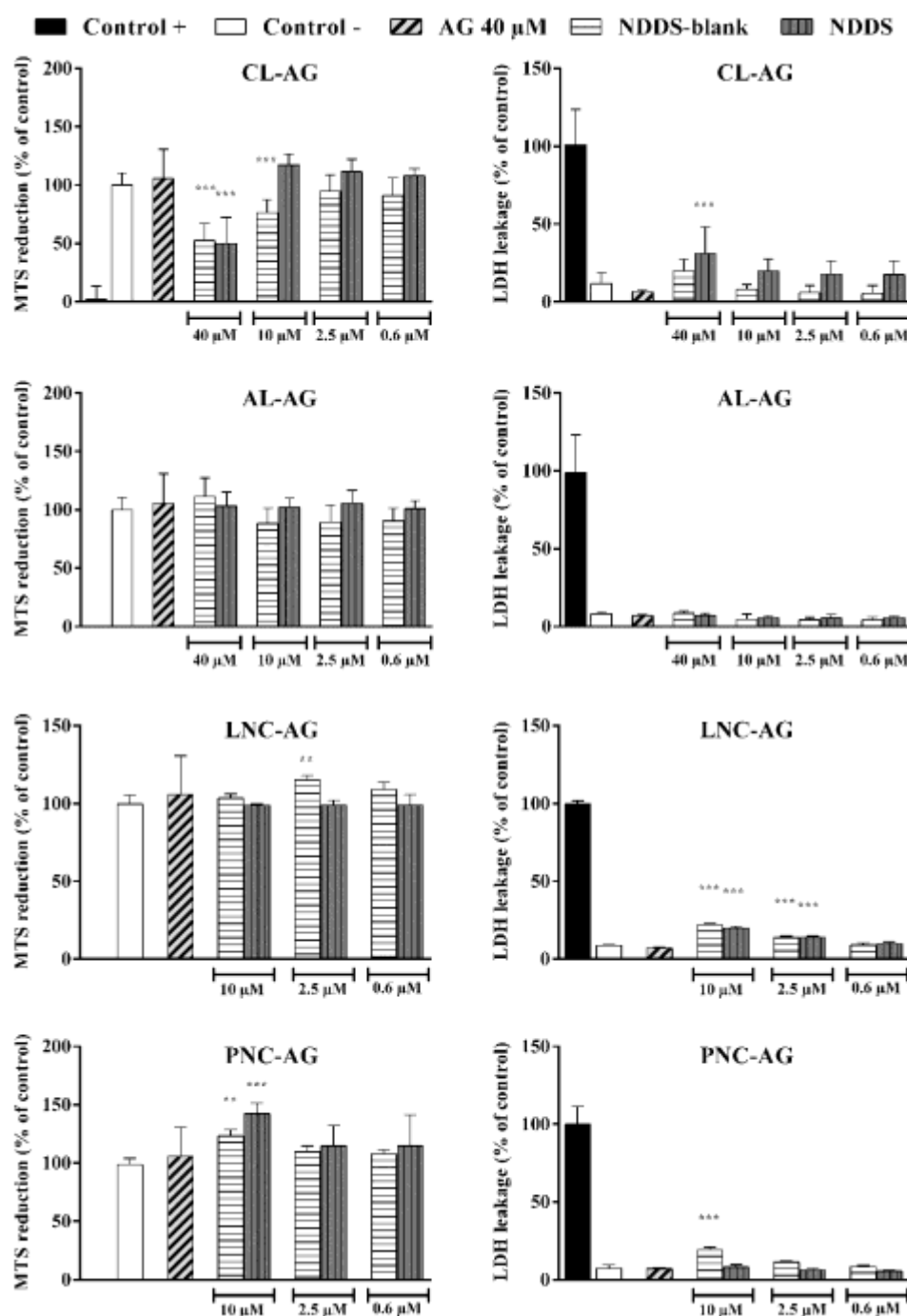


Figure 3.5: Cytotoxicity of AG, CL-AG, CL-blank, AL-AG, AL-blank, LNC-AG, LNC-blank, PNC-AG and PNC-blank on hCMEC/D3 cells. The cells were treated for 24 h. At the end of the incubation period, cell viability was determined by the MTS reduction assay and cell necrosis was quantified by LDH assay, as described in Publication 2 section 2.11. (Oneway ANOVA with Dunnett's post-test. p < 0.1 is denoted by (*), p < 0.01 by (**) and p < 0.001 by (***)).

CHAPTER 3

In Neuro2a cells, CL-blank and CL-AG significantly reduced cell viability in MTS assay and enhanced LDH leakage in LDH assay at 40 μ M concentrations. Similar effects were observed for LNC-blank and LNC-AG at 10 μ M concentrations. However, AL-blank, AL-AG, PNC-blank and PNC-AG did not show any signs of toxicity in both assays up to the highest studied concentrations.

Considering the drug loading capacity (Publication 2, Table 3) of the NDDSs, they were non-toxic to hCMEC/D3 and Neuro2a cells up to moderate to high concentrations.

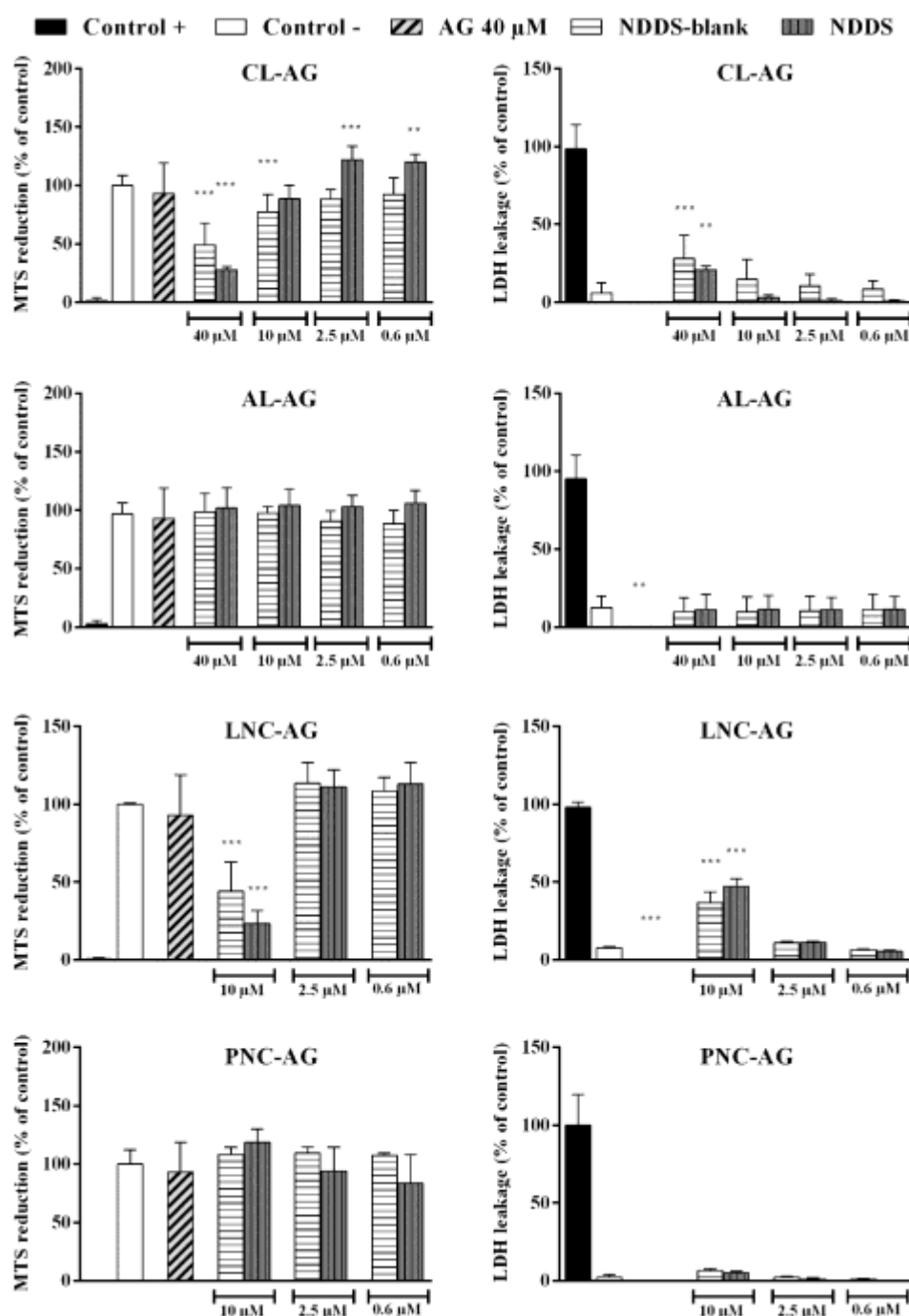


Figure 3.6: Cytotoxicity of AG, CL-AG, CL-blank, AL-AG, AL-blank, LNC-AG, LNC-blank, PNC-AG and PNC-blank on Neuro2a cells. The cells were treated for 24 h. At the end of the incubation period, cell viability was determined by the MTS reduction assay and cell necrosis was quantified by LDH assay, as described in section 2.11. (Oneway ANOVA with Dunnett's post-test. $p < 0.1$ is denoted by (*), $p < 0.01$ by (**) and $p < 0.001$ by (***)).

3.3.2.3 Discussion (additional unpublished results)

It was hypothesized in publication 2 that drug concentration in CL-AG decreased due to possible degradation of the partially deprotonated AG that was perhaps adsorbed on the CL surface due to electrostatic attraction and/or hydrogen bond formation. Reduction of AG concentration was not observed in the other formulations where AG was protected from aqueous environments. Formation of cyclodextrin complex with AG had the possibility to hide the drug in the cyclodextrin core, which could improve stability of the molecule like previously observed for curcumin (Tonnesen et al., 2002). Moreover, the AG-cyclodextrin complex could be encapsulated in the core of liposomes to prepare DCLs as an effort to improve the drug loading capacity. Therefore, two aqueous soluble AG-HP β CD complexes were prepared, AG complex with 50 mM and 100 mM HP β CD, and were encapsulated within CL core to prepare DCL-AG and DCL-AG2. However, the drug loading capacity of both DCLs were significantly lower compared to CL-AG. Therefore, the DCLs seemed less promising and were not further characterized. Moreover, the ability of the cyclodextrin complexes to protect AG from possible degradation in aqueous environment was assessed by evaluating the storage stability of the complexes in solution form. By day 14, AG concentration significantly decreased to 87% of initial concentration in case of the 50 mM complex. However, the 100 mM complex was comparatively stable in the same conditions although a tendency of AG concentration decrease was observed. Freeze-drying improves the storage stability of the complexes and they were stable throughout the study period (84 days). AG is known to form 1:1 complex with HP β CD. If the HP β CD concentration is increased from 50 to 100 mM, that will shift the equilibrium (as per Le Châtelier's principle) to produce more complexes and reduce the concentration of free AG (Figure 3.8). Therefore, at 100 mM HP β CD concentration, more AG-HP β CD complexes is produced which improves the protection of the drug molecule from aqueous environment and improves its stability.

CHAPTER 3

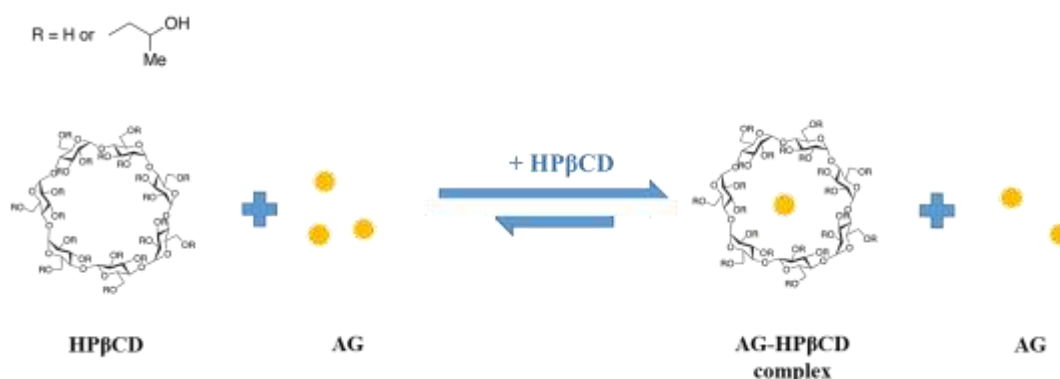


Figure 3.8: Shift of equilibrium between free AG and AG-HP β CD complex as concentration of HP β CD was increased.

Freeze-drying significantly improved the stability of the complex and they were completely stable at 4°C up to 84 days. Therefore, to improve the stability of the CL-AG, lyophilization was performed in presence of optimized concentration of trehalose (a commonly used lyoprotectant) and the freeze-dried liposomes were stored at 4°C. At specified time points, the liposomes were rehydrated and physicochemical characteristics of the formulation were evaluated. Lyophilization significantly improved the stability of the CL-AG and drug concentrations in the formulation did not decrease up to 7 weeks. Further studies are required to have better understanding about the mechanism of possible AG degradation in aqueous environments.

Cytotoxicity of the NDDSs on hCMEC/D3 cells and on Neuro2a cells was evaluated. The CLs showed antiproliferative activity on hCMEC/D3 cells from 683 $\mu\text{g/mL}$, whereas it showed both antiproliferative and cytotoxic effects from 683 $\mu\text{g/mL}$ on Neuro2a cells. The ALs did not show any antiproliferative or cytotoxic effects at the tested concentrations. The LNCs showed signs of cellular toxicity on hCMEC/D3 cells at 109 $\mu\text{g/mL}$, and both cytotoxic and antiproliferative effects on Neuro2a cells at 436 $\mu\text{g/mL}$. The PNC-blank showed cytotoxicity on hCMEC/D3 cells from 189 $\mu\text{g/mL}$. Antiproliferative activity or cytotoxicity can be due to certain excipients in the formulation i.e. the CLs has tertiary nitrogen group containing cationic cholesterol derivative which can act as certain kinase inhibitor and cause toxicity (Lv et al., 2006). However, extent of internalization for each nanovector may vary from one cell line to another, and their effects can depend on the uptake pathway. Moreover, results from commonly used cytotoxicity studies can vary due

to differences in sensitivity (Borenfreund et al., 1988; Fotakis and Timbrell, 2006). Therefore, two assays were performed in this study and only CL and LNC showed toxicity on both assays on Neuro2a cells at very high concentrations i.e. 683 $\mu\text{g/mL}$ and 436 $\mu\text{g/mL}$ respectively. Overall, the NDDSs were non-toxic up to high concentrations on these cells lines.

3.4. Conclusion of chapter 3

In this part of the study, we developed and characterized two liposomal and two nanocapsule formulations and characterized them as potential injectable nanocarriers for low-molecular weight hydrophobic molecules. The liposome formulation was selected based on a previously published literature (Bellavance et al., 2010). In that study, a non-PEGylated liposome formulation containing DPPC, DOPE and DC-Chol showed significant internalization and intracellular delivery of their cargo within 6 hours in GBM cells. Although this formulation was very promising *in vitro*, the absence of PEG-coating on its surface and its positive zeta potential (not measured in the published article, about +47 mV according to our experiments, results not shown) can be unfavorable for *in vivo* study as both will facilitate plasma protein adsorption and rapid clearance by RES systems. The authors intended to perform a future *in vivo* study by administering the non-PEGylated positively charged liposome by intra-arterial cerebral infusion to avoid the liver (major site of RES elimination) (Bellavance et al., 2010). However, no follow-up *in vivo* studies were published until now. Furthermore, the addition of PEG-coating on the liposome surface did hinder the cellular internalization and slowed down the intracellular delivery compared to the non-PEGylated liposome at 24 hours, but the uptake was similar up to 4 hours and only varied at long contact time (Bellavance et al., 2010). In the context of *in vivo* study, the PEGylated formulation could be promising as their uptake and intracellular delivery was similar up to 4 hours, may have prolonged circulation half-life after i.v. administration and can have more penetration radius in brain tissue after local delivery by CED, compared to the non-PEGylated formulation (MacKay et al., 2005). Therefore, the PEGylated liposome was chosen for preparation, modification, characterization and comparison with other formulations.

The LNCs are well known nanocarriers that have been used for delivery of lipophilic drug molecules in numerous studies (Lacoeuille et al., 2007; Saliou et al., 2013). Moreover,

CHAPTER 3

they have shown promising results as potential drug delivery systems for glioblastoma (Allard et al., 2010; Huynh et al., 2012). Additionally, their composition and nature of core material are very different from liposomes. Therefore, a comparison between LNC and liposomes as drug delivery systems for low-molecular weight hydrophobic drugs seemed interesting.

The use of polyphosphate blocks with PEG to produce copolymers instead of the commonly used carboester block copolymers e.g. PEG-PLA, PEG-PGA and PEG-PLGA for preparing nanocarriers can have several advantages. Their surface-active properties can aid in the stability of the developed nanocarriers like other amphiphilic polymers (Lopalco et al., 2015). Additionally, their chemical structure has resemblance with biomacromolecules i.e. DNA and RNA, and do not create highly acidic biodegradable products (Yilmaz and Jerome, 2016). Moreover, the additional valence of phosphorus compared to carbon (5 vs 4, respectively) gives more opportunity to polymer scientists for physicochemical modification in order to achieve desired properties for intended application (Yilmaz and Jerome, 2016). Among various PEG-polyphosphate polymers, the PEG₁₂₀-b-(PBP-co-Ptoco)₉ showed no toxicity on HUVEC cells up to very high concentrations (Vanslambrouck, 2015). Due to its promising characteristics, a nanovector formulation (PNC) was prepared for the first time using this polymer and the characteristics of PNC was compared with the liposomes and the LNC.

Size of the nanocarriers is an important parameter as capacity of the NDDSs to cross the BBB can be size dependent. As potential injectable nanocarriers, their size was kept between 59-145 nm (measured by DLS and NTA). This size range may allow the i.v. administered nanocarriers to passively accumulate into the brain tumors through the compromised BBTB (Steiniger et al., 2004). All the nanocarriers showed stability in serum up to 6 h and did not show high complement protein consumption, including the positively charged CL due to the PEG coating on its surface. All the nanocarriers except CL were stable during storage as dispersions. However, lyophilization of CL significantly improved its stability. Moreover, the NDDSs were non-toxic up to quite high concentrations on the various tested cell lines. The drug release from the nanocapsules (LNC and PNC) was significantly more controlled compared to the liposomes. The liposomes showed quick release profiles and may release maximum amount of encapsulated drug in the systemic circulation before reaching the tumor tissue after i.v,

CHAPTER 3

administration. Therefore, the nanocapsule formulations were more promising for future studies. Among the nanocapsules, the LNC had smaller size, more controlled release profile after 24 h and lower complement consumption compared to the PNC. It allows easy manufacturing, and the process does not involve organic solvents, suitable for scale-up. Therefore, LNC was selected among the NDDSs for the next studies.

The LNCs are known for their capability to revert lysosome integrity after endocytosis, and about 90 % of the nanocarrier can escape and deliver their cargo to extra endolysosomal targets, possibly due to the presence of Kolliphor® HS15 (Paillard et al., 2010). Paillard et al. showed that the uptake of LNC in F98 rat GBM cells was an active process, and occurred mainly through clathrin/caveolae-independent endocytosis. However, rate and pathway of LNC internalization is cell specific as expression of interacting plasma membrane moieties and endocytosis components varies from cell line to another (Paillard et al., 2010; Roger et al., 2009). Moreover, alteration of surface characteristics of LNC can also alter cellular internalization. Hence, to evaluate the potential of LNCs as potential hydrophobic drug encapsulating NDDS, intended for future clinical GBM treatment, it is necessary to investigate the cellular internalization profile of the nanovector in human GBM cell lines.

Therefore, the next chapter of the thesis is focused on evaluation and enhancement of LNC internalization in human GBM cell line by altering its surface characteristics. Additionally, possible cellular internalization pathways of the optimized formulation will be investigated. Additionally, the novel ferrocifen-derivate molecule FcTriOH, which is a low molecular weight hydrophobic molecule like AG and also promising for GBM treatment will be encapsulated in the LNC. The *in vitro* efficacy of the LNC-AG and LNC-FcTriOH formulations (with/without modified surface characteristics) on the human GBM cell will be assessed. Finally, preliminary *in vivo* studies will be performed on murine GBM models to assess the toxicity and efficacy of the drug-loaded LNCs after local or systemic administrations.

Acknowledgements

We would like to thank Dr. Julie Laloy, Anne-Sophie Delvigne and Prof. Jean-Michel Dogne (Namur Nanosafety Centre (NNC), Department of Pharmacy, University of Namur) for their support in the *in vitro* cytotoxicity studies.

3.5. References

- Allard, E., Jarnet, D., Vessieres, A., Vinchon-Petit, S., Jaouen, G., Benoit, J.P., Passirani, C., 2010. Local delivery of ferrociphenol lipid nanocapsules followed by external radiotherapy as a synergistic treatment against intracranial 9L glioma xenograft. *Pharm. Res.* 27, 56-64.
- Allard, E., Passirani, C., Benoit, J.P., 2009. Convection-enhanced delivery of nanocarriers for the treatment of brain tumors. *Biomaterials* 30, 2302-2318.
- Allard, E., Passirani, C., Garcion, E., Pigeon, P., Vessieres, A., Jaouen, G., Benoit, J.P., 2008. Lipid nanocapsules loaded with an organometallic tamoxifen derivative as a novel drug-carrier system for experimental malignant gliomas. *J. Control. Release* 130, 146-153.
- Baeten, E., Vanslambrouck, S., Jérôme, C., Lecomte, P., Junkers, T., 2016. Anionic flow polymerizations toward functional polyphosphoesters in microreactors: Polymerization and UV-modification. *Eur. Polym. J.* 80, 208-218.
- Bellavance, M.A., Poirier, M.B., Fortin, D., 2010. Uptake and intracellular release kinetics of liposome formulations in glioma cells. *Int. J. Pharm.* 395, 251-259.
- Bernardi, A., Braganhol, E., Jager, E., Figueiro, F., Edelweiss, M.I., Pohlmann, A.R., Guterres, S.S., Battastini, A.M., 2009. Indomethacin-loaded nanocapsules treatment reduces in vivo glioblastoma growth in a rat glioma model. *Cancer Lett.* 281, 53-63.
- Bhattacharjee, S., 2016. DLS and zeta potential - What they are and what they are not? *J. Control. Release* 235, 337-351.
- Blanco, E., Shen, H., Ferrari, M., 2015. Principles of nanoparticle design for overcoming biological barriers to drug delivery. *Nat. Biotechnol.* 33, 941-951.
- Borenfreund, E., Babich, H., Martin-Alguacil, N., 1988. Comparisons of two in vitro cytotoxicity assays-The neutral red (NR) and tetrazolium MTT tests. *Toxicol. In Vitro* 2, 1-6.
- Brigger, I., Morizet, J., Aubert, G., Chacun, H., Terrier-Lacombe, M.J., Couvreur, P., Vassal, G., 2002. Poly(ethylene glycol)-coated hexadecylcyanoacrylate nanospheres display a combined effect for brain tumor targeting. *J. Pharmacol. Exp. Ther.* 303, 928-936.
- Cajot, S., Lautram, N., Passirani, C., Jerome, C., 2011. Design of reversibly core cross-linked micelles sensitive to reductive environment. *J. Control. Release* 152, 30-36.
- Calvo, P., Gouritin, B., Chacun, H., Desmaële, D., D'Angelo, J., Noel, J.-P., Georgin, D., Fattal, E., Andreux, J.P., Couvreur, P., 2001. Long-circulating PEGylated polycyanoacrylate nanoparticles as new drug carrier for brain delivery. *Pharm. Res.* 18, 1157-1166.
- Capriotti, A.L., Caracciolo, G., Cavaliere, C., Foglia, P., Pozzi, D., Samperi, R., Lagana, A., 2012. Do plasma proteins distinguish between liposomes of varying charge density? *J. Proteomics* 75, 1924-1932.
- Caracciolo, G., 2015. Liposome-protein corona in a physiological environment: challenges and opportunities for targeted delivery of nanomedicines. *Nanomedicine* 11, 543-557.
- Clement, B., Grignard, B., Koole, L., Jérôme, C., Lecomte, P., 2012. Metal-free strategies for the synthesis of functional and well-defined polyphosphoesters. *Macromolecules* 45, 4476-4486.

CHAPTER 3

- De Melo, N.F., De Araujo, D.R., Grillo, R., Moraes, C.M., De Matos, A.P., de Paula, E., Rosa, A.H., Fraceto, L.F., 2012. Benzocaine-loaded polymeric nanocapsules: study of the anesthetic activities. *J. Pharm. Sci.* 101, 1157-1165.
- Eavarone, D.A., Yu, X., Bellamkonda, R.V., 2000. Targeted drug delivery to C6 glioma by transferrin-coupled liposomes. *J. Biomed. Mater. Res.* 51, 10-14.
- Engelmann, C., Blot, E., Panis, Y., Bauer, S., Trochon, V., Nagy, H., Lu, H., Soria, C., 2002. Apigenin—strong cytostatic and anti-angiogenic action *in vitro* contrasted by lack of efficacy *in vivo*. *Phytomedicine* 9, 489-495.
- Favaro, G., Clementi, C., Romani, A., Vickackaite, V., 2007. Acidochromism and ionochromism of luteolin and apigenin, the main components of the naturally occurring yellow weld: a spectrophotometric and fluorimetric study. *J. Fluoresc.* 17, 707-714.
- Felgner, P.L., Ringold, G.M., 1989. Cationic liposome-mediated transfection. *Nature* 337, 387-388.
- Filipe, V., Hawe, A., Jiskoot, W., 2010. Critical evaluation of Nanoparticle Tracking Analysis (NTA) by NanoSight for the measurement of nanoparticles and protein aggregates. *Pharm. Res.* 27, 796-810.
- Fotakis, G., Timbrell, J.A., 2006. *In vitro* cytotoxicity assays: comparison of LDH, neutral red, MTT and protein assay in hepatoma cell lines following exposure to cadmium chloride. *Toxicol. Lett.* 160, 171-177.
- Fu, J.Y., Blatchford, D.R., Tetley, L., Dufes, C., 2009. Tumor regression after systemic administration of tocotrienol entrapped in tumor-targeted vesicles. *J. Control. Release* 140, 95-99.
- Gao, H., He, Q., 2014. The interaction of nanoparticles with plasma proteins and the consequent influence on nanoparticles behavior. *Expert opinion on drug delivery* 11, 409-420.
- Gradolatto, A., Basly, J.P., Berges, R., Teyssier, C., Chagnon, M.C., Siess, M.H., Canivenc-Lavier, M.C., 2005. Pharmacokinetics and metabolism of apigenin in female and male rats after a single oral administration. *Drug Metab. Dispos.* 33, 49-54.
- Gradolatto, A., Canivenc-Lavier, M.C., Basly, J.P., Siess, M.H., Teyssier, C., 2004. Metabolism of apigenin by rat liver phase I and phase ii enzymes and by isolated perfused rat liver. *Drug Metab. Dispos.* 32, 58-65.
- He, C., Hu, Y., Yin, L., Tang, C., Yin, C., 2010. Effects of particle size and surface charge on cellular uptake and biodistribution of polymeric nanoparticles. *Biomaterials* 31, 3657-3666.
- Heurtault, B., Saulnier, P., Pech, B., Venier-Julienne, M.-C., Proust, J.-E., Phan-Tan-Luu, R., Benoît, J.-P., 2003. The influence of lipid nanocapsule composition on their size distribution. *Eur. J. Pharm. Sci.* 18, 55-61.
- Holder, A.L., Goth-Goldstein, R., Lucas, D., Koshland, C.P., 2012. Particle-induced artifacts in the MTT and LDH viability assays. *Chem. Res. Toxicol.* 25, 1885-1892.
- Huynh, N.T., Passirani, C., Allard-Vannier, E., Lemaire, L., Roux, J., Garcion, E., Vessieres, A., Benoit, J.P., 2012. Administration-dependent efficacy of ferrociphenol lipid nanocapsules for the treatment of intracranial 9L rat gliosarcoma. *Int. J. Pharm.* 423, 55-62.
- Iyer, A.K., Khaled, G., Fang, J., Maeda, H., 2006. Exploiting the enhanced permeability and retention effect for tumor targeting. *Drug discovery today* 11, 812-818.

CHAPTER 3

- Jeon, S.I., Lee, J.H., Andrade, J.D., De Gennes, P.G., 1991. Protein—surface interactions in the presence of polyethylene oxide. *J. Colloid Interface Sci.* 142, 149-158.
- Karim, R., Palazzo, C., Evrard, B., Piel, G., 2016. Nanocarriers for the treatment of glioblastoma multiforme: Current state-of-the-art. *J. Control. Release* 227, 23-37.
- Karim, R., Palazzo, C., Laloy, J., Delvigne, A.S., Vanslambrouck, S., Jerome, C., Lepeltier, E., Orange, F., Dogne, J.M., Evrard, B., Passirani, C., Piel, G., 2017a. Development and Evaluation of Injectable Nanosized Drug Delivery Systems for Apigenin. *Int. J. Pharm.*
- Karim, R., Somani, S., Al Robaian, M., Mullin, M., Amor, R., McConnell, G., Dufes, C., 2017b. Tumor regression after intravenous administration of targeted vesicles entrapping the vitamin E α -tocotrienol. *J. Control. Release* 246, 79-87.
- Kroll, A., Pillukat, M.H., Hahn, D., Schnekenburger, J., 2009. Current in vitro methods in nanoparticle risk assessment: limitations and challenges. *Eur. J. Pharm. Biopharm.* 72, 370-377.
- Lacoeuille, F., Hindré, F., Moal, F., Roux, J., Passirani, C., Couturier, O., Calès, P., Le Jeune, J.-J., Lamprecht, A., Benoit, J.-P., 2007. In vivo evaluation of lipid nanocapsules as a promising colloidal carrier for paclitaxel. *Int. J. Pharm.* 344, 143-149.
- Laine, A.-L., Clavreul, A., Rousseau, A., Tétaud, C., Vessieres, A., Garcion, E., Jaouen, G., Aubert, L., Guilbert, M., Benoit, J.-P., 2014a. Inhibition of ectopic glioma tumor growth by a potent ferrocenyl drug loaded into stealth lipid nanocapsules. *Nanomedicine* 10, 1667-1677.
- Laine, A.L., Gravier, J., Henry, M., Sancey, L., Bejaud, J., Pancani, E., Wiber, M., Texier, I., Coll, J.L., Benoit, J.P., Passirani, C., 2014b. Conventional versus stealth lipid nanoparticles: formulation and in vivo fate prediction through FRET monitoring. *J. Control. Release* 188, 1-8.
- Lamprecht, A., Bouligand, Y., Benoit, J.P., 2002. New lipid nanocapsules exhibit sustained release properties for amiodarone. *J. Control. Release* 84, 59-68.
- Lappalainen, K., Jaaskelainen, I., Syrjanen, K., Urtti, A., Syrjanen, S., 1994. Comparison of cell proliferation and toxicity assays using two cationic liposomes. *Pharm. Res.* 11, 1127-1131.
- Lee, J.H., Zhou, H.Y., Cho, S.Y., Kim, Y.S., Lee, Y.S., Jeong, C.S., 2007. Anti-inflammatory mechanisms of apigenin: inhibition of cyclooxygenase-2 expression, adhesion of monocytes to human umbilical vein endothelial cells, and expression of cellular adhesion molecules. *Arch. Pharm. Res.* 30, 1318-1327.
- Lertsutthiwong, P., Noomun, K., Jongaroonngamsang, N., Rojsitthisak, P., Nimmannit, U., 2008. Preparation of alginate nanocapsules containing turmeric oil. *Carbohydr. Polym.* 74, 209-214.
- Li, B., Robinson, D.H., Birt, D.F., 1997. Evaluation of properties of apigenin and [G-3H]apigenin and analytic method development. *J. Pharm. Sci.* 86, 721-725.
- Li, F., Zhao, X., Wang, H., Zhao, R., Ji, T., Ren, H., Anderson, G.J., Nie, G., Hao, J., 2015. Multiple layer-by-layer lipid-polymer hybrid nanoparticles for improved FOLFIRINOX chemotherapy in pancreatic tumor models. *Advanced Functional Materials* 25, 788-798.
- Lim, L.Y., Koh, P.Y., Somani, S., Al Robaian, M., Karim, R., Yean, Y.L., Mitchell, J., Tate, R.J., Edrada-Ebel, R., Blatchford, D.R., Mullin, M., Dufes, C., 2015. Tumor

CHAPTER 3

regression following intravenous administration of lactoferrin- and lactoferricin-bearing dendriplexes. *Nanomedicine* 11, 1445-1454.

Liu, Y., Lu, W., 2012. Recent advances in brain tumor-targeted nano-drug delivery systems. *Expert opinion on drug delivery* 9, 671-686.

Lobner, D., 2000. Comparison of the LDH and MTT assays for quantifying cell death: validity for neuronal apoptosis? *J. Neurosci. Methods* 96, 147-152.

Lopalco, A., Ali, H., Denora, N., Rytting, E., 2015. Oxcarbazepine-loaded polymeric nanoparticles: development and permeability studies across in vitro models of the blood-brain barrier and human placental trophoblast. *International journal of nanomedicine* 10, 1985-1996.

Lv, H., Zhang, S., Wang, B., Cui, S., Yan, J., 2006. Toxicity of cationic lipids and cationic polymers in gene delivery. *J. Control. Release* 114, 100-109.

MacKay, J.A., Deen, D.F., Szoka, F.C., Jr., 2005. Distribution in brain of liposomes after convection enhanced delivery; modulation by particle charge, particle diameter, and presence of steric coating. *Brain Res.* 1035, 139-153.

Meerasa, A., G Huang, J., X Gu, F., 2011. CH50: A revisited hemolytic complement consumption assay for evaluation of nanoparticles and blood plasma protein interaction. *Current Drug Delivery* 8, 290-298.

Moore, T.L., Rodriguez-Lorenzo, L., Hirsch, V., Balog, S., Urban, D., Jud, C., Rothen-Rutishauser, B., Lattuada, M., Petri-Fink, A., 2015. Nanoparticle colloidal stability in cell culture media and impact on cellular interactions. *Chem. Soc. Rev.* 44, 6287-6305.

Mora-Huertas, C.E., Fessi, H., Elaissari, A., 2010. Polymer-based nanocapsules for drug delivery. *Int. J. Pharm.* 385, 113-142.

Mora-Huertas, C.E., Garrigues, O., Fessi, H., Elaissari, A., 2012. Nanocapsules prepared via nanoprecipitation and emulsification-diffusion methods: comparative study. *Eur. J. Pharm. Biopharm.* 80, 235-239.

Mosqueira, V.C., Legrand, P., Morgat, J.L., Vert, M., Mysiakine, E., Gref, R., Devissaguet, J.P., Barratt, G., 2001. Biodistribution of long-circulating PEG-grafted nanocapsules in mice: effects of PEG chain length and density. *Pharm. Res.* 18, 1411-1419.

Nag, O.K., Awasthi, V., 2013. Surface engineering of liposomes for stealth behavior. *Pharmaceutics* 5, 542-569.

Nag, O.K., Yadav, V.R., Hedrick, A., Awasthi, V., 2013. Post-modification of preformed liposomes with novel non-phospholipid poly(ethylene glycol)-conjugated hexadecylcarbamoylmethyl hexadecanoic acid for enhanced circulation persistence in vivo. *Int. J. Pharm.* 446, 119-129.

Nel, A.E., Madler, L., Velegol, D., Xia, T., Hoek, E.M., Somasundaran, P., Klaessig, F., Castranova, V., Thompson, M., 2009. Understanding biophysicochemical interactions at the nano-bio interface. *Nat. Mater.* 8, 543-557.

Paillard, A., Hindre, F., Vignes-Colombeix, C., Benoit, J.P., Garcion, E., 2010. The importance of endo-lysosomal escape with lipid nanocapsules for drug subcellular bioavailability. *Biomaterials* 31, 7542-7554.

Palchetti, S., Colapicchioni, V., Digiaco, L., Caracciolo, G., Pozzi, D., Capriotti, A.L., La Barbera, G., Lagana, A., 2016. The protein corona of circulating PEGylated liposomes. *Biochim. Biophys. Acta* 1858, 189-196.

CHAPTER 3

- Papay, Z.E., Sebestyen, Z., Ludanyi, K., Kallai, N., Balogh, E., Kosa, A., Somavarapu, S., Boddi, B., Antal, I., 2016. Comparative evaluation of the effect of cyclodextrins and pH on aqueous solubility of apigenin. *J. Pharm. Biomed. Anal.* 117, 210-216.
- Patel, D., Shukla, S., Gupta, S., 2007. Apigenin and cancer chemoprevention: progress, potential and promise (review). *Int. J. Oncol.* 30, 233-245.
- Peer, D., Karp, J.M., Hong, S., Farokhzad, O.C., Margalit, R., Langer, R., 2007. Nanocarriers as an emerging platform for cancer therapy. *Nat. Nanotechnol.* 2, 751-760.
- Rabanel, J.M., Hildgen, P., Banquy, X., 2014. Assessment of PEG on polymeric particles surface, a key step in drug carrier translation. *J. Control. Release* 185, 71-87.
- Roger, E., Lagarce, F., Garcion, E., Benoit, J.P., 2009. Lipid nanocarriers improve paclitaxel transport throughout human intestinal epithelial cells by using vesicle-mediated transcytosis. *J. Control. Release* 140, 174-181.
- Romanova, D., Vachalkova, A., Cipak, L., Ovesna, Z., Rauko, P., 2001. Study of antioxidant effect of apigenin, luteolin and quercetin by DNA protective method. *Neoplasma* 48, 104-107.
- Ruozi, B., Belletti, D., Tombesi, A., Tosi, G., Bondioli, L., Forni, F., Vandelli, M.A., 2011. AFM, ESEM, TEM, and CLSM in liposomal characterization: a comparative study. *International journal of nanomedicine* 6, 557-563.
- Saliou, B., Thomas, O., Lautram, N., Clavreul, A., Hureaux, J., Urban, T., Benoit, J.P., Lagarce, F., 2013. Development and in vitro evaluation of a novel lipid nanocapsule formulation of etoposide. *Eur. J. Pharm. Sci.* 50, 172-180.
- Senior, J., Crawley, J.C., Gregoriadis, G., 1985. Tissue distribution of liposomes exhibiting long half-lives in the circulation after intravenous injection. *Biochim. Biophys. Acta* 839, 1-8.
- Sharma, A., Sharma, U.S., Straubinger, R.M., 1996. Paclitaxel-liposomes for intracavitary therapy of intraperitoneal P388 leukemia. *Cancer Lett.* 107, 265-272.
- Shukla, S., Gupta, S., 2010. Apigenin: a promising molecule for cancer prevention. *Pharm. Res.* 27, 962-978.
- Steiniger, S.C., Kreuter, J., Khalansky, A.S., Skidan, I.N., Bobruskin, A.I., Smirnova, Z.S., Severin, S.E., Uhl, R., Kock, M., Geiger, K.D., Gelperina, S.E., 2004. Chemotherapy of glioblastoma in rats using doxorubicin-loaded nanoparticles. *Int. J. Cancer* 109, 759-767.
- Straubinger, R.M., Sharma, A., Murray, M., Mayhew, E., 1993. Novel Taxol formulations: Taxol-containing liposomes. *J. Natl. Cancer Inst.*, 69-78.
- Thomas, O., Lagarce, F., 2013. Lipid Nanocapsules: A Nanocarrier Suitable for Scale-Up Process. *Journal of Drug Delivery Science and Technology* 23, 555-559.
- Tonnesen, H.H., Masson, M., Loftsson, T., 2002. Studies of curcumin and curcuminoids. XXVII. Cyclodextrin complexation: solubility, chemical and photochemical stability. *Int. J. Pharm.* 244, 127-135.
- Tripodo, G., Pasut, G., Trapani, A., Mero, A., Lasorsa, F.M., Chlapanidas, T., Trapani, G., Mandracchia, D., 2015. Inulin-D-alpha-tocopherol succinate (INVITE) nanomicelles as a platform for effective intravenous administration of curcumin. *Biomacromolecules* 16, 550-557.
- Tungjai, M., Poompimon, W., Loetchutin, C., Kothan, S., Dechsupa, N., Mankhetkorn, S., 2008. Spectrophotometric characterization of behavior and the predominant species of

CHAPTER 3

flavonoids in physiological buffer: determination of solubility, lipophilicity and anticancer efficacy. *Open Drug Deliv. J.* 2, 10-19.

Vanslambrouck, S., 2015. Polyphosphate-based amphiphilic copolymers: synthesis and application to drug nanocarriers. University of Liège, Liège, Belgium.

Vonarbourg, A., Passirani, C., Saulnier, P., Simard, P., Leroux, J.C., Benoit, J.P., 2006. Evaluation of pegylated lipid nanocapsules versus complement system activation and macrophage uptake. *J. Biomed. Mater. Res.* 78, 620-628.

Wan, L., Guo, C., Yu, Q., Li, Y., Wang, X., Wang, X., Chen, C., 2007. Quantitative determination of apigenin and its metabolism in rat plasma after intravenous bolus administration by HPLC coupled with tandem mass spectrometry. *Journal of Chromatography B* 855, 286-289.

Wang, P., Henning, S.M., Heber, D., 2010. Limitations of MTT and MTS-based assays for measurement of antiproliferative activity of green tea polyphenols. *PLoS One* 5, e10202.

Watnasirichaikul, S., Rades, T., Tucker, I.G., Davies, N.M., 2002. Effects of formulation variables on characteristics of poly (ethylcyanoacrylate) nanocapsules prepared from w/o microemulsions. *Int. J. Pharm.* 235, 237-246.

Wei, X., Gao, J., Zhan, C., Xie, C., Chai, Z., Ran, D., Ying, M., Zheng, P., Lu, W., 2015. Liposome-based glioma targeted drug delivery enabled by stable peptide ligands. *J. Control. Release* 218, 13-21.

Wolfram, J., Suri, K., Yang, Y., Shen, J., Celia, C., Fresta, M., Zhao, Y., Shen, H., Ferrari, M., 2014. Shrinkage of pegylated and non-pegylated liposomes in serum. *Colloids Surf B Biointerfaces* 114, 294-300.

www.malvern.com, 2017. Technical notes, p. 4.

Xu, X., Yu, L., Chen, G., 2006. Determination of flavonoids in *Portulaca oleracea* L. by capillary electrophoresis with electrochemical detection. *J. Pharm. Biomed. Anal.* 41, 493-499.

Yilmaz, Z.E., Jerome, C., 2016. Polyphosphoesters: New Trends in Synthesis and Drug Delivery Applications. *Macromol. Biosci.* 16, 1745-1761.

Yilmaz, Z.E., Vanslambrouck, S., Cajot, S., Thiry, J., Debuigne, A., Lecomte, P., Jérôme, C., Riva, R., 2016. Core cross-linked micelles of polyphosphoester containing amphiphilic block copolymers as drug nanocarriers. *RSC Adv.* 6, 42081-42088.

Yuan, J.-L., Liu, Z.-G., Hu, Z., Zou, G.-L., 2007. Study on interaction between apigenin and human serum albumin by spectroscopy and molecular modeling. *Journal of Photochemistry and Photobiology A: Chemistry* 191, 104-113.

Zanotto-Filho, A., Coradini, K., Braganhol, E., Schroder, R., de Oliveira, C.M., Simoes-Pires, A., Battastini, A.M., Pohlmann, A.R., Guterres, S.S., Forcelini, C.M., Beck, R.C., Moreira, J.C., 2013. Curcumin-loaded lipid-core nanocapsules as a strategy to improve pharmacological efficacy of curcumin in glioma treatment. *Eur. J. Pharm. Biopharm.* 83, 156-167.

Zhang, J., Huang, Y., Liu, D., Gao, Y., Qian, S., 2013. Preparation of apigenin nanocrystals using supercritical antisolvent process for dissolution and bioavailability enhancement. *Eur. J. Pharm. Sci.* 48, 740-747.

Zhang, J., Liu, D., Huang, Y., Gao, Y., Qian, S., 2012. Biopharmaceutics classification and intestinal absorption study of apigenin. *Int. J. Pharm.* 436, 311-317.

CHAPTER 3

- Zhang, L., Gu, F.X., Chan, J.M., Wang, A.Z., Langer, R.S., Farokhzad, O.C., 2008. Nanoparticles in medicine: therapeutic applications and developments. *Clin. Pharmacol. Ther.* 83, 761-769.
- Zhao, L., Zhang, L., Meng, L., Wang, J., Zhai, G., 2013. Design and evaluation of a self-microemulsifying drug delivery system for apigenin. *Drug Dev. Ind. Pharm.* 39, 662-669.
- Zheng, P.-W., Chiang, L.-C., Lin, C.-C., 2005. Apigenin induced apoptosis through p53-dependent pathway in human cervical carcinoma cells. *Life Sci.* 76, 1367-1379.

***Chapter 4: Surface-functionalization of lipid
nanocapsules for targeted drug delivery to human
glioblastoma cells***

4. SURFACE-FUNCTIONALIZATION OF LIPID NANOCAPSULES FOR TARGETED DRUG DELIVERY TO HUMAN GLIOBLASTOMA CELLS

4.1. Introduction

This chapter concerns about the surface functionalization of LNCs to enhance their internalization into human glioblastoma cells in order to improve their efficacy as GBM-targeting nanovector.

One of the toughest tasks in oncology is the drug delivery to brain-cancers like GBM. The major reason behind the failure of conventional chemotherapy is the BBB, which blocks the blood-to-brain passage of majority of the drug molecules (Pardridge, 2012). The use of nanocarriers can be a promising strategy to delivery drugs to brain tumor by several aspects. Long-circulating nanocarriers with appropriate size can bypass the BBB by EPR effect and accumulate in tumor tissue (Bernardi et al., 2009; Guo et al., 2011). However, EPR effect generally occur in considerably lower extent in brain tumors compared to peripheral tumors (Liu and Lu, 2012).

Surface-functionalization of the NDDSs with suitable moieties to achieve active targeting towards the BBB and/or the brain tumor tissue is another promising approach to enhance drug delivery to brain tumors (Beduneau et al., 2007). The surface-functionalizing ligands used for cerebral drug delivery can be peptides, proteins, mAb, surfactants or simpler molecules like sugars (Liu and Lu, 2012). Examples of brain-targeting ligands commonly used for nanocarrier surface-functionalization are the human immune deficiency virus type 1 (HIV-1) transcriptional activator protein derived TAT peptide (Gupta et al., 2007), the integrin targeting cyclic arginine–glycine–aspartic acid (cRGD) peptide (Zhan et al., 2010), endogenous proteins like Tf (Liu et al., 2013) and lactoferrin (Lf) (Pang et al., 2010), OX26 mAb (Yue et al., 2014), surfactants like PS80 (Ambruosi et al., 2006) and P188 (Wohlfart et al., 2011), and sugar molecule D-glucosamine (Dhanikula et al., 2008).

A neurofilament light subunit derived tubulin binding site peptide, i.e. NFL-TBS.40-63 (NFL), has been reported to be internalized by human, rat and mouse glioma cell lines (Berges et al., 2012a). The peptide internalization into various GBM cells was significantly higher compared to corresponding healthy astrocytes. Moreover, the peptide preferentially inhibited viability, proliferation and migration of the GBM cells, whereas

the astrocytes were not affected after similar treatment. Therefore, this peptide had the potential to be used as a GBM targeting-ligand if used at low concentrations (below its pharmacologically active concentrations) to functionalize NDDS surfaces. Balzeau et al. used this peptide to functionalize LNC surface and improved uptake of the nanocarrier into mouse GBM cells (Balzeau et al., 2013).

Surface-functionalization of nanovectors can be targeted to BBB cells only (to enhance their uptake in whole brain), can be dual-targeted to BBB and brain-tumor cells (using multiple ligands, or by single ligand that target both BBB and tumor cells), can be targeted towards BBTB, or can be targeted only to brain-tumor cells (efficacy relies on EPR effect, or developed for local administration) (Liu and Lu, 2012). However, no published reports of BBB/BBTB-targeting capability of the NFL peptide are available.

A targeting-moiety can be attached with the nanocarrier by several methods i.e. adsorption, chemical-linkage with nanovector surface, or chemical-linkage with the distal end of surface-coating hydrophilic polymer (Torchilin, 2005). Balzeau et al. reported that chemical linkage of the NFL peptide with the distal end of DSPE-PEG₂₀₀₀ (used as hydrophilic coating on LNC surface) hampered the GBM-targeting activity of the peptide significantly and uptake of this nanovector in mouse GBM cells was similar to the control LNC (non-functionalized) (Balzeau et al., 2013). However, simple adsorption of the peptide on LNC surface significantly enhanced nanovector internalization in mouse GBM cells.

The brain tumor targeted-nanovectors chiefly utilize carrier-mediated transport (CMT), receptor-mediated endocytosis (RME), and adsorptive-mediated endocytosis (AME) systems of the BBB and/or the brain-tumor cells (Beduneau et al., 2007) and enhances cellular internalization of the NDDSs. Cellular internalization of nanocarriers chiefly occur by various endocytosis pathways in mammalian cells (Figure 4.1) (Conner and Schmid, 2003). The endocytosis process occurs in several steps. Initially, the nanocarrier is entrapped in membrane invaginations that form intracellular vesicles called endosomes or phagosomes characterized by distinctive internalization machinery. Subsequently, the endosomes carry the nanovectors to other dedicated cytoplasmic vesicles which direct their contents toward various destinations. Lastly, the nanovector is supplied to different cellular compartments, sent back to the extracellular environment (exocytosis) or transported across the cells (transcytosis) (Sahay et al., 2010). Broadly, endocytosis can be

categorized into two groups, phagocytosis and pinocytosis. Phagocytosis occurs mainly in some particular cells called phagocytes (macrophages, neutrophils, monocytes and dendritic cells) (Aderem and Underhill, 1999), can internalize particles up to 20 μm and nanocarriers that are opsonized are generally engulfed by this process (Sahay et al., 2010). Pinocytosis can be sub-divided into several other categories (on the basis of the proteins involved in the mechanism) i.e. macropinocytosis, clathrin-dependent endocytosis, caveolin-dependent endocytosis and clathrin-caveolin independent endocytosis. Various nanocarrier characteristics (e.g. size, shape, surface charge and surface ligands) and cellular features (cell types and expression of receptors or transporters) can influence the complex nanovector-cell interaction, and most nanoparticles are internalized by multiple endocytosis pathways (Bareford and Swaan, 2007; Conner and Schmid, 2003; Sahay et al., 2010).

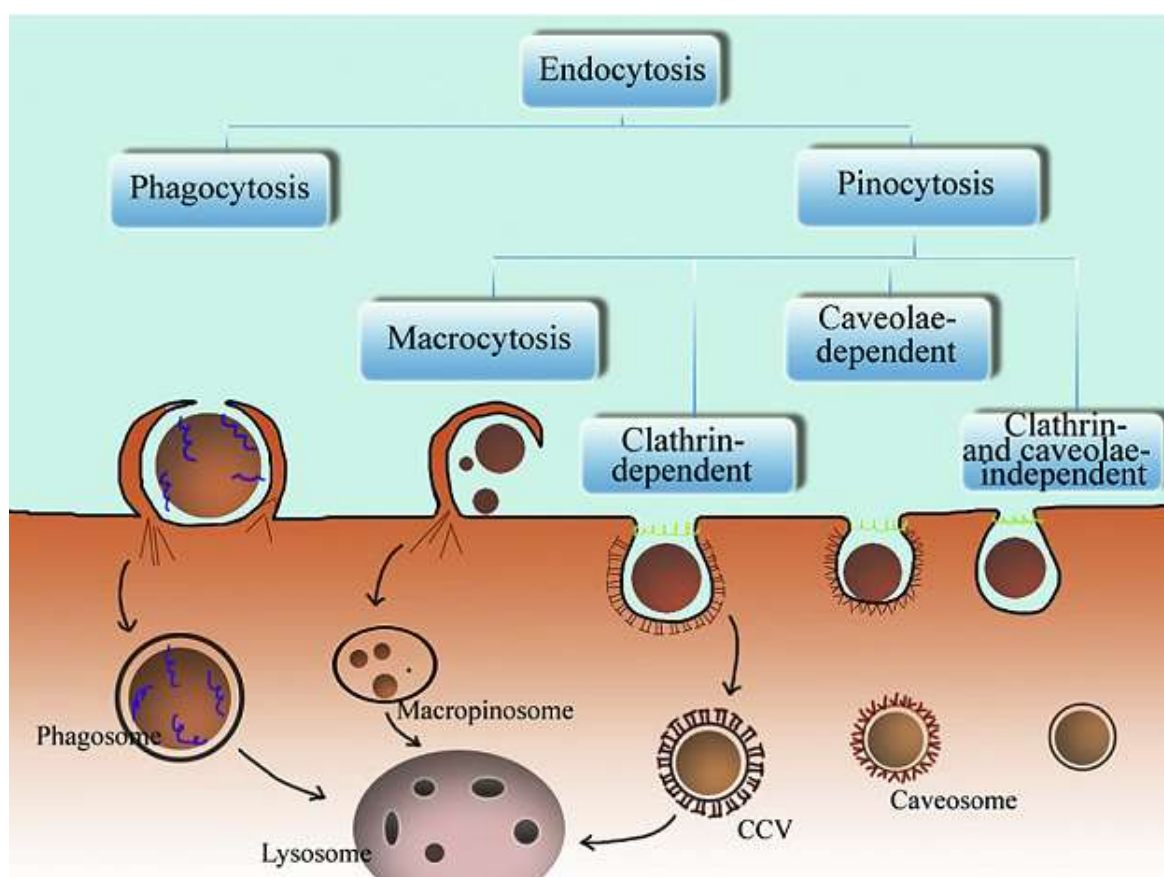


Figure 4.1: Various endocytosis pathways for nanocarrier internalization in mammalian cells (Kou et al., 2013).

Study of intracellular trafficking of nanocarriers can be important to understand the intracellular fate of the cargo, especially if they are carrying drug molecules sensitive to lysosomal degradation, and may help to understand the reason of success or failure of the therapy. The evaluation of the intracellular trafficking of NDDSs is mostly done by two methods. One method is called ‘pulse-chase’ method where cells are treated before or concurrently (of nanocarriers) with known endocytosis pathway markers and the colocalization of the nanovector and the marker is followed (Lepinoux-Chambaud and Eyer, 2013). In the other method, specific endocytosis pathways are blocked by pretreating the cells with pharmacological inhibitors (Mercer and Helenius, 2009) and the effect of such treatments are evaluated by exposing the cells to the NDDSs for certain time. However, such endocytosis markers and inhibitors are hardly selective towards one pathway and often impacts of multiple pathways (Ivanov, 2008). Therefore, combination of two methods is preferred for authenticating the endocytosis mechanism. Moreover, more than one technique, i.e. flow cytometry and confocal microscopy, can be used to investigate the internalization pattern of nanocarriers and further strengthen the results.

In the previous chapter, the LNCs were identified as one of the potential i.v. administrable NDDSs for hydrophobic drugs, among the 4 developed nanocarriers. In this chapter, the LNC surface was functionalized with NFL peptide in order to improve its internalization into human GBM cell line. The developed LNCs were physicochemically characterized, the interaction between LNC and NFL was evaluated, and their complement consumption in human serum was determined. Additionally, effect of surface-functionalizing NFL concentration on LNC internalization into human GBM cells and on BBB permeability of the nanocarriers was evaluated. GBM-targeting capability of the nanocolloids was evaluated by comparing their uptake into NHA and human GBM cells. Additionally, possible pathways of peptide-functionalized LNC internalization in the GBM cell line was assessed. Furthermore, two promising hydrophobic molecules for GBM treatment i.e. AG and FcTriOH were encapsulated in the LNC formulations and their *in vitro* antiproliferative activity on human GBM cells was evaluated. The possible synergy between AG and FcTriOH was also assessed. Finally, antitumor activity of the developed LNCs was evaluated in ectopic and orthotopic human GBM tumor models in nude mice.

A part of this chapter has been prepared as an article (to be submitted for publication) entitled 'Enhanced and targeted internalization of lipid nanocapsules in human glioblastoma cells: effect of surface-functionalizing NFL peptide' and available at 4.3.1.

4.2. Summary of the results

The objective of this chapter was to functionalize the surface of LNCs with GBM-targeting ligands in order to enhance their cellular internalization preferentially into human GBM cells compared to NHA. Previously, adsorption of NFL peptide on LNC (without long chain PEG) surface significantly enhanced the uptake of the nanocarrier into mouse GBM cells, whereas covalent-coupling with LNC-DSPE-PEG₂₀₀₀ hampered the activity of the peptide (Balzeau et al., 2013). Therefore, we chose the adsorption technique to functionalize the LNCs with different concentrations of NFL. The LNC composition described in chapter 3 was modified by removing the DSPE-mPEG₂₀₀₀ to formulate the LNCs in this study, so that NFL peptide adsorption on nanovector surface was maximized and its interaction with cell membranes was not weakened (Torchilin et al., 2001).

As the concentration of fluorescent-labelled NFL peptide (fluoNFL) was increased from 1 mM to 3 mM to prepare LNC-fluoNFL1 and LNC-fluoNFL3 respectively, the size of the LNCs also became bigger. The control LNCs had size of 57 nm, whereas the diameters of LNC-fluoNFL1 and LNC-fluoNFL3 were larger by 4 nm and 7 nm respectively. The diameter of the 3 formulations were within acceptable limits for i.v. administration and for diffusion through brain extracellular space (Allard et al., 2009b; Fu et al., 2011; Thorne and Nicholson, 2006). PDI of the NFL-functionalized LNCs was slightly higher compared to control LNCs, although it was < 0.2 for all three formulations, showing their monodispersity. The zeta potential of the control LNC was -2.2 mV, whereas it was +0.5 mV and +4.9 mV for LNC-fluoNFL1 and LNC-fluoNFL3 respectively. The change of zeta potential can be explained by the slightly net positive charge of the peptide (Berges et al., 2012b).

To evaluate the effect of NFL-functionalization on complement activation, complement consumption of the nanovectors in human serum was evaluated. The CH50 unit consumption of the LNC-fluoNFL1 was similar to control LNC, whereas consumption of the LNC-fluoNFL3 was slightly higher. This can be due to the higher particle size or positive zeta potential of the LNC-fluoNFL3 compared to the other two nanovectors

(Harashima et al., 1994; Vonarbourg et al., 2006a). However, the complement consumptions by all three formulations were little even at high particle surface area and should not be rapidly recognized by the MPS after systemic administration, and the nanocapsules may have prolonged plasma circulation half-life. This would be beneficial for the nanovectors to cross the fenestrated BBTB by EPR effect and accumulate in brain-tumors.

We evaluated the interaction between the LNC and the peptide in the LNC-fluoNFL3 by incubating the nanovector with various concentrations of NaCl and Tris buffer solutions, and subsequently measuring their size using DLS. The diameter of the LNC-fluoNFL3 was not affected by NaCl solutions and up to 0.05 M Tris buffer. It can be hypothesized that more hydrophobic forces, hydrogen bonds and/or Van der Waal's forces were involved in LNC and fluoNFL interaction in LNC-fluoNFL3, resulting higher resistance to NaCl or Tris induced peptide desorption compared to the LNC-NFL formulation in previous study (Carradori et al., 2016). Additionally, peptide desorption rate from the LNC surface was evaluated by dialyzing the LNC-fluoNFL3 against Tris buffer solution at 37°C. Desorption of fluoNFL from LNC surface was slow and gradual, and only 33.6% peptide was desorbed after 6 h. Therefore, the peptide may not be desorbed rapidly from LNC surface after large dilutions and the formulation could be promising for i.v. administration.

The concentration of LNC-adsorbed fluoNFL was quantified indirectly HPLC. The concentration of LNC adsorbed fluoNFL in LNC-NFL1 was 0.4% (w/w), whereas it was 2.49% (w/w) for LNC-fluoNFL3. This was surprising as 53% of 1 mM fluoNFL in the LNC-fluoNFL1 and only 3% of 3 mM fluoNFL in LNC-fluoNFL3 were free. However, results of experiment evaluating the fluoNFL desorption from LNC surface also indicated a high percentage of fluoNFL adsorption in LNC-fluoNFL3. The exact reason for such high percentage of adsorption is unknown. Further study is necessary to understand the mechanism for the high peptide adsorption percentage in LNC-fluoNFL3. The calculated number of peptides on surfaces of LNC-fluoNFL1 and LNC-fluoNFL3 were 243 and 1534 per LNC particle respectively. The higher number of peptide molecules per LNC particle may enhance the interaction with the human GBM cells and impact on rate and extent of nanocarrier internalization, and can improve efficacy of the delivery system.

The cellular uptake kinetics of the developed nanocapsules in a human GBM cell line i.e. U87MG were determined by flow cytometry, to evaluate their potential as human GBM targeting NDDSs. The nanocapsule internalization into U87MG cells at every time point (0.5 h, 1 h, 6 h and 24 h) was dependent on NFL concentration, and occurred as following: LNC-fluoNFL3 > LNC-fluoNFL1 > LNC. Moreover, it was observed that the 24 h peptide adsorption step was essential to maximize LNC internalization. Additionally, confocal microscopy images confirmed the higher uptake of LNC-fluoNFL3 compared to LNC. It was also observed from the images that majority of the NFL-functionalized LNCs were localized into the cytoplasm, whereas the non-functionalized LNC was mostly attached to the cell membrane. This can significantly lower the amount of nanocarriers required for achieving a certain intracellular drug concentration in GBM cells, and may reduce side effects on healthy tissue if the internalization enhancement is targeted towards the cancerous cell.

The internalization of control LNC and LNC-fluoNFL3 into NHA was measured. The uptake of the LNC-fluoNFL3 was significantly lower into NHA compared to U87MG cells, whereas it was the opposite for control LNCs. Therefore, the LNC-fluoNFL3 internalization was more targeted towards the human GBM cells compared to healthy astrocytes. This can aid to improve efficacy, reduce required dose and decrease toxicity.

The uptake of the LNC-fluoNFL3 into U87MG cells was found to be energy-dependent active process and occurred chiefly by macropinocytosis, clathrin-dependent and caveolin-dependent endocytosis; similar to the peptide solution. As cargoes taken up by these pathways can end up in lysosomes, the NFL-functionalized LNCs may not be suitable to deliver drugs prone to lysosomal degradation (e.g. nucleic acids or proteins) in U87MG cells, unless it can escape from the endo-lysosomal compartments like LNC (Paillard et al., 2010). Therefore, intracellular trafficking on NFL-functionalized LNCs should be further investigated.

The effect of NFL-functionalization on BBB permeability of the LNCs was evaluated using the well-established hCMEC/D3 cell monolayer *in vitro* BBB model (Poller et al., 2008). The functionalization with NFL did not enhance the passage of LNCs through the BBB. However, further repetitions of this test should be performed with lower concentrations of LNCs as a tendency of reduced integrity of the cell monolayer after LNC treatment was observed. Moreover, cellular uptake of NFL peptide in the BBB cells

and its permeability across the cell monolayer model has to be investigated to see if the peptide actually has capacity to cross the BBB.

FcTriOH and AG, the two promising hydrophobic molecules for GBM therapy were encapsulated in the LNCs with high encapsulation efficiency (99.8% and 93.5% respectively) and drug-loading (2.67% and 0.55% w/w respectively). The encapsulation of FcTriOH reduced the particle diameter by 7-8 nm compared to corresponding unloaded LNCs similar to previous reports (Allard et al., 2008; Huynh et al., 2012), although no significant difference in zeta potential was observed. AG encapsulation did not alter size or zeta potential of the LNCs. The *in vitro* antiproliferative activity of the drug solutions and their LNC formulations against U87MG cells were evaluated by MTS assay. Moreover, possible synergy among the two drugs at different ratios were assessed by the Chou-Talalay method (Chou, 2010), and no synergy between the drugs were observed at the various tested combination ratios. The IC_{50} of FcTriOH, LNC-FcTriOH and LNC-FcTriOH-fluoNFL3 were 1.31, 1.05 and 0.46 μM respectively. The IC_{50} of AG, LNC-AG and LNC-AG-FcTriOH were 31.8, 15.1 and 6.2 μM respectively. Therefore, encapsulation of the drugs within the NFL-functionalized LNC reduced IC_{50} compared to free drug and non-functionalized LNC encapsulated drug. This could reduce the minimum effective dose of the drugs if the NFL-functionalized LNCs can reach the brain tumor tissue while retaining the peptides on their surface to achieve high internalization and better efficacy.

Preliminary *in vivo* studies using ectopic and orthotopic U87MG tumor models in nude mice were performed to evaluate possible antitumor activity and/or toxicity after treatment with FcTriOH and AG formulations. For the ectopic tumor model, the treatments were administered by i.v. route (two injections). A gradual reduction of relative tumor volume was observed since the beginning of the treatment with FcTriOH-loaded LNCs. A significant difference, i.e. 40.1 % and 44.2 % lower relative tumor volume for LNC-FcTriOH and FcTriOH-fluoNFL3 respectively (compared to the saline treated group), was observed on day 17. However, the tumor reduction effect of the FcTriOH treatments was not observed from day 24 (two weeks after the last injection). The tumor rapidly grew back and no significant difference in relative tumor volume was observed. This possibly occurred as the drug was eliminated leading its antiproliferative effect to fade and the tumor to grow back. The LNC-AG-NFL3 (LNC-AG was not tested) showed no significant tumor reducing activity compared to control. No signs of toxicity were observed and the

therapy was well tolerated. Therefore, the number of injections and/or dose should be increased in future studies to possibly achieve tumor regression after FcTriOH-loaded LNC treatment and to observe the possible effect of NFL-functionalization.

For the orthotopic tumor model, the treatments were administered locally to the brain tumor by CED to bypass the BBB. MRI acquisitions revealed that LNC administration created lesions in the brain and the average lesion volumes of the non-functionalized LNCs (blank or drug-loaded) were smaller compared to NFL-functionalized LNCs, possibly due to lower cellular uptake of the LNC without NFL. Diffusion tensor imaging (DTI) revealed that the LNC-fluoNFL3 treated groups had certain regions in their lesions which possibly had reduced tissue cellularity, lysis and/or necrosis due to treatment; which could be a predictor for therapy response evaluation for cerebral tumors (Hamstra et al., 2005; Mardor et al., 2003). The median survival of saline, LNC-FcTriOH-fluoNFL3, LNC-FcTriOH, LNC-blank, LNC-blank-fluoNFL3 and LNC-AG-fluoNFL3 treated groups was 37.5, 38, 43, 45.5, 45.5 and 47 days respectively. It can be hypothesized that the higher cellular internalization property of NFL-functionalized LNCs created larger brain lesions by the intrinsic toxicity of the nanocapsules whereas the additional activity of the FcTriOH molecule damaged larger healthy regions of brain leading to a potential toxicity, side effects and earlier mortality of the LNC-FcTriOH treated groups compared to the other groups. The enhanced survival of the blank LNC (with/without NFL) treated groups were possibly due to nanoparticle induced cytotoxic effects. The slightly higher median survival of the AG-loaded LNC-NFL3 compared to the blank LNCs can be due to neuroprotective and neurotrophic effects of AG (Zhao et al., 2013a; Zhao et al., 2013b).

Therefore, further studies are necessary for both of the GBM tumor models to optimize the LNC dosages by i.v. and CED routes in order to translate the promising *in vitro* results into *in vivo* experiments by obtaining a balance between antitumor activity and toxicity.

4.3. Results

4.3.1. Publication 3 (to be submitted in ACS Nano): Enhanced and targeted internalization of lipid nanocapsules in human glioblastoma cells: effect of surface-functionalizing NFL peptide

ENHANCED AND TARGETED INTERNALIZATION OF LIPID NANOCAPSULES IN HUMAN GLIOBLASTOMA CELLS: EFFECT OF SURFACE-FUNCTIONALIZING NFL PEPTIDE

Reatul Karim^{1,2}, Elise Lepeltier², Lucille Esnault², Pascal Pigeon^{3,4}, Laurent Lemaire², Claudio Palazzo¹, Claire Lépinoux-Chambaud², Gerard Jaouen⁴, Joel Eyer², Géraldine Piel¹, Catherine Passirani²

¹ LTPB, CIRM, University of Liège, Liège, Belgium

² MINT, UNIV Angers, INSERM 1066, CNRS 6021, Université Bretagne Loire, Angers, France

³ UPMC Univ Paris 06, Sorbonne Univ, CNRS, UMR 8232, IPCM, F-75005 Paris, France

⁴ PSL Chim ParisTech, 11 Rue Pierre & Marie Curie, F-75005 Paris, France

Corresponding author: reatul.karim@ulg.ac.be

Abstract

In this study, the fluorescent-labelled NFL-TBS.40-63 peptide (fluoNFL) concentration on lipid nanocapsule (LNC) was optimized to enhance its delivery to human glioblastoma cells. The physicochemical properties of the developed LNCs were characterized. Additionally, peptide-adsorption on LNC surface and interaction between the peptide and the nanocarrier, and desorption rate of the peptide from the nanocarrier was determined. The interaction between peptide and LNC possibly occurs by hydrogen bonding, Van der Waal's forces or hydrophobic forces. Moreover, desorption of fluoNFL from LNC surface was found to be slow and gradual. Furthermore, it was observed that the rate and extent of LNC internalization in the U87MG human glioblastoma cells were dependent on the surface-functionalizing fluoNFL concentration. In addition, we showed that the uptake of fluoNFL functionalized LNC was preferentially targeted towards glioblastoma cells compared to healthy human astrocytes. The uptake of the fluoNFL-functionalized LNCs in the human GBM cell line was energy-dependent and occurred possibly by macropinocytosis, clathrin-mediated and caveolin-mediated endocytosis. A novel ferrocifen-type molecule (FcTriOH) was then encapsulated in the LNCs and the functionalization reduced its IC₅₀ compared to other tested formulations against U87MG cells. In the preliminary study on the subcutaneous human GBM tumor model in nude mice, a significant reduction in relative tumor volume was observed one week after the 2nd i.v. injection and the significant difference was maintained for a week. These results show that optimization of NFL-TBS.40-63 peptide concentration on LNC surface is a promising strategy for enhanced and targeted nanocarrier internalization in human glioblastoma cells, and the FcTriOH-loaded LNCs are promising therapy approach for glioblastoma.

Keywords: Lipid nanocapsule, glioblastoma, ferrocifen, cell-penetrating peptide, NFL-TBS.40-63

1. Introduction

Glioblastoma multiforme (GBM) is one of the most prevalent, and fatal primary brain tumor classified as the World Health Organization as a Grade IV CNS tumor (Louis et al., 2016). Although remarkable progress in diagnostic methods and treatment strategies has been achieved in the last few decades, the median survival only altered from 8.3 to 14.6 months over the last 60 years after present multimodal therapy (surgical resection followed by radiotherapy plus chemotherapy) (Netsky et al., 1950; Stupp et al., 2009; Thomas et al., 2014). Therefore, new therapeutic approaches for treatment of GBM are necessary.

Nanosized-drug delivery systems (NDDSs) have appeared as a promising strategy for drug delivery for cancer therapy, including brain cancers. The NDDSs can have numerous beneficial characteristics i.e. prolonged blood circulation time, improved bioavailability and biocompatibility of hydrophobic drugs, controlled drug release and site-targeted drug delivery (Peer et al., 2007). Moreover, long circulating nanocarriers with appropriate size may accumulate in brain tumors after crossing the blood-brain barrier (BBB) by enhanced permeability and retention (EPR) effect, and improve survival time of animals (Bernardi et al., 2009). Among various nanocarriers, lipid nanocapsules (LNCs) have been reported in numerous literatures as promising NDDS for carrying hydrophobic drugs due to their characteristic oily core (Huynh et al., 2009). One of the promising features of LNC formulation is its easy and organic solvent free preparation technique that can be easy to scale-up for future industrial purpose (Thomas and Lagarce, 2013). LNCs were evaluated and showed promising *in vitro* and *in vivo* results against GBM in numerous studies (Allard et al., 2009a; Roger et al., 2012; Zanutto-Filho et al., 2013).

In order to enhance the site-specific drug delivery to GBM, the surface of the NDDSs can be modified by adding various GBM-targeting ligands (Fu et al., 2012; Liu et al., 2013; Wei et al., 2015; Yang et al., 2013). A neurofilament light subunit derived 24 amino acid tubulin binding site peptide called NFL-TBS.40-63 (NFL) was reported to preferentially internalize into human, rat and mouse GBM cells compared to corresponding healthy cells (Berges et al., 2012a). This peptide was evaluated in multiple studies as potential GBM-targeting moiety on LNC surface in rat or mouse GBM cell lines (Balzeau et al., 2013; Laine et al., 2012). However, based on these studies and in order to be more clinically relevant, it is necessary to evaluate the selective delivery capability of NFL-functionalized

LNC into human GBM cell line. Moreover, the concentration of the GBM targeting ligand should also be optimized to further improve its delivery to GBM cells. Therefore, the aim of this study was to evaluate the effect of the LNC surface-adsorbed NFL concentration on the nanovector internalization into human GBM cells in order to avoid a potential toxicity on healthy cells. The effect of NFL adsorption on the physicochemical characteristics of LNC was evaluated. Additionally, impact of salt concentration on NFL-desorption from the LNC surface was studied. Moreover, influence of NFL-adsorption on the complement consumption by the formulations was investigated by CH50 assay. A comparative cellular internalization kinetic study into human GBM cells with the various developed LNCs was performed and confirmed by confocal microscopy study. Targeting ability of the NFL-functionalized LNC towards GBM cells was also assessed by comparing its uptake into both GBM cells and astrocytes under identical conditions. Possible internalization pathway of the functionalized-LNC into the human GBM cell line was assessed. Furthermore, a novel ferrocifen-type anticancer molecule, FcTriOH, was encapsulated in the LNCs and the effect of the LNC functionalization on its antiproliferative activity was measured. Finally, an *in vivo* study was performed on an ectopic GBM model in mice in order to observe possible therapeutic or toxic effects after systemic delivery of the formulations.

2. Materials and methods

2.1. Materials

Macrogol 15 hydroxystearate (Kolliphor® HS15) was purchased from BASF (Germany). Hydrogenated phosphatidylcholine from soybean (Lipoid S PC-3) was provided from Lipoid GmbH (Germany), caprylic/capric triglycerides (Labrafac Lipophile WL1349) was supplied by Gattefosse (France). FcTriOH was provided by PSL Chim ParisTech (France). 5,6-FAM labelled NFL.TBS-40.63 peptide (fluoNFL) was purchased from Polypeptide Laboratories (France).

The human glioblastoma cell line U87MG was collected from ATCC (USA). Normal human astrocytes (NHA), astrocyte basal medium (ABM), SingleQuots™ kit supplements & growth factors, L-glutamine, penicillin-streptomycin and Dulbecco's modified Eagle's medium with 1 g/L L-glucose (DMEM) were provided by Lonza (France). Methyl-β-

cyclodextrin (M β CD), 5-(N,N-dimethyl) amiloride hydrochloride (DAM), chlorpromazine (CP), phalloidin–tetramethylrhodamine-B-isothiocyanate (phalloidin-TRITC), sodium azide and 2-deoxy-D-glucose were purchased from Sigma (Germany). Phorbol-12-myristate-13- acetate (PMA) was collected from Abcam (France). 4-(4-(dihexadecylamino)styryl)-N-methylpyridinium iodide (DiA), 4',6-diamidino-2-phenylindole (DAPI), Trypsin-EDTA 1x, non-essential amino acids solution 100x (NEAA), fetal bovine serum (FBS) and ProLong Gold antifade were collected from Thermo Fisher Scientific (USA). 3-carboxymethoxyphenyl-2-(4-sulfophenyl)-2H-tetrazolium (MTS) and phenazine methosulfate (PMS) was purchased from Promega (USA).

Normal human serum (NHS) was provided by the “Etablissement Français du Sang” (Angers, France). Sheep erythrocytes and hemolysin were purchased from Eurobio (France). Sodium chloride (NaCl) was purchased from Prolabo (Fontenay-sous-bois, France). Ultra-pure water (UPW) was obtained from a Millipore filtration system. All the other reagents and chemicals were of analytical grade.

2.2. Preparation of lipid nanocapsules

2.2.1. Preparation of stock lipid nanocapsules

Stock LNC (LNC-stock) was prepared using phase inversion temperature technique (Heurtault et al., 2002). In brief, Kolliphor® HS15 (16.9 % w/w), Lipoid® S PC-3 (1.5 % w/w), Labrafac Lipophile WL1349 (20.6 % w/w), NaCl (1.8 % w/w) and UPW (59.2 % w/w) were mixed under magnetic stirring at 60°C for 15 min. Three heating-cooling cycles were performed between 90°C and 60°C. During the last cooling step, when the temperature was in the phase inversion zone (78-83°C), ice-cold UPW was added (final concentration 88.4 % w/w) to induce irreversible shock and form the LNC-stock. The nanocapsules were then passed through 0.2 μ m cellulose acetate filter to remove any aggregates and stored at 4°C.

DiA-labelled stock LNC was prepared by incorporating 0.1% (w/w) DiA in the formulation at the first step with other excipients.

2.2.2. Preparation of fluoNFL functionalized lipid nanocapsules and lipid nanocapsules

1 mL of stock LNC (LNC-stock) was stirred at room temperature for 24 h with 0.369 mL of 1 mM (0.86 % w/w) (similar to (Balzeau et al., 2013; Carradori et al., 2016)) or 3 mM (2.57 % w/w) fluoNFL solution (in water) to prepare the fluoNFL functionalized LNCs (LNC-fluoNFL1 and LNC-fluoNFL3 respectively). Similarly, 1 mL of the LNC stock was stirred at room temperature for 24 h with 0.369 mL of UPW to produce final control LNC. The DiA labelled LNC was also functionalized with the fluoNFL by same mentioned method.

2.2.3. Preparation of FcTriOH-loaded lipid nanocapsules

The FcTriOH-loaded LNC (LNC-FcTriOH) was prepared according to step 2.2.1., excepted FcTriOH (0.9 % w/w) was added at the first step of the formulation with the other excipients. Subsequently, fluoNFL was adsorbed at their surface according to 2.2.2. to produce drug loaded NFL-functionalized LNCs.

2.2.4. Optimization of lipid nanocapsules for in vivo studies

For *in vivo* studies, the amount of ice-cold UPW used to induce shock to produce the LNCs was adjusted (final concentration 70.9% w/w) to produce concentrated LNCs according to previously published article (Huynh et al., 2012). NaCl concentration was also adjusted to keep the final formulations isotonic with blood.

2.3. Characterization of the lipid nanocapsules

2.3.1. Dynamic light scattering, laser-Doppler electrophoresis and nanoparticle tracking analysis

The mean diameter and polydispersity index (PDI) of the LNCs were determined by dynamic light scattering (DLS) technique using Zetasizer Nano ZS (Malvern Instruments Ltd, UK). The LNCs were diluted 100-folds in UPW before the analysis. The measurements were performed at backscatter angle of 173°. The measured average values were calculated from 3 runs, with 10 measurements within each run.

Zeta potential of the nanocarriers was measured using laser Doppler micro-electrophoresis using Zetasizer Nano ZS (Malvern Instruments Ltd, UK).

Additionally, the particle concentration in the control LNC dispersion was determined using nanoparticle tracking analysis (NTA) as described previously (Karim et al., 2017a). The NTA was carried out using the NanoSight NS300 (Malvern Instruments Ltd, UK).

Briefly, the NDDS samples were diluted to optimum concentrations with UPW and were infused in the sample chamber using a syringe pump at 30 $\mu\text{L}/\text{min}$ rate. A 405 nm laser was used to illuminate the particles, and their Brownian motion was recorded into three 60s videos (25 fps) using the sCMOS type camera of the instrument. Subsequently, the NTA software (NTA 3.2 Dev Build 3.2.16) analyzed the recordings, tracked the motion of the particles and calculated the number of particles in the samples. The experiment was performed in triplicate.

2.3.2. High-performance liquid chromatography

2.3.2.1. Peptide concentration on LNC surface

The peptide concentration was indirectly measured by quantifying the free peptide present in the formulations using a supplier recommended HPLC method. Briefly, the fluoNFL functionalized LNCs were filtered by centrifugation at 4000 g for 30 min using Amicon Ultra-0.5 mL centrifugal filters having molecular weight cut off (MWCO) 100 kD (Millipore). The filtrate containing the free fluoNFL was collected and the peptide dosage was performed in a HPLC system (Waters, France). A C18 analytical column (250 x 4.6 mm, 5 μm , Waters, France) was used at room temperature. 0.1% TFA in UPW and 0.1% TFA in acetonitrile were used as mobile phases (gradient: 80:20 \rightarrow 55:25, 25 min). Flow rate was 1 mL/min, injection volume was 10 μL and fluoNFL was quantified by an UV detector at λ of 220 nm. Analysis of the data was performed by Empower 3 software (Waters). Retention time was of 18 min. Calibration curves were established by quantifying the area under the curves (AUCs) of 1-100 $\mu\text{g}/\text{mL}$ solutions of fluoNFL in UPW. The peptide solution and LNC alone were also filtered and quantified as positive and negative controls.

2.3.2.2. FcTriOH concentration in LNCs

To quantify total (encapsulated and unencapsulated) drug concentration, LNCs were broken by mixing vigorously with an appropriate volume of ethanol (40 folds for LNCs prepared for *in vitro* experiments, 100-folds for concentrated LNCs prepared for *in vivo*) to keep dissolved drug concentration between 5-75 $\mu\text{g}/\text{mL}$. To quantify unencapsulated drug concentration, formulations were placed on centrifugal concentrator devices with polyethersulfone membrane (MWCO 30 kD, Amicon Ultra-500, Millipore) and centrifuged at 4000 g for 30 minutes to separate the free drug from the rest of the

formulation. The filtrates containing unencapsulated drug were collected and ethanol (2-folds) was added to solubilize any undissolved drug. Drug dosage in the above-mentioned samples was performed in a HPLC system (Waters, France). A C18 analytical column (250 x 4.6 mm, 5 µm, Waters, France) was used at room temperature. UPW and acetonitrile (45:55, v/v) were used as mobile phases. Flow rate was 1 mL/min, injection volume was 10 µL and FcTriOH was detected at 304 nm. Analysis of the data was performed by Empower 3 software (Waters). Retention time of FcTriOH was 8.1 min.

EE (%) was calculated using the following equation:

$$EE (\%) = \frac{(\text{Total drug conc. in LNC} - \text{unencapsulated drug conc. in LNC}) \times 100}{\text{Theoretical drug conc. in LNC}}$$

Drug loading was calculated using the following equation:

$$\text{Drug loading (\% w/w)} = \frac{\text{Encapsulated drug conc. in LNC} \times 100}{\text{Conc. of LNC}}$$

2.3.3. Interaction between LNC and fluoNFL

The LNC-fluoNFL3 and control LNCs were diluted in UPW or in various concentrations (0.005, 0.05, 0.15, 0.25, 0.5 and 1 M) of NaCl or Tris buffer, incubated for 30 minutes before measuring their size by DLS technique mentioned in 2.3.1. (Carradori et al., 2016). Additionally, LNC- fluoNFL3 and control fluoNFL solutions were taken in dialysis bags (MWCO 100 kD, Spectra/Por® biotech grade cellulose ester membrane, SpectrumLabs, Netherlands) and dialyzed against Tris buffer (0.05 M, pH 7.4) at 37°C, stirred at 75 rpm. At various time points (0.25, 0.5, 0.75, 1, 2, 3, 4, 6 and 24 h) samples were collected from the receiver chamber and amount of the free peptide was quantified using the HPLC method mentioned in 2.3.2.1.

2.4. Complement consumption assay (CH50 assay)

The residual hemolytic capacity of NHS towards antibody-sensitized sheep erythrocytes after incubation with different LNC formulations was measured to evaluate the complement activation by the formulations (Cajot et al., 2011). In brief (Karim et al., 2017a), aliquots of NHS were incubated with increasing concentrations of the LNCs at 37°C for 1 h. Subsequently, the different volumes of the NHS were incubated with a fixed volume of hemolysin-sensitized sheep erythrocytes at 37°C for 45 min. The volume of serum that can lyse 50% of the erythrocytes was calculated (“CH50 units”) for each

sample and percentage of CH50 unit consumption relative to negative control was determined as described previously (Vonarbourg et al., 2006b). Particle number in the LNC dispersion was determined by NTA and nanocarrier concentration per mL of NHS was calculated according to following equation:

$$\text{Particle number per mL of NHS} = \text{Particle conc. in NDDS dispersion} \times \frac{\text{vol. of NDDS added}}{\text{vol. of NHS}}$$

Subsequently, surface area of the NDDSs per mL of NHS was calculated according to the following equation:

$$\text{Surface area} = \text{Particle number per mL of NHS} \times \pi \times (\text{average particle diameter})^2$$

The CH50 unit consumption by the different LNCs were compared by plotting the percentage of CH50 unit consumption as a function of their surface area.

2.5. Cell culture

The human glioblastoma cell line U87MG was cultured at 37°C under 5% CO₂ in DMEM supplemented with 10% FBS, 5% L-glutamine, 5% NEAA and 5% penicillin-streptomycin. NHA was cultured at 37°C under 5% CO₂ in ABM supplemented by the ‘AGM SingleQuot™ Kit’. The cells were passaged once they were about 70 % confluence.

2.6. Flow cytometry

2.6.1. Kinetics of LNC internalization in U87MG cells

The kinetics of internalization of the DiA-labelled LNCs (LNC-DiA, LNC-DiA-fluoNFL1 and LNC-DiA-fluoNFL3) in U87MG cells was assessed using the BD FACSCanto™ II flow cytometer (BD Biosciences). In brief, cells were seeded in 6-well plates at 5×10^5 cells/well concentration for 24 hours. Subsequently, they were treated with the different DiA-labelled LNCs (1.23 mg/mL) for 0.5, 1, 6 and 24 h. Afterwards, the cells were washed three times with ice-cold phosphate buffer saline 1x (PBS), detached by incubating 5-10 minutes with Trypsin-EDTA 1x. The cells were then centrifuged at 2000 rpm for 5 minutes, the supernatant was aspirated and the cell pellet was re-dispersed in PBS. The centrifugation and re-dispersion cycle was repeated twice more. Finally, the cells were suspended in trypan blue (final trypan blue concentration 0.12% w/v) and the percentage of DiA positive (DiA^{+ve}) cells were analyzed by the flow cytometer. Each

experiment was performed in triplicate and 20,000 events per sample were analyzed in each experiment.

2.6.2. Targeting-capability of fluoNFL-functionalized LNC towards GBM cells compared to healthy cells

To assess the targeting-capability of the fluoNFL-functionalized LNC towards GBM cells compared to healthy cells, NHA was treated for 1 h and 6 h with LNC-DiA-fluoNFL3 (method 2.6.1.) at 37°C and percentage of DiA^{+ve} cells was measured using the above mentioned method, and compared with the results of U87MG cells.

2.6.3. Mechanism of fluoNFL-functionalized LNC internalization in U87MG cells

To evaluate the dependency of NFL-functionalized LNC cellular internalization on energy, U87MG cells were pre-incubated for 30 min at 4°C or pretreated for 30 minutes at 37 °C (NaN₃ 10 mM and 2-deoxy-D-glucose 6 mM) to deplete cellular ATP (Lepinoux-Chambaud and Eyer, 2013). Subsequently, the cells were treated for 1 and 6 h with the LNC-DiA-fluoNFL3 and percentage of DiA^{+ve} cells were measured by the above mentioned method.

To investigate the possible pathways of LNC-DiA-fluoNFL3 internalization in U87MG, cells were pretreated with different inhibitors (MβCD 10 mg/mL, DAM 1 mM, CP 50 μM and PMA 10 μg/mL) for 30 min at 37°C (Lepinoux-Chambaud and Eyer, 2013) followed by 1 h treatment with the nanocarrier and percentage of DiA^{+ve} was quantified.

In all the above mentioned conditions (37 °C, pre-incubation at 4 °C, pre-treatment for ATP depletion, and pre-treatment with various inhibitors), internalization of fluoNFL (at equivalent concentration of LNC-DiA-fluoNFL3) in U87MG cells was assessed by measuring FAM^{+ve} cells to assess if the fluoNFL by itself regulates the internalization of NFL-functionalized LNC.

2.7. Confocal microscopy

To visualize the effects of the fluoNFL peptide on LNC internalization, U87MG cells were seeded (3×10^4 cells/well) in 24 well plates containing coverslips and incubated at 37°C for 72 h (medium was carefully replaced every 24 h) to allow the cells to grow on the coverslips. Subsequently, the cells were treated with 1.23 mg/mL of LNC-DiA or LNC-DiA-fluoNFL3 for 1 h and 6 h at 37 °C. Afterwards, the cells were washed three

times with PBS and fixed with 4 % paraformaldehyde for 20 min at room temperature. Then, the cells were washed twice with PBS and permeabilized by incubation with 0.1% Triton X-100 for 10 min. The cells were washed twice with PBS and incubated with 0.7 μ M of phalloidin-TRITC for 1 h at room temperature. Subsequently, the cells were washed twice with PBS and incubated with 3 μ M DAPI for 10 minutes. Finally, the cells were washed 3-times with PBS and the coverslips were mounted using ProLong Gold antifade mounting medium. The cells were then visualized and images were captured by a confocal microscope (LSM 700 Zeiss). DAPI was excited with a 405 nm laser and recorded at 409-453 nm (blue channel), DiA was excited with a 458 nm laser and recorded at 558-666 nm (green channel) whereas TRITC was excited with a 561 nm laser and recorded at 564-632 nm (red channel).

2.8. Cell viability

Viability of the U87MG cells to various LNC treatments was assessed by MTS assay (Balzeau et al., 2013). In brief, the U87MG cells were seeded in 96 well plates (5×10^3 cells/well) and incubated for 24 h. Then the medium was replaced with various concentrations of LNCs (LNC-blank, LNC-FcTriOH and LNC-FcTriOH-fluoNFL3), FcTriOH and fluoNFL in DMEM and treated for 72 hours at 37°C. After that, each well content was replaced with 100 μ L of fresh DMEM. Additionally, 20 μ L of MTS-PMS (20:1) mixture was added in each well and incubated at 37°C for 2 h. Absorbance of the samples at 490 nm was recorded using a microplate reader (SpectraMax M2, Molecular Devices). The absorbance of the cells incubated with only DMEM was considered as 100% of cell survival (Abs^{+ve}), and the cells treated by 0.5% Triton X-100 was considered as 0% (Abs^{-ve}). Cell survival was calculated using the following equation:

$$\text{Cell survival (\%)} = [(Abs^{\text{sample}} - Abs^{-ve}) \div (Abs^{+ve} - Abs^{-ve})] \times 100$$

2.9. *In vivo* studies

The *in vivo* studies were performed following the guidelines of the European regulations. The experimental protocol was approved by the ‘French Ministry of National Education, Higher Education and Research’: APAFIS 8292 and APAFIS 8293. Seven weeks old female NMRI nude mice were collected from Janvier Labs (France). The animals were kept in the animal facility for one week for acclimatization and were given sufficient food and water throughout the study.

2.9.1. Preliminary study in ectopic xenograft model

After acclimatization period, the animals were anesthetized by temporary exposure to 2% isoflurane in oxygen to induce anesthesia followed by 1.5% isoflurane in oxygen delivered by face mask to maintain it. The U87MG cells were trypsinized and washed three times before injected subcutaneously in the right flank of the mice (2×10^6 cells in 50 μ L PBS). When the tumor became palpable, tumor volume was measured using an electronic caliper using the following equation: $\text{Volume} = \pi/6 \times \text{length} \times \text{width}^2$. Seven days after cell injection, the mice were divided into 5 groups to have similar average tumor volume. The animals were anesthetized (by above mentioned method) and received the following treatments by injections in the tail vein on day 7 and day 10- Group 1: 70 μ L Saline (n = 7); Group 2: 70 μ L of LNC-blank equivalent to 822.4 mg LNC per kg of body weight (n = 8); Group 3: 70 μ L of LNC-blank-fluoNFL3 equivalent to 822.4 mg LNC and 21.5 mg peptide per kg of body weight (n = 8), Group 4: 70 μ L of LNC-FcTriOH equivalent to 20 mg FcTriOH per kg of body weight (equivalent to 822.4 mg LNC per kg of body weight) (n = 8); Group 5: 70 μ L of LNC-FcTriOH-fluoNFL3 equivalent to 20 mg FcTriOH per kg of body weight (equivalent to 822.4 mg LNC and 21.5 mg peptide per kg of body weight) (n = 8). The length and width of the tumor was followed regularly (every day in the first week of treatment and then 3-times a week). Weight and behavior of the animals were daily followed.

2.10. Statistical analysis

The experiments were performed at least 3 times. Results obtained from the experiments were analyzed statistically using GraphPad Prism[®] software. Mean and standard deviation (SD) were determined and values are represented as Mean \pm SD. T-test or One way analysis of variance (ANOVA) (with Bonferroni post-test to compare among individual groups, and Dunnett's post-test to compare with control) was performed in the respective fields. P-value less than 0.05 (p < 0.05) was considered to be statistically significant.

3. Results

3.1. Physicochemical characteristics of the nanocapsules

Particle size, PDI and zeta potential of the different nanocapsule formulations determined by DLS and laser Doppler electrophoresis are given in Table 1. The investigational conditions, i.e. LNC concentrations, sample viscosities, temperature and sample

conductivity were consistent among the measurements. The control LNC had a size of 57 ± 2 nm, PDI of 0.08 ± 0.01 and zeta potential of -2.2 ± 0.9 mV. LNC-fluoNFL1 had a size of 61 ± 1 nm, PDI of 0.12 ± 0.02 and zeta potential of 0.5 ± 0.7 mV (Table 1). Additionally, LNC-fluoNFL3 had the highest values among the three formulations i.e. size of 64 ± 1 nm, PDI of 0.15 ± 0.02 and zeta potential of 4.9 ± 1.5 mV. Concentration of the adsorbed fluoNFL (% w/w), determined by HPLC, on LNC-fluoNFL1 and LNC-fluoNFL3 was of 0.40 ± 0.01 % and 2.49 ± 0.01 % respectively.

Encapsulation of FcTriOH in LNC (LNC-FcTriOH) significantly ($p < 0.001$) reduced the particle size to 50 ± 2 nm, compared to control LNC. Drug-loading of LNC-FcTriOH was 2.67 % (w/w) with encapsulation efficiency of 99.8 ± 2.3 %. After fluoNFL adsorption, the size of LNC-FcTriOH-fluoNFL3 was 58 ± 1 nm which was significantly ($p < 0.001$) larger compared to LNC-FcTriOH. After peptide adsorption, the LNC size increased consistently for control LNC and LNC-FcTriOH (7 nm and 8 nm respectively). PDI and zeta potential was not altered after FcTriOH encapsulation with/without fluoNFL functionalization compared to respective unloaded LNCs.

Table 1: Physicochemical characteristics of the nanocapsules

Formulation	Size (nm)	PDI	Zeta potential (mV)
Control LNC	57 ± 2	0.08 ± 0.01	-2.2 ± 0.9
LNC -fluoNFL1	$61 \pm 1^{**}$	$0.12 \pm 0.02^{**}$	$0.5 \pm 0.7^{**}$
LNC-fluoNFL3	$64 \pm 1^{***}$	$0.15 \pm 0.02^{***}$	$4.9 \pm 1.5^{***}$
LNC-FcTriOH	$50 \pm 2^{***}$	0.06 ± 0.02	-2.3 ± 1.3
LNC-FcTriOH-fluoNFL3	58 ± 1	$0.15 \pm 0.08^*$	$3.4 \pm 0.6^{***}$

(Oneway ANOVA with Dunnett's post-test. $p < 0.1$ is denoted by (*), $p < 0.01$ by (**) and $p < 0.001$ by (***), $n=6$)

3.2. Interaction between LNC and fluoNFL

The interaction between the LNC surface and NFL peptide in a formulation equivalent to LNC-fluoNFL1 was described previously (Carradori et al., 2016). To understand the interaction between the LNC surface and fluoNFL, the LNC-fluoNFL3 and LNC as control were incubated for 30 min in UPW and different concentrations of NaCl or Tris

buffer pH 7.4. Subsequently, their size was measured in DLS (Figure 1). The size of LNC-fluoNFL3 remained significantly different compared to control LNC as NaCl concentration was increased up to 1 mM. However, as concentration of Tris buffer increased above 0.05 M, the size of LNC-fluoNFL3 was reduced and its significant difference compared to control LNC was lost.

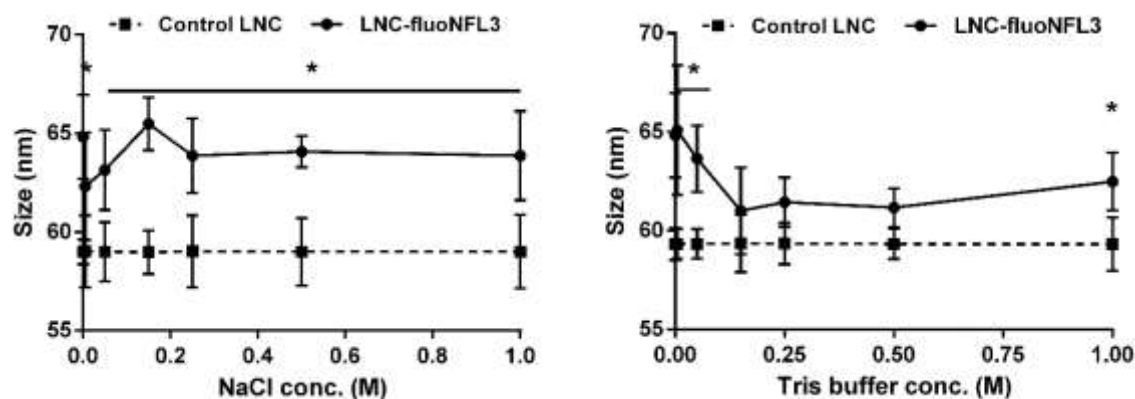


Figure 1: Mean particle sizes of control LNC and LNC-fluoNFL3 in various concentrations of NaCl and Tris buffer (t-test. $p < 0.1$ is denoted by (*), $p < 0.01$ by (**) and $p < 0.001$ by (***), $n = 3$).

Moreover, LNC-fluoNFL3 was dialyzed against 0.05 M Tris buffer at 37°C and 75 rpm using a dialysis bag having MWCO 100 kD. At various time points, the amount of fluoNFL in the receiver chamber (desorbed from the formulation) was quantified by HPLC. The peptide solution was dialyzed and quantified in the receiver chamber as control. The control peptide solution reached the receiver chamber very quickly and more than 90% of the peptide was recovered by 1 h. However, a slow and gradual desorption of the peptide was observed (Figure 2) from the LNC surface and only 6% peptide desorption occurred by 30 min and reached 33 % by 6 h.

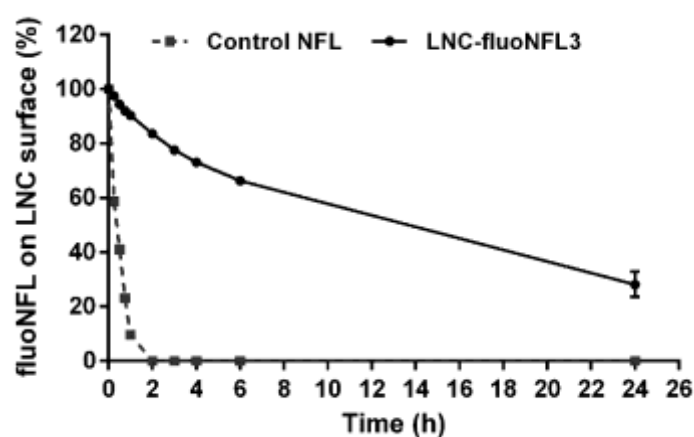


Figure 2: FluoNFL desorption kinetics from LNC-fluoNFL3 surface in 0.05 M Tris buffer pH 7.4 at 37°C and 75 rpm.

3.3. Complement consumption by the nanocapsules

Complement consumption by the control LNC and the fluoNFL-functionalized LNCs was assessed by the CH50 assay. The particle concentration in the control LNC was quantified by NTA and was used to calculate surface area of the LNC formulations. The percentage of CH50 unit consumptions by the control LNC, and the peptide functionalized LNCs were plotted against surface area of the nanocapsules in 1 mL of NHS (Figure 3). The complement consumption by all three nanocapsules increased as surface area of the nanovectors increased per mL of NHS. The percentage of CH50 unit consumption by control LNC and LNC-fluoNFL1 was similar and reached only 9.8 and 7.6 % respectively at around 700 cm²/mL NHS. The complement consumption by LNC-fluoNFL3 was slightly higher and reached 21.0 % at the same surface area.

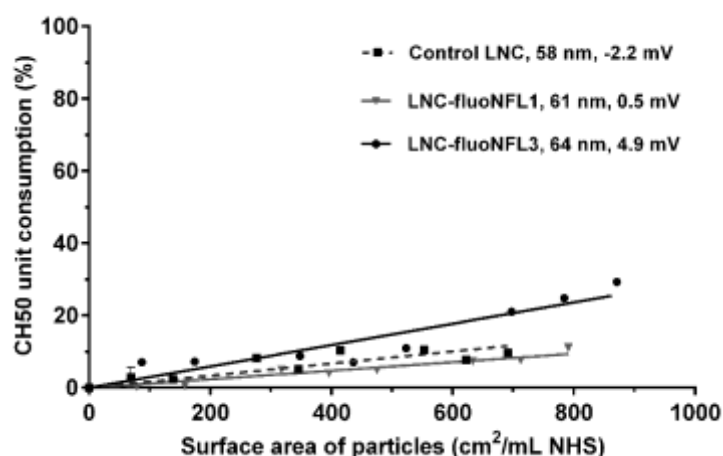


Figure 3: Complement consumption at 37°C by control LNC, LNC-fluoNFL1 and LNC-fluoNFL3.

3.4. Effect of surface-functionalizing fluoNFL concentration on LNC internalization into human GBM cells

The U87MG cells were treated with DiA-labelled LNCs (LNC-DiA, LNC-DiA-fluoNFL1 and LNC-DiA-fluoNFL3) for 30 min, 1 h, 6 h and 24 h to assess their cellular internalization at each time point (Figure 4). For each formulation, the cellular uptake increased as time was increased, showing the time dependency of the cell internalization. The internalization of LNC-DiA was 0.2, 0.8, 2.3 and 11.8 % after 30 min, 1 h, 6 h and 24 h respectively. LNC-DiA-fluoNFL1 uptake was 1.2, 2.7, 46.5 and 81.9 % after 30 min, 1 h, 6 h and 24 h respectively; whereas it was 8.4, 16.6, 72.4 and 86.2 % for LNC-DiA-fluoNFL3. At each time point, the cellular internalization of LNC-DiA-fluoNFL3 was significantly higher compared to LNC-DiA-fluoNFL1 and LNC-DiA, whereas uptake of LNC-DiA-fluoNFL1 was significantly higher compared to LNC-DiA.

Moreover, to investigate the necessity of the peptide adsorption on LNC (during the formulation of LNC-fluoNFL3) to enhance its cellular uptake, DiA-labelled LNC and fluoNFL (at same peptide concentration as LNC-DiA-fluoNFL3) were mixed to prepare ‘LNC-DiA & fluoNFL imm. mix.’ and the cells were treated immediately for 1 h at 37°C. The uptake of the immediate mixture was significantly lower (3.9-folds) compared to LNC-DiA-fluoNFL3, but slightly higher compared to LNC-DiA (Figure 5).

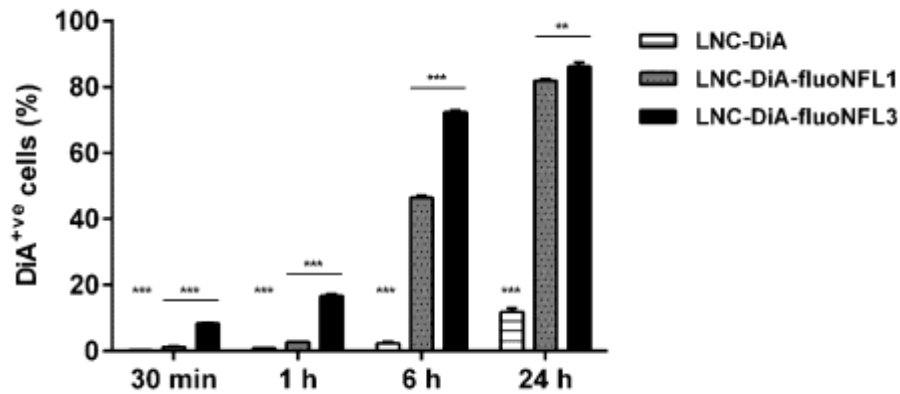


Figure 4. Enhancement of LNC internalization at 37°C in U87MG cells with increasing concentration of the fluoNFL peptide on LNC surface. The cells were incubated with 1.23 mg/mL of LNC-DiA, LNC-DiA-NFL1 and LNC-DiA-fluoNFL3 for 30 min, 1 h, 6 h and 24 h. Twenty thousand events per sample were analyzed and percentages of DiA⁺ cells were measured. The experiments were performed in triplicate. Statistical analysis was performed with oneway ANOVA with Tukey post-hoc test ($p < 0.1$ is denoted by (*), $p < 0.01$ by (**), and $p < 0.001$ by (***), $n=3$).

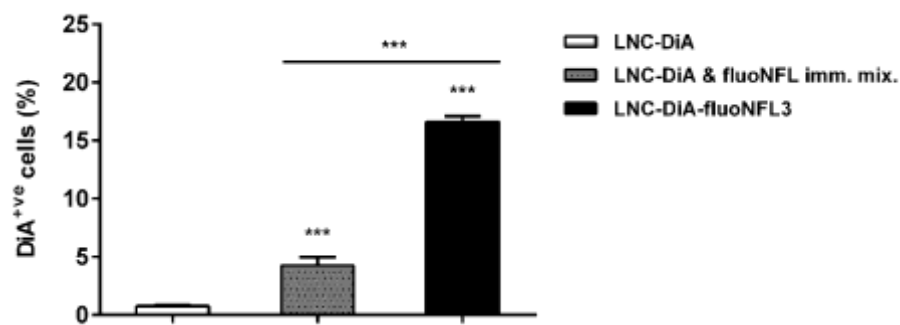


Figure 5: Internalization of LNC-DiA, immediate mixture of LNC-DiA and fluoNFL3, and LNC-DiA-fluoNFL3 in U87MG cells at 37°C after 1 h. The cells were incubated with 1.23 mg/mL of LNC-DiA, 'LNC-DiA & fluoNFL imm. mix.' and LNC-DiA-fluoNFL3 for 1 h. Twenty thousand events per sample were analyzed and percentage of DiA⁺ cells were measured. The experiments were performed in triplicate. Statistical analysis was performed with oneway ANOVA with Tukey post-hoc test ($p < 0.1$ is denoted by (*), $p < 0.01$ by (**), and $p < 0.001$ by (***), $n=3$).

Additionally, the higher cellular internalization of LNC-fluoNFL3 compared to control LNC was visualized by confocal microscopy (Figure 6). The cells were first treated by LNC-DiA (green dye) and LNC-DiA-fluoNFL3 for 6 h, followed by staining of their nuclei (DAPI staining: blue) and cytoskeleton (phalloidin-TRITC staining: red) for capturing confocal images. The DiA signal was much higher for the fluoNFL-functionalized LNC compared to control LNC, and nearly each cell had numerous DiA signal throughout its cytoplasm (Figure 5a). To see if the LNCs were on the cell surface or inside the cytoplasm, orthogonal sections of the stacked images were analyzed (Figure 5b). Indeed, nearly all fluoNFL-functionalized LNCs were observed inside the cytoplasm of the cells and each cell had internalized lots of nanocapsules. In comparison, the control LNC were situated predominantly on the cell surface rather than inside the cytoplasm.

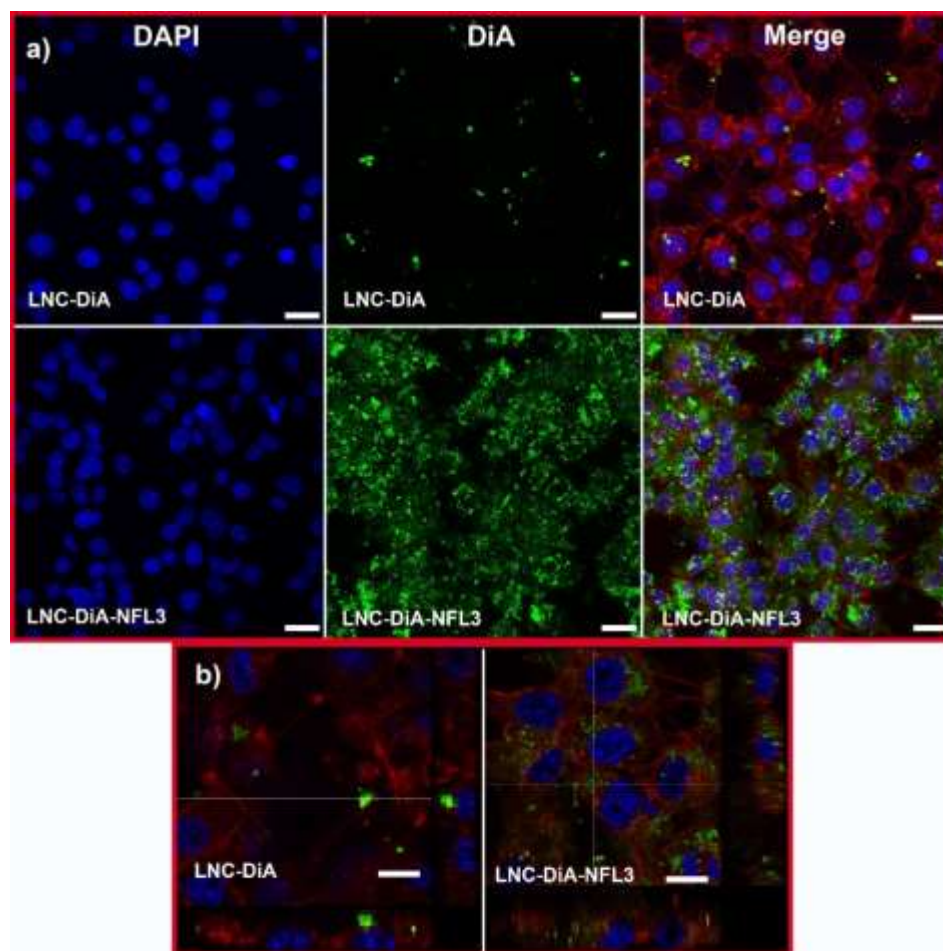


Figure 6. Representative confocal microscopy images of enhanced LNC internalization in U87MG cells due to LNC surface-functionalizing fluoNFL peptide. a) Cells were treated at 37°C for 6 h with 1.23 mg/mL of LNC-DiA and LNC-DiA-NFL3. Blue is DAPI staining (nuclei), green is DiA (LNC) and red is phalloidin-TRITC staining (F-actin, cytoskeleton). White bar = 20 μm . b) Orthogonal sections of U87MG cells treated 6 h with LNC-DiA and LNC-DiA-NFL3. Majority of LNC-DiA-NFL3 was localized into cell cytoplasm, whereas LNC-DiA was chiefly localized on cell surface. Blue is DAPI staining (nuclei), green is DiA (LNC) and red is phalloidin-TRITC staining (F-actin, cytoskeleton). White bar = 10 μm .

3.5. Preferential accumulation of fluoNFL functionalized lipid nanocapsules in human GBM cells compared to normal human astrocytes

To inspect the targeting capability of the fluoNFL-functionalized LNC towards human GBM cells, internalization of DiA-labelled LNC and LNC-fluoNFL3 into NHA were measured and compared with the uptake in U87MG cells. The internalization of LNC was significantly higher in NHA compared to U87MG cells at 1 h and 6 h (Figure 7 and Figure 8). Surface-functionalization with the fluoNFL peptide significantly enhanced the uptake of LNC in NHA by 5.2-folds and 3.5-folds at 1 h and 6 h respectively (Figure 7), compared to control LNC (LNC-DiA). In contrast, LNC functionalization with fluoNFL enhanced the LNC uptake into U87MG cells by 21.6-folds and 31.5-folds at 1 h and 6h respectively, compared to control LNC.

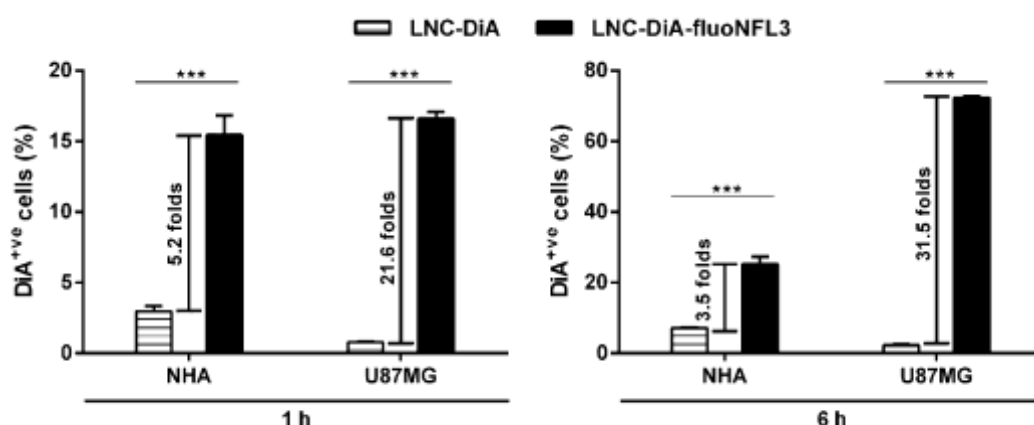


Figure 7: Enhanced LNC Internalization in NHA and U87MG cells due to LNC surface functionalization using fluoNFL peptide. The cells were incubated with 1.23 mg/mL of LNC-DiA and LNC-DiA-fluoNFL3 for 1 h and 6 h. Twenty thousand events per sample were analyzed and percentages of DiA⁺ cells were measured. The experiments were performed in triplicate. Statistical analysis was performed with t-test ($p < 0.1$ is denoted by (*), $p < 0.01$ by (**), and $p < 0.001$ by (***), $n=3$).

Although there was no significant difference of LNC-DiA-fluoNFL3 internalization in NHA and U87MG cells at 1 h, the uptake was significantly higher (4.4-folds) in the GBM cells by 6 h (Figure 8).

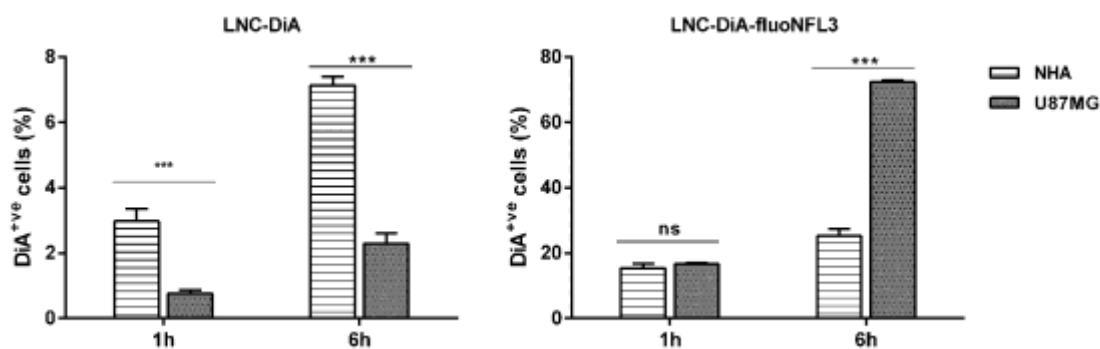


Figure 8: Higher LNC-DiA internalization into NHA compared to U87MG cells, whereas LNC-DiA-fluoNFL3 is internalized preferentially into U87MG cells compared to NHA. The cells were incubated with 1.23 mg/mL of LNC-DiA or LNC-DiA-fluoNFL3 for 1 h and 6 h. Twenty thousand events per sample were analyzed and percentages of DiA⁺ve cells were measured. The experiments were performed in triplicate. Statistical analysis was performed with t-test ($p < 0.1$ is denoted by (*), $p < 0.01$ by (**), and $p < 0.001$ by (***), $n=3$).

3.6. Mechanisms of fluoNFL-functionalized lipid nanocapsule internalization in U87MG human glioblastoma cell

To evaluate the possible mechanism of LNC-fluoNFL3 internalization in U87MG cells, the cells were treated with the DiA-labelled nanocapsule in different energetic conditions i.e. at 4°C and ATP-depleted conditions for 1 h and 6 h (Figure 9a). At 4°C, the internalization of LNC-DiA-fluoNFL3 was almost completely stopped both at 1 h and 6 h and therefore the alteration was significant compared to the normal conditions (n.c.). In ATP-depleted conditions, LNC-DiA-fluoNFL3 uptake was near 0 % after 1 h, but increased to about 25 % of the n.c after 6 h. At 1 h, the LNC-DiA-fluoNFL3 uptake was similar in both conditions (4°C and ATP-depleted), but significantly different after 6 h. Internalization of fluoNFL solution was significantly and similarly reduced at 4°C and ATP-depleted condition at 1 h compared to n.c. (Figure 9b). Therefore, LNC-fluoNFL3 uptake in U87MG cells is temperature and energy-dependent process, similarly to fluoNFL as previously reported (Berges et al., 2012a).

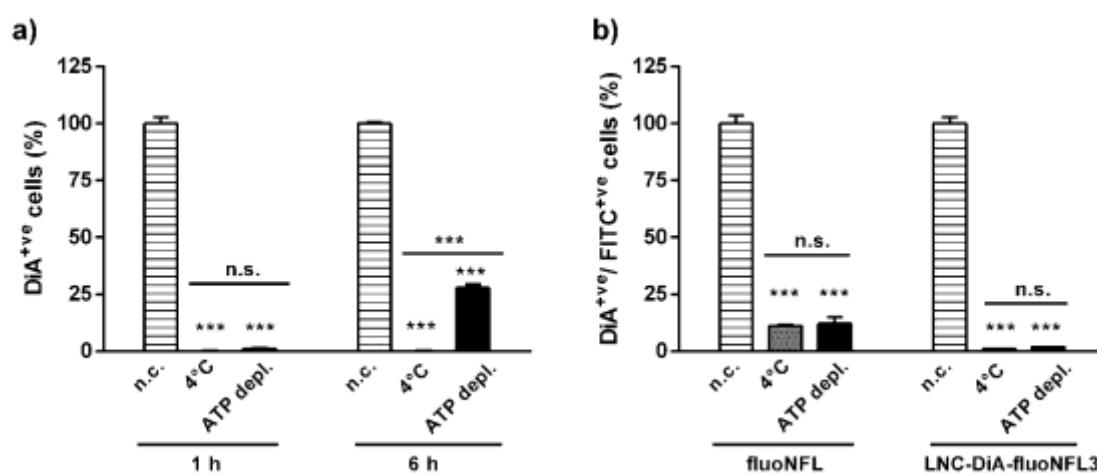


Figure 9: a) LNC-DiA-fluoNFL3 internalization in U87MG cells at different energetic conditions. The cells were incubated with 1.23 mg/mL of LNC-DiA-fluoNFL3 for 1 h and 6 h at 37°C (n.c.), 4°C and ATP-depleted conditions. b) Comparison of internalization of fluoNFL and LNC-DiA-fluoNFL3 in U87MG cells at different energetic conditions at 1 h. Twenty thousand events per sample were analyzed and percentages of DiA⁺ve cells (for LNC-DiA-fluoNFL3) or FAM⁺ve cells (for fluoNFL) were measured. The experiments were performed in triplicate. Statistical analysis was performed with oneway ANOVA with Tukey post-hoc test (p < 0.1 is denoted by (*), p < 0.01 by (**), and p < 0.001 by (***), n=3).

To further evaluate the possible uptake pathway(s) of the peptide-functionalized LNC, exclusion of particular endocytosis mechanisms was achieved by using inhibitors of the foremost endocytosis pathways. The cells were pretreated for 30 minutes with different inhibitors followed by 1 h treatment with the LNC-DiA-NFL3. LNC uptake was significantly inhibited in presence of each of these inhibitors (Figure 10a). LNC-DiA-NFL3 internalization was the lowest in presence of DAM, followed by CP, MβCD and PMA. A strong correlation between fluoNFL internalization and LNC-DiA-FluoNFL3 uptake was observed (Figure 10b). Like the functionalized-LNC, fluoNFL uptake was most strongly inhibited by DAM, followed by similar inhibition in presence of CP and MβCD, and lastly PMA.

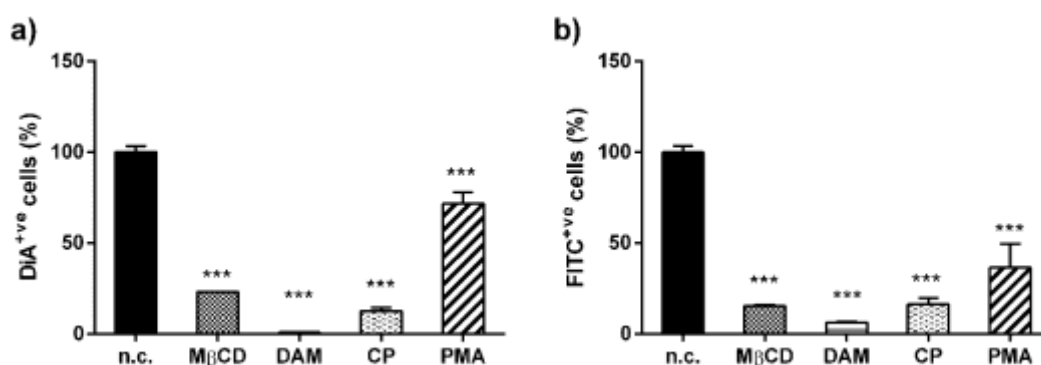


Figure 10: Internalization of LNC-DiA-fluoNFL3 (a) and fluoNFL (b) in U87MG cells at 37°C (n.c.) after 30 min pretreatment with various inhibitors (MβCD, DAM, CP and PMA) followed by 1 h incubation with the nanocapsule (1.23 mg/mL) or the peptide solution (equivalent fluoNFL concentration of LNC-DiA-fluoNFL3). Twenty thousand events per sample were analyzed and percentages of DiA⁺ve cells (for LNC-DiA-fluoNFL3) or FAM⁺ve cells (for fluoNFL) were measured. The experiments were performed in triplicate. Statistical analysis was performed with oneway ANOVA with Tukey post-hoc test (p < 0.1 is denoted by (*), p < 0.01 by (**), and p < 0.001 by (***), n=3).

3.7. Cytotoxicity on U87MG cells

To evaluate the cytotoxicity of FcTriOH loaded LNC formulations, cell viability was evaluated by MTS assay after 72 h of treatment with the formulations. The IC₅₀ of FcTriOH solution was of 1.31 μM which was slightly reduced to 1.05 μM as the drug was loaded in LNC. However, the peptide-functionalized LNC-FcTriOH-NFL3 had the lowest IC₅₀ of 0.46 μM, which was 2.8-folds and 2.3-folds lower compared to the drug solution and the drug-loaded non-functionalized LNC (LNC-FcTriOH). The control LNC showed toxicity at much higher concentration (IC₅₀ 22.2 μM) compared to the drug-loaded LNCs. The fluoNFL solution did not show any toxicity in the tested concentrations (Supplementary data).

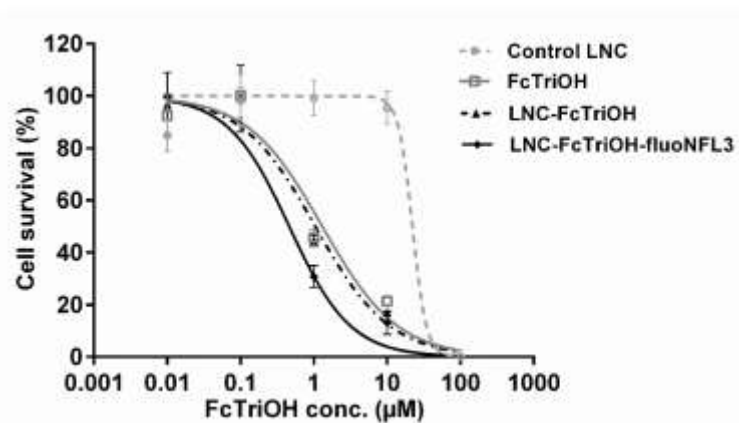


Figure 11. Cytotoxicity of various LNCs (control LNC, LNC-FcTriOH and LNC-FcTriOH-NFL3) and FcTriOH solution on U87MG cells after 72 h treatment, measured by MTS assay.

3.8. *In vivo* studies

3.8.1. *Preliminary study in ectopic xenograft model*

Nude NMRI mice were subcutaneously inoculated with human U87MG cells to acquire preliminary knowledge of possible tumor reduction efficacy and toxicity of the developed formulations after i.v. administration. After 7 days of cell implantation, the average tumor volume was around 70 mm³ and the animals were divided into five groups and injected intravenously with 70 μL of treatments (20 mg FcTriOH per kg body weight, or 822.4 mg LNC with/without 21.5 mg peptide per kg of body weight) on day 7 and day 10 (Figure 12). The relative tumor volume of the saline and the LNC-blank treated mice gradually increased from day 7 until the end of the study, whereas it was stable until day 17 and then augmented for LNC-blank-fluoNFL3 treated group. For the FcTriOH treated groups (LNC-FcTriOH and LNC-FcTriOH-fluoNFL3), relative tumor volume gradually decreased up to day 17, remained smaller than their initial volume (at the first treatment injection day) up to day 22, and then increased gradually. Compared to saline treated group, the relative tumor growth for LNC-FcTriOH and LNC-FcTriOH-fluoNFL3 treated groups were significantly lower (40.1 and 44.2 % respectively) at day 17 of the study (Figure 12). This significant difference was maintained up to day 22 of the study, and was absent afterwards due to high standard deviation.

None of the mice showed any immediate or delayed behavioral signs of pain or toxicity after the treatments were administered. Moreover, they were growing gradually as evident from their relative weight which increased about 20 % at the end of the study period.

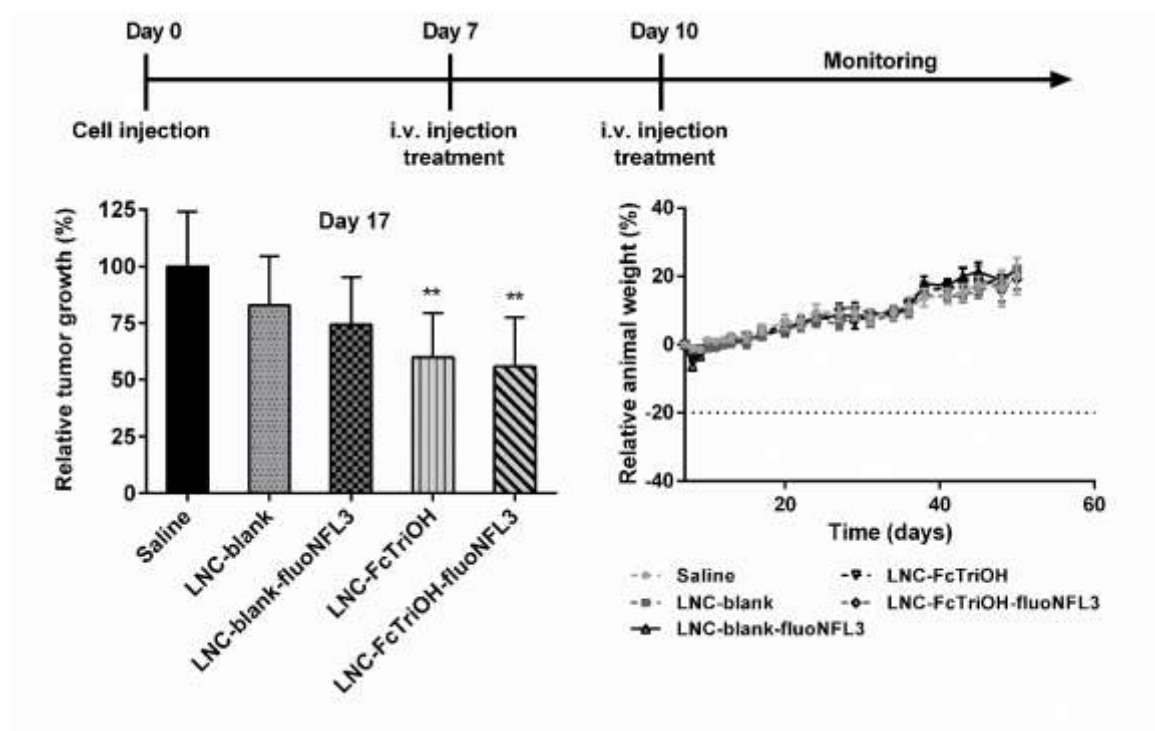


Figure 12: Relative tumor growth (on day 17) and relative animal weight of subcutaneous U87MG human glioblastoma tumor bearing mice. Each mouse was injected with 2×10^6 cells (in 50 μ L PBS) in the right flank on day 0 of the study. As the average tumor volume reached about 70 mm³ after one week, the mice received their treatment (equivalent to 20 mg FcTriOH per kg of body weight) by i.v. injections on day 7 and day 10. Mouse weight, behavior and tumor volume was followed regularly. Statistical analysis was performed with oneway ANOVA with Tukey post-hoc test ($p < 0.1$ is denoted by (*), $p < 0.01$ by (**), and $p < 0.001$ by (***), $n=8$)

4. Discussion

The aim of this study was to optimize the concentration of fluoNFL peptide on LNC surface to enhance their internalization in human GBM cells, in order to improve their efficacy as a drug delivery system for GBM. LNCs are promising nanovectors for carrying hydrophobic anticancer molecules and has been used in numerous preclinical studies using

various GBM tumor models and different administration routes (Allard et al., 2009a; Allard et al., 2010; Huynh et al., 2012). However, GBM tumors are known to develop resistance to such treatments (Haar et al., 2012). Therefore, enhancement of cellular internalization of LNCs in GBM cells by optimizing their surface characteristics can be a promising approach to improve therapeutic efficacy. The NFL peptide was reported to preferentially enter in GBM cells from diverse origins (human, rat and mouse) compared to corresponding healthy cerebral cells, and showed possible therapeutic benefits at certain concentrations (Berges et al., 2012a). The potential of this peptide as a GBM-targeting ligand to functionalize LNC surface was investigated by Balzeau et al., and increased cellular uptake of LNCs into mouse GBM cells (Balzeau et al., 2013). In this study, we evaluated the capability of NFL-peptide to act as a targeting ligand for the U87MG human GBM cells and we evaluated the effect of surface-functionalizing NFL concentration on cellular internalization of LNC. Finally, we tested the efficacy of NFL-LNC encapsulating a ferrocifen-type anticancer molecule, FcTriOH.

The surface-functionalization of LNCs was performed by simply adsorbing different amounts of the peptide onto LNC surface over 24 h period. As size, zeta potential and surface coating can profoundly impact on the *in vivo* fate of the nanovectors (Straubinger et al., 1993), these properties of the developed LNCs were characterized (Table 1). The particle size of the control LNC was 57 ± 2 nm, whereas diameter of the LNC-fluoNFL1 (NFL 1 mM) and LNC-fluoNFL3 (NFL 3 mM) were about 4 nm and 7 nm higher respectively signifying a potential higher amount of fluoNFL adsorbed to the surface. Similarly, peptide adsorption augmented the zeta potential of the LNC-fluoNFL1 and LNC-fluoNFL3 by +2 and +7 mV respectively compared to control LNC. This variation of surface charge can be explained by the net positive charge of the NFL peptide (Berges et al., 2012b). The changes in size and zeta potential for LNC-fluoNFL1 were similar to the one reported by Carradori et al. (Carradori et al., 2016). Moreover, the LNC size after fluoNFL adsorption was well below 100 nm which can be beneficial for diffusion in the cerebral extracellular space (Allard et al., 2009a; Allard et al., 2009b). The PDI of all three formulations were less than 0.2, therefore they can be considered as monodispersed. The concentration of the LNC-adsorbed fluoNFL was quantified indirectly by measuring the free peptide concentration after separating them using centrifugal filters with MWCO 100 kD. The concentration of LNC-adsorbed peptide in LNC-fluoNFL1 was 0.40 % w/w

which was in correspondence with the concentration reported by Balzeau et al. and Carradori et al. (Balzeau et al., 2013; Carradori et al., 2016). The concentration of LNC adsorbed fluoNFL in LNC-fluoNFL3 was 2.49 % (w/w) which was about 6-folds higher compared to LNC-fluoNFL1 although the concentration of peptide initially added was only 3-folds higher. The number of peptide molecules per LNC particle can be calculated from the particle concentration obtained by NTA and the adsorbed NFL concentration quantified by HPLC. About 243 and 1534 peptides were adsorbed per LNC particle in LNC-fluoNFL1 and LNC-fluoNFL3 respectively. Torchilin et al. calculated number of TAT peptides on 200 nm liposomes in a different method and found about 500 peptides per liposome (Torchilin et al., 2001), which was between the number of fluoNFL observed in our formulations. About 0.016 and 0.102 fluoNFL molecules will be present per nm² surface area in LNC-fluoNFL1 and LNC-fluoNFL3 respectively, whereas up to 5.4 short chain PEG molecules (comes from Kolliphor HS15) per nm² surface area can be present. The exact reason for such high percentage of adsorption is unknown. It can be hypothesized that 3-folds increased peptide concentration during the 24 h adsorption step possibly increased the likelihood of collision and amplified the LNC-peptide and peptide-peptide interactions, which in combination may have resulted the high adsorption. Physical entanglement between adjacent peptide molecules might also occur in presence of LNCs at this concentration, resulting restrained peptide movement and increased adsorption (Yu and Zheng, 2011). Moreover, the aqueous dispersion of LNCs became semi-solid after adsorption of 4 mM fluoNFL (therefore NFL concentrations above 3 mM were not tested). This also indicated that the peptide-LNC mixture may started to form a network at high peptide concentrations. Self-assembly peptides has been described to form hydrogels in the literature (Zhou et al., 2009). Alteration in environmental conditions (e.g. pH and ionic strength) can trigger interaction among peptide chains resulting physical cross-linking and filament growth to form viscoelastic solids (Larsen et al., 2009). Addition of LNC dispersion may alter such environmental conditions of the peptide solution and result formation of semi-solids. However, further study is necessary to understand the exact reason for the high adsorption percentage.

Balzeau et al. has reported that the NFL interacts with the polar PEG chains of the Kolliphor (Balzeau et al., 2013) whereas Carradori et al. suggested that the interaction was possibly by a combination of electrostatic forces and other weak forces i.e. Van der

Waal's forces and hydrophobic forces (Carradori et al., 2016). We evaluated the effect of NaCl and Tris buffer concentration on LNC-fluoNFL3 size by incubation with different concentrations of these solutions and subsequently measuring their diameter in DLS (Figure 1). Contrasting to previous studies, the significant difference of nanocapsule diameter compared to control LNC was maintained nearly throughout the NaCl concentration range. However, Tris buffer impacted more the size of LNC-fluoNFL3 compared to NaCl, and no significant difference of particle size was observed above 0.05 M concentration. It can be hypothesized that the possible self-entanglement of the peptide in LNC-fluoNFL3 involves more inter-chain interactions (e.g. hydrogen bond, hydrophobic forces and/or Van der Waal's forces) and therefore resisted the impact of high NaCl concentrations, but loses its significant size difference with control LNC in higher Tris concentrations. To evaluate if the fluoNFL will be rapidly removed from the LNC surface after dilution, LNC-fluoNFL3 was put in a dialysis bag (MWCO 100 kD) and was dialyzed against 1x Tris buffer solution at 37°C and 75 rpm. Free peptide concentration was quantified from the receiver compartment by HPLC. Desorption of the fluoNFL from LNC surface was slow and gradual and only 33.6 % peptide was desorbed after 6 h (Figure 2). Moreover, NFL-functionalized LNCs was reported to maintain their characteristics in cell culture medium (Carradori et al., 2016). Therefore, the LNC-fluoNFL3 formulation can be promising for administration by i.v. injection. Additionally, this experimentation about the fluoNFL desorption from LNC surface by dialysis method also indicated a high percentage of fluoNFL adsorption in LNC-fluoNFL3. About 94.4% and 90.4% of the added peptide were remaining in the dialysis chamber after 30 min and 1 h dialysis respectively for LNC-fluoNFL3, whereas it was only 41.1% and 9.6% for the control fluoNFL solution (same initial concentration as LNC-fluoNFL3). Theoretically, up to 59% of the added 3 mM peptide in LNC-fluoNFL3 should be able to cross the dialysis membrane to reach the receiver chamber after 30 min dialysis, if they were free. Therefore, this results also showed that the peptide adsorption percentage in LNC-fluoNFL3 was possibly very high and further study is necessary to understand the mechanism.

As the size and zeta potential of the LNC was altered after fluoNFL adsorption, it could impact the *in vivo* fate of the nanocarrier. Enhanced particle size and positive zeta potential may significantly increase complement protein consumption by nanoparticles,

leading to rapid removal from systemic circulation by the mononuclear phagocytic system (MPS) (Vonarbourg et al., 2006a; Vonarbourg et al., 2006b). The CH50 unit consumption by the LNC-fluoNFL1 was similar to what shown by the control LNC. However, the CH50 unit consumption by the LNC-fluoNFL3 was slightly enhanced compared to the other two formulations. This can be attributed to the increased size as surface area recognition by the complement is proportional to the particle diameter (Harashima et al., 1996), or to the altered zeta potential (Vonarbourg et al., 2006a). Overall, the complement consumption by all three formulations were low even at high surface area (calculated by NTA (Karim et al., 2017a)) and should not be quickly removed from bloodstream by MPS.

Previously, Balzeau et al. showed that the internalization of LNC in mouse GBM cells can be enhanced by adsorbing the NFL peptide on its surface (Balzeau et al., 2013). However, cellular uptake on nanocarriers can be cell specific as the interacting plasma membrane composition (i.e. ligands, receptors and endocytosis apparatus) vary among cell lines (Paillard et al., 2010). Therefore, as a potential therapeutic strategy for human disease, it was necessary to characterize the internalization kinetics of the LNC with/without the surface-adsorbed NFL peptide in a human GBM cell line at a non-toxic concentration. Moreover, Lépinoux-Chambaud et al. reported that the extent and pathway of NFL internalization into U87MG cells were dependent on the extracellular peptide concentration (Lépinoux-Chambaud and Eyer, 2013). Therefore, the effect of LNC surface-functionalizing fluoNFL peptide concentration on LNC internalization by U87MG human GBM cells was evaluated in this study. For this purpose, the LNCs were fluorescently labelled by encapsulation of DiA and their cellular uptake was quantified by fluorescence-activated cell sorting (FACS). The LNC concentration used for the cellular uptake studies was 1.23 mg/mL, which was selected based on previously described safe concentrations of LNC and NFL peptide (Balzeau et al., 2013; Carradori et al., 2016; Lépinoux-Chambaud and Eyer, 2013). To identify and separate dead cells, the FACS samples were suspended in 0.12 % w/v of trypan blue for the measurements in flow cytometer and signals in 655 nm long-pass filter was detected. Trypan blue can enter inside cells with damaged membrane, complex with proteins and emit fluorescence around 660 nm that can be detected in FACS (Avelar-Freitas et al., 2014; Patino et al., 2015). However, maximum 0.1% dead cells were detected in the FACS samples which confirms

that the LNC concentration used for treatment of cells was non-toxic. The internalization of all three formulations increased with time (Figure 4). At each time point, the uptake of LNC-DiA-fluoNFL3 was significantly higher compared to LNC-DiA-fluoNFL1 and LNC-DiA, whereas the internalization of LNC-DiA-fluoNFL1 was significantly higher compared to LNC-DiA. It was also observed that the peptide needs to be absorbed onto the LNC surface (by 24 h stirring) for maximizing LNC internalization as the uptake of 'LNC-DiA and fluoNFL immediate mixture' was significantly lower compared to LNC-DiA-fluoNFL3 (Figure 5). Therefore, the internalization of nanocapsules into U87MG cells is dependent on the concentration of NFL on LNC surface. Confocal microscopy images visually confirmed the much higher cellular uptake of LNC-DiA-fluoNFL3 compared to LNC-DiA (Figure 6a), and showed that majority of the NFL-functionalized LNC was into the cytoplasm whereas the LNC-DiA was mostly attached to the cell membrane (Figure 6b). It has been shown for the first time that the NFL peptide concentration (as a targeting-ligand) onto nanocarrier surface can have significant impact on the rate and the extent of the nanovector cellular internalization. Therefore, this strategy can be used to improve nanocarrier targeting efficiency to other GBM cells, even to other type of cells in which the peptide can efficiently enter i.e. brain neural stem cells (Berges et al., 2012a; Carradori et al., 2016; Lepinoux-Chambaud et al., 2016).

Previously, Paillard et al. reported that the internalization of LNC was not preferentially targeted into GBM cells and entered also healthy astrocytes (Paillard et al., 2010). Therefore, to investigate the targeting capacity of the LNC-fluoNFL3 towards U87MG cells, LNC-DiA and LNC-DiA-fluoNFL3 were incubated with NHA and their cellular uptake after 1 h and 6 h was measured and compared with their uptake in U87MG cells (Figure 7). At 1 h, no significant difference was observed between LNC-fluoNFL3 internalization in NHA and U87MG cells (Figure 8). However, the rate of LNC-fluoNFL3 internalization was much faster in the GBM cell and the nanovector entered significantly more in the cancer cell compared to NHA. Therefore, the cellular internalization of LNC-fluoNFL3 was more targeted towards the human GBM cells compared to healthy cells.

To investigate the possible pathway(s) of LNC-fluoNFL3 internalization in U87MG cells, its uptake was followed in different energetic conditions and in presence of various endocytosis pathway inhibitors. The internalization of the nanocarrier was significantly reduced (compared to 37°C) when incubated at different energetic conditions (4°C and

ATP-depleted condition) (Figure 9a). Thus, the LNC-fluoNFL3 uptake in U87MG cell was an energy-dependent active process. Comparable trend was observed in cellular uptake of the fluoNFL alone (Figure 9b) which was also mentioned in previously reports (Berges et al., 2012a).

The dependency of cellular uptake on energy indicates that the internalization possibly occurs by endocytosis. To further illustrate about the particular internalization pathway(s) involved, the cells were pretreated with various inhibitors of the chief endocytosis pathways. Treatment with M β CD depletes cholesterol and inhibits both clathrin- and caveolin-mediated endocytosis, DAM prevents macropinocytosis, chlorpromazine blocks clathrin-dependent endocytosis and PMA impedes caveolin-dependent endocytosis (Paillard et al., 2010; Sahay et al., 2010). As previously reported for the NFL peptide (Lepinoux-Chambaud and Eyer, 2013) (also observed in our experiments, Figure 10b), the internalization of the LNC-fluoNFL3 was not dependent on one particular endocytosis pathway, rather on several and its uptake was significantly reduced compared when cells were pretreated with these inhibitors (Figure 10a). Taken together, the predominant pathways involved in NFL-functionalized LNC internalization were macropinocytosis, clathrin-dependent and caveolin-dependent endocytosis; similar to the peptide solution. The very low uptake of the non-functionalized LNC into U87MG cells up to 6 h was not suitable to be used as control for evaluating its cellular uptake mechanisms. Moreover, we tried the 24 h time point for determining the possible LNC internalization pathways. But the cells did not survive up to 24 h in presence of the different endocytosis inhibitors and the mechanism of LNC uptake in U87MG cells could not be determined by this method. Therefore, it cannot be concluded if the NFL-peptide dictated the internalization of peptide-functionalized LNCs into U87MG cells. As cargoes taken up by macropinocytosis and clathrin-dependent endocytosis (and caveolin-dependent endocytosis to some extent) can end up in lysosomes, the NFL-functionalized LNCs may not be the suitable choice to deliver drugs prone to lysosomal degradation (e.g. nucleic acids or proteins) in U87MG cells, unless it can escape from the endo-lysosomal compartments, like LNC (Paillard et al., 2010). Therefore, intracellular trafficking on NFL-functionalized LNCs should be further investigated.

A promising ferrocifen-type anticancer drug FcTriOH was encapsulated in the LNCs and its *in vitro* antiproliferative activity was assessed by MTS assay. The cells were treated

with 0.1-100 μM of FcTriOH and its formulations for 72 h. Up to 0.1 μM , cell survival was above 80% for all treatment groups (Figure 11). Between 0.1-10 μM , the cell survival percentage drastically reduces for cells treated with FcTriOH, LNC-FcTriOH and LNC-FcTriOH-fluoNFL3 resulting in IC_{50} values of 1.31 μM , 1.05 μM and 0.46 μM respectively. The survival of the cells treated with control LNC reduced significantly between 10 and 100 μM with an IC_{50} of 22.5 μM . Corresponding concentrations of fluoNFL solution did not alter cell viability (supplementary data) which was also reported previously (Berges et al., 2012a).

In the preliminary *in vivo* study, an U87MG subcutaneous GBM tumor model was used to evaluate potential tumor reduction efficacy or possible toxicity after two tail vein injections equivalent to 20 mg/kg FcTriOH. As no previous reports about FcTriOH administration in animals were available, the dose was chosen based on previous *in vivo* studies involving other ferrocifen molecules (Laine et al., 2014). The two i.v. injections were given on day 7 and day 10. A tendency of relative tumor volume gradual reduction was observed since the beginning of the treatment with FcTriOH-loaded LNCs. A significant difference i.e. 40.1 % and 44.2 % lower relative tumor volume for LNC-FcTriOH and FcTriOH-fluoNFL3 respectively, compared to the saline treated group, was observed on by day 17 (Figure 12) which was maintained up to day 22. The mouse showed no behavioral signs of pain or irritation immediately after the injection. Additionally, no sign of toxicity were observed as the weight of the mice never reduced. Therefore, the therapy was well tolerated. However, the tumor reduction effect of the FcTriOH treatments was not observed from day 24 (two weeks after the last injection). The tumor rapidly grew back and no significant difference in relative tumor volume was observed. This possibly occurs as the drug is eliminated leading its antiproliferative effect to fade and the tumor to grow back. In fact, several preclinical studies have used much higher number (6 to 20) of i.v. injections (Karim et al., 2017b; Laine et al., 2014) and observed a significant difference on tumor growth. In clinical practice, chemotherapy is generally administered in several cycles; a treatment period followed by a waiting period for the patient to wash-out and recover from the side effect of the drug. The cycle frequencies are optimized depending on the treatment used. In future studies, the number of injections and/or dose should be increased to possibly achieve tumor regression after FcTriOH-loaded LNC treatment. Although the relative tumor volume of LNC-FcTriOH

treated and LNC-FcTriOH-fluoNFL3 treated groups between on 17 was significantly lower from saline treated groups, the difference among themselves were not significant. However, the average value was slightly lower for NFL-functionalized LNC treated groups. The tendency could be more clearly observed if more injections are given in the future studies.

The NFL-peptide concentration of LNC surface can be further increased for additional enhancement of its internalization in human GBM cells. However, the currently used preparation technique is not suitable for this purpose as precipitates were observed in NFL peptide solutions above 3 mM, probably due to its aqueous solubility limit. However, higher amounts of peptide can be added by altering the volume of NFL solution added before the adsorption step. Additionally, suitable chemical-grafting methods can be evaluated to covalently couple the peptide to LNC surface or to the distal end of suitable spacer molecules.

5. Conclusion

In this study, we have showed that the NFL peptide can enhance the uptake of LNC in human GBM cells in a dose-dependent manner. Moreover, the peptide-functionalized LNCs reached the cytoplasm at much higher concentration compared to the non-functionalized control LNCs. Additionally, the peptide functionalized LNCs were preferentially accumulated in GBM cells compared to healthy human astrocytes showing the targeting capacity of the nanovector. The internalization of this nanoparticle in the U87MG cells was energy-dependent and occurred by a combination of macropinocytosis, clathrin-mediated and caveolin-mediated endocytosis, similar pathway as the NFL peptide solution. Encapsulation of FcTriOH in the GBM targeting LNC resulted in a decreased IC₅₀. The preliminary *in vivo* study in an ectopic human GBM xenograft model showed that the drug-loaded LNC therapy was well tolerated after i.v. administration and their tumor reduction efficacy was promising. However, more cycles of chemotherapy seemed necessary for future experiments. Moreover, NFL peptide concentration can be further enhanced on LNC surface to further improve its uptake in GBM cells. Overall, enhancement of NFL peptide concentration on LNC surface is a promising strategy for greater and targeted nanocarrier internalization in human glioblastoma cells, and the FcTriOH-loaded LNCs are promising therapy approach for glioblastoma.

Acknowledgements

The authors would like to thank Pierre Legras (Service Commun d'Animalerie Hospitalo-Universitaire, Angers, France) for his technical assistance in animal experiments, and Dr. Rodolphe Perrot (Service Commun d'Imageries et d'Analyses Microscopiques, University of Angers) for his support in confocal microscopy. This work was supported by the NanoFar Consortium of the Erasmus Mundus program; and Fonds Léon Fredericq, CHU, University of Liege, Liege, Belgium.

Appendix A. Supplementary data

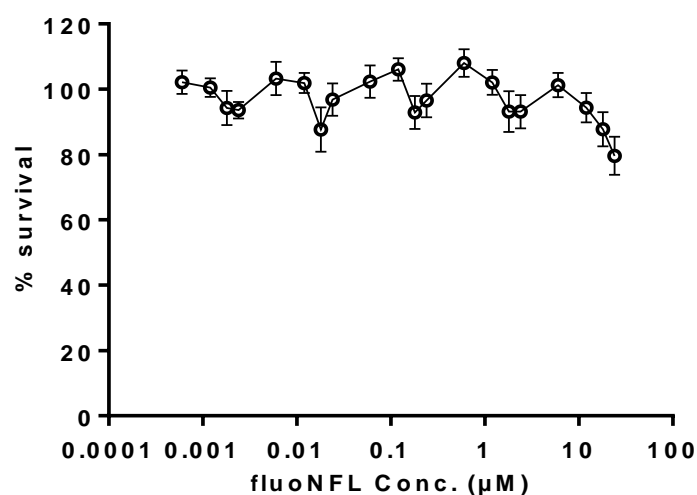


Figure S1: Cytotoxicity of fluoNFL solution on U87MG cells after 72 h treatment, measured by MTS assay.

4.3.2. Additional data

4.3.2.1 Blood-brain-barrier permeability of lipid nanocapsules and NFL-functionalized lipid nanocapsules

The NFL peptide was reported for enhancing nanocarrier uptake in GBM cells (Balzeau et al., 2013). However, the effect of NFL-functionalization of LNCs on their BBB permeability was never reported. The BBB permeability of the various developed LNCs was evaluated using the *in vitro* BBB model using hCMEC/D3 cell line. This is a human cerebral microvascular endothelial cell line which is reported to express the major

properties of the BBB i.e. expression of junction complexes (Weksler et al., 2005), and has been used as a consistent *in vitro* model to evaluate drug transport across the BBB (Poller et al., 2008).

For the transport assays, optimum excitation (455 nm) and emission wavelengths (650 nm) for detection of DiA in the culture media was determined by scanning its solution in a spectrophotometer (Infinite M200 Pro, Tecan). Subsequently, a calibration curve was prepared to correlate the fluorescence signals to the various concentrations of DiA-labelled LNCs (use of LNCs was necessary as DiA signal intensity increases when it is in contact with lipids). The cells were cultured using EndoGROTM-MV Complete Culture Media Kit® (Millipore) on 24 well hanging call culture inserts with 0.4 µm pores (Millicell, Millipore) placed on a 24 well plate (Millipore). Before the LNC permeability studies, integrity of the hCMEC/D3 cell monolayers in all the inserts was assessed by lucifer yellow (LY) rejection method according to previously described protocols (Millipore, 2016). Once the integrity of the monolayers confirmed, DiA-labelled LNCs (LNC-DiA, LNC-DiA-NFL1 and LNC-DiA-NFL3. 0.48 mg/mL in FBS) were placed on the apical chamber of the well. At defined time points, samples were collected from the basal chamber and the volume was immediately replaced with fresh medium. The fluorescence intensity of the samples was measured in the spectrophotometer to know the LNC concentration in the basal sample. At the end of the nanocarrier permeability study, another LY rejection test was performed to determine the monolayer integrity. Only results from the inserts with intact cell monolayer were considered for permeability calculation.

However, no significant difference was observed in the permeability of the different LNCs (with or without NFL-functionalization) at any time points (Figure 4.2). The LNC passage was faster up to 2 h and reached about 31-42%. Subsequent rate of permeability was slower and gradually increased to 36-49% after 6 h. Therefore, it seemed that the NFL peptide did not enhance the passage of LNCs through the BBB model. However, it is necessary to consider that the dilutions of the nanocarriers during sample preparation was performed using FBS (instead of buffers used in other studies (Markoutsas et al., 2011)), to mimic the *in vivo* situation. Therefore, it is possible that the LNCs were covered by serum proteins resulting the similar passage of the formulations.

We only included the results from the inserts which showed acceptable LY rejection at the end of the study, an increase in LY passage (about 6-14%) was evident in these samples as well. Additionally, the LY passage was higher than the acceptable range for a few samples (which were not considered to calculate the LNC passage) indicating that the cell monolayer was disrupted in these cases. Possibly, the LNCs affected the BBB monolayers by disrupting the junction complexes or by causing cell deaths, resulting monolayer disruption and increased LY permeability. Therefore, further repetitions of this test should be performed with lower concentrations of LNCs. Moreover, cellular uptake of NFL peptide in the BBB cells and its permeability across the cell monolayer model has to be investigated to see if the peptide actually has capacity to cross the BBB. If the peptide shows promising properties, it can be chemically linked with the LNCs with suitable hydrophilic spacer molecules and tested for possible enhancement of nanocarrier BBB permeability.

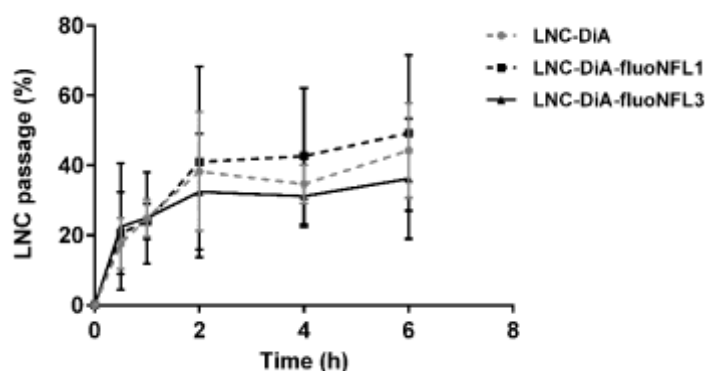


Figure 4.2: *In vitro* blood-brain-barrier permeability of lipid nanocapsules measured using the hCMEC/D3 cell monolayer model (n=3).

4.3.2.2 Possibility of synergy between AG and FcTriOH:

Although AG is known for its antioxidant activity (Romanova et al., 2001), it has been also reported for its prooxidant activity (Galati et al., 2002; Xu et al., 2011). Flavonoids under specific conditions can show their prooxidant activity and cause oxidative damage to cellular components by producing ROS (Prochazkova et al., 2011). As oxidative damage is one of the possible mechanisms of action FcTriOH, it is possible that AG and FcTriOH may have synergistic effect. To evaluate possible synergy, we used the ‘Chou-Talalay method’ for drug combination study. This method is a unified theory based on a

derivative from ‘mass-action law’ theory, called ‘median-effect equation’ (Chou, 2010; Chou, 2006). The method can quantitatively describe synergism, antagonism or additive effect in drug combinations by calculating combination index (CI) (Chou, 2010) based on simple *in vitro* cell proliferation assays i.e. MTS assay. The value of CI is < 1 in case of synergism, whereas it is >1 for antagonism and $=1$ for additive effect. Synergism and antagonism are further divided into several categories ranging from ‘slight’ to ‘very strong’. The experimental design involves treatment of cells with the drug molecules alone and also in combinations at different ratios and evaluating their effect on cell proliferation. The calculation can be performed easily on the software called ‘CompuSyn’ developed by ComboSyn Inc (Chou, 2006). We evaluated different combinations of FcTriOH and AG solutions on U87MG cells using MTS assay (n=12) to evaluate any potential synergism (Table 4.1). The activity of the combinations at their IC_{50} can be classified in groups ranging from moderate antagonism to strong antagonism. As no synergy between the drugs were observed, formulations co-encapsulating FcTriOH and AG were not developed.

Table 4.1: Combination index (CI) values of different AG and FcTriOH combinations calculated from the results of MTS assay using CompuSyn software.

Molar ratio of FcTriOH and AG (FcTriOH:AG)	Combination index at IC_{50}
1: 0.4	2.02
1: 0.2	3.45
1: 0.1	1.68
1: 0.05	1.70
1: 100	1.33
2: 100	1.30

4.3.2.3 Efficacy and/or toxicity of the FcTriOH formulations in orthotopic xenograft model

Nude NMRI mice were injected with human U87MG cells in the brain to develop orthotopic tumor xenografts and were treated subsequently by CED to gain preliminary understanding of possible efficacy and/or toxicity of the LNCs after local administration into the brain. After acclimatization period, the animals were divided into 5 groups (4 mice per group) and were anesthetized by intraperitoneal injection of ketamine-xylazine mixture (100 mg/kg and 13 mg/kg respectively). The head of the animal was immobilized on a stereotaxic frame (Stoelting Co.) and an incision was made on the scalp. A hole was

created using a drill at 2.1 mm lateral and 0.5 mm anterior from the bregma. Then, a Hamilton 10 μL syringe (700 series) fitted with a 26G needle was loaded with U87MG cells (1×10^7 cells/mL of DMEM) and was inserted into the brain very slowly through the drilled hole up to 3.2 mm depth (from the bregma), waited 3 min before going up by 0.1 mm, and 3 μL of the cell suspension (3×10^4 cells) was injected very slowly over 5 min. The needle was kept static for 5 min before withdrawing it very slowly (0.5 mm/min). The incision was closed using a suture. On day 7, MRI (Biospec 70/20 Avance III, Bruker, France) was performed according to protocol described in (Danhier et al., 2015), to determine the possible location and size of the tumor. On day 8, the animals were anesthetized and surgery was made in the above mentioned method to put the treatment-loaded syringe (Hamilton 10 μL syringe, 1700 series, 32G needle) at the same coordinates from the bregma, except the depth that was chosen individually for each mouse based on the MRI scan from the previous day to have the injection point near the middle of the tumor. The animals received the treatment by CED at a rate of 0.37 $\mu\text{L}/\text{min}$ for 20 min, using a pump (PHD 2000 infusion, Harvard Apparatus, France). Group 1: 7.4 μL Saline ($n = 4$); Group 2: 7.4 μL of LNC-blank ($n = 4$); Group 3: 7.4 μL of LNC-blank-fluoNFL3 ($n = 4$), Group 4: 7.4 μL of LNC-FcTriOH equivalent to 2 mg FcTriOH per kg of body weight ($n = 4$); Group 5: 7.4 μL of LNC-FcTriOH-fluoNFL3 equivalent to 2 mg FcTriOH per kg of body weight ($n = 4$). MRI scans were performed on day 13 and day 22. Weight and behavior of the animals were daily followed.

MRI (T2-weighted) on day 7 was performed to evaluate brain lesions/tumors due to cells injection and their positions (Figure 4.3). The treatments were administered on the following day (day 8) by CED at suitable depths (individually determined for each mouse based on the MRI images) to have the best possibility to reach the whole region of tumor lesion. Survival of the mice was followed and Kaplan-Meier survival graph was prepared (Figure 4.5). The median survival of the saline treated and LNC-FcTriOH-fluoNFL3 treated groups were 37.5 and 38 days, whereas it was 43 days for LNC-FcTriOH treated group and 45.5 days for LNC-blank and LNC-blank-fluoNFL3 treated groups.

MR image acquisition was performed on day 13 and day 22 to follow up the evolution of the lesions. The mean brain lesion/tumor sizes at day 7 were small and similar between the groups (0.39-0.55 mm^3) (Figure 4.5). However, the brain lesions on day 13 (6 days after LNC administration by CED) were different between groups. The lesions of saline treated

group remained similar to day 7 with an average volume of $0.47 \pm 0.20 \text{ mm}^3$, whereas the lesion size increased for other groups. The lesion size of LNC-blank, LNC-blank-fluoNFL3, LNC-FcTriOH and LNC-FcTriOH-fluoNFL3 treated groups were $1.76 \pm 1.10 \text{ mm}^3$, $5.06 \pm 2.33 \text{ mm}^3$, $1.94 \pm 0.88 \text{ mm}^3$ and $5.81 \pm 2.07 \text{ mm}^3$ respectively. The lesion size of the NFL functionalized LNCs at day 13 were significantly higher from the saline group and their respective lesions at day 7. The mean lesion size increased at day 22 for all groups compared to day 13, except the lesions that were reduced for LNC-FcTriOH-NFL3 treated mice. However, the lesion sizes were not significantly different from day 13. Additionally, DTI on 1-2 mice from each group was performed on day 12, 17, and 22 which revealed that the NFL-functionalized LNC (with or without FcTriOH) treated groups had parts of lesions with comparatively high ADC i.e. between 1.54×10^{-3} to $2.01 \times 10^{-3} \text{ mm}^2/\text{sec}$, compared to ADC around $0.85 \times 10^{-3} \text{ mm}^2/\text{sec}$ and $0.65 \times 10^{-3} \text{ mm}^2/\text{sec}$ for lesions of other treatment groups and control healthy brain respectively (Figure 4.4).

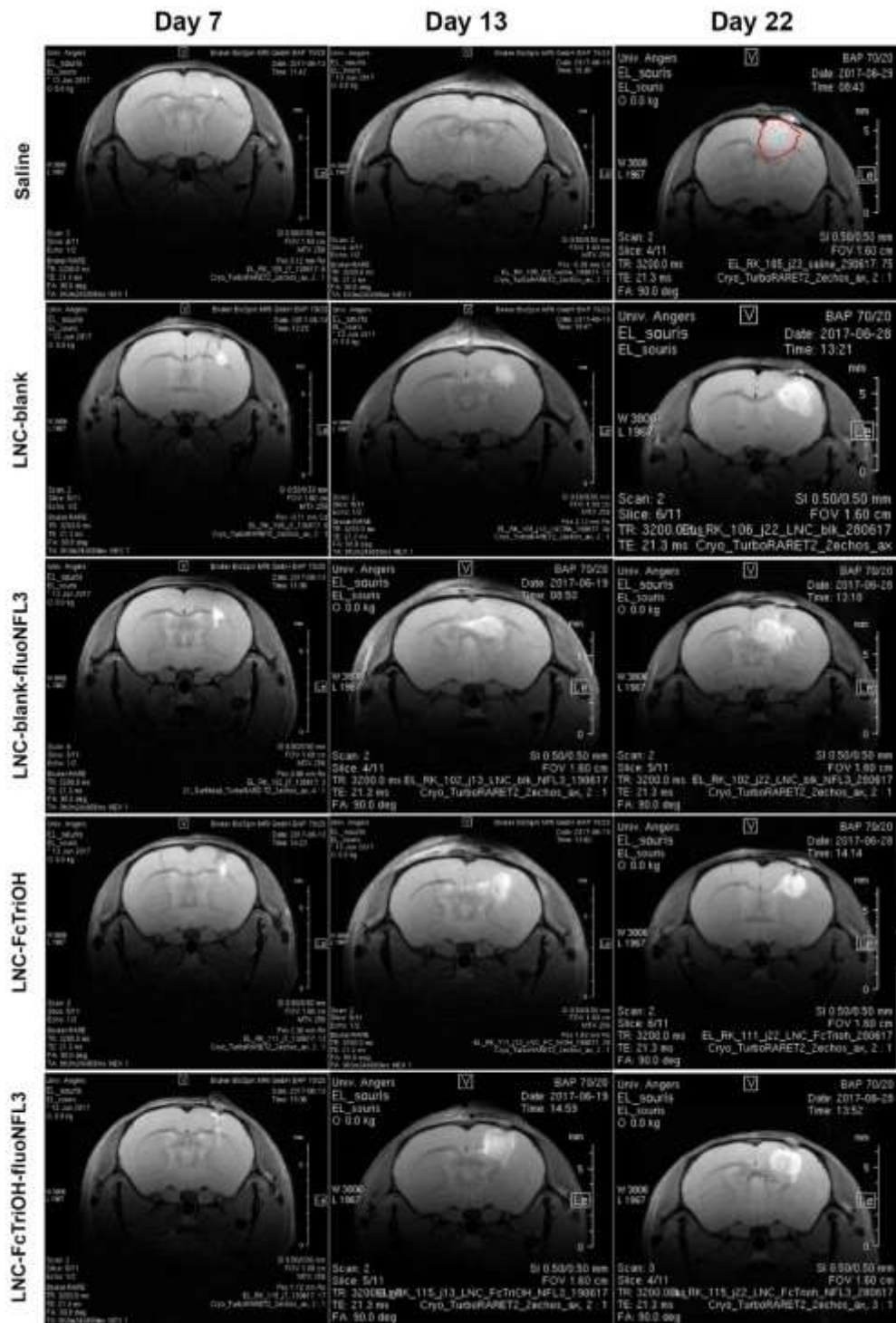


Figure 4.3: Representative T2-weighted MR images of longitudinal brain sections showing brain-lesions on day 7 (prior treatment), day 13 and day 22 of the study. For the saline group, the tumor/lesion on day 22 is shown by the red line. For the other groups, the lesion is visible by the lighter zone.

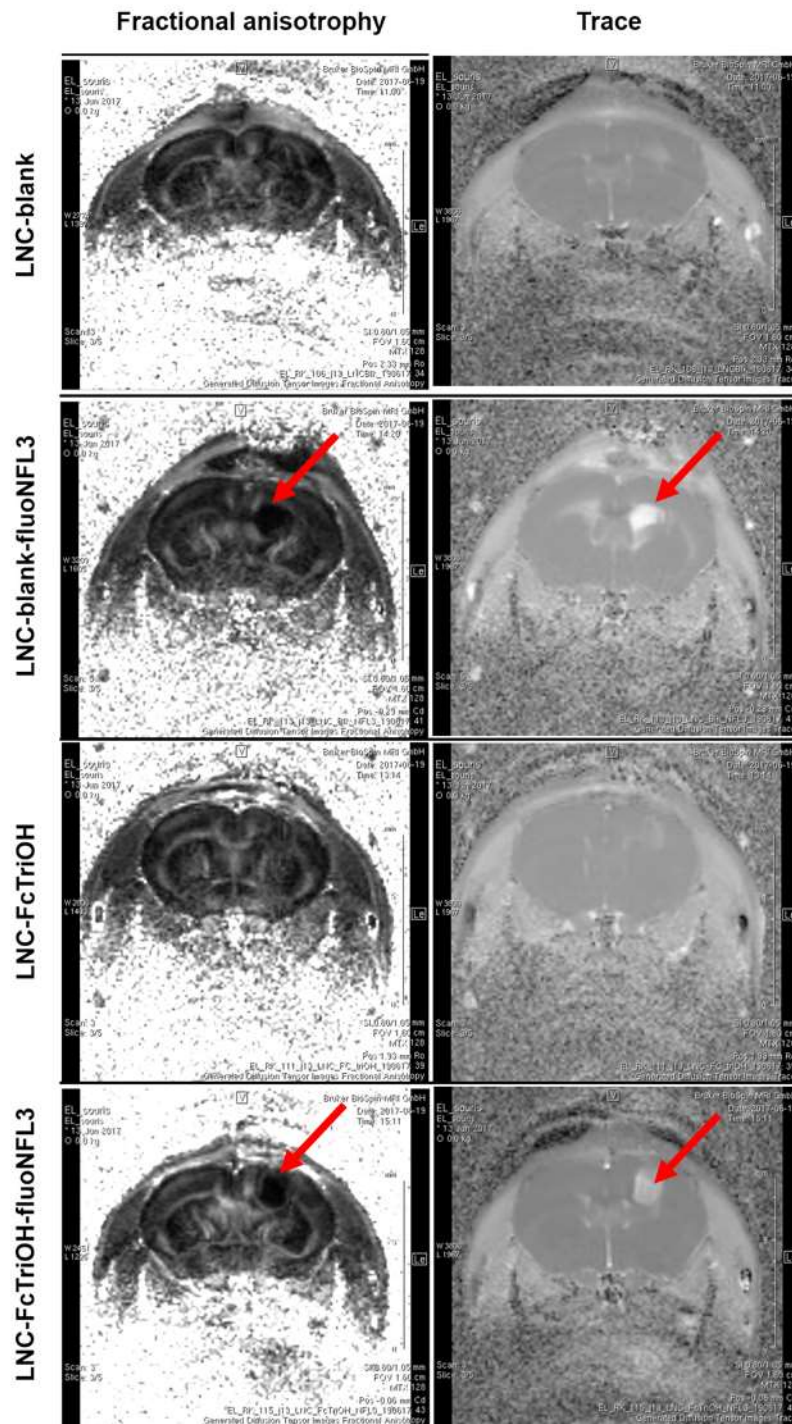


Figure 4.4: Representative diffusion tensor images (fractional anisotropy and trace) of a longitudinal brain section showing brain-lesions on day 13 of the study. For the NFL-functionalized LNC treated groups, the tumor/lesions had certain regions (indicated by the red arrows, appears black in fractional anisotropy and white in trace images) with high ADC values compared to non-functionalized LNC treated groups.

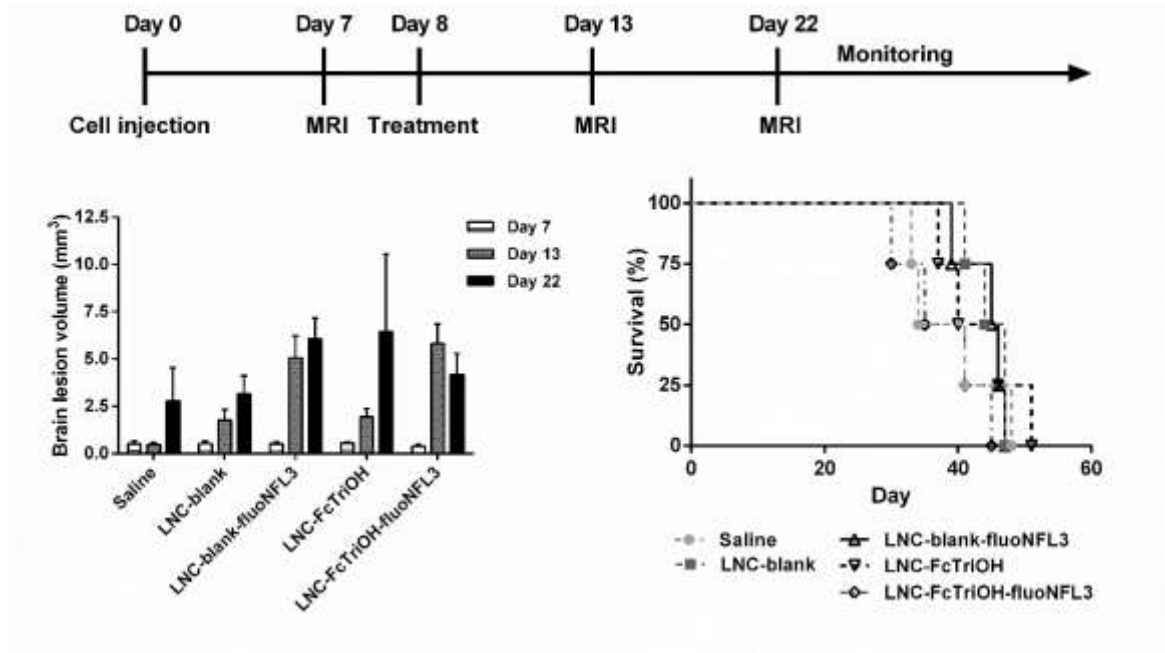


Figure 4.5: Brain lesion volumes calculated from manually selected region of interests in T2-weighted MR images, and Kaplan-Meier survival curves for U87MG tumor bearing mice treated with saline, or various LNCs administered by CED on day 8 after cell injection in the brain (n=4).

The significantly higher lesion size on day 13 (day 6 after treatment) for NFL-functionalized LNCs compared to other groups (Figure 4.5) is possibly due to the higher cellular uptake on the LNCs due to the NFL peptide functionalization which corresponds to the results observed *in vitro*. DTI of 1-2 mice per group revealed that the LNC-fluoNFL3 treated (with/without FcTriOH) had certain regions in their lesions which had 2-3-folds higher ADC values compared to the tumors of other groups (Figure 4.4). This high ADC value regions signifies alteration in tissue cellularity, possible lysis and necrosis in that region due to treatment (Patterson et al., 2008). The cell shrinkage and necrosis increase the available extracellular space and allow additional movement of water molecule resulting in the ADC increase. Moreover, several studies mentioned that treatment inducing an increase in ADC could be a predictor for response evaluation for cerebral tumors (Hamstra et al., 2005; Mardor et al., 2003). However, the treatment with LNC-FcTriOH-fluoNFL3 did not increase the median survival (38 days) of the animals

compared to the saline groups (37.5 days), possibly due to its toxicity. In comparison, median survival of LNC-blank and LNC-blank-fluoNFL3 was 45.5 days, whereas it was 43 and 47 days for LNC-FcTriOH and LNC-AG-fluoNFL3 respectively. We can hypothesize that the higher cellular internalization property of NFL-functionalized LNCs created larger brain lesions (evident from the lesion size seen on MRI at day 13) by the intrinsic toxicity of the nanocapsules. Moreover, the additional activity of the FcTriOH molecule damaged large healthy regions of brain leading to a potential toxicity, side effects and earlier mortality of the LNC-FcTriOH treated groups compared to the other groups. Similarly, Laine et al. reported toxicity induced survival reduction of rats after CED of FcDiOH-loaded GBM targeted LNCs, compared to the control group (Laine et al., 2012). However, the possible evolution towards lysis or necrotic regions after CED of peptide-functionalized LNCs can be promising if the dose can be optimized either by reducing the LNC concentration, or by reducing the injection volume. Additionally, further study is necessary to understand the relationship of injection volume and LNC concentration with the volume of treatment induced lesion to optimize the dosage.

4.3.2.4 Preparation of AG-LNCs, their efficacy and/or toxicity of the AG formulations in ectopic and orthotopic xenograft model

The LNC-AG were prepared according to step 2.2.1 of publication 3, except 0.2 % w/w AG (Indis NV, Belgium) was added at the first step with the other ingredients. Subsequently, LNC-AG-fluoNFL1 and LNC-AG-fluoNFL3 were produced by adsorbing fluoNFL on LNC-AG surface according to step 2.2.2 of publication 3. AG concentration in the LNCs was determined by the method described in 2.4 of publication 2.

The encapsulation of AG in the LNCs did not alter the size distribution and zeta potential compared to the corresponding unloaded LNCs (results not shown). Drug loading of AG in the LNC was of 0.55 % (w/w) with an encapsulation efficiency of 93.5 ± 3.3 %. Cytotoxicity of the AG-loaded LNCs on U87MG cells was evaluated by MTS assay described in section 2.8 of publication 3. After 72 h of treatment, IC_{50} of the drug solution was observed as 31.8 μ M (Figure 4.6) which was reduced to 15.1 μ M after entrapment in LNC. The control LNC had an IC_{50} of 19.2 μ M (equivalent dose), whereas the AG-loaded surface functionalized LNC (LNC-AG-fluoNFL3) had an IC_{50} of 6.2 μ M. The peptide solution did not affect cell viability at equivalent test concentrations (additional data of publication 3).

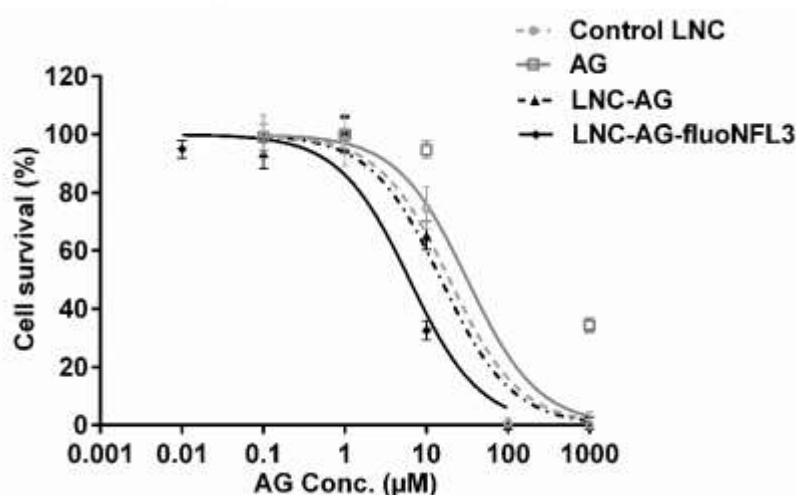


Figure 4.6: Cytotoxicity of control LNC, LNC-AG and LNC-AG-NFL3 and AG solution on U87MG cells after 72 h treatment, measured by MTS assay.

To assess the possible tolerability and efficacy of the AG-loaded LNCs in GBM models in mice, the LNC-AG-fluoNFL3 was administered by i.v. injections in mice (n=5) bearing subcutaneous U87MG tumors and in intracranial U87MG tumor bearing mice by CED (n=5) (according to method described in section 2.9.1 of publication 3 and section 3.2.2.2 respectively). The dose administered in the subcutaneous tumor model was of 4.5 mg AG per kg body weight of animals (70 μL) which was lower than the dose given for FcTriOH-LNCs due to the lower drug loading of AG in LNC. No sign of toxicity were observed in the animals. However, there was no significant reduction in relative tumor volume compared to the saline treated and LNC-fluoNFL3 treated groups. In the intracranial tumor bearing mice, 7.4 μL of the treatment (AG 0.5 mg/kg) was administered by CED. Interestingly, on the MRI on day 13, the average lesion size created by the formulation was smaller ($3.2 \pm 1.2 \text{ mm}^3$) compared to the other NFL-functionalized LNC treatments in publication 3. This can be due to the neuroprotective effects of AG that was observed in mice models and possibly acted by reducing oxidative stress, inflammation and macroglia activation (Patil et al., 2014). Additionally, cytoprotective effect of AG was observed by Stump et al. at low drug concentrations (Stump et al., 2017). Moreover, median survival of the LNC-AG-fluoNFL3 treated group was 47 days compared to 45.5 days for LNC-blank and LNC-blank-NFL3 treated groups. This can be also due to the neuroprotective and neurotrophic effects of AG (Zhao et al., 2013a; Zhao et al., 2013b). Therefore, further

studies with more animals are necessary to fully understand whether the increased survival of the AG-treated mice is a result of balancing neuroprotective activity of AG against the intrinsic toxicity of the nanocapsules, or a significant therapeutic effect.

4.4. Conclusion of chapter 4

In this chapter, we have improved the GBM targeting fluoNFL peptide concentration on LNC surface, leading to significantly enhanced cellular internalization compared to non-functionalized LNC and LNC functionalized with weak fluoNFL concentration. Addition of higher concentrations of NFL (e.g. 4 mM) was hindered as the aqueous dispersion of LNCs became semi-solid after adsorption of 4 mM fluoNFL. Due to this reasons, NFL concentrations above 3 mM were not tested. The formulation technique possibly need to be optimized to further enhance NFL concentration onto LNCs.

The preferential uptake of the functionalized LNC in human GBM cells was observed, compared to healthy human astrocytes. The cellular uptake pathway was also characterized. BBB permeability of the LNCs were assessed although further experiments would be necessary to fully understand the outcomes. Moreover, LNCs (with and without peptide functionalization) encapsulating FcTriOH and AG were developed and characterized. The FcTriOH loaded LNCs induced significant reduction of tumor size after only two i.v. injections in subcutaneous U87MG tumor bearing mice, although the effect was not anymore significant 14 days after the 2nd injection possibly due to elimination of the drug by that time. Another *in vivo* study on the same tumor model will be performed soon with more number of injections in order to validate the efficacy of the formulations.

In the intracranial GBM model, cerebral lesions as a side effect of the treatment was observed after local administration in the brain by CED and the mouse treated with the peptide-functionalized FcTriOH loaded LNC had similar median survival as the saline treated groups. However, the DTI revealed that the GBM-targeted LNCs possibly had a lytic or necrotic region in their lesions with very high ADC values. This could be interesting as treatment-induced high ADC values can be an indicator of therapy response and, in previous studies, only patients with increased ADC showed response. Therefore, optimization of the administered dose is necessary.

Chemotherapy can be administered at an intermittent frequency using a suitable administration route that was optimized and validated according to the type and grade of

cancer in clinical studies. For balancing the treatment efficacy with the toxic side effects, several parameters i.e. maximum tolerable unit dose, minimum effective dose, dosing frequency and duration of the dose should be determined (Strother et al., 2001). Various dose optimization techniques including computerized mathematical modelling can be used (Canal et al., 1998; Chmielecki et al., 2011; Saito et al., 2004). Moreover, histological-toxicological studies can be performed to have understanding of the changes occurring in the tissue microenvironment after treatment.

To our knowledge, these were the first preclinical studies where the activity and/or toxicity of the FcTriOH-loaded formulations were performed. These studies gave valuable insights of clinically relevant treatment strategies which can benefit for optimization.

Acknowledgements

We would like to thank Dr. Julie Laloy, Anne-Sophie Delvigne and Prof. Jean-Michel Dogne (Namur Nanosafety Centre (NNC), Department of Pharmacy, University of Namur) for their support in the *in vitro* BBB permeability study.

4.5. References

- Aderem, A., Underhill, D.M., 1999. Mechanisms of phagocytosis in macrophages. *Annu. Rev. Immunol.* 17, 593-623.
- Allard, E., Huynh, N.T., Vessieres, A., Pigeon, P., Jaouen, G., Benoit, J.P., Passirani, C., 2009a. Dose effect activity of ferrocifen-loaded lipid nanocapsules on a 9L-glioma model. *Int. J. Pharm.* 379, 317-323.
- Allard, E., Jarnet, D., Vessieres, A., Vinchon-Petit, S., Jaouen, G., Benoit, J.P., Passirani, C., 2010. Local delivery of ferrociphenol lipid nanocapsules followed by external radiotherapy as a synergistic treatment against intracranial 9L glioma xenograft. *Pharm. Res.* 27, 56-64.
- Allard, E., Passirani, C., Benoit, J.P., 2009b. Convection-enhanced delivery of nanocarriers for the treatment of brain tumors. *Biomaterials* 30, 2302-2318.
- Allard, E., Passirani, C., Garcion, E., Pigeon, P., Vessieres, A., Jaouen, G., Benoit, J.P., 2008. Lipid nanocapsules loaded with an organometallic tamoxifen derivative as a novel drug-carrier system for experimental malignant gliomas. *J. Control. Release* 130, 146-153.
- Ambruosi, A., Gelperina, S., Khalansky, A., Tanski, S., Theisen, A., Kreuter, J., 2006. Influence of surfactants, polymer and doxorubicin loading on the anti-tumour effect of poly (butyl cyanoacrylate) nanoparticles in a rat glioma model. *J. Microencapsul.* 23, 582-592.
- Avelar-Freitas, B.A., Almeida, V.G., Pinto, M.C.X., Mourão, F.A.G., Massensini, A.R., Martins-Filho, O.A., Rocha-Vieira, E., Brito-Melo, G.E.A., 2014. Trypan blue exclusion assay by flow cytometry. *Braz. J. Med. Biol. Res.* 47, 307-3015.
- Balzeau, J., Pinier, M., Berges, R., Saulnier, P., Benoit, J.P., Eyer, J., 2013. The effect of functionalizing lipid nanocapsules with NFL-TBS.40-63 peptide on their uptake by glioblastoma cells. *Biomaterials* 34, 3381-3389.
- Bareford, L.M., Swaan, P.W., 2007. Endocytic mechanisms for targeted drug delivery. *Advanced drug delivery reviews* 59, 748-758.
- Beduneau, A., Saulnier, P., Benoit, J.P., 2007. Active targeting of brain tumors using nanocarriers. *Biomaterials* 28, 4947-4967.
- Berges, R., Balzeau, J., Peterson, A.C., Eyer, J., 2012a. A tubulin binding peptide targets glioma cells disrupting their microtubules, blocking migration, and inducing apoptosis. *Mol. Ther.* 20, 1367-1377.
- Berges, R., Balzeau, J., Takahashi, M., Prevost, C., Eyer, J., 2012b. Structure-function analysis of the glioma targeting NFL-TBS.40-63 peptide corresponding to the tubulin-binding site on the light neurofilament subunit. *PLoS One* 7, e49436.
- Bernardi, A., Braganhol, E., Jager, E., Figueiro, F., Edelweiss, M.I., Pohlmann, A.R., Guterres, S.S., Battastini, A.M., 2009. Indomethacin-loaded nanocapsules treatment reduces in vivo glioblastoma growth in a rat glioma model. *Cancer Lett.* 281, 53-63.
- Cajot, S., Lautram, N., Passirani, C., Jerome, C., 2011. Design of reversibly core cross-linked micelles sensitive to reductive environment. *J. Control. Release* 152, 30-36.
- Canal, P., Chatelut, E., Guichard, S., 1998. Practical treatment guide for dose individualisation in cancer chemotherapy. *Drugs* 56, 1019-1038.
- Carradori, D., Saulnier, P., Preat, V., des Rieux, A., Eyer, J., 2016. NFL-lipid nanocapsules for brain neural stem cell targeting in vitro and in vivo. *J. Control. Release* 238, 253-262.

- Chmielecki, J., Foo, J., Oxnard, G.R., Hutchinson, K., Ohashi, K., Somwar, R., Wang, L., Amato, K.R., Arcila, M., Sos, M.L., Socci, N.D., Viale, A., de Stanchina, E., Ginsberg, M.S., Thomas, R.K., Kris, M.G., Inoue, A., Ladanyi, M., Miller, V.A., Michor, F., Pao, W., 2011. Optimization of dosing for EGFR-mutant non-small cell lung cancer with evolutionary cancer modeling. *Sci. Transl. Med.* 3, 90ra59.
- Chou, T.-C., 2010. Drug combination studies and their synergy quantification using the Chou-Talalay method. *Cancer Res.* 70, 440-446.
- Chou, T.C., 2006. Theoretical basis, experimental design, and computerized simulation of synergism and antagonism in drug combination studies. *Pharmacol. Rev.* 58, 621-681.
- Conner, S.D., Schmid, S.L., 2003. Regulated portals of entry into the cell. *Nature* 422, 37-44.
- Danhier, F., Messaoudi, K., Lemaire, L., Benoit, J.P., Lagarce, F., 2015. Combined anti-Galectin-1 and anti-EGFR siRNA-loaded chitosan-lipid nanocapsules decrease temozolomide resistance in glioblastoma: in vivo evaluation. *Int. J. Pharm.* 481, 154-161.
- Dhanikula, R.S., Argaw, A., Bouchard, J.F., Hildgen, P., 2008. Methotrexate loaded polyether-copolyester dendrimers for the treatment of gliomas: enhanced efficacy and intratumoral transport capability. *Mol. Pharm.* 5, 105-116.
- Fu, J.Y., Zhang, W., Blatchford, D.R., Tetley, L., McConnell, G., Dufes, C., 2011. Novel tocotrienol-entrapping vesicles can eradicate solid tumors after intravenous administration. *J. Control. Release* 154, 20-26.
- Fu, Y., An, N., Li, K., Zheng, Y., Liang, A., 2012. Chlorotoxin-conjugated nanoparticles as potential glioma-targeted drugs. *J. Neurooncol.* 107, 457-462.
- Galati, G., Sabzevari, O., Wilson, J.X., O'Brien, P.J., 2002. Prooxidant activity and cellular effects of the phenoxyl radicals of dietary flavonoids and other polyphenolics. *Toxicology* 177, 91-104.
- Guo, L., Fan, L., Pang, Z., Ren, J., Ren, Y., Li, J., Chen, J., Wen, Z., Jiang, X., 2011. TRAIL and doxorubicin combination enhances anti-glioblastoma effect based on passive tumor targeting of liposomes. *J. Control. Release* 154, 93-102.
- Gupta, B., Levchenko, T.S., Torchilin, V.P., 2007. TAT peptide-modified liposomes provide enhanced gene delivery to intracranial human brain tumor xenografts in nude mice. *Oncol. Res.* 16, 351-359.
- Haar, C.P., Hebbar, P., Wallace, G.C.t., Das, A., Vandergrift, W.A., 3rd, Smith, J.A., Giglio, P., Patel, S.J., Ray, S.K., Banik, N.L., 2012. Drug resistance in glioblastoma: a mini review. *Neurochem. Res.* 37, 1192-1200.
- Hamstra, D.A., Chenevert, T.L., Moffat, B.A., Johnson, T.D., Meyer, C.R., Mukherji, S.K., Quint, D.J., Gebarski, S.S., Fan, X., Tsien, C.I., Lawrence, T.S., Junck, L., Rehemtulla, A., Ross, B.D., 2005. Evaluation of the functional diffusion map as an early biomarker of time-to-progression and overall survival in high-grade glioma. *Proc. Natl. Acad. Sci. U. S. A.* 102, 16759-16764.
- Harashima, H., Huong, T.M., Ishida, T., Manabe, Y., Matsuo, H., Kiwada, H., 1996. Synergistic effect between size and cholesterol content in the enhanced hepatic uptake clearance of liposomes through complement activation in rats. *Pharm. Res.* 13, 1704-1709.
- Harashima, H., Sakata, K., Funato, K., Kiwada, H., 1994. Enhanced hepatic uptake of liposomes through complement activation depending on the size of liposomes. *Pharm. Res.* 11, 402-406.

- Heurtault, B., Saulnier, P., Pech, B., Proust, J.E., Benoit, J.P., 2002. A novel phase inversion-based process for the preparation of lipid nanocarriers. *Pharm. Res.* 19, 875-880.
- Huynh, N.T., Passirani, C., Allard-Vannier, E., Lemaire, L., Roux, J., Garcion, E., Vessieres, A., Benoit, J.P., 2012. Administration-dependent efficacy of ferrociphenol lipid nanocapsules for the treatment of intracranial 9L rat gliosarcoma. *Int. J. Pharm.* 423, 55-62.
- Huynh, N.T., Passirani, C., Saulnier, P., Benoit, J.P., 2009. Lipid nanocapsules: a new platform for nanomedicine. *Int. J. Pharm.* 379, 201-209.
- Ivanov, A.I., 2008. Pharmacological inhibition of endocytic pathways: is it specific enough to be useful? *Methods Mol. Biol.* 440, 15-33.
- Karim, R., Palazzo, C., Laloy, J., Delvigne, A.S., Vanslambrouck, S., Jerome, C., Lepeltier, E., Orange, F., Dogne, J.M., Evrard, B., Passirani, C., Piel, G., 2017a. Development and Evaluation of Injectable Nanosized Drug Delivery Systems for Apigenin. *Int. J. Pharm.*
- Karim, R., Somani, S., Al Robaian, M., Mullin, M., Amor, R., McConnell, G., Dufes, C., 2017b. Tumor regression after intravenous administration of targeted vesicles entrapping the vitamin E α -tocotrienol. *J. Control. Release* 246, 79-87.
- Kou, L., Sun, J., Zhai, Y., He, Z., 2013. The endocytosis and intracellular fate of nanomedicines: Implication for rational design. *Asian Journal of Pharmaceutical Sciences* 8, 1-10.
- Laine, A.-L., Clavreul, A., Rousseau, A., Tétaud, C., Vessieres, A., Garcion, E., Jaouen, G., Aubert, L., Guilbert, M., Benoit, J.-P., 2014. Inhibition of ectopic glioma tumor growth by a potent ferrocenyl drug loaded into stealth lipid nanocapsules. *Nanomedicine* 10, 1667-1677.
- Laine, A.L., Huynh, N.T., Clavreul, A., Balzeau, J., Bejaud, J., Vessieres, A., Benoit, J.P., Eyer, J., Passirani, C., 2012. Brain tumour targeting strategies via coated ferrociphenol lipid nanocapsules. *Eur. J. Pharm. Biopharm.* 81, 690-693.
- Larsen, T.H., Branco, M.C., Rajagopal, K., Schneider, J.P., Furst, E.M., 2009. Sequence-dependent gelation kinetics of β -hairpin peptide hydrogels. *Macromolecules* 42, 8443-8450.
- Lepinoux-Chambaud, C., Barreau, K., Eyer, J., 2016. The Neurofilament-Derived Peptide NFL-TBS.40-63 Targets Neural Stem Cells and Affects Their Properties. *Stem cells translational medicine* 5, 901-913.
- Lepinoux-Chambaud, C., Eyer, J., 2013. The NFL-TBS.40-63 anti-glioblastoma peptide enters selectively in glioma cells by endocytosis. *Int. J. Pharm.* 454, 738-747.
- Liu, G., Shen, H., Mao, J., Zhang, L., Jiang, Z., Sun, T., Lan, Q., Zhang, Z., 2013. Transferrin modified graphene oxide for glioma-targeted drug delivery: in vitro and in vivo evaluations. *ACS Appl Mater Interfaces* 5, 6909-6914.
- Liu, Y., Lu, W., 2012. Recent advances in brain tumor-targeted nano-drug delivery systems. *Expert opinion on drug delivery* 9, 671-686.
- Louis, D.N., Perry, A., Reifenberger, G., von Deimling, A., Figarella-Branger, D., Cavenee, W.K., Ohgaki, H., Wiestler, O.D., Kleihues, P., Ellison, D.W., 2016. The 2016 World Health Organization Classification of Tumors of the Central Nervous System: a summary. *Acta Neuropathol.* 131, 803-820.
- Mardor, Y., Pfeffer, R., Spiegelmann, R., Roth, Y., Maier, S.E., Nissim, O., Berger, R., Glicksman, A., Baram, J., Orenstein, A., Cohen, J.S., Tichler, T., 2003. Early detection of

- response to radiation therapy in patients with brain malignancies using conventional and high b-value diffusion-weighted magnetic resonance imaging. *J. Clin. Oncol.* 21, 1094-1100.
- Markoutsas, E., Pampalakis, G., Niarakis, A., Romero, I.A., Weksler, B., Couraud, P.O., Antimisiaris, S.G., 2011. Uptake and permeability studies of BBB-targeting immunoliposomes using the hCMEC/D3 cell line. *Eur. J. Pharm. Biopharm.* 77, 265-274.
- Mercer, J., Helenius, A., 2009. Virus entry by macropinocytosis. *Nat. Cell Biol.* 11, 510-520.
- Millipore, 2016. Monolayer integrity measurements and drug transport guidelines. Millipore.
- Netsky, M.G., August, B., Fowler, W., 1950. The longevity of patients with glioblastoma multiforme. *J. Neurosurg.* 7, 261-269.
- Paillard, A., Hindre, F., Vignes-Colombeix, C., Benoit, J.P., Garcion, E., 2010. The importance of endo-lysosomal escape with lipid nanocapsules for drug subcellular bioavailability. *Biomaterials* 31, 7542-7554.
- Pang, Z., Feng, L., Hua, R., Chen, J., Gao, H., Pan, S., Jiang, X., Zhang, P., 2010. Lactoferrin-conjugated biodegradable polymersome holding doxorubicin and tetrandrine for chemotherapy of glioma rats. *Mol. Pharm.* 7, 1995-2005.
- Pardridge, W.M., 2012. Drug transport across the blood-brain barrier. *J. Cereb. Blood Flow Metab.* 32, 1959-1972.
- Patil, S.P., Jain, P.D., Sancheti, J.S., Ghumatkar, P.J., Tambe, R., Sathaye, S., 2014. Neuroprotective and neurotrophic effects of Apigenin and Luteolin in MPTP induced parkinsonism in mice. *Neuropharmacology* 86, 192-202.
- Patino, T., Soriano, J., Barrios, L., Ibanez, E., Nogues, C., 2015. Surface modification of microparticles causes differential uptake responses in normal and tumoral human breast epithelial cells. *Sci. Rep.* 5, 11371.
- Patterson, D.M., Padhani, A.R., Collins, D.J., 2008. Technology insight: water diffusion MRI-a potential new biomarker of response to cancer therapy. *Nat. Clin. Pract. Oncol.* 5, 220-233.
- Peer, D., Karp, J.M., Hong, S., Farokhzad, O.C., Margalit, R., Langer, R., 2007. Nanocarriers as an emerging platform for cancer therapy. *Nat. Nanotechnol.* 2, 751-760.
- Poller, B., Gutmann, H., Krahenbuhl, S., Weksler, B., Romero, I., Couraud, P.O., Tuffin, G., Drewe, J., Huwyler, J., 2008. The human brain endothelial cell line hCMEC/D3 as a human blood-brain barrier model for drug transport studies. *J. Neurochem.* 107, 1358-1368.
- Prochazkova, D., Bousova, I., Wilhelmova, N., 2011. Antioxidant and prooxidant properties of flavonoids. *Fitoterapia* 82, 513-523.
- Roger, M., Clavreul, A., Huynh, N.T., Passirani, C., Schiller, P., Vessieres, A., Montero-Menei, C., Menei, P., 2012. Ferrociphenol lipid nanocapsule delivery by mesenchymal stromal cells in brain tumor therapy. *Int. J. Pharm.* 423, 63-68.
- Romanova, D., Vachalkova, A., Cipak, L., Ovesna, Z., Rauko, P., 2001. Study of antioxidant effect of apigenin, luteolin and quercetin by DNA protective method. *Neoplasma* 48, 104-107.
- Sahay, G., Alakhova, D.Y., Kabanov, A.V., 2010. Endocytosis of nanomedicines. *J. Control. Release* 145, 182-195.

- Saito, R., Bringas, J.R., McKnight, T.R., Wendland, M.F., Mamot, C., Drummond, D.C., Kirpotin, D.B., Park, J.W., Berger, M.S., Bankiewicz, K.S., 2004. Distribution of liposomes into brain and rat brain tumor models by convection-enhanced delivery monitored with magnetic resonance imaging. *Cancer Res.* 64, 2572-2579.
- Straubinger, R.M., Sharma, A., Murray, M., Mayhew, E., 1993. Novel Taxol formulations: Taxol-containing liposomes. *J. Natl. Cancer Inst.*, 69-78.
- Strother, D., Ashley, D., Kellie, S.J., Patel, A., Jones-Wallace, D., Thompson, S., Heideman, R., Benaim, E., Krance, R., Bowman, L., Gajjar, A., 2001. Feasibility of four consecutive high-dose chemotherapy cycles with stem-cell rescue for patients with newly diagnosed medulloblastoma or supratentorial primitive neuroectodermal tumor after craniospinal radiotherapy: results of a collaborative study. *J. Clin. Oncol.* 19, 2696-2704.
- Stump, T.A., Santee, B.N., Williams, L.P., Kunze, R.A., Heinze, C.E., Huseman, E.D., Gryka, R.J., Simpson, D.S., Amos, S., 2017. The antiproliferative and apoptotic effects of apigenin on glioblastoma cells. *J. Pharm. Pharmacol.*
- Stupp, R., Hegi, M.E., Mason, W.P., van den Bent, M.J., Taphoorn, M.J., Janzer, R.C., Ludwin, S.K., Allgeier, A., Fisher, B., Belanger, K., Hau, P., Brandes, A.A., Gijtenbeek, J., Marosi, C., Vecht, C.J., Mokhtari, K., Wesseling, P., Villa, S., Eisenhauer, E., Gorlia, T., Weller, M., Lacombe, D., Cairncross, J.G., Mirimanoff, R.O., European Organisation for, R., Treatment of Cancer Brain, T., Radiation Oncology, G., National Cancer Institute of Canada Clinical Trials, G., 2009. Effects of radiotherapy with concomitant and adjuvant temozolomide versus radiotherapy alone on survival in glioblastoma in a randomised phase III study: 5-year analysis of the EORTC-NCIC trial. *Lancet Oncol.* 10, 459-466.
- Thomas, A.A., Brennan, C.W., DeAngelis, L.M., Omuro, A.M., 2014. Emerging therapies for glioblastoma. *JAMA neurology* 71, 1437-1444.
- Thomas, O., Lagarce, F., 2013. Lipid Nanocapsules: A Nanocarrier Suitable for Scale-Up Process. *Journal of Drug Delivery Science and Technology* 23, 555-559.
- Thorne, R.G., Nicholson, C., 2006. In vivo diffusion analysis with quantum dots and dextrans predicts the width of brain extracellular space. *Proc. Natl. Acad. Sci. U. S. A.* 103, 5567-5572.
- Torchilin, V.P., 2005. Recent advances with liposomes as pharmaceutical carriers. *Nature reviews. Drug discovery* 4, 145-160.
- Torchilin, V.P., Rammohan, R., Weissig, V., Levchenko, T.S., 2001. TAT peptide on the surface of liposomes affords their efficient intracellular delivery even at low temperature and in the presence of metabolic inhibitors. *P. Natl. Acad. Sci. USA* 98, 8786-8791.
- Vonarbourg, A., Passirani, C., Saulnier, P., Benoit, J.P., 2006a. Parameters influencing the stealthiness of colloidal drug delivery systems. *Biomaterials* 27, 4356-4373.
- Vonarbourg, A., Passirani, C., Saulnier, P., Simard, P., Leroux, J.C., Benoit, J.P., 2006b. Evaluation of pegylated lipid nanocapsules versus complement system activation and macrophage uptake. *J. Biomed. Mater. Res.* 78, 620-628.
- Wei, X., Gao, J., Zhan, C., Xie, C., Chai, Z., Ran, D., Ying, M., Zheng, P., Lu, W., 2015. Liposome-based glioma targeted drug delivery enabled by stable peptide ligands. *J. Control. Release* 218, 13-21.
- Weksler, B.B., Subileau, E.A., Perriere, N., Charneau, P., Holloway, K., Leveque, M., Tricoire-Leignel, H., Nicotra, A., Bourdoulous, S., Turowski, P., Male, D.K., Roux, F., Greenwood, J., Romero, I.A., Couraud, P.O., 2005. Blood-brain barrier-specific properties of a human adult brain endothelial cell line. *FASEB J.* 19, 1872-1874.

- Wohlfart, S., Khalansky, A.S., Gelperina, S., Maksimenko, O., Bernreuther, C., Glatzel, M., Kreuter, J., 2011. Efficient chemotherapy of rat glioblastoma using doxorubicin-loaded PLGA nanoparticles with different stabilizers. *PLoS One* 6, e19121.
- Xu, Y., Xin, Y., Diao, Y., Lu, C., Fu, J., Luo, L., Yin, Z., 2011. Synergistic effects of apigenin and paclitaxel on apoptosis of cancer cells. *PLoS One* 6, e29169.
- Yang, Y., Yan, Z., Wei, D., Zhong, J., Liu, L., Zhang, L., Wang, F., Wei, X., Xie, C., Lu, W., He, D., 2013. Tumor-penetrating peptide functionalization enhances the anti-glioblastoma effect of doxorubicin liposomes. *Nanotechnology* 24, 405101.
- Yu, X., Zheng, J., 2011. Polymorphic structures of Alzheimer's beta-amyloid globulomers. *PLoS One* 6, e20575.
- Yue, P.J., He, L., Qiu, S.W., Li, Y., Liao, Y.J., Li, X.P., Xie, D., Peng, Y., 2014. OX26/CTX-conjugated PEGylated liposome as a dual-targeting gene delivery system for brain glioma. *Mol. Cancer* 13, 191.
- Zanotto-Filho, A., Coradini, K., Braganhol, E., Schroder, R., de Oliveira, C.M., Simoes-Pires, A., Battastini, A.M., Pohlmann, A.R., Guterres, S.S., Forcelini, C.M., Beck, R.C., Moreira, J.C., 2013. Curcumin-loaded lipid-core nanocapsules as a strategy to improve pharmacological efficacy of curcumin in glioma treatment. *Eur. J. Pharm. Biopharm.* 83, 156-167.
- Zhan, C., Gu, B., Xie, C., Li, J., Liu, Y., Lu, W., 2010. Cyclic RGD conjugated poly(ethylene glycol)-co-poly(lactic acid) micelle enhances paclitaxel anti-glioblastoma effect. *J. Control. Release* 143, 136-142.
- Zhao, L., Wang, J.L., Liu, R., Li, X.X., Li, J.F., Zhang, L., 2013a. Neuroprotective, anti-amyloidogenic and neurotrophic effects of apigenin in an Alzheimer's disease mouse model. *Molecules* 18, 9949-9965.
- Zhao, L., Wang, J.L., Wang, Y.R., Fa, X.Z., 2013b. Apigenin attenuates copper-mediated beta-amyloid neurotoxicity through antioxidation, mitochondrion protection and MAPK signal inactivation in an AD cell model. *Brain Res.* 1492, 33-45.
- Zhou, M., Smith, A.M., Das, A.K., Hodson, N.W., Collins, R.F., Ulijn, R.V., Gough, J.E., 2009. Self-assembled peptide-based hydrogels as scaffolds for anchorage-dependent cells. *Biomaterials* 30, 2523-2530.

***Chapter 5: General discussion, conclusion and
perspectives***

5. GENERAL DISCUSSION, CONCLUSION AND PERSPECTIVES

5.1. General discussion

The word ‘glioma’ was primarily mentioned in the 1864 as a distinct type of brain tumor separate from other tumors of the CNS (DeAngelis and Mellinghoff, 2011). One of the first reported surgical removal of glioma occurred in 1884 (Bennett, 1885) although no modern diagnostic imaging techniques were available at that moment. The X-ray was discovered in 1885, whereas stereotaxic device and surgical microscope were available about 65 year later (Bianco et al., 2017; Spiegel et al., 1947). However, it was established by 1960 that surgical removal of the tumor resulted better prognosis in GBM patients compared to untreated groups (Roth and Elvidge, 1960). The currently used diagnostic techniques i.e. CT scan and MRI were available around 1970s (Ambrose, 1973; Lauterbur, 1989) which allowed surgeons to have detailed information on the location and size of the tumor and make decisions on the extent of surgical resection. RT for brain tumors started around 1940s and became a standardized post-surgery treatment for GBM around 1970s (Gzell et al., 2017). To improve patient survival, numerous chemotherapies were investigated as concomitant of RT. The present standard concomitant and adjuvant chemotherapy TMZ was introduced around 2002 and improved median survival by 2.5 months which was 12.1 months for RT alone (Stupp et al., 2005). Substantial progress has been made in the understanding of GBM pathology and molecular biology in the last few decades. The recently published ‘2016 WHO Classification of Tumors of the Central Nervous System’ included for the first time a molecular genetic feature (IDH gene mutation) to classify and divide GBM into three sub-categories i.e. IDH-wildtype GBM, IDH-mutant GBM and GBM not otherwise specified (GBM NOS) (Louis et al., 2016). Despite the advances achieved, GBM still remains as a fatal disease, therefore numerous studies are ongoing to evaluate the potential of new drug molecules for its treatment.

Various naturally occurring flavonoids have been reported to show promising *in vitro* activity against GBM cells i.e. antiproliferative activity, apoptosis induction, reduction in cell metabolism and decreased cell migration (Santos et al., 2015). AG is one of these promising flavonoids which showed significant *in vitro* antiproliferative and apoptotic effects against GBM cells from human and animal sources (Chen et al., 2016; Feng et al., 2012; Parajuli et al., 2009; Santos et al., 2015; Stump et al., 2017). Das et al. reported that

treatment with AG induced apoptosis in two human GBM cell lines, but not on human healthy astrocytes (Das et al., 2010). While reported several times as a promising molecule for GBM treatment, only one *in vivo* study evaluating efficacy of AG against GBM is available (Engelmann et al., 2002). The intrinsic very low aqueous solubility and unavailability of biocompatible solvents of AG makes it challenging to administrate in preclinical studies. The studies reporting injectable AG formulations are also rare (Das et al., 2013; Ding et al., 2013).

Several platinum coordination complexes i.e. cisplatin, oxaliplatin and carboplatin have already reached the market as proven chemotherapeutics for various cancers and showed the potential of organometallic drugs. Many other metal-based (e.g. ruthenium, gold, and titanium) complexes have been extensively evaluated as potential anticancer agents in the last decades (Muhammad and Guo, 2014). An interesting group of organometallic compounds are the iron-based ferrocenes which inspired chemists to develop anticancer molecules since the 1970s (Fiorina et al., 1978). Ever since, numerous ferrocene-compounds, e.g. ferrocenyl-paclitaxels, ferrocenyl-docetaxels and ferrocene-embedded flavonoids (Peres et al., 2017; Wieczorek et al., 2016), have been reported for their potential anticancer properties. The most studied ferrocene complexes are the ferrocifen family, which are ferrocenyl-tamoxifens and their derivatives (Nguyen et al., 2007). Several ferrocifen molecules showed promising *in vitro* activity against GBM cells, while being significantly less toxic to astrocytes (Allard et al., 2008). However, nanoencapsulation of these molecules is required before moving to the preclinical studies due to their intrinsic low aqueous solubility (Allard et al., 2009a; Allard et al., 2008; Huynh et al., 2012). A new ferrocifen-derivative, the FcTriOH that has never been tested before on human GBM cells, was tested in this work as a potential candidate.

AG and FcTriOH, are both low molecular-weight molecules, which could be promising for treatment of GBM, but having both a problem to face in order to advance to preclinical studies: their low aqueous solubility. That is why the work done in this thesis, was focused on solving this issue and presented three key tasks:

1. To develop several nanocarriers as potential i.v. delivery systems for the low molecular-weight hydrophobic drugs, and compare their characteristics to identify the most promising nanovector.

2. To optimize the most promising nanocarrier to improve its targeting towards GBM cells, along with the *in vitro* evaluation of the drug-loaded nanocarriers.
3. To perform preliminary *in vivo* studies on two murine GBM models (ectopic and orthotopic) to assess their possible antitumor activity and/or toxic effects when the formulations were administered using two different routes (i.v. and intracranial).

Task 1: Identifying the most suitable nanocarrier

There are several types of nanocarriers available, and many of each category are described in literature for their promising properties as delivery system for brain diseases (Liu and Lu, 2012). Nanovectors can cross the BBB by two major ways. Firstly, nanocolloids with optimum size and hydrophilic surface-coating can cross the integrity-impaired BBTB (at advanced tumor stage) by EPR effect and accumulate in cerebral tumor tissue (Bernardi et al., 2009; Brigger et al., 2002; Guo et al., 2011b). Secondly, nanocarrier surfaces can be functionalized with various targeting ligands that binds to various receptors or transporters on the BBB to enhance the permeability of the nanovector and cerebral accumulation of the drug (Miura et al., 2013; Ying et al., 2010; Yue et al., 2014).

Among different nanocarriers, liposomes are one of the most frequently studied and almost all (except Abraxane, an albumin nanoparticle bound paclitaxel) clinically approved NDDSs for various cancer treatments are liposomes (Anselmo and Mitragotri, 2016). To begin our formulation, we chose to start with a cationic and pH-sensitive liposome which was reported to have promising cellular uptake, and released their cargo in the cytosol within 24 h in rat and human GBM cells (Bellavance et al., 2010). The authors designed several liposomes by modification from a clinically approved liposome, called Daunoxome. However, the liposome with the most efficient *in vitro* cellular uptake and cytosolic delivery (due to its cationic property by DC-Chol and pH-sensitivity by DOPE) was non-PEGylated. Therefore its *in vivo* utilization would be challenging due to non-specific interactions, opsonization and rapid removal by RES (Bellavance et al., 2010; Wasungu and Hoekstra, 2006). In comparison, the PEG-modified liposome has better possibility to reach the target site and it showed comparable cellular uptake with the non-PEGylated formulation up to 4 h in the U-118 human GBM cell (Bellavance et al., 2010). Therefore, we added DSPE-mPEG₂₀₀₀ in the formulation to compose the CL (DPPC, DC-Chol, DOPE, DSPE-mPEG₂₀₀₀) (Table 5.1). Subsequently, we replaced DC-Chol with

equimolar cholesterol to prepare the AL, and added AG as AG-HP in order to compare their characteristics (Figure 5.1).

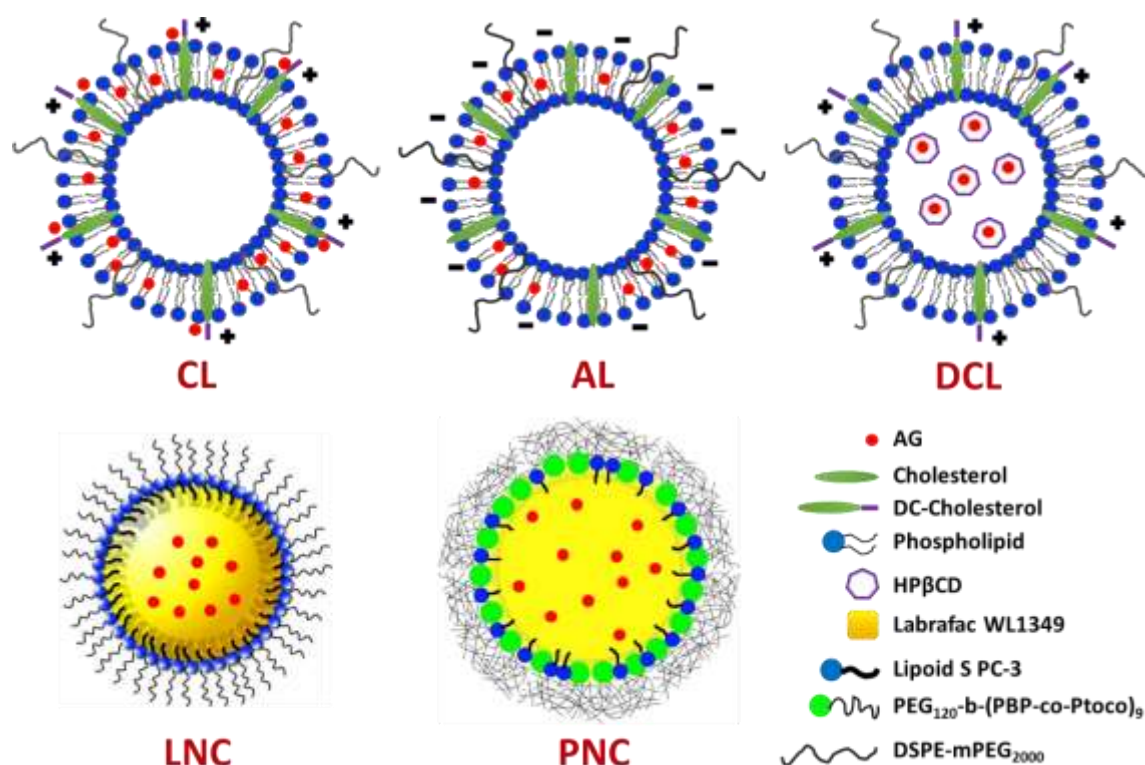


Figure 5.1: Theoretical structures of the AG-loaded CL, AL, DCL, LNC and PNC

Table 5.1: Compositions of the AG-loaded CL, AL, LNC and PNC

Ingredients and their respective percentages in the NDDSs (% w/w)										
CL*		AL*		DCL and DCL2*			LNC**		PNC**	
DPPC	39.1	DPPC	41.7	DPPC	16.8	10.6	Kolliphor	41.1	Polymer	20.1
DC-Chol	22.0	Chol	16.9	DC-Chol	9.4	6.0	Lipoid	3.6	Lipoid	10.8
DOPE	30.5	DOPE	32.5	DOPE	13.1	8.3	Labrafac	49.9	Labrafac	67.9
PEG	6.5	PEG	6.9	PEG	2.8	1.8	PEG	4.8	AG	1.2
AG	1.8	AG	1.9	AG-CD	58.0	72.4	AG	0.6		

PEG: DSPE-mPEG₂₀₀₀, Polymer: PEG₁₂₀-b-(PBP-co-Ptoco)₉, Labrafac: Labrafac Lipophile WL1349, Lipoid: Lipoid S PC-3, AG-CD: AG-HPβCD complex (w/w ratio 1:71.5)

* Molar ratio of the DPPC, DOPE, DC-Chol/Chol, PEG and AG in CL, AL, DCL and DCL2 were same, but varies in w/w % due to weight difference between DC-Chol and Chol, or presence of additional HPβCD (in DCLs).

** Molecular weight of Labrafac WL1349 is not mentioned by manufacturer. Therefore molar ratio calculation was not possible for LNC and PNC.

Additionally, LNCs were already reported for encapsulation of various hydrophobic drug molecules (Lamprecht and Benoit, 2006; Lamprecht et al., 2002) including several ferrocifens (Allard et al., 2009a; Allard et al., 2008; Clavreul et al., 2015) with more than 90 % of encapsulation efficiency. They were known for their capacity of inhibiting P-gp (Lamprecht and Benoit, 2006), endo-lysosomal escape (Paillard et al., 2010), and were able to reduce tumor progression in multi-drug resistant GBM in rats (Garcion et al., 2006). Therefore, LNC were promising as injectable nanocarriers for hydrophobic drugs and were selected for encapsulating AG and FcTriOH.

Moreover, a newly synthesized tocopherol modified PEG-b-polyphosphate copolymer (PEG₁₂₀-b-(PBP-co-Ptoco)₉), synthesized in the 'Center For Education and Research for Macromolecules' (CERM) as a promising amphiphilic copolymer with low toxicity (Vanslambrouck, 2015), was provided to us in order to evaluate its potential to be formulated in a nanocarrier. Due to its non-ionic surface properties, it seemed a good candidate to act as a LNC shell component (like Kolliphor HS15) and we prepared the PNC (Composition in table 5.1).

For development, characterization and comparison of the nanocarriers, we used AG as a model molecule among the two molecules of interest as it is easier to handle due to its nontoxic nature. FcTriOH require special precautions during handling, formulation and characterization.

To be administered by i.v. route, nanocarriers generally need to keep their size between 20-200 nm, as too small nanovectors can be cleared by glomerular filtration and too large NDDSs will be cleared by the MPS systems (Lian and Ho, 2001). Moreover, PEGylated nanocarriers with a similar size range have the possibility to preferentially gather in brain tumors by enhanced extravasation through the compromised BBTB (Siegal et al., 1995). Some common alterations that occur in the BBB near the GBM tumors are: enhanced vascular wall thickness, TJ opening (more significant as the tumor grows), absence of occludin, or presence of non-functional occludin, increased fenestrations and enhanced pinocytic vacuoles (Garcia-Garcia et al., 2005).

Table 5.2: Summary of the characteristics of the AG-loaded CL, AL, DCL, DCL2, LNC and PNC (/: parameter not determined)

Characteristics	CL	AL	DCL	DCL2	LNC	PNC
Mean diameter (nm)*	144 ± 1	142 ± 6	136 ± 3	134 ± 3	59 ± 2	145 ± 7
PDI	0.04 ± 0.01	0.12 ± 0.02	0.05 ± 0.01	0.04 ± 0.03	0.11 ± 0.03	0.11 ± 0.02
Zeta potential (mV)	43.2 ± 1.2	-27.4 ± 2.3	30.2 ± 1.0	32.2 ± 3.1	-24.9 ± 6.0	-16.2 ± 4.4
EE (%)	71 ± 2	34 ± 1	21.2 ± 6.1	15.1 ± 3.6	82 ± 5	84 ± 4
Mass yield (%)	80 ± 3	86 ± 5	77.4 ± 6.7	73.8 ± 2.3	72 ± 2	81 ± 4
Drug loading capacity (% w/w)	1.65 ± 0.02	0.65 ± 0.03	0.51 ± 0.16	0.75 ± 0.16	0.62 ± 0.05	1.43 ± 0.06
Storage stability (as dispersions)	3 days	Min. 14 days	/	/	Min. 14 days	Min. 14 days
Stability in serum	Min. 6 h	Min. 6 h	/	/	Min. 6 h	Min. 24 h
Complement consumption (CH50%)	Low	Low	/	/	Very low	Moderate
Drug release	Immediate	Immediate	/	/	Sustained	Sustained

The **size** (measured by DLS) of the CL, AL, LNC and PNC we developed were of 144 ± 1, 142 ± 6, 59 ± 2 and 145 ± 7 nm respectively. Additionally, we have used NTA technique to confirm their size and the results obtained were in accordance. Calvo et al. reported that 137 ± 21 nm PEG-PHDCA nanoparticles penetrated into the brain in significantly higher amount after tail vein injection in healthy mice and rats, compared to PS80 coated PHDCA particles (159 ± 25 nm), P908 coated PHDCA particles (147 ± 30 nm) and uncoated PHDCA particles (164 ± 57 nm) (Calvo et al., 2001). Moreover, PEG-PHDCA nanoparticles (146-161 nm) accumulated 3.1-folds and 4-8 folds more in 9L gliosarcoma tumors and healthy brain regions respectively in Fischer rats compared to PHDCA nanospheres (135-161 nm), with a tumor-to-brain ratio of 11 (Brigger et al., 2002). Additionally, tail vein injection of PEGylated liposomes (98-116 nm) entrapping DOX and TNF-related apoptosis inducing ligand (TRAIL) combination resulted better antitumor efficacy and improved survival by 9-16 days of intracranial U87MG tumor bearing mice, compared to other treatment groups (Guo et al., 2011b). Furthermore, Bernardi et al. reported significantly reduced tumor size and enhanced survival time of C6 glioma bearing rats after intraperitoneal administration of indomethacin-loaded polycaprolactone-

capric/caprylic triglyceride based nanocapsules with a size about 240 nm, compared to other control groups (Bernardi et al., 2009). The concentration of the nanocapsules was about 6-folds higher in glioma bearing rats compared to healthy and sham-operated rats indicating the presence of integrity-compromised BBB and possible EPR effect that enhances the nanocapsule brain-penetration (Bernardi et al., 2009). Therefore, the size of all our NDDSs (CL, AL, LNC and PNC) was within acceptable limits for parenterally injectable nanocarriers for the brain drug delivery.

Surface charge is another important parameter that impacts on the *in vivo* fate of the nanovectors, as it can influence the interaction with serum proteins and subsequently the clearance by RES (Caracciolo, 2015). All the NDDSs developed were negatively charged (AL -27.4 mV, LNC -24.9 mV and PNC -16.2 mV) except CL (+43 mV). Positive surface charge can benefit from higher cellular uptake, but can cause more toxicity as well as an increased MPS recognition (Nel et al., 2009). Therefore, the CL had more possibility to adsorb large amount of serum proteins and form a corona as the post-insertion of the PEG chains during its formulation reduced the zeta potential only by 4 mV (+47 mV before PEGylation). The negatively charged NDDSs should theoretically have less unspecific interactions, but may also have less cellular internalization compared to the CL. The potential stealth characteristics of the nanocarriers was evaluated by their stability in serum and their complement consumption properties, which are discussed later.

Drug loading of the NDDSs is another important factor that can influence the efficacy and the toxicity of nanovectors. NDDSs with high drug loading will require less amount (weight) of particles to deliver an equal amount of drug compared to low drug-loading particles, therefore they may have a better efficacy and a lower toxicity (although toxicity will also depend on composition). Interestingly, CL resulted in 2.5-folds higher drug loading capacity compared to AL. As the only difference between CL and AL was the absence of the DC-chain (which imparts positive charge) on the later, we hypothesized that AG had charge interaction with CL and resulted in the higher drug-loading. AG is a hydrophobic molecule and has a very low aqueous solubility (1.35 µg/mL) (Li et al., 1997). However, the two pKa values (6.6 and 9.3 (Favaro et al., 2007)) of AG allows it to be partially deprotonated at physiological pH with a possible equilibrium between the ionized and non-ionized forms (Favaro et al., 2007; Papay et al., 2016; Tungjai et al., 2008). Therefore, AG was probably entrapped within the phospholipid bilayer of AL,

whereas AG⁻ was probably both entrapped in the lipid bilayer and adsorbed onto CL surface by electrostatic, hydrogen and/or hydrophobic forces. Similar bond formation was described by Yuan et al. while characterizing the interaction between AG and HSA in their complex by spectroscopy and molecular modeling (Yuan et al., 2007). Additionally, Papay et al. described an electrostatic repulsion between AG and sulfobutylether- β -CD, an anionic CD derivative (Papay et al., 2016).

Among the nanocapsule formulations (LNC and PNC), an increased percentage of core-oil lead to an increased AG-loading. The LNC had a drug loading of 0.62 % w/w and 49.9 % core oil, whereas the PNC had drug loading of 1.43 % w/w with 67.9 % core-oil. Additionally, the higher drug loading in PNC can be due to its lower lipid-drug ratio compared to LNC (65.6 and 83.2 respectively), which was possibly achieved due to the use of organic solvents to pre-solubilize AG for PNC preparation.

The **EE** of the NDDSs possibly varied depending upon several factors i.e. lipid-drug ratio, surface charge, and drug pre-solubilization (in organic solvents). The EE of CL, AL, LNC and PNC were 71, 34, 82 and 84% respectively. Compared to the liposomes, the nanocapsules had higher lipid-drug ratio resulting higher EE. However, although the lipid-drug ratio of LNC was much higher, the drug-presolubilization in organic solvent facilitated the encapsulation process resulting higher encapsulation for PNC. The CL, AL and PNC were formulated with the organic solutions of AG. But, the PNC had highest EE due to higher lipid drug ratio, followed by CL which had higher EE compared to AL due to possible charged interactions with the drug.

These strategies i.e. use of charged lipids, pre-solubilizing the drug or optimization of the core oil percentage to have a balance between particle size and AG-loading can be used to improve EE and drug-loading in future formulations for drugs with similar characteristics.

The **storage stability** of the drug-loaded NDDSs is another important issue that was evaluated by the physical stability of the nanocarriers and the chemical stability of the drug molecule AG, when stored as dispersions at 4°C. Generally, steric repulsion among the nanovector particles hinders particle aggregation and improves physical stability (Lian and Ho, 2001), whereas protection of the active ingredient from the external environment can improve chemical stability of the drug. The sizes of all the nanocarriers were stable throughout the study period of 14 days which can be a due to steric repulsion. Regarding chemical stability, a reduction of drug concentration was observed only for CL. As AG is

a polyphenolic molecule, it can be chemically degraded by oxidation when in contact with aqueous environments. AG should be encapsulated between lipid molecules in AL, LNC and PNC which should protect the drug from the external environment. Only in CL, the surface adsorbed drug was exposed to aqueous environments which possibly resulted the degradation. This hypothesis was supported by the decrease of AG concentration in AG-HP β CD complex that was stored at 4°C as an aqueous solution. Additionally, two DCL formulations were prepared by entrapping different amounts of AG-HP β CD aqueous soluble complex in the CL core. As the DCLs had significantly lower (more than 2-folds) drug loading capacity compared to CL, and due to the degradation pattern of AG-HP β CD complex, the DCL formulations were not further studied. However, the lyophilization of CL (in presence of 5% trehalose) and the AG-HP β CD complex significantly improved its storage stability up to 12 weeks. Further extended stability studies should be performed with AL, LNC and PNC to evaluate their long-term stability as aqueous dispersions, although freeze-drying of the NDDSs might be necessary to achieve long-standing storage stability.

As injectable formulations, the NDDSs will come into contact with a large quantity of **serum proteins** after i.v. administration and have possibility (especially cationic NDDSs) to form a protein-corona which will alter its physicochemical characteristics (synthetic identity) and create a new biological identity which will regulate its physiological response (Figure 5.2) (Nel et al., 2009). The characteristics of the protein-corona depend on the nanocarrier size, surface properties and lipid composition (Capriotti et al., 2012; Caracciolo, 2015; Lundqvist et al., 2008). To evaluate the stability of the developed NDDSs in biological fluids, we incubated the nanocarriers in 50 % FBS at 37 °C and followed their size overtime using DLS, a method established by Palchetti et al. (Palchetti et al., 2016). All the nanocarriers were stable up to 6 h, and did not form any protein corona or aggregates. Therefore, the NDDSs were stable after large dilution in serum and did not form aggregates, or protein corona due to the steric repulsion by their surface PEG chains.

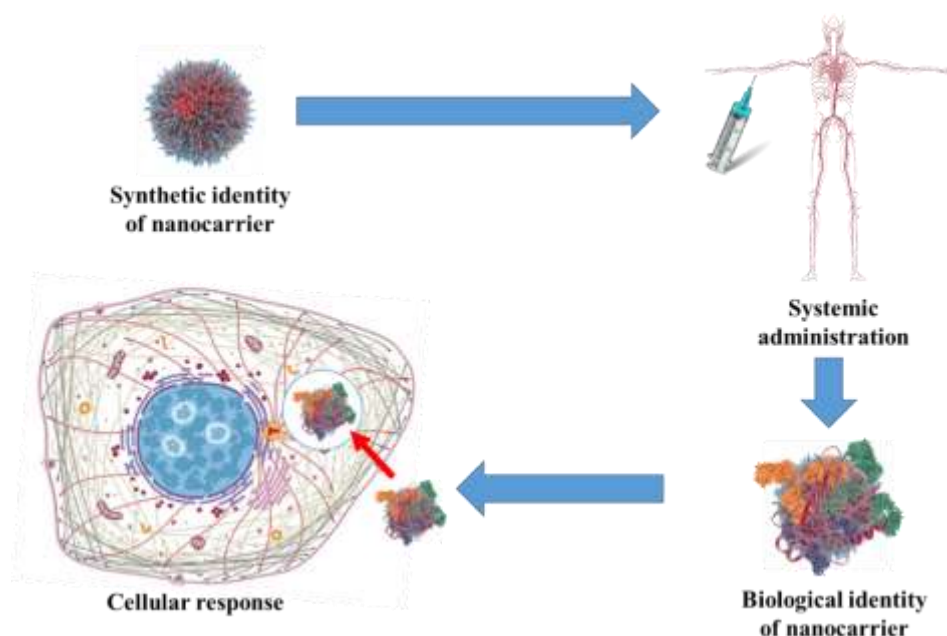


Figure 5.2: Alteration of physicochemical characteristics of nanocarriers (size, zeta potential, surface chemistry) after systemic administration due to interaction with serum components and creation of biological identity which regulates their interaction with cells.

The low interaction of the nanocarriers with serum components was also observed from the results of the **complement consumption** assay, where the nanocarriers consumed very low percentage of CH50 units even at very high surface area per mL of serum. Additionally, the NDDSs were **nontoxic** to endothelial cells, human BBB cells and neuronal cells up to reasonably high concentrations (lowest toxic concentration was shown by CLs at 171 $\mu\text{g/mL}$).

An important criteria of an ideal nanocarrier for i.v. administration is its **sustained drug release property** (Danhier et al., 2010). Nanocarriers might be in systemic circulation for significant time, before accumulating in tumor tissue. Therefore, an ideal nanocarrier should release the entrapped drug in a controlled manner, to keep sufficient amounts of drug when it reaches the tumor. For example, paclitaxel-loaded glioma-targeting peptide modified PEG-PLGA NPs released about 50% drug at 24 h (at pH 7.4) which gradually reached about 70% after 72 h (Lv et al., 2016). DOX encapsulating PLGA/HAS NPs showed a biphasic release with an initial burst release followed by a much slower gradual release phase, and released about 60% drug after 60 h (Wohlfart et al., 2011). Among the developed NDDSs, only the nanocapsules showed sustained release characteristics

possibly due to encapsulation of the drug in their core and better membrane rigidity. The liposomes showed quick release characteristics and therefore were considered as less suitable for i.v. administration.

In summary, among the four developed NDDSs, LNC and PNC were most promising. The particle size of the PNC can be possibly reduced by controlling the percentage of the core-oil in the composition. Moreover, it would be possible to produce the PNC by the phase-inversion technique like LNCs, if the copolymer is stable at heated conditions. Further studies are planned to fully evaluate the potential of this polymer. Additionally, the liposome formulations will require formulation optimization to achieve sustained release characteristics and to obtain a smaller size. However, the most promising characteristics was shown by the LNCs due to their easier and organic solvent free manufacturing (suitable for scale-up), more sustained release property and smaller size compared to the other formulations. Therefore, LNCs were chosen for further optimization to improve their targeting towards GBM cells.

Task 2: Optimization of LNC formulation to improve its targeting towards human GBM cells

In this part of the study, surface-functionalization of the LNC was performed to improve its targeting towards human GBM cells. Although the LNCs were described for their capability to inhibit P-gp (Garcion et al., 2006; Lamprecht and Benoit, 2006) and escape endosomes to deliver their cargo into the cytoplasm, they were also reported to be non-selective (rat glioma cells and astrocytes) (Paillard et al., 2010). This can be problematic not only for local delivery of the formulation (i.e. stereotactic bolus injection and CED), but also if LNCs are planned to be used by temporary BBB opening-strategies.

Functionalization of nanocarrier surface with GBM-targeting ligands can enhance the uptake of the nanovector in GBM cells. For instance, grafting Tf on liposome surface significantly enhanced (70% internalization) in C6 GBM cells, compared to PEGylated, nonPEGylated and albumin-functionalized PEGylated liposomes (14, 54 and 34% uptake respectively) (Eavarone et al., 2000). Similarly, lactoferrin-functionalized solid lipid NPs were significantly more (2.8-folds) internalized in U87MG cells compared to unfunctionalized solid lipid NPs (Singh et al., 2016). Likewise, Guo et al. reported that

addition of AS1411 DNA aptamer (targets cancer cells and tumor neovasculature) on PEG-PLGA NP enhanced C6 cell internalization of the nanovector by 2-folds, compared to the unmodified PLGA-PEG NP (Guo et al., 2011a). Treatment of intracranial C6 tumor bearing rats with paclitaxel (PTX) loaded PLGA-PEG-AP NP (i.v. administration) enhanced the median survival by 4 days (31 days) compared to non-functionalized PLGA-PEG-PTX NP (Guo et al., 2011a). Moreover, surface functionalization of PEG-PLA-PTX micelles with a cyclic RGD peptide (cRGDyK) increased the *in vitro* cytotoxicity on U87MG GBM cells by 2-folds, accumulated in subcutaneous and intracranial tumors after i.v. administration and enhanced median survival time of intracranial U87MG tumor bearing mice to 48 days compared to 41.5 days of the non-functionalized micelle (Zhan et al., 2010). Additionally, Gu et al. reported that surface-functionalization of PEG-PLA NP with MT1-AF7p peptide (MT1) (Gu et al., 2013a) and surface-functionalization of PEG-PCL NP with an activatable low molecular weight protamine (ALMWP) (Gu et al., 2013b) significantly enhanced cellular internalization of the NPs in C6 glioma cells, specific accumulation in intracranial tumor tissue in nude mice and enhanced median survivals after treatment with PTX-loaded targeted NP compared to other treatment groups.

Therefore, to improve their targeting towards GBM cells, LNC-surface functionalization with the peptide NFL-TBS.40-.63 (NFL) was intended.

The NFL peptide was reported to preferentially accumulate in the GBM cells compared to astrocytes, therefore it has the potential to be used as a targeting ligand for GBM (Berges et al., 2012a). Additionally, it has been shown that NFL peptide uptake in human glioblastoma cells occurs chiefly during its active proliferative phases (Lepinoux-Chambaud and Eyer, 2013). This peptide has some similarities with common CPPs e.g. it has 24 amino acids (AA) (< 30 AA) and is slightly cationic at physiological pH. In contrast, it is composed of only 2 arginines and no lysine which are generally abundant in CPPs (Berges et al., 2012b). Additionally, it cannot translocate directly across the cell membrane of U87MG cells, and no conventional cell surface recognition is needed for its uptake in this cell line.

Balzeau et al. reported that NFL-adsorption on LNC surface significantly increased nanocarrier internalization in mouse GBM cells (Balzeau et al., 2013). Different grafting methods were evaluated to attach the peptide to the distal end of DSPE-PEG₂₀₀₀ (biotin- or amino- modified) chains on the LNC surface, but no significant difference in cellular

uptake was observed compared to non-functionalized LNCs, possibly due to structural and functional modifications of the peptide (Balzeau et al., 2013). Moreover, Torchilin et al. reported that presence of PEG-coating creates steric hindrance among CPP-liposome interaction and number of TAT peptides attached to liposome surface was reduced about 4 folds (Torchilin et al., 2001). Presence of PEG-coating also inhibited TAT peptide-to-cell interaction possibly by steric hindrance and prevented cellular internalization of liposomes (Torchilin et al., 2001). As there was no reported suitable spacer for fluoNFL and because the peptide had to be adsorbed on the LNC surface, we modified the LNC composition described in chapter 3, by removing the DSPE-mPEG₂₀₀₀ to formulate the LNC in chapter 4, in order to retain its targeting activity. However, we tested the complement consumption of the LNC without DSPE-mPEG₂₀₀₀ and we confirmed that the complement consumption of the newly formed LNC was also very low, owing to the PEG chains contained in Kolliphor HS15.

Although in a previous study it was already showed that NFL-adsorption increased significantly the LNC uptake in GBM cells, the internalization of LNC-NFL in healthy mouse astrocytes was similar, therefore the formulation would not preferentially internalize in GBM cells (Balzeau et al., 2013). This phenomenon was observed at all tested concentrations (1/1000 to 1/100) of the formulation. However, NFL uptake in all the cell lines (GBM and astrocytes) were dependent on the available peptide concentration (Berges et al., 2012a) and its internalization mechanism in U87MG cells was also concentration-dependent (Lepinoux-Chambaud and Eyer, 2013). Therefore, we hypothesized that if the peptide concentration on LNC surface could be increased compared to Balzeau et al. (Balzeau et al., 2013), the internalization of the nanocarrier in U87MG cells might also increase. If this increase could occur at a faster rate compared to astrocytes, the preferential uptake of the LNC in GBM cells might be achieved. Moreover, the internalization rate and pathways are cell line specific: therefore, the results could be intrinsically different according the cell line used. Additionally, time of incubation can be another factor to study as cellular internalization processes may require longer time compared to the incubation time used in previous report (Balzeau et al., 2013).

In our study, we have shown that the internalization of LNC in U87MG cells is dependent on incubation time and NFL peptide concentration on the nanocarrier surface. Resembling to Balzeau et al. (Balzeau et al., 2013), we also observed that the 24 h adsorption of the

peptide on LNC surface was necessary to maximize nanocarrier internalization in U87MG cells. Confocal microscopy images demonstrated that the LNC-fluoNFL3 formulation (containing 3 times more NFL than in previous studies) was located in very high concentrations throughout the cytoplasm of the U87MG cells at 6 h, whereas the control LNC was chiefly membrane bound at very low percentage. Interestingly, the uptake of control LNC in U87MG cells was very low (2.3 % at 6h and 11.8 % at 24 h), and internalization in healthy astrocytes (NHA) was significantly higher (3-folds after 6 h). In contrast, internalization of LNC-fluoNFL3 was 2.9-folds higher in U87MG cells after 6 h compared to NHA. Therefore, the LNC-fluoNFL3 was preferentially internalized in GBM cells compared to healthy astrocytes.

Additionally, we have shown in this study that the internalization of LNC-fluoNFL3 in U87MG cells was energy-dependent, similar to the internalization pattern of the peptide alone (Berges et al., 2012a). Similarly, Gu et al. reported that the internalization of PEG-PLA-MT1 NPs and PEG-PCL-ALMWP NPs in C6 cells were energy-dependent and occurred by macropinocytosis and lipid-raft endocytosis (Gu et al., 2013a; Gu et al., 2013b). We showed that the internalization of LNC-fluoNFL3 in U87MG cells occurs by all three major endocytosis pathways i.e. macropinocytosis, clathrin-dependent and caveolin-dependent endocytosis, similar to the previously reported uptake pathway of the peptide alone (Lepinoux-Chambaud and Eyer, 2013). Lipid-raft endocytosis can be another major pathway of LNC-fluoNFL3 uptake (endocytosis inhibition by M β CD), although some studies described it as a combination of clathrin-dependent and caveolin-dependent endocytosis (Lepinoux-Chambaud and Eyer, 2013), and several classifications of endocytosis pathways exist (Sahay et al., 2010). However, macropinocytosis and lipid-raft endocytosis (or combination of clathrin- and caveolin-dependent endocytosis) are described as major cell internalization pathways for CPP-functionalized cargos with MW > 30000 Da (Torchilin, 2008). Interestingly, internalization of NFL in U87MG cells occurs only by caveolin-dependent endocytosis at low NFL concentrations and other pathways only gets involved from concentration above 5 μ M (Lepinoux-Chambaud and Eyer, 2013). As the NFL peptide is regulating the internalization pathway of LNC-fluoNFL3, caveolin-dependent uptake might be the major uptake pathway of the NFL-functionalized LNC and the other pathways may activate at higher concentrations possibly due to saturation. After formation, caveolar vesicles move and traffic with the aid of actin

and cellular microtubules, fuse with caveosomes or multivesicular bodies, and may reach cytosol and nuclei through endoplasmic reticulum (Sahay et al., 2010). As this pathway can avoid degradation by lysosomal enzymes (Carver and Schnitzer, 2003; Medina-Kauwe, 2007), it can be advantageous for degradation-prone drugs (nucleic acids and proteins) to avoid possible breakdown in lysosome and reach certain cellular organelles e.g. nucleus or endoplasmic reticulum (Sahay et al., 2010). However, AG chiefly inhibits activity of CK2 which is present in numerous subcellular compartments (Faust and Montenarh, 2000) and identified in both the cytoplasm and nucleus of human GBM cells (Zheng et al., 2013). FcTriOH, like other ferrocifens, would require activation by oxidation by intracellular enzymes to form the cytotoxic quinone methide, radicals and/or ROS (Jaouen et al., 2015; Wang et al., 2015). Therefore, both AG and FcTriOH would possibly needs to reach the cytoplasm.

Additionally, encapsulation of FcTriOH and AG was achieved with high encapsulation efficiency (>90 %). The drug-loaded NFL-functionalized LNCs showed lower IC₅₀ values compared to the drug-loaded non-functionalized LNCs against U87MG cells in MTS assay.

Moreover, *in vitro* BBB permeability of the nanocapsules were evaluated using hCMEC/D3 monolayer model. Although, it seemed from the results that NFL peptide do not aid in the BBB permeability of the LNC, further experiments would be necessary to confirm the results and to understand the interaction between the NFL peptide and the BBB cells.

In summary, we have increased the NFL peptide concentration on LNC surface and significantly enhanced its internalization in a human GBM cell line compared to healthy human astrocytes. The internalization mechanism of the peptide-functionalized LNC in U87MG cells was characterized and it seemed to follow the pathway of the peptide. Moreover, encapsulation of AG and FcTriOH in NFL-functionalized LNC seemed to improve their activity in the U87MG cells. Therefore, preliminary *in vivo* studies with these formulations were planned to evaluate their potential efficacy and/or side effects or toxicity in preclinical animal models.

Task 3: Preliminary *in vivo* assessment of efficacy and/or toxicity of drug-loaded optimized LNCs

The last part of the study was focused on the preliminary *in vivo* evaluation of the formulations, in a subcutaneous (ectopic) and an intracranial (orthotopic) U87MG tumor models in nude mice with two different administration routes: i.v., and intracranial. Nanocarriers administered by different drug administration routes have to overcome different biological barriers before reaching the target site. In the ectopic U87MG tumor model, the LNCs after i.v. administration have to hinder protein corona formation, avoid capture by the MPS, have less nonspecific distribution and pass through the fenestrated neovasculature before reaching the tumor tissue. Additionally, they have to overcome the interstitial pressure gradients to penetrate deeper into the tumors, enter into the internalized in the cells and avoid P-gp efflux to finally reach their target site (Figure 5.3) (Blanco et al., 2015).

Intraperitoneal route of administration is more commonly used in small animal models in which i.v. injections are challenging (Turner et al., 2011). Intraperitoneally administered nanovectors have an additional absorption step at the beginning before reaching the systemic circulation and the absorption occurs firstly in the mesenteric vessels which goes into portal circulation (Lukas et al., 1971).

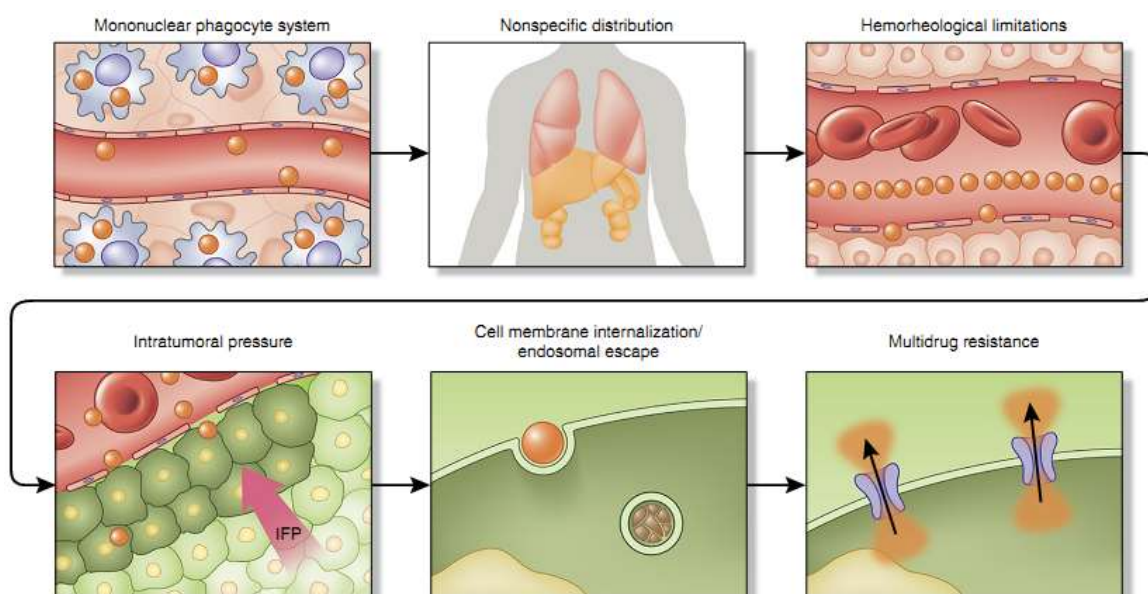


Figure 5.3: Biological barriers to overcome by intravenously administered nanocarriers. IFP, interstitial fluid pressure (Blanco et al., 2015).

Route of administration of nanovectors can influence on its *in vivo* fate. Chang et al. reported that lung and kidney levels of amphotericin B (AmpB) were higher after i.v. administration of liposomal AmpB, compared to intraperitoneal administration in mice (Chang et al., 2010). Moreover, more AmpB was present in spleens after intraperitoneal injection (compared to i.v.) whereas liver AmpB levels were similar for both administration routes. The peak serum AmpB level was reached after 0.5 h of i.v. injection, compared to 2 h after intraperitoneal injection, although the peak serum levels were higher after intraperitoneal injections (Chang et al., 2010). Reddy et al. reported significantly higher (about 8-folds) tumor accumulation of etoposide-loaded tripalmitin NPs after intraperitoneal administration compared to i.v. administration in mice with subcutaneously implanted Dalton's lymphoma tumors (Harivardhan Reddy et al., 2005). Significantly high brain distribution was also detected after intraperitoneal injections (Harivardhan Reddy et al., 2005). Moreover, Zhang et al. reported higher toxicity of gold NPs administered by intraperitoneal route, compared to i.v. route (Zhang et al., 2010). We utilized the i.v. route for LNC administration in mice with ectopic GBM tumors in the preliminary study.

In the subcutaneous tumor model, two i.v. injections of the formulations were given to evaluate the efficacy and/or toxicity of the formulations. Two i.v. injections on day 7 and day 10 after cell injection resulted in significant reduction in relative tumor volume for the groups treated with LNC-FcTriOH and LNC-FcTriOH-fluoNFL3, compared to saline treated group. The significant reduction was observed from day 17 and was abolished on day 24 (2 weeks after last injection). Although the difference between LNC-FcTriOH and LNC-FcTriOH-fluoNFL3 was not significant, the relative tumor volume of the peptide-functionalized LNC-FcTriOH was slightly lower than the respective non-functionalized group. AG-loaded LNC-fluoNFL3 did not show any tumor reduction capacity. No toxicity was observed in any of the groups. Therefore, optimization of chemotherapy dosage regimen with FcTriOH-loaded LNCs seemed necessary. Chemotherapy in clinical practice is generally given over several cycles, and each cycle has multiple dose administrations. Therefore, another *in vivo* study with a greater number of injections (possibly through intraperitoneal route) will be performed soon.

In the intracranial U87MG tumor model, the treatment was administered by CED to bypass the BBB. Subsequently, the LNCs have to diffuse through the brain extracellular space to maximize their volume of distribution (V_d) and reach the tumor cells that are distant from the injection site (Figure 5.4). Various parameters can impact on the LNC distribution which can be divided into technical parameters and nanocarrier physicochemical parameters (Allard et al., 2009b). Among technical parameters, catheter/needle size, needle design and infusion rate are important parameters that need to be adjusted. Needles with bigger diameter increase the chance of backflow and reduce the V_d (Chen et al., 1999; Kroll et al., 1996). Therefore, a 32-gauge needle was used in our experiments during the CED which reduces the chance of backflow (Allard et al., 2009b). Moreover, single end port type needle was used to have a spherical and high V_d (Bauman et al., 2003). The infusion rate was kept below 0.5 $\mu\text{L}/\text{min}$ to minimize backflow (Allard et al., 2009b; Degen et al., 2003). Among nanocarrier physicochemical properties, size of the LNCs were between 50-65 nm which is within the suitable range for passage through brain extracellular space as previously described (Allard et al., 2009a; Thorne and Nicholson, 2006).

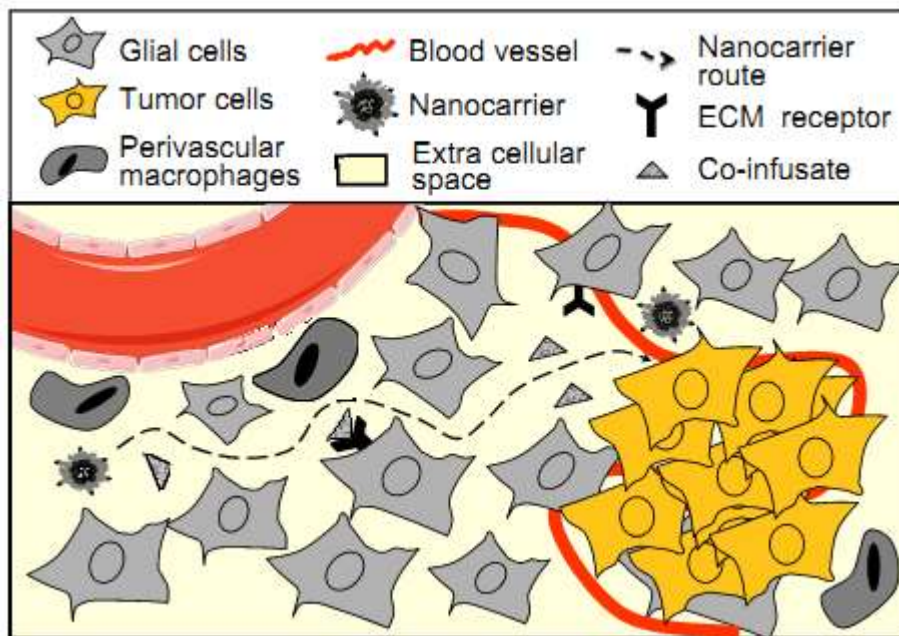


Figure 5.4: Passage of nanocarrier through brain extracellular space after convection enhanced delivery (Allard et al., 2009b).

MRI after 5 days of treatment administration showed that the LNCs possibly resulted lesions in the brain due to toxicity. Similar observations were reported by Huynh et al. (Huynh et al., 2012). They observed brain lesions 14 days after CED of non-functionalized LNC by MRI (Huynh et al., 2012). Similarly, Laine et al reported possible toxicity after CED of surface-functionalized LNCs, which reduced the median survival of rats compared to control group (Laine et al., 2012). Interestingly, MRI scans on day 13 revealed that the lesion size created by NFL-functionalized LNCs (with or without FcTriOH) was significantly larger compared to control group and non-functionalized LNC treated groups. Therefore, it was evident that NFL-functionalized LNCs entered into higher percentage in brain cells (healthy or cancerous) creating larger lesions by their toxicity, as their concentration after CED decreases gradually from the injection site. Moreover, DTI revealed that the LNC-NFL3 treated groups (with or without FcTriOH) had a part of the lesion which had much higher ADC values, compared to other parts and to the control groups. Such high ADC values are often predictor of treatment response and indicates less cellularity in that region due to possible lysis or necrosis of cells (Patterson et al., 2008). Chen et al. showed that CED of different concentrations (25, 50 and 100%) of BSA did not significantly alter the V_d which was about 20 mm^3 (Chen et al., 1999). Kroll et al. increased the CED dose of mono crystalline iron oxide nanocompounds (MIONs) by 5-folds, and observed 4.9-folds increase of V_d at $0.2 \text{ }\mu\text{L/min}$ infusion rate (Kroll et al., 1996). So, dose of the nanocarrier was the major parameter that impacts on V_d . Hence, optimization of the LNC-NFL3 dose by CED can be a promising strategy for GBM treatment. Dose of the LNC can be optimized by reducing the concentration of nanocarrier (while keeping the injection volume same) or by reducing the volume of injection.

However, to make more efficient administration in the brain tumor by CED, larger animal models can be beneficial. Mouse brain tumors are very small and it is very difficult to inject directly within the tumor. For example, a 3 mm^3 spherical brain tumor would have a radius of 0.89 mm, whereas a 32 Gauge needle have a 0.23 mm outer diameter. A 20 mm^3 tumor will have a radius of only 1.68 mm. Therefore, it is difficult to administer the dose exactly in the tumor core and a larger animal model e.g. rats can be used in the future for CED optimization.

5.2. Conclusion and Perspectives

In this thesis, four nanocarriers i.e. a cationic liposome, an anionic liposome, a lipid nanocapsule and a novel PEG-b-polyphosphate polymer-based nanocapsule were developed, characterized and compared as prospective injectable nanocarriers for low-molecular weight hydrophobic drugs. Among the developed NDDSs, the potential of the nanocapsule formulations as injectable nanocarriers for low-molecular weight drugs were observed. Subsequently, the lipid nanocapsules were modified by surface-functionalization with NFL peptide. The importance of enhancing targeting-moiety concentration for achieving preferential internalization in the desired cell was shown. Promising *in vivo* activity of a novel ferrocifen-derivative i.e. FcTriOH was also observed for the first time. The knowledge obtained in this thesis can be beneficial for further optimization of the FcTriOH therapy and targeted delivery of LNCs towards GBM tumors in forthcoming studies.

In near future, another *in vivo* study on the subcutaneous U87MG tumor model will be performed with higher number of injections in order to optimize the chemotherapy dosage. A pharmacokinetic and a biodistribution study of the LNC-FcTriOH and the LNC-FcTriOH-NFL3 after i.v. administration could be performed to have better understanding about the effect of the functionalization on the drug accumulation sites, pathway of metabolism and elimination. Additionally, optimization of the CED administration can be evaluated, preferentially in larger animals like rats to ensure injection inside the tumor core. The dose optimization can be performed by adapting the LNC concentration and/or also the injection volume, and their influence on the V_d of the formulations should be followed.

Further studies are necessary to understand why AG does not show its activity *in vivo*. High intracellular dose of AG might be required to exert its pharmacological activity which can be a limiting factor for nanoparticle based drug delivery. Moreover, AG inhibits the activity of an upstream serine/threonine selective protein kinase CK2 which has hundreds of downstream cell signaling modulators and some of which may counteract and inhibit its antiGBM activity pathways. Therefore, further detailed study of effect of AG on cell signaling pathway of GBM can be performed.

Additionally, a suitable covalent coupling strategy can be investigated to link the NFL peptide at the distal end of a spacer molecule on that is longer than the PEG chains of nanocarrier surface. Various chemical linking strategies, their efficacy and effect on the GBM-targeting property of NFL should be evaluated in order to find the optimum peptide grafting technique. Moreover, the stability of the NFL-grafted nanovector during storage and in biological medium, and its interaction with serum proteins should be studied to predict its *in vivo* fate. Additionally, pharmacokinetics of the NFL-coupled nanocarrier and the NFL-adsorbed nanocarrier should be studied in healthy and GBM animal models, and compared to illustrate the necessity and benefits of the coupling technique.

Furthermore, theranostic nanocarriers encapsulating FcTriOH can be developed using the NFL-functionalization strategy in order to treat GBM and also monitor the treatment response. This would give immense opportunity to modify the therapy according to patient's requirements and would be a crucial point for moving towards personalized medicine. The advancement of diagnostic imaging techniques and the nanotechnology may allow disease progression monitoring throughout the total treatment regimen. Co-encapsulation of imaging agent with FcTriOH in NFL-functionalized LNC can be one of the strategies to develop theranostic nanocarriers for GBM. Development of other type of NFL-functionalized nanovectors (e.g. liposomes and PNPs) should be also evaluated for comparing the efficacy of the nanocarriers as theranostic tool for GBM.

Moreover, further analysis with the FcTriOH molecule should be performed to understand its exact mechanism of action in human GBM cells. As ROS production is one of the major mechanisms of ferrochins (Jaouen et al., 2015), co-administration of the drug with other redox modulators can be a promising approach to improve their efficacy and selectivity towards GBM cells. GBM cells are already in high ROS state which is necessary for their increased proliferation rate (Salazar-Ramiro et al., 2016). However, reduction in cellular redox buffers, e.g. reduced glutathione (GSH) which protects the cells from the oxidant damage, can weaken the cells response to oxidative damage and improve the efficacy of ROS producing drugs (Khan et al., 2012; Romero-Canelón et al., 2015).

NFL-peptide was used also for targeted delivery of LNCs to brain-neural stem cells (Carradori et al., 2016). Therefore the LNC-fluoNFL3 formulation with higher NFL peptide on surface may improve the targeting capability, which can be investigated.

5.3. References

- Allard, E., Huynh, N.T., Vessieres, A., Pigeon, P., Jaouen, G., Benoit, J.P., Passirani, C., 2009a. Dose effect activity of ferrocifen-loaded lipid nanocapsules on a 9L-glioma model. *Int. J. Pharm.* 379, 317-323.
- Allard, E., Passirani, C., Benoit, J.P., 2009b. Convection-enhanced delivery of nanocarriers for the treatment of brain tumors. *Biomaterials* 30, 2302-2318.
- Allard, E., Passirani, C., Garcion, E., Pigeon, P., Vessieres, A., Jaouen, G., Benoit, J.P., 2008. Lipid nanocapsules loaded with an organometallic tamoxifen derivative as a novel drug-carrier system for experimental malignant gliomas. *J. Control. Release* 130, 146-153.
- Ambrose, J., 1973. Computerized transverse axial scanning (tomography). 2. Clinical application. *Br. J. Radiol.* 46, 1023-1047.
- Anselmo, A.C., Mitragotri, S., 2016. Nanoparticles in the clinic. *Bioengineering & Translational Medicine* 1, 10-29.
- Balzeau, J., Pinier, M., Berges, R., Saulnier, P., Benoit, J.P., Eyer, J., 2013. The effect of functionalizing lipid nanocapsules with NFL-TBS.40-63 peptide on their uptake by glioblastoma cells. *Biomaterials* 34, 3381-3389.
- Bauman, M., Gillies, G., Raghavan, R., Brady, M., Pedain, C., 2003. Physical characterization of neurocatheter performance in a brain phantom gelatin with nanoscale porosity: steady-state and oscillatory flows. *Nanotechnology* 15, 92.
- Bellavance, M.A., Poirier, M.B., Fortin, D., 2010. Uptake and intracellular release kinetics of liposome formulations in glioma cells. *Int. J. Pharm.* 395, 251-259.
- Bennett, A.H., 1885. Case of Cerebral Tumour. *Med. Chir. Trans.* 68, 243-275.
- Berges, R., Balzeau, J., Peterson, A.C., Eyer, J., 2012a. A tubulin binding peptide targets glioma cells disrupting their microtubules, blocking migration, and inducing apoptosis. *Mol. Ther.* 20, 1367-1377.
- Berges, R., Balzeau, J., Takahashi, M., Prevost, C., Eyer, J., 2012b. Structure-function analysis of the glioma targeting NFL-TBS.40-63 peptide corresponding to the tubulin-binding site on the light neurofilament subunit. *PLoS One* 7, e49436.
- Bernardi, A., Braganhol, E., Jager, E., Figueiro, F., Edelweiss, M.I., Pohlmann, A.R., Guterres, S.S., Battastini, A.M., 2009. Indomethacin-loaded nanocapsules treatment reduces in vivo glioblastoma growth in a rat glioma model. *Cancer Lett.* 281, 53-63.
- Bianco, J., Bastiancich, C., Jankovski, A., des Rieux, A., Preat, V., Danhier, F., 2017. On glioblastoma and the search for a cure: where do we stand? *Cell. Mol. Life Sci.*, 2451-2466.
- Blanco, E., Shen, H., Ferrari, M., 2015. Principles of nanoparticle design for overcoming biological barriers to drug delivery. *Nat. Biotechnol.* 33, 941-951.
- Brigger, I., Morizet, J., Aubert, G., Chacun, H., Terrier-Lacombe, M.J., Couvreur, P., Vassal, G., 2002. Poly(ethylene glycol)-coated hexadecylcyanoacrylate nanospheres display a combined effect for brain tumor targeting. *J. Pharmacol. Exp. Ther.* 303, 928-936.
- Calvo, P., Gouritin, B., Chacun, H., Desmaële, D., D'Angelo, J., Noel, J.-P., Georgin, D., Fattal, E., Andreux, J.P., Couvreur, P., 2001. Long-circulating PEGylated polycyanoacrylate nanoparticles as new drug carrier for brain delivery. *Pharm. Res.* 18, 1157-1166.

- Capriotti, A.L., Caracciolo, G., Cavaliere, C., Foglia, P., Pozzi, D., Samperi, R., Lagana, A., 2012. Do plasma proteins distinguish between liposomes of varying charge density? *J. Proteomics* 75, 1924-1932.
- Caracciolo, G., 2015. Liposome-protein corona in a physiological environment: challenges and opportunities for targeted delivery of nanomedicines. *Nanomedicine* 11, 543-557.
- Carradori, D., Saulnier, P., Preat, V., des Rieux, A., Eyer, J., 2016. NFL-lipid nanocapsules for brain neural stem cell targeting *in vitro* and *in vivo*. *J. Control. Release* 238, 253-262.
- Carver, L.A., Schnitzer, J.E., 2003. Caveolae: mining little caves for new cancer targets. *Nat. Rev. Cancer* 3, 571-581.
- Chang, T., Olson, J.A., Proffitt, R.T., Adler-Moore, J.P., 2010. Differences in tissue drug concentrations following intravenous versus intraperitoneal treatment with amphotericin B deoxycholate or liposomal amphotericin B. *Med. Mycol.* 48, 430-435.
- Chen, M.Y., Lonser, R.R., Morrison, P.F., Governale, L.S., Oldfield, E.H., 1999. Variables affecting convection-enhanced delivery to the striatum: a systematic examination of rate of infusion, cannula size, infusate concentration, and tissue-cannula sealing time. *J. Neurosurg.* 90, 315-320.
- Chen, X.J., Wu, M.Y., Li, D.H., You, J., 2016. Apigenin inhibits glioma cell growth through promoting microRNA-16 and suppression of BCL-2 and nuclear factor-kappaB/MMP9. *Mol Med Rep* 14, 2352-2358.
- Clavreul, A., Montagu, A., Laine, A.L., Tetaud, C., Lautram, N., Franconi, F., Passirani, C., Vessieres, A., Montero-Menei, C.N., Menei, P., 2015. Targeting and treatment of glioblastomas with human mesenchymal stem cells carrying ferrociphenol lipid nanocapsules. *International journal of nanomedicine* 10, 1259-1271.
- Danhier, F., Feron, O., Preat, V., 2010. To exploit the tumor microenvironment: Passive and active tumor targeting of nanocarriers for anti-cancer drug delivery. *J. Control. Release* 148, 135-146.
- Das, A., Banik, N.L., Ray, S.K., 2010. Flavonoids activated caspases for apoptosis in human glioblastoma T98G and U87MG cells but not in human normal astrocytes. *Cancer* 116, 164-176.
- Das, S., Das, J., Samadder, A., Paul, A., Khuda-Bukhsh, A.R., 2013. Strategic formulation of apigenin-loaded PLGA nanoparticles for intracellular trafficking, DNA targeting and improved therapeutic effects in skin melanoma *in vitro*. *Toxicol. Lett.* 223, 124-138.
- DeAngelis, L.M., Mellingerhoff, I.K., 2011. Virchow 2011 or How to ID(H) Human Glioblastoma. *J. Clin. Oncol.* 29, 4473-4474.
- Degen, J.W., Walbridge, S., Vortmeyer, A.O., Oldfield, E.H., Lonser, R.R., 2003. Safety and efficacy of convection-enhanced delivery of gemcitabine or carboplatin in a malignant glioma model in rats. *J. Neurosurg.* 99, 893-898.
- Ding, B., Chen, H., Wang, C., Zhai, Y., Zhai, G., 2013. Preparation and *in vitro* evaluation of apigenin loaded lipid nanocapsules. *Journal of nanoscience and nanotechnology* 13, 6546-6552.
- Eavarone, D.A., Yu, X., Bellamkonda, R.V., 2000. Targeted drug delivery to C6 glioma by transferrin-coupled liposomes. *J. Biomed. Mater. Res.* 51, 10-14.
- Engelmann, C., Blot, E., Panis, Y., Bauer, S., Trochon, V., Nagy, H., Lu, H., Soria, C., 2002. Apigenin—strong cytostatic and anti-angiogenic action *in vitro* contrasted by lack of efficacy *in vivo*. *Phytomedicine* 9, 489-495.

- Faust, M., Montenarh, M., 2000. Subcellular localization of protein kinase CK2. A key to its function? *Cell Tissue Res.* 301, 329-340.
- Favaro, G., Clementi, C., Romani, A., Vickackaite, V., 2007. Acidochromism and ionochromism of luteolin and apigenin, the main components of the naturally occurring yellow weld: a spectrophotometric and fluorimetric study. *J. Fluoresc.* 17, 707-714.
- Feng, X., Zhou, Q., Liu, C., Tao, M.-L., 2012. Drug screening study using glioma stem-like cells. *Mol. Med. Report.* 6, 1117-1120.
- Fiorina, V.J., Dubois, R.J., Brynes, S., 1978. Ferrocenyl polyamines as agents for the chemioimmunotherapy of cancer. *J. Med. Chem.* 21, 393-395.
- Garcia-Garcia, E., Andrieux, K., Gil, S., Couvreur, P., 2005. Colloidal carriers and blood-brain barrier (BBB) translocation: a way to deliver drugs to the brain? *Int. J. Pharm.* 298, 274-292.
- Garcion, E., Lamprecht, A., Heurtault, B., Paillard, A., Aubert-Pouessel, A., Denizot, B., Menei, P., Benoit, J.P., 2006. A new generation of anticancer, drug-loaded, colloidal vectors reverses multidrug resistance in glioma and reduces tumor progression in rats. *Mol. Cancer Ther.* 5, 1710-1722.
- Gu, G., Gao, X., Hu, Q., Kang, T., Liu, Z., Jiang, M., Miao, D., Song, Q., Yao, L., Tu, Y., Pang, Z., Chen, H., Jiang, X., Chen, J., 2013a. The influence of the penetrating peptide iRGD on the effect of paclitaxel-loaded MT1-AF7p-conjugated nanoparticles on glioma cells. *Biomaterials* 34, 5138-5148.
- Gu, G., Xia, H., Hu, Q., Liu, Z., Jiang, M., Kang, T., Miao, D., Tu, Y., Pang, Z., Song, Q., Yao, L., Chen, H., Gao, X., Chen, J., 2013b. PEG-co-PCL nanoparticles modified with MMP-2/9 activatable low molecular weight protamine for enhanced targeted glioblastoma therapy. *Biomaterials* 34, 196-208.
- Guo, J., Gao, X., Su, L., Xia, H., Gu, G., Pang, Z., Jiang, X., Yao, L., Chen, J., Chen, H., 2011a. Aptamer-functionalized PEG-PLGA nanoparticles for enhanced anti-glioma drug delivery. *Biomaterials* 32, 8010-8020.
- Guo, L., Fan, L., Pang, Z., Ren, J., Ren, Y., Li, J., Chen, J., Wen, Z., Jiang, X., 2011b. TRAIL and doxorubicin combination enhances anti-glioblastoma effect based on passive tumor targeting of liposomes. *J. Control. Release* 154, 93-102.
- Gzell, C., Back, M., Wheeler, H., Bailey, D., Foote, M., 2017. Radiotherapy in Glioblastoma: the Past, the Present and the Future. *Clin. Oncol. (R. Coll. Radiol.)* 29, 15-25.
- Harivardhan Reddy, L., Sharma, R.K., Chuttani, K., Mishra, A.K., Murthy, R.S., 2005. Influence of administration route on tumor uptake and biodistribution of etoposide loaded solid lipid nanoparticles in Dalton's lymphoma tumor bearing mice. *J. Control. Release* 105, 185-198.
- Huynh, N.T., Passirani, C., Allard-Vannier, E., Lemaire, L., Roux, J., Garcion, E., Vessieres, A., Benoit, J.P., 2012. Administration-dependent efficacy of ferrociphenol lipid nanocapsules for the treatment of intracranial 9L rat gliosarcoma. *Int. J. Pharm.* 423, 55-62.
- Jaouen, G., Vessieres, A., Top, S., 2015. Ferrocifen type anti cancer drugs. *Chem. Soc. Rev.* 44, 8802-8817.
- Khan, M., Yi, F., Rasul, A., Li, T., Wang, N., Gao, H., Gao, R., Ma, T., 2012. Alantolactone induces apoptosis in glioblastoma cells via GSH depletion, ROS generation, and mitochondrial dysfunction. *IUBMB life* 64, 783-794.

- Kroll, R.A., Pagel, M.A., Muldoon, L.L., Roman-Goldstein, S., Neuwelt, E.A., 1996. Increasing volume of distribution to the brain with interstitial infusion: dose, rather than convection, might be the most important factor. *Neurosurgery* 38, 746-752; discussion 752-744.
- Laine, A.L., Huynh, N.T., Clavreul, A., Balzeau, J., Bejaud, J., Vessieres, A., Benoit, J.P., Eyer, J., Passirani, C., 2012. Brain tumour targeting strategies via coated ferrociphenol lipid nanocapsules. *Eur. J. Pharm. Biopharm.* 81, 690-693.
- Lamprecht, A., Benoit, J.P., 2006. Etoposide nanocarriers suppress glioma cell growth by intracellular drug delivery and simultaneous P-glycoprotein inhibition. *J. Control. Release* 112, 208-213.
- Lamprecht, A., Bouligand, Y., Benoit, J.P., 2002. New lipid nanocapsules exhibit sustained release properties for amiodarone. *J. Control. Release* 84, 59-68.
- Lauterbur, P.C., 1989. Image formation by induced local interactions. Examples employing nuclear magnetic resonance. 1973. *Clin. Orthop. Relat. Res.*, 3-6.
- Lepinoux-Chambaud, C., Eyer, J., 2013. The NFL-TBS.40-63 anti-glioblastoma peptide enters selectively in glioma cells by endocytosis. *Int. J. Pharm.* 454, 738-747.
- Li, B., Robinson, D.H., Birt, D.F., 1997. Evaluation of properties of apigenin and [G-3H]apigenin and analytic method development. *J. Pharm. Sci.* 86, 721-725.
- Lian, T., Ho, R.J., 2001. Trends and developments in liposome drug delivery systems. *J. Pharm. Sci.* 90, 667-680.
- Liu, Y., Lu, W., 2012. Recent advances in brain tumor-targeted nano-drug delivery systems. *Expert opinion on drug delivery* 9, 671-686.
- Louis, D.N., Perry, A., Reifenberger, G., von Deimling, A., Figarella-Branger, D., Cavenee, W.K., Ohgaki, H., Wiestler, O.D., Kleihues, P., Ellison, D.W., 2016. The 2016 World Health Organization Classification of Tumors of the Central Nervous System: a summary. *Acta Neuropathol.* 131, 803-820.
- Lukas, G., Brindle, S.D., Greengard, P., 1971. The route of absorption of intraperitoneally administered compounds. *J. Pharmacol. Exp. Ther.* 178, 562-564.
- Lundqvist, M., Stigler, J., Elia, G., Lynch, I., Cedervall, T., Dawson, K.A., 2008. Nanoparticle size and surface properties determine the protein corona with possible implications for biological impacts. *Proc. Natl. Acad. Sci. U. S. A.* 105, 14265-14270.
- Lv, L., Jiang, Y., Liu, X., Wang, B., Lv, W., Zhao, Y., Shi, H., Hu, Q., Xin, H., Xu, Q., Gu, Z., 2016. Enhanced Antiglioblastoma Efficacy of Neovasculature and Glioma Cells Dual Targeted Nanoparticles. *Mol. Pharm.* 13, 3506-3517.
- Medina-Kauwe, L.K., 2007. "Alternative" endocytic mechanisms exploited by pathogens: new avenues for therapeutic delivery? *Advanced drug delivery reviews* 59, 798-809.
- Miura, Y., Takenaka, T., Toh, K., Wu, S., Nishihara, H., Kano, M.R., Ino, Y., Nomoto, T., Matsumoto, Y., Koyama, H., Cabral, H., Nishiyama, N., Kataoka, K., 2013. Cyclic RGD-linked polymeric micelles for targeted delivery of platinum anticancer drugs to glioblastoma through the blood-brain tumor barrier. *ACS Nano* 7, 8583-8592.
- Muhammad, N., Guo, Z., 2014. Metal-based anticancer chemotherapeutic agents. *Curr. Opin. Chem. Biol.* 19, 144-153.
- Nel, A.E., Madler, L., Velegol, D., Xia, T., Hoek, E.M., Somasundaran, P., Klaessig, F., Castranova, V., Thompson, M., 2009. Understanding biophysicochemical interactions at the nano-bio interface. *Nat. Mater.* 8, 543-557.

- Nguyen, A., Vessi res, A., Hillard, E.A., Top, S., Pigeon, P., Jaouen, G., 2007. Ferrocifens and ferrocifenols as new potential weapons against breast cancer. *CHIMIA International Journal for Chemistry* 61, 716-724.
- Paillard, A., Hindre, F., Vignes-Colombeix, C., Benoit, J.P., Garcion, E., 2010. The importance of endo-lysosomal escape with lipid nanocapsules for drug subcellular bioavailability. *Biomaterials* 31, 7542-7554.
- Palchetti, S., Colapicchioni, V., Digiaco, L., Caracciolo, G., Pozzi, D., Capriotti, A.L., La Barbera, G., Lagana, A., 2016. The protein corona of circulating PEGylated liposomes. *Biochim. Biophys. Acta* 1858, 189-196.
- Papay, Z.E., Sebestyen, Z., Ludanyi, K., Kallai, N., Balogh, E., Kosa, A., Somavarapu, S., Boddi, B., Antal, I., 2016. Comparative evaluation of the effect of cyclodextrins and pH on aqueous solubility of apigenin. *J. Pharm. Biomed. Anal.* 117, 210-216.
- Parajuli, P., Joshee, N., Rimando, A.M., Mittal, S., Yadav, A.K., 2009. In vitro antitumor mechanisms of various *Scutellaria* extracts and constituent flavonoids. *Planta Med.* 75, 41-48.
- Patterson, D.M., Padhani, A.R., Collins, D.J., 2008. Technology insight: water diffusion MRI--a potential new biomarker of response to cancer therapy. *Nat. Clin. Pract. Oncol.* 5, 220-233.
- Peres, B., Nasr, R., Zariouh, M., Lecerf-Schmidt, F., Di Pietro, A., Baubichon-Cortay, H., Boumendjel, A., 2017. Ferrocene-embedded flavonoids targeting the Achilles heel of multidrug-resistant cancer cells through collateral sensitivity. *Eur. J. Med. Chem.* 130, 346-353.
- Romero-Canel n, I., Mos, M., Sadler, P.J., 2015. Enhancement of Selectivity of an Organometallic Anticancer Agent by Redox Modulation. *J. Med. Chem.* 58, 7874-7880.
- Roth, J.G., Elvidge, A.R., 1960. Glioblastoma multiforme: a clinical survey. *J. Neurosurg.* 17, 736-750.
- Sahay, G., Alakhova, D.Y., Kabanov, A.V., 2010. Endocytosis of nanomedicines. *J. Control. Release* 145, 182-195.
- Salazar-Ramiro, A., Ram rez-Ortega, D., P rez de la Cruz, V., H rnandez-Pedro, N.Y., Gonz lez-Esquivel, D.F., Sotelo, J., Pineda, B., 2016. Role of Redox Status in Development of Glioblastoma. *Front. Immunol.* 7, 156.
- Santos, B.L., Oliveira, M.N., Coelho, P.L., Pitanga, B.P., da Silva, A.B., Adelita, T., Silva, V.D., Costa Mde, F., El-Bacha, R.S., Tardy, M., Chneiweiss, H., Junier, M.P., Moura-Neto, V., Costa, S.L., 2015. Flavonoids suppress human glioblastoma cell growth by inhibiting cell metabolism, migration, and by regulating extracellular matrix proteins and metalloproteinases expression. *Chem. Biol. Interact.* 242, 123-138.
- Siegal, T., Horowitz, A., Gabizon, A., 1995. Doxorubicin encapsulated in sterically stabilized liposomes for the treatment of a brain tumor model: biodistribution and therapeutic efficacy. *J. Neurosurg.* 83, 1029-1037.
- Singh, I., Swami, R., Pooja, D., Jeengar, M.K., Khan, W., Sistla, R., 2016. Lactoferrin bioconjugated solid lipid nanoparticles: a new drug delivery system for potential brain targeting. *J. Drug Target.* 24, 212-223.
- Spiegel, E.A., Wycis, H.T., Marks, M., Lee, A.J., 1947. Stereotaxic Apparatus for Operations on the Human Brain. *Science* 106, 349-350.

- Stump, T.A., Santee, B.N., Williams, L.P., Kunze, R.A., Heinze, C.E., Huseman, E.D., Gryka, R.J., Simpson, D.S., Amos, S., 2017. The antiproliferative and apoptotic effects of apigenin on glioblastoma cells. *J. Pharm. Pharmacol.*
- Stupp, R., Mason, W.P., van den Bent, M.J., Weller, M., Fisher, B., Taphoorn, M.J., Belanger, K., Brandes, A.A., Marosi, C., Bogdahn, U., Curschmann, J., Janzer, R.C., Ludwin, S.K., Gorlia, T., Allgeier, A., Lacombe, D., Cairncross, J.G., Eisenhauer, E., Mirimanoff, R.O., 2005. Radiotherapy plus concomitant and adjuvant temozolomide for glioblastoma. *N. Engl. J. Med.* 352, 987-996.
- Thorne, R.G., Nicholson, C., 2006. In vivo diffusion analysis with quantum dots and dextrans predicts the width of brain extracellular space. *Proc. Natl. Acad. Sci. U. S. A.* 103, 5567-5572.
- Torchilin, V.P., 2008. Cell penetrating peptide-modified pharmaceutical nanocarriers for intracellular drug and gene delivery. *Biopolymers* 90, 604-610.
- Torchilin, V.P., Rammohan, R., Weissig, V., Levchenko, T.S., 2001. TAT peptide on the surface of liposomes affords their efficient intracellular delivery even at low temperature and in the presence of metabolic inhibitors. *P. Natl. Acad. Sci. USA* 98, 8786-8791.
- Tungjai, M., Poompimon, W., Loetchutin, C., Kothan, S., Dechsupa, N., Mankhetkorn, S., 2008. Spectrophotometric characterization of behavior and the predominant species of flavonoids in physiological buffer: determination of solubility, lipophilicity and anticancer efficacy. *Open Drug Deliv. J.* 2, 10-19.
- Turner, P.V., Brabb, T., Pekow, C., Vasbinder, M.A., 2011. Administration of Substances to Laboratory Animals: Routes of Administration and Factors to Consider. *Journal of the American Association for Laboratory Animal Science : JAALAS* 50, 600-613.
- Vanslambrouck, S., 2015. Polyphosphate-based amphiphilic copolymers: synthesis and application to drug nanocarriers. University of Liège, Liège, Belgium.
- Wang, Y., Pigeon, P., Top, S., McGlinchey, M.J., Jaouen, G., 2015. Organometallic Antitumor Compounds: Ferrocenyls as Precursors to Quinone Methides. *Angew. Chem. Int. Ed. Engl.* 54, 10230-10233.
- Wasungu, L., Hoekstra, D., 2006. Cationic lipids, lipoplexes and intracellular delivery of genes. *J. Control. Release* 116, 255-264.
- Wieczorek, A., Blauz, A., Zal, A., Arabshahi, H.J., Reynisson, J., Hartinger, C.G., Rychlik, B., Plazuk, D., 2016. Ferrocenyl Paclitaxel and Docetaxel Derivatives: Impact of an Organometallic Moiety on the Mode of Action of Taxanes. *Chemistry (Easton)* 22, 11413-11421.
- Wohlfart, S., Khalansky, A.S., Gelperina, S., Maksimenko, O., Bernreuther, C., Glatzel, M., Kreuter, J., 2011. Efficient Chemotherapy of Rat Glioblastoma Using Doxorubicin-Loaded PLGA Nanoparticles with Different Stabilizers. *PLoS One* 6, e19121.
- Ying, X., Wen, H., Lu, W.L., Du, J., Guo, J., Tian, W., Men, Y., Zhang, Y., Li, R.J., Yang, T.Y., Shang, D.W., Lou, J.N., Zhang, L.R., Zhang, Q., 2010. Dual-targeting daunorubicin liposomes improve the therapeutic efficacy of brain glioma in animals. *J. Control. Release* 141, 183-192.
- Yuan, J.-L., Liu, Z.-G., Hu, Z., Zou, G.-L., 2007. Study on interaction between apigenin and human serum albumin by spectroscopy and molecular modeling. *Journal of Photochemistry and Photobiology A: Chemistry* 191, 104-113.

- Yue, P.J., He, L., Qiu, S.W., Li, Y., Liao, Y.J., Li, X.P., Xie, D., Peng, Y., 2014. OX26/CTX-conjugated PEGylated liposome as a dual-targeting gene delivery system for brain glioma. *Mol. Cancer* 13, 191.
- Zhan, C., Gu, B., Xie, C., Li, J., Liu, Y., Lu, W., 2010. Cyclic RGD conjugated poly(ethylene glycol)-co-poly(lactic acid) micelle enhances paclitaxel anti-glioblastoma effect. *J. Control. Release* 143, 136-142.
- Zhang, X.D., Wu, H.Y., Wu, D., Wang, Y.Y., Chang, J.H., Zhai, Z.B., Meng, A.M., Liu, P.X., Zhang, L.A., Fan, F.Y., 2010. Toxicologic effects of gold nanoparticles in vivo by different administration routes. *International journal of nanomedicine* 5, 771-781.
- Zheng, Y., McFarland, B.C., Drygin, D., Yu, H., Bellis, S.L., Kim, H., Bredel, M., Benveniste, E.N., 2013. Targeting protein kinase CK2 suppresses prosurvival signaling pathways and growth of glioblastoma. *Clin. Cancer Res.* 19, 6484-6494.

